Petrography, geochemistry and provenance of Saudi Arabian Palaeozoic sandstones

vom Fachbereich Material- und Geowissenschaften
der Technische Universität Darmstadt
zur Erlangung des Grades
Doktor rerum naturalium (Dr. rer. nat.)
genehmigte Dissertation

von Diplom-Geologe Alexander Bassis aus Malsch

TECHNISCHE UNIVERSITÄT DARMSTADT

Referenten:
Prof. Dr. Matthias Hinderer
Prof. Dr. Christoph Schüth

Tag der Einreichung: 05.12.2016
Tag der mündlichen Prüfung: 18.04.2017

Darmstadt 2017
D17

Declaration of Authorship

I hereby certify that the complete work to this PhD thesis

'Petrography, geochemistry and provenance of Saudi Arabian Palaeozoic sandstones.'

was done by me and only with the use of the referenced literature and the described methods.

…….. ……

Place, date Signature

'There is no real ending. It’s just the place where you stop the story.'

Frank Herbert

Index

Abstract
Zusammenfassung
1. Introduction ... 1
1.1. Aims ... 1
1.2. Concept ... 2
1.3. Study areas ... 3
2. Geological background ... 5
2.1. Arabian Plate evolution ... 5
2.2. Stratigraphic framework of northern and central Saudi Arabia ... 7
2.2.1. Saq Formation ... 7
2.2.2. Qasim Formation ... 7
2.2.3. Sarah and Zarqa formations ... 8
2.2.4. Qalibah Formation: Qusaiba Member ... 9
2.2.5. Qalibah Formation: Sharawra Member ... 10
2.2.6. Tawil Formation ... 12
2.2.7. Jauf Formation ... 12
2.2.8. Jubah Formation ... 13
2.2.9. Unayzah Formation ... 13
2.3. Stratigraphic framework of southern Saudi Arabia ... 15
2.3.1. Dibsiyah Formation ... 15
2.3.2. Sanamah Formation ... 15
2.3.3. Qalibah Formation: Qusaiba Member ... 16
2.3.4. Khusayyayn Formation ... 16
2.3.5. Juwayl Formation ... 16
2.4. Provenance, chemostratigraphy and heavy mineral studies ... 18
3. Provenance analysis ... 21
3.1. A short history of provenance analysis ... 21
3.2. Heavy minerals ... 23
3.2.1. Heavy mineral indices ... 24
3.2.2. Rutile ... 25
3.2.3. Garnet ... 26
3.2.4. Zircon ... 26
4. Methods and material ... 28
4.1. Sampling ... 28
4.2. Sample preparation ... 29
4.3. Petrography and standard heavy mineral analysis ... 30
4.4. Geochemical analysis ... 32
4.5. Single-grain analysis ... 32
5. Results ... 33
5.1. Petrography ... 33
5.2. Geochemistry ... 36
5.3. Major elements ... 37
5.4. Trace elements ... 39
5.4.1. Large-ion lithophile elements (LILE): Rb, Ba, Sr, Cs ... 39
5.4.2. High field strength elements (HFSE): Th, U, Y, Zr, Hf, Nb, Ta ... 39
5.4.3. Transition trace elements (TTE): Sc, Cu, Ni ... 42
5.4.4. Rare earth elements (REE): La, Ce, Pr, Nd, Sm, Eu, Gd, Tb, Dy, Ho, Er, Yb ... 42
5.5. Standard heavy mineral analysis ... 47
5.5.1. Zircon-tourmaline-rutile index (ZTR) ... 49
5.5.2. Rutile:zircon index (RZi) ... 50
5.5.3. Garnet:zircon index (GZi) ... 50
5.5.4. Apatite:tourmaline index (ATi) ... 50
5.5.5. Staurolite:tourmaline index (STi) ... 50
5.5.6. Opaque phases ... 50
5.5.7. Cross-plots ... 51
5.6. Single-grain analysis ... 53
5.6.1. Rutile chemistry ... 53
5.6.2. Garnet chemistry ... 53
5.6.3. Zircon morphotypology ... 54

6. Discussion 58
6.1. Source area weathering 58
6.2. Sedimentary recycling 63
6.3. Tectonic setting 66
6.4. Provenance 72
6.5. Chemostratigraphy 75
6.6. Standard heavy mineral analysis 80
6.7. Rutile varietal studies 86
6.8. Garnet varietal studies 87
6.9. Zircon morphotypology 89
6.10. An integrated approach to provenance analysis 90
7. The Khida Terrane: A closer look at a potential source for Palaeozoic sandstones in southern Saudi Arabia 95
7.1. Geological setting 95
7.2. Previous studies 98
7.3. Geology of the Muhayil area 100
7.4. Methodology 101
7.5. Results 101
7.5.1. Petrography 101
7.5.2. Geochemistry 104
7.6. Discussion 106
7.7. Summary and outlook 109
8. Conclusions and outlook 110
Acknowledgements
References
Annex
Curriculum vitae

Figures

Figure 1: Principal of an integrated multi-proxy provenance analysis and analytical methods as utilised in this study. 2

Figure 2: (a) Simplified geologic map of the Arabian Peninsula showing the study areas (modified after Powers, 1968). (b) Geologic map of the southern Saudi Arabian study area ('Wajid area') with sample locations (modified after Keller et al., 2011). (c) Geologic map of the northern Saudi Arabian study area ('Tabuk area') with sample locations (modified after Pollastro et al., 1998). 4

Figure 3: Simplified stratigraphic column of both study areas. 6

Figure 4: (a) Saq Fm. with large-scale trough cross-bedding, Highway 70. (b) Qasim Fm. unconformably overlying Precambrian basement near Hail. (c) Sarah Fm. cutting into the Qasim Fm. W of Al Qara. (d) Bioturbated fine-grained sandstone, Sharawra Mbr, W of the Qusaiba Depression. (e) Medium-grained, SiO_2-cemented sandstone of the Tawil Fm., W of Dawmut al Jandal. (f) Shales interbedded with fine- to medium-grained sandstone of the Subbat Mbr., Jauf Fm., Dawmut al Jandal. (g) Fine- to medium grained sandstone with abundand ripples, Jubah Fm., W of Sakaka. (h) Well sorted, medium-grained sandstone of the Unayzah Fm., E of the Qusaiba Depression. 11

Figure 5: (a) Planolites traces, Qasim Formation, west of Al Qara. (b) Middle to Late Darriwilian didymograptids, Hanadir Member, Qasim Formation, Sarah Ridge. (c) & (d) Burrow traces and echinoderm fragments, Sharawra Member, Qalibah Formation, west of Qusaiba Depression. (e) & (f) Zoophycos and unidentified fossil wood, Jubah Formation, approximately 25 km north of Sakaka. 14

Figure 6: (a) *Skolithos* piperock of the Dibsiyah Fm. at Jabal Nafla. (b) Intensive Fe-/Mn-cementation in the Sanamah Fm., Jabal Atheer. (c) Glacial striations striking ~150°, Sanamah Fm., SW of Wadi Ad Dawasir. (d) Khusayyayn Fm. Resting on the Qusaiba Mbr. of the Qalibah Fm., Hima/Nawan. (e) Slumping structures above planar cross-bedded sandstone in the Khusayyayn Fm., Jabal Abood. (f) Planar cross-bedded sandstone above laminated shales of the Juwayl Fm., Jabal Seab. 17

Figure 7: Sample preparation and analytical scheme. 28

Figure 8: (a) Sawing of samples with a rock saw for thin section preparation and further disintegration. (b) Grinding of disintegrated sample for geochemical analysis in a vibratory disc mill with a tungsten carbide set to a grain size of <63 µm. (c) Dry sieving of disintegrated sample to separate 63–125 µm grain size fraction. (d) Density separation of heavy mineral fraction in a separator funnel filled with sodium polytungstate. 29

Figure 9: QFL diagrams for lithological classification (modified after McBride, 1963). 33

Figure 10: Thin section photographs of Palaeozoic sandstones. 34

Figure 11: Major elements concentrations plotted against Al_2O_3 concentration for samples from the Tabuk area. 36

Figure 12: Major elements concentrations plotted against Al_2O_3 concentration for samples from the Wajid area. 40

Figure 13: Spider plots for trace elements normalised to the average UCC (from Taylor and McLennan, 2009; McLennan, 2001) for samples from the Tabuk area. 41

Figure 14: Spider plots for trace elements normalised to the average UCC (from Taylor and McLennan, 2009; McLennan, 2001) for samples from the Wajid area. 42

Figure 15: REE patterns for samples from the Tabuk area, chondrite-normalised after McDonough and Sun (1995). 45

Figure 16: REE patterns for samples from the Wajid area, chondrite-normalised after McDonough and Sun (1995). 46

Figure 17: Translucent heavy mineral distribution of Saudi Arabian Palaeozoic sandstones in their inferred stratigraphical order. 49

Figure 18: Photomicrographs of the most common heavy minerals. 51

Figure 19: Different heavy mineral indices of samples from both study areas, plotted in their inferred stratigraphical succession. 52

Figure 20: Frequency histograms of rutile temperature distribution from the Tabuk (a) and Wajid (b) areas. Inlays in (a) and (b) show the distribution of rutile source rock lithologies for lower and upper parts of the successions. 54

Figure 21: Results of garnet chemical analysis. (a) Garnet classification scheme after Mange and Morton (2007). (b), (c) and (d) Percentage distribution of garnet types in the Jauf, Jubah and Juwayl formations, respectively. 56

Figure 22: CL-images showing the different zircon morphotypes encountered, their characteristic features and internal structures. 57

Figure 23: Results of the zircon morphotype classification. 57

Figure 24: A-CN-K diagram, modified after Nesbitt and Young (1984), showing idealized weathering trends for some common magmatic rocks. 62

Figure 25: Th/Sc vs. Zr/Sc plot (modified after McLennan et al., 1993) showing zircon enrichment interpreted as sedimentary recycling. 65

Figure 26: Tectonic discrimination diagrams (modified after Dickinson et al., 1983). (a) & (b) Tabuk area; (c) & (d) Wajid area. 67

Figure 27: Tectonic setting discrimination diagrams after Roser and Korsch (1986) (a & b) and provenance discrimination diagram after Roser and Korsch (1988) (c & d) for the Tabuk and Wajid areas. 69

Figure 28: Tectonic setting discrimination diagrams after Verma and Armstrong-Altrin (2013). (a) Tabuk area; (b) Wajid area. 70

Figure 29: Ternary Ni-V-Th*10 diagram for source rock discrimination (modified after Bracciali et al. (2007). (a) Tabuk area; (b) Wajid area. 71

Figure 30: (a) and (b): Plots of Th/U vs. Th (modified after McLennan et al., 1993) for the Tabuk and Wajid areas, respectively. (c) and (d): Plots of Th/Sc vs. Th/U for the Tabuk and Wajid areas, respectively. (e) Enlarged detail of (d). 73

Figure 31: Cluster dendrogram showing association of samples from both study areas. 75

Figure 32: Scatter plot of the two most significant components of a principal component analysis (PCA). (b) biplot of variables; grey area represents range Wajid area samples without outliers; (c) scree plot of principal components vs. eigenvalues. 78

Figure 33: Scatter plot of the PCA with a reduced data set. (a) Arrangement of samples; (b) biplot of variables; (c) scree plot of principal components vs. eigenvalues. 79

Figure 34: Sketch map of the Arabian Peninsula and surrounding areas (modified after Powers, 1968; Avigad et al., 2005; Meinhold et al., 2013b). 83

Figure 35: Scatter plot of the two most significant components of a principal component analysis (PCA). (a) Arrangement of samples; (b) biplot of variables; (c) scree plot of principal components vs. eigenvalues. 91

Figure 36: Compilation and comparison of provenance sensitive parameters of different methods used to identify and correlate 4 provenance events in the Tabuk and Wajid areas. 94

Figure 37: (a) Overview map of the Arabian Shield, showing the Khida Terrane and the Muhayil area (modified after Stoeser et al. 2001). (b) Map of the Muhayil area in the southern Khida Terrane (modified after Stoeser et al., 2001), showing sample locations from literature and this study. 96

Figure 38: (a) QAPF classification diagram after Streckeisen (1974); (b) TAS classification diagram after Middlemost (1994). 102

Figure 39: Thin section photographs of basement samples from the Muhayil area. (a), (b) Zinnwaldite alkali-feldspar granite (sample AB-SA39), containing idiomorphic magmatic garnet (I) and zinnwaldite mica (II). (c), (d) Meta-psammite (sample AB-SA45) with mm-scale layers, containing Cr-spinel (III). (e), (f) Biotite granitic orthogneiss (sample AB-SA51) containing quartz with undulose extinction (IV) and altered feldspar (V). 103

Figure 40: Results of the geochemical characterisation scheme for granitic rocks after Frost et al. (2001). (a) MALI; (b) Fe*; (c) ASI. 104

Figure 41: REE patterns for samples from the Khida Terrane, chondrite-normalised after McDonough and Sun (1995). 105

Figure 42: Set of 5 tectonic discrimination diagrams after Verma et al. (2013). 107

Tables

Table 1: Relative stability during burial diagenesis and in weathering profiles for some of the most important heavy minerals (modified after Morton and Hallsworth, 1999, 2007). 23

Table 2: Overview of utilised heavy mineral indices (modified after Morton and Hallsworth, 1994). 24

Table 3: Palaeozoic sampling sites and outcrops with GPS coordinates. 31

Table 4: Modal composition and framework mineralogy for Palaeozoic sandstones. 35

Table 5: Correlation matrix of selected major and trace elements. 38

Table 6: Correlation matrix of selected major elements, Zr, Th, U and selected REE-ratios. 44

Table 7: Heavy mineral composition and heavy mineral indices of Palaeozoic sandstones. 48

Table 8: Distribution of mafic and felsic rutiles in both study areas. 53

Table 9: Mean values of different weathering indices for Palaeozoic formations from the Tabuk and Wajid areas. 60

Table 10: Calculations of discriminant functions for tectonic discrimination diagrams of Roser and Korsch (1988) and Verma and Armstrong-Altrin (2013) for high silica rocks (63–95% SiO_2). 68

Table 11: Simplified timeline of the events leading to the assembly of Gondwana. 95

Table 12: Published ages for Khida Terrane rocks. 99

Table 13: GPS coordinates and short description of samples from the Khida Terrane, including the lithological descriptions of Stoeser et al. (2001). 101

Table 14: Summarised results of different petrographic and geochemical classification schemes for samples from the Khida Terrane. 102

Table 15: Results of the geochemical characterisation scheme for granitic rocks after Frost et al. (2001). 104

Table 16: Calculations of discriminant functions for tectonic discrimination diagrams of Verma et al. (2013) utilising trace element concentrations in ppm for for acidic magmas. 109

Abbreviations

ACM – active continental margin
Afsp – alkali feldspar
Alm – almandine
Alt – alterated grain
AP – Arabian Plate Tectonostratigraphic Megasequence
Apt – apatite
ATi – apatite:tourmaline index
ANS – Arabian-Nubian Shield
bio – biotite
Chr – chromite
CIA – chemical index of alteration
CL – cathodoluminescence
CM – cement
cpx – clinopyroxene
cSi – coarse silt
DF – discriminant function
EMP – electron microprobe
En – enstatite
Epd – epidote
fS – fine sand
Grs – grossular
Grt – garnet
GS – grain size
GZi – garnet:zircon index
hbl – hornblende
HFSE – high field strength elements
Ky – kyanite
LA-ICP-MS – laser ablation inductively coupled plasma mass spectrometry
Lf – lithic fragments
LILE – large-ion lithophile elements
Lt – total lithic fragments including Qp
LT – Lower Tabuk
LW – Lower Wajid
MI – mineralogical maturity index
mS – medium sand
Mzt – monazite
OIA – ocean island arc
olv – olivine
Opq – opaque grains
opx – orthopyroxene
OUC – old upper continental crust
PAAS – Post-Archean Australian Shale
PC – principal component
PCA – principal component analysis
PE – provenance event
PIA – plagioclase index of alteration
Plag – plagioclase feldspar
PMa – pseudomatrix
PM – passive margin
Prp – pyrope
px – pyroxene
Q% – relative abundance of quartz
Qm – monocrystalline quartz
Qmu – monocrystalline quartz with undulose extinction
Qp – polycrystalline quartz
REE – rare earth element (HREE – heavy REE; LREE – light REE)
RS – recycled sedimentary
RTi – rutile:tourmaline index
rtl – rutile
SHMA – standard heavy mineral analysis

Sph – sphene
Sps – spessartine
STi – staurolite:tourmaline index
Stl – staurolite
Trem – tremolite
trm – tourmaline
TTE – transition trace elements
UCC – Upper Continental Crust
UT – Upper Tabuk
UW – Upper Wajid
YDA – young differentiated arc
YUA – young undifferentiated arc
zrc – zircon
ZTR – zircon-tourmaline-rutile index

Equations

(equation 1)..... 25
(equation 2)..... 25
(equation 3)..... 43
(equation 4)..... 58
(equation 5)..... 59

Abstract

The Arabian Peninsula hosts a thick Palaeozoic succession, ranging from the Cambrian through the Permian. It not only contains deposits of the two major Palaeozoic glaciations, but also holds both the major Palaeozoic hydrocarbon source and reservoir rocks. In addition, Palaeozoic sandstones serve as important aquifers. The succession is dominated by highly mature quartz arenites, as seen in thin sections. It is starved of fossils and very uniform in lithology. This creates unique problems for the interpretation of provenance and tectonic setting as well as for stratigraphic correlations. In order to better understand provenance, tectonic setting and stratigraphic relationships, the petrography, major and trace element geochemistry, heavy mineral assemblages and single-grain geochemistry of sandstones were studied. Samples were taken in several field campaigns from two study areas in southern (Wajid area) as well as central and northern (Tabuk area) Saudi Arabia. The data set presented here is the first comprehensive study to cover the entire Palaeozoic succession in both the southern and northern part of the Arabian Peninsula. Tectonic discrimination diagrams suggest that deposition of sandstones took place in an intracratonic setting, which is in accordance with the established model for the evolution of the Arabian Plate. The collisional signal from some samples is a relic from the last stages of the amalgamation of Gondwana, carried into the basin by glaciogenic sediments. Major and trace element geochemistry indicate the Neoproterozoic basement of the nearby Arabian Shield as the most likely source for the detritus. An influx of fresh material, probably sourced from the Shield, did occur in the upper Palaeozoic units of southern Saudi Arabia but did not reach the northern study area. Petrographic and geochemical observations have proven to be unsuitable to assess the influence of sedimentary recycling versus strong weathering and reworking during deposition in highly mature quartz arenites. A (meta-) sedimentary source for the Palaeozoic sandstones could therefore neither be proven nor refuted. Multivariate cluster and principal component analysis of geochemical data revealed significant differences between the two study areas. They further allowed differentiating between the lower and upper parts of the southern Saudi Arabian Palaeozoic succession. The heavy mineral assemblages reflect the mineralogical maturity of the Saudi Arabian Palaeozoic siliciclastics. They are dominated by the ultra-stable phases zircon, tourmaline and rutile. Less stable accessories are apatite, staurolite and garnet. Standard heavy mineral analysis of samples from both study areas reveals distinct changes in provenance. Cambrian–Ordovician sandstones are first-cycle sediments, probably sourced from the Arabian-Nubian Shield. The overlying, Hirnantian glaciogenic deposits consist of recycled Cambrian–Ordovician material. Devonian–Permian sandstones show a significant influx of fresh basement material, as attested by an increase of meta-stable heavy minerals. Single-grain geochemical analysis of rutile and garnet has proven to be a powerful supplementary technique. Rutile varietal studies reveal distinct differences in host rock lithologies between the two study areas. Zr-in-rutile thermometry identified granulite-facies detritus in the lower Palaeozoic of the Tabuk area and has the potential to further define source areas. The distribution patterns of garnet host rock lithologies are remarkably similar in both study areas. They are dominated by amphibolite-facies metasediments and intermediate to felsic igneous rocks. Garnets derived from granulite-facies metasediments, which are scarce in the Arabian-Nubian Shield, also occur. Possible source rocks for high-grade garnets can be found in Yemen or further south in the Mozambique Belt. A closer look was taken at the Khida Terrane – a block of old continental crust situated at the southeastern margin of the Arabian Shield. The Khida Terrane contains various Palaeo- to Neoproterozoic igneous suites as well as metasedimentary successions and is a potential source area for Palaeozoic sediments. Geochemical analyses revealed a collisional setting of most igneous samples. Petrographical observations showed the presence of primary igneous garnet and zinnwaldite mica in one igneous sample and significant amounts of Cr-spinel in a metasediment.

Zusammenfassung

Die Arabische Halbinsel beherbergt eine mächtige paläozoische Abfolge, die vom Kambrium bis zum Ende des Perms reicht. Diese Abfolge beinhaltet nicht nur Spuren der zwei großen paläozoischen Vereisungen, sondern enthält auch die wichtigsten paläozoischen Mutter- und Speichergesteine für Kohlenwasserstoffe. Paläozoische Sandsteine dienen weiterhin als wichtige Grundwasserleiter. Die Abfolge wird beherrscht von hochmaturen Quarzareniten, wie Dünnschliffe zeigen. Sie ist sehr arm an Fossilien und von einer sehr uniformen Lithologie. Dies schafft einzigartige Probleme für die Interpretation von Provenienz und tektonischem Regime sowie stratigraphischen Korrelationen. Um die Sedimentprovenienz, das tektonische Regime und stratigraphische Zusammenhänge besser zu verstehen wurden die Petrographie, Haupt- und Spurenelementgeochemie, Schwermineralogie und Einzelmineralgeochemie untersucht. Die Proben wurden während mehrerer Geländekampagnen in zwei Arbeitsgebieten im südlichen (Wajid Gebiet) sowie zentralen bis nördlichen (Tabuk Gebiet) Saudi-Arabien genommen. Der hier präsentierte Datensatz ist der erste, der die gesamte paläozoische Abfolge sowohl im Süden wie auch im Norden der Arabischen Halbinsel abdeckt. Diagramme zur Unterscheidung des tektonischen Regimes zeigen, dass die Ablagerung der Sandsteine auf einem passiven Kontinentalrand stattfand. Dies ist in Übereinstimmung mit dem etablierten Modell der Evolution des Arabischen Platte. Das Kollisionsorogen-Signal, welches in einigen Proben sichtbar ist, ist ein Relikt der Endphase der Amalgamation von Gondwana. Dieses Signal wurde durch glazigene Sedimente ins Becken getragen. Haupt- und Spurenelementgeochemie deuten auf das neoproterozoische Grundgebirge des nahegelegenen Arabischen Schildes als die wahrscheinlichste Sedimentquelle hin. Ein Zustrom frischen Materials, welches wahrscheinlich vom Schild abgetragen wurde, fand im späten Paläozoikum im südlichen Arbeitsgebiet statt. Dieser Zustrom erreichte nicht das nördliche Arbeitsgebiet. Es zeigte sich, dass petrographische und geochemische Untersuchungen alleine nicht ausreichen, um den Einfluss von Wiederaufarbeitung des Sediments gegen starke Verwitterung sowie Aufarbeitung während der Ablagerung in hochmaturen Quarzareniten abzugrenzen. Für die paläozoischen Sandsteine konnte daher eine (meta-) sedimentäre Quelle weder bestätigt noch widerlegt werden. Multivariate Cluster- sowie Hauptkomponentenanalyse geochemischer Daten deckten signifikante Unterschiede zwischen beiden Arbeitsgebieten auf. Sie erlaubten es weiterhin, zwischen dem unteren und oberen Teil der Abfolge im Süden Saudi-Arabiens zu unterscheiden. Die Schwermineralsuites spiegeln die hohe mineralogische Reife der saudi-arabischen paläozoischen Siliziklastika wider. Sie werden von den hochstabilen Phasen Zirkon, Turmalin und Rutil dominiert. Weniger stabile Akzessorien sind Apatit, Staurolith und Granat. Standardschwermineralanalysen von Proben aus beiden Arbeitsgebieten enthüllen eindeutige Änderungen in der Provenienz. Sandsteine des Kambro-Ordoviz sind 'first-cycle' Sedimente, welche wahrscheinlich vom Arabisch-Nubischen Schild stammen. Die hangenden, hirnantischen glazigenen Ablagerungen bestehen aus wiederaufgearbeitetem kambro-ordovizischem Material. Devonisch-permische Sandsteine zeigen einen signifikanten Eintrag von frischem Grundgebirgsmaterial, wie durch den Anstieg an metastabilen Schwermineralen belegt wird. Einzelmineralgeochemische Analysen von Rutilen und Granaten haben sich als vielversprechende, ergänzende Methode entpuppt. Einzelmineraluntersuchungen an Rutilen enthüllten distinkte Unterschiede in den Liefergesteinslithologien der beiden Arbeitsgebiete. Durch Zr-in-Rutil Thermometrie konnte granulitfazieller Detritus im unteren Paläozoikum des Tabuk Gebietes identifiziert werden. Diese Methode hat das Potenzial, Liefergebiete noch genauer zu definieren. Die Verteilungsmuster der Liefergebietslithologien von Granaten beider Arbeitsgebiete sind sich bemerkenswert ähnlich. Sie werden beide von amphibolitfaziellen Metasedimenten und intermediären bis felsischen Magmatiten beherrscht. Granate aus granulitfaziellen Metasedimenten, welche im Arabisch-Nubischen Schild selten sind, kommen ebenfalls vor. Mögliche Liefergesteine für hochmetamorphe Granate befinden sich im Jemen oder weiter südlich im Mosambik-Gürtel. Das Khida Terrane, ein Block alter kontinentaler Kruste am südöstlichen Rand des Arabischen Schildes, wurde näher beleuchtet. Das Khida Terrane beherbergt verschiedene paläo- und neoproterozoische magmatische und metasedimentäre Gesteine und ist ein potenzielles Liefergebiet paläozoischer Sedimente. Geochemische Analysen offenbarten ein Kollisionssetting für die meisten magmatischen Proben. Petrographische Beobachtungen zeigten die Präsenz von primärem magmatischem Granat und Zinnwaldit Glimmer in einer magmatischen Probe sowie signifikante Mengen von Cr-Spinell in einem Metasediment.

1. Introduction

Saudi Arabian Palaeozoic sediments have been and are still intensely studied since the 1950s (e.g. Thralls and Hasson, 1956; Powers et al., 1966; BRGM, 1985; McGillivray and Husseini, 1992; Stump et al., 1995; Alsharhan and Nairn, 1997; Edgell, 1997; Sharland et al., 2001; GTZ/DCo, 2009; Al-Ajmi et al., 2015), both for economic and scientific reasons. They not only represent significant source and host rocks for hydrocarbons, but also recently gained importance as groundwater reservoirs (Schubert et al., 2011; Al-Ajmi et al., 2014; Salman et al., 2014) for the increasing demands of the desert kingdom. Majestic outcrops along the Arabian Shield are a natural laboratory and lend themselves perfectly to be studied with the classic tools of sedimentology: lithological and geophysical outcrop logging, petrography, facies models and architectural element studies, sequence stratigraphy, and basin analysis. Well-logs, cores and seismic help to link surface with subsurface. Yet, despite of more than half a decade of research, there still remain some glaring questions addressed in this study:

(1) What is the provenance of this highly mature siliciclastic succession?

(2) What was the influence of the two major Palaeozoic glaciations on sediment distribution?

(3) How can the different sandstones units in southern, central and northern Saudi Arabia be correlated?

This study aims to shed new light on these questions. The first comprehensive data set, containing petrographic data from thin sections as well as major and trace element geochemistry is presented. It covers the entire Palaeozoic successions in both southern and central/northern Saudi Arabia.

1.1. Aims

The aims of this PhD thesis are

- Compile a review and synopsis of the stratigraphy, tectonic setting and provenance of Palaeozoic Saudi Arabian siliciclastics
- Create a comprehensive petrographical and geochemical data set covering the entire Palaeozoic succession in northern, central and southern Saudi Arabia
- Use this data set, supported by published data, to identify changes in petrography, geochemistry and heavy mineral assemblage in order to find and evaluate new markers for stratigraphical correlations
- Perform an integrated multi-proxy provenance analysis
- Identify the provenance and potential source rocks of Palaeozoic sandstones, either proximal in and around the Arabian-Nubian Shield (ANS) or distal in East and Central Africa
- Characterise northern, central and southern Saudi Arabian Palaeozoic sedimentary basins: Did they share the same catchment system over time?
- Identify the influence of the Late Ordovician (Hirnantian) and Carboniferous–Permian glaciations on sandstone provenance and sediment dispersal
- Use heavy mineral data and chemical composition to link Saudi Arabian Palaeozoic sandstones with their counterparts in northern Gondwana: Libya, Jordan, Israel

1.2. Concept

The fundamental concept of this PhD thesis is based on an integrated and multi-proxy provenance analysis (Figure 1), i.e. the identification of source rocks for detritus and the tectonic setting of the sedimentary basins. A multi-proxy approach is necessary since Saudi Arabian Palaeozoic sandstones are highly mature and starved of provenance-indicative features. Therefore a wide array of data was collected, including petrographic, geochemical and heavy mineral data. Emphasis was put on lithologies suitable for heavy mineral analysis, but samples were collected from representative units of all major formations exposed in northern, central and southern Saudi Arabia. This makes it possible to not only identify stratigraphical, but also spatial provenance changes and to compare the evolutions of two sedimentary basins. Samples were collected during a two month-long field campaign in 2013 and sent to Germany. Most laboratory and microscopic work was done at the Institute for Applied Geosciences of TU Darmstadt. Whole-rock geochemical analysis was performed at the Geoscience Center at the University of Göttingen. Major element composition of some samples was measured at the Institute for Geosciences at the University of Mainz. The multiple data was then compiled into a single data base and further supplemented by published data. Multivariate studies and principal component analysis was carried out on selected factors. Several parts of this thesis are published and/or are submitted to international journals or were presented at conferences.

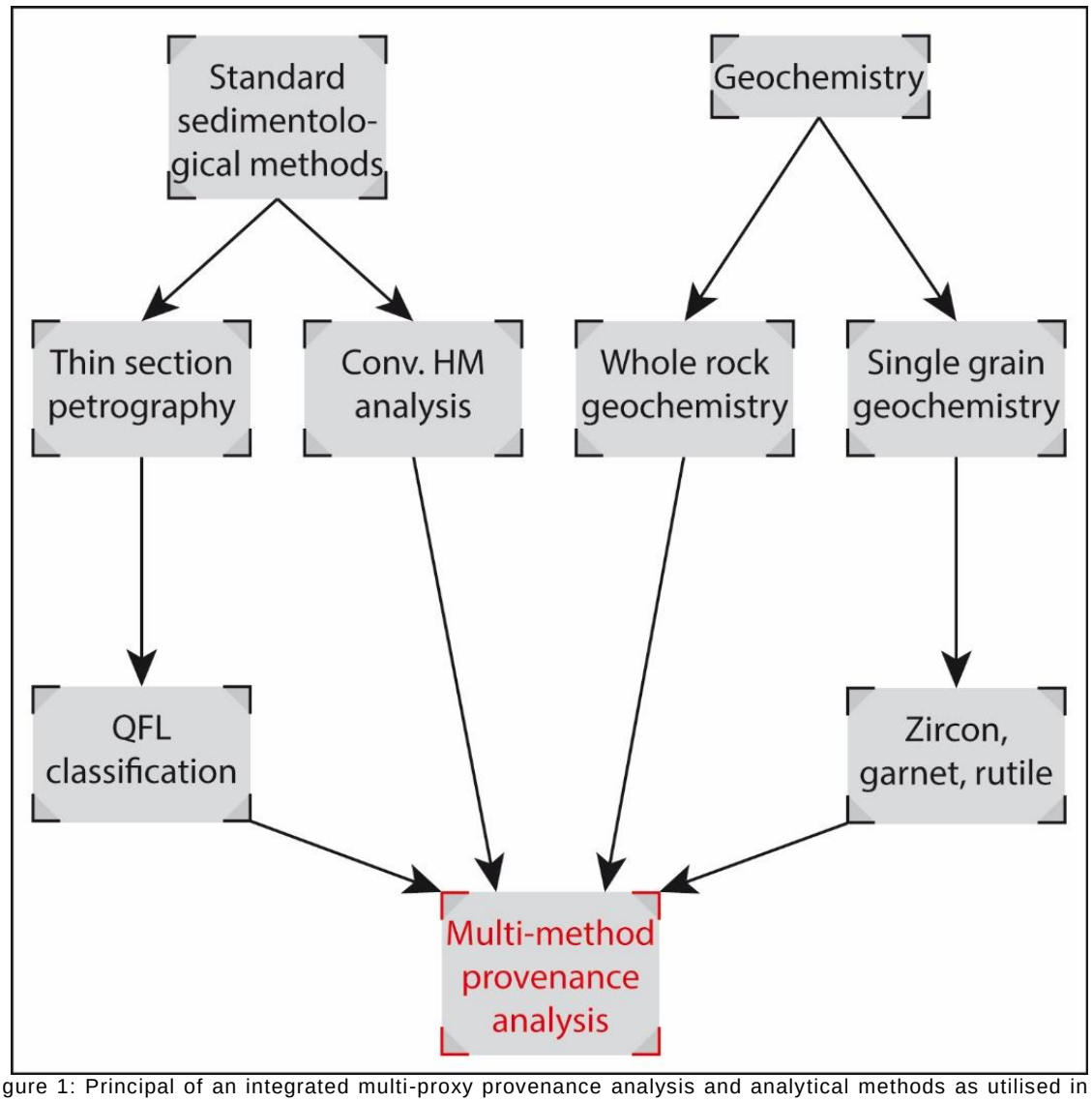

Figure 1: Principal of an integrated multi-proxy provenance analysis and analytical methods as utilised in this study.

1.3. Study areas

The Arabian Plate hosts a Phanerozoic clastic sedimentary succession several kilometres thick, which ranges over the entire Palaeozoic time frame, from the Cambrian to the Permian. However the succession, which was deposited on a largely stable, flat shelf, contains several prominent hiatuses, i.e. unconformities (Powers et al., 1966, Sharland et al. 2001). Palaeozoic sediments crop out in a narrow band west of the Arabian Shield (Figure 2a), where they have a thickness of about 500 m at the surface and generally dip gently towards the east. In the subsurface, the Palaeozoic siliciclastics can reach a thickness of over 4,500 m and show great hydrocarbon and groundwater reservoir potential (Al-Ajmi et al., 2015). They are dominated by highly mature clastic sediments up to the Permian Khuff Formation, where the sedimentation regime switches to a mainly carbonatic one.

In order to compare and characterise the two main Palaeozoic sedimentary basins today exposed in Saudi Arabia, samples were taken from two study areas. These are located in the northern/central and southern part of the Kingdom of Saudi Arabia (Figure 2a). The northern/central study area ('Tabuk area', Figure 2c) is located along the eastern to north-eastern edge of the Arabian Shield and further north around the cities of Sakaka and Dawmut al Jandal. Further to the north and east the Palaeozoic sediments disappear under younger strata and the sands of the Nefud and Dahna deserts. The western margin of the Palaeozoic outcrop belt is marked by the Arabian Shield. As a consequence of the opening of the Red Sea and erosion following the uplift of the rift shoulders, no extensive Palaeozoic outcrops are preserved on the Arabian Shield. While Palaeozoic units continue to crop out in a thin band towards the south, the direct contact with strata from the Wajid outcrop belt is not exposed. The Tabuk area as defined in this study is geographically extensive and can be further divided into three separate outcrop areas. The first is to the east of the Arabian Shield, around the city of Buraida and along the Qusaiba Depression. There Hirnantian, Silurian and Carboniferous–Permian strata are exposed. The second outcrop area stretches from Hail at the north-eastern corner of the Arabian Shield to the west, along its northern margin. Cambrian–Ordovician sandstones crop out impressively and are easily accessible from the highway. The third outcrop area is further to the north, beyond the Nefud Desert, around the cities of Sakaka and Al Jawf. This area features well preserved Devonian successions, again easily accessible from the highway.

The Wajid area in the south is a much more compact outcrop belt (Figure 2b). Its northern boundary is at Wadi Ad Dawasir, while to the east and south the Palaeozoic succession disappears under Mesozoic strata and the Rub' Al Khali Desert. As in northern and central Saudi Arabia, the eastern extent of the Wajid outcrop belt is marked by the basement rocks of the Arabian Shield, though some outliers remain around Najran and Hima. Most samples from southern Saudi Arabia have been collected southwest of Wadi Ad Dawasir. Outcrops from all Palaeozoic formations can be found there. Another outcrop area is located at the southern end of Wajid outcrop belt. At the town of Hima, Devonian sandstones resting directly on basement are exposed as well as Silurian shales.

The clastic succession is overall devoid of fossils, with only minor occurrences of graptolites, trace fossils such as *Cruziana* or *Skolithos* (Powers et al., 1966), some Devonian fish scales (Evans et al., 1991; Forey et al., 1992) and plant remains in younger strata. Microfossils are almost absent in outcrops due to intense and deep weathering, but can be well preserved in the subsurface (Senalp and Al-Duaiji, 1995; Stump et al., 1995; Stump and van der Eem, 1995; Le Hérissé et al., 2007; Hints et al., 2015; Le Hérissé et al., 2015; Paris et al., 2015a,b; Strother et al., 2015; Wellman et al., 2015). This lack of fossils makes precise dating difficult at best. Saudi Arabian Palaeozoic stratigraphy still mainly relies on lithostratigraphic correlations, which can be unreliable in such extensive, highly mature successions. Other successful stratigraphic tools are heavy mineral stratigraphy and chemostratigraphy, which so far have only been published by a few workers and often only for isolated Palaeozoic units (Powers et al., 1966; Hussain, 2001; Hussain and Abdullatif, 2004; Al-Harbi and Khan, 2005; Hussain, 2007; Al-Harbi and Khan, 2008, 2011). A comprehensive database, covering the entire Palaeozoic succession on a regional scope and combining petrographic and geochemical data is still lacking.

Evidence of both the Late Ordovician (Hirnantian) as well as the Carboniferous–Permian glaciations can be found in southern and northern Arabia, such as glacial striations, dropstones, glacio-fluvial conglomerates and tunnel valleys (Keller et al., 2011). In the Wajid area very mature, medium- to fine-grained quartz arenites make up most of the sedimentary column with only minor shaly intercalations. The most prominent shale unit, the Qusaiba 'hot shale', can be correlated throughout the basin and is the source rock for Palaeozoic oil reservoirs south of Riyadh and the Khuff gas (Bishop, 1995). The depositional environment ranges from (glacio-) fluvial to shallow marine (Al-Ajmi et al., 2015). The sedimentary succession in the Tabuk area is similar to southern Saudi Arabia in both lithology and depositional setting. Yet it contains more fine-grained material, especially in Ordovician and Devonian sedimentary rocks, pointing to a more distal depositional environment.

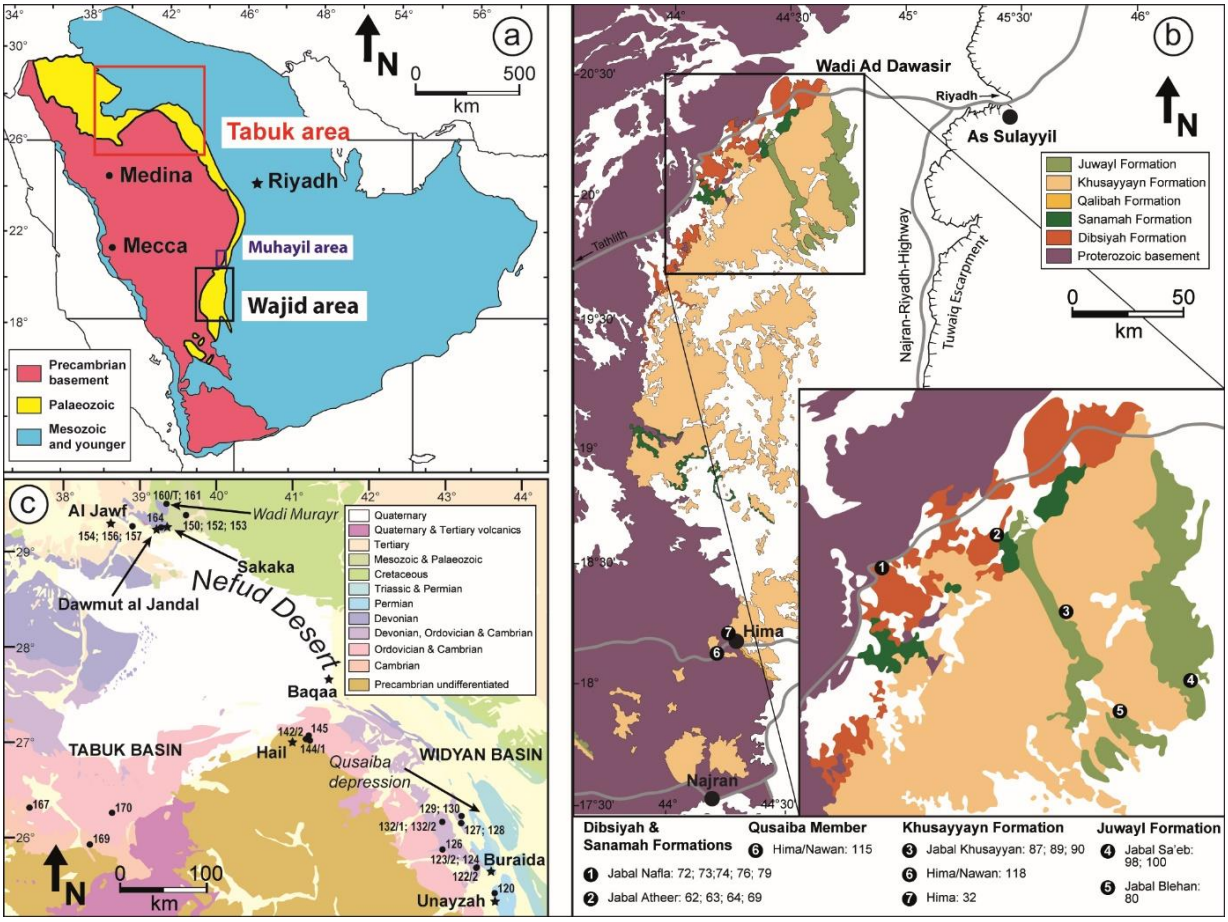

Figure 2: (a) Simplified geologic map of the Arabian Peninsula showing the study areas (modified after Powers, 1968). (b) Geologic map of the southern Saudi Arabian study area ('Wajid area') with sample locations (modified after Keller et al., 2011). (c) Geologic map of the northern Saudi Arabian study area ('Tabuk area') with sample locations (modified after Pollastro et al., 1998).

2. Geological background

2.1. Arabian Plate evolution

During the final stages of the Pan-African Orogeny in the late Neoproterozoic, a collage of juvenile arcs and enclaves of pre-Neoproterozoic crust attached onto Gondwana, forming the ANS, which makes up a prominent part of the basement of the Arabian Plate (e.g. Johnson et al., 2011). Arabia remained part of Gondwana for the entire Palaeozoic and much of the Mesozoic. After final amalgamation of the supercontinent, a vast depositional platform developed on its northern (in present-day coordinates) passive margin. This sedimentary system stretched over modern-day North Africa, Turkey, Iran and the Arabian Peninsula. During the early Palaeozoic, especially the Cambrian–Ordovician, a vast amount of highly mature sandstones were deposited (Avigad et al., 2005). Squire et al. (2006) postulated a super-fan system which has been confirmed to have reached Libya and southern Jordan (Meinhold et al., 2013b). On the Arabian Peninsula, the Phanerozoic sediments were deposited on the continental crust of the Arabian Shield, forming the so called 'Arabian Platform'. Throughout most of the Palaeozoic, the Arabian Platform was situated further inland from the passive margin to the north and east, thus representing an intracratonic setting. In the north and east (present-day coordinates), the platform was separated from the Palaeo-Tethys by the Anatolian and Iranian blocks, respectively. Beginning subduction of the Palaeo-Tethys under these blocks in the Late Devonian caused a switch to a back-arc setting in the northern and eastern parts of the Arabian Platform (McGillivray and Husseini, 1992; Sharland et al., 2001). Rifting along the Zagros suture in the late Carboniferous resulted in the separation of the Cimmerian Plate from Gondwana and the opening of the Neo-Tethys (McGillivray and Husseini, 1992; Sharland et al., 2001). Low subsidence rates and the high stability of the Arabian Plate throughout most of the Palaeozoic resulted in a ‘layer cake’ stratigraphy (Bishop, 1995). Sediments were deposited mostly in fluvial to shallow marine conditions. Accommodation was largely controlled by eustacy. Major flooding events were caused by exceptional rises of the eustatic sea level, like those connected to deglaciation (Sharland et al., 2001).

At the beginning of the Palaeozoic, much of northern Gondwana had been peneplained. On the Arabian Plate, which was situated between 20°S and 40°S and moving further south (Sharland et al., 2001), existed a broad clastic shelf. This shelf lay adjacent to exposed Pan-African basement rocks of the ANS. On this peneplain, mature quartz arenites were deposited (Konert et al., 2001). During the Middle to Late Ordovician, changes in eustacy or a possible rifting event across the Arabian Plate caused fluctuating sea levels on the northeastern shelf (Sharland et al., 2001). This led to the deposition of the Middle to Upper Ordovician shale members of the otherwise coarse Qasim Formation (Sharland et al., 2001). In the Late Ordovician, Gondwana had moved further south, moving the Arabian Plate into palaeolatitutes of 40°S to 60°S (Sharland et al., 2001). This brought Arabia into the reach of the polar ice cap of the Hirnantian glaciation, causing sub-glacial erosion across the platform (Vaslet, 1990; Keller et al., 2011). In northern, central and southern Arabia, tunnel-valleys, radiating away from the ANS, incised deeply into platform sediments (Sharland et al., 2001; Le Heron et al., 2009). On this regional unconformity, the Sarah/Zarqa and Sanamah formations were then deposited. With the demise of the Hirnantian ice-age, sea-level rapidly rose in response to deglaciation. This 2nd order post-glacial sea level rise flooded not only the Arabian Platform, but large parts of northern Gondwana. The Arabian Plate remained in high southern latitudes without major tectonic activity. Anoxic conditions and sediment starvation in the early Silurian helped create the prolific, organic-rich ‘hot shales’. Represented by the Qusaiba Member of the Qalibah Formation in Saudi Arabia, these shales are the main source rocks for Palaeozoic hydrocarbon reservoirs in North Africa and the Middle East (Lüning et al., 2000; Konert et al., 2001; Sharland et al., 2001). Tectonically quiet conditions continued throughout most of the Devonian. Gondwana moved north again, bringing the Arabian Plate into a more moderate latitudinal position, around a minimum of 30°S by the Late Devonian (Sharland et al., 2001). Sedimentation took place in an epicontinental, dominantly shallow marine, intracratonic setting. Devonian rocks are not as well preserved as other Palaeozoic units, especially in central Saudi Arabia. Regional uplift and erosion on structural highs associated with the following 'Hercynian Event' removed large parts of the Devonian

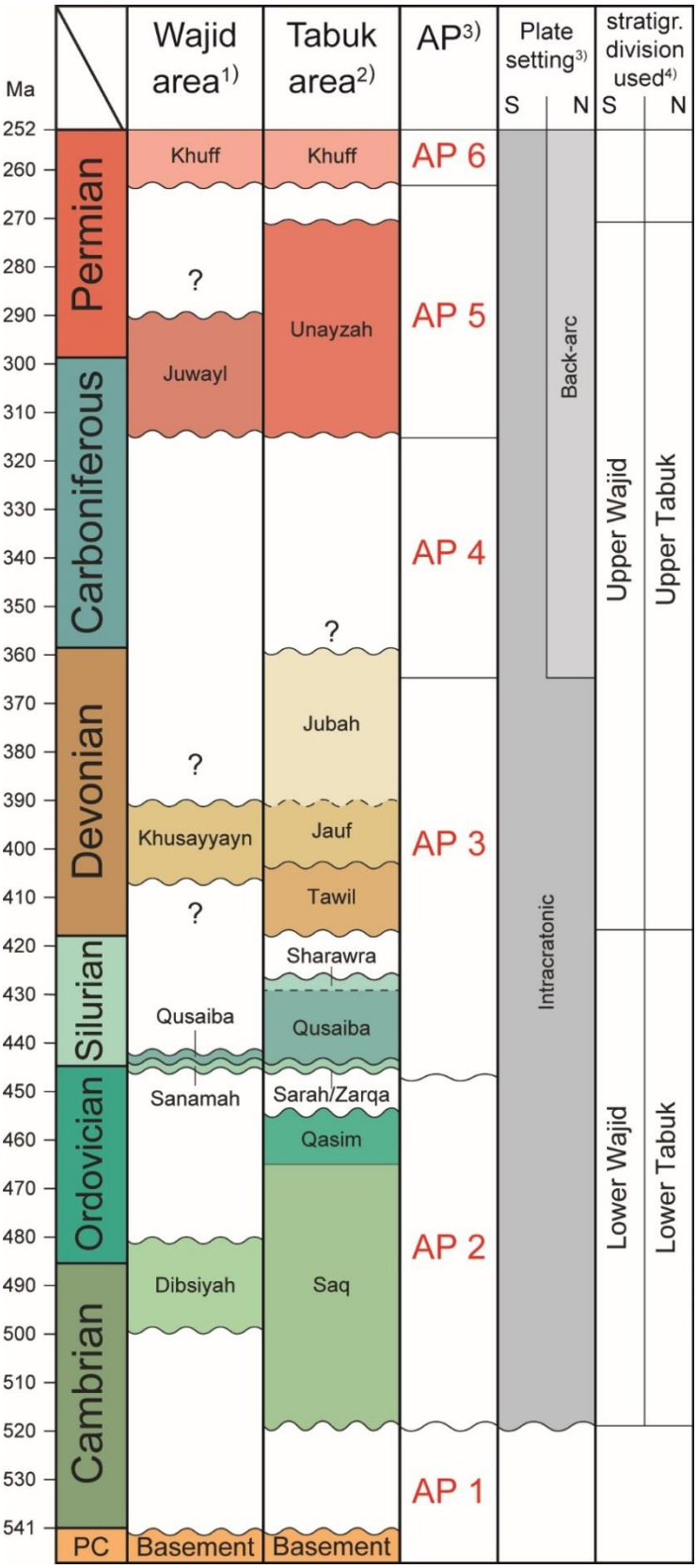

Figure 3: Simplified stratigraphic column of both study areas. Modified after 1) Al-Ajmi et al. (2015); 2) Al-Laboun (2010); 3) Sharland et al., (2001); AP = Arabian Plate Sequences according to Sharland et al. (2001); 4) informal stratigraphic subdivision used in this study.

strata (McGillivray and Husseini, 1992; Sharland et al., 2001; Al-Ramadan et al., 2004; Laboun, 2013). North and south of the central Arabian Arch, some Devonian units are preserved: the Tawil, Jauf, Jubah formations of northern Saudi Arabia and especially the impressive Khusayyayn Formation in the south. The Carboniferous is almost completely missing, due to erosion and non-deposition (Konert et al., 2001). Yet, it brought significant change to Arabian Platform evolution. The beginning subduction of the Palaeo-Tethys led to the development of an overall back-arc setting in northern and eastern Arabia, while the south and west stayed intracratonic (Sharland et al., 2001). The plate again moved to higher latitudes (~40°S), rotated clockwise by ~90° and gently tilted to the northeast (Konert et al., 2001; Sharland et al., 2001). During the end of the Carboniferous thermal uplift started in Oman. While at the northern and eastern plate margins the Zagros back-arc rift developed, an intracratonic setting persisted in the south and west (Sharland et al., 2001). Arabia again reached high southern latitudes of up to 40°S (Sharland et al., 2001). The Carboniferous–Permian brought with it the second large Palaeozoic glaciation of Gondwana. Glacial and peri-glacial sediments of the Unayzah C Member and Juwayl Formation were deposited on the Hercynian ('pre-Unayzah') unconformity (Le Heron et al., 2009; Keller et al., 2011). Glacial advance was toward the north and northwest in northern Arabia and to the south and southeast in southern Arabia, away from the main ice shield, as evidenced by direction of tunnel valleys and striated surfaces (Hinderer et al., 2009; Khalifa, 2015). The glacial to fluvial Unayzah Formation is the primary Palaeozoic hydrocarbon reservoir of the Arabian Peninsula, mainly sourced from the Silurian Qusaiba Shale (McGillivray and Husseini, 1992). During the Permian the Arabian Plate moved rapidly northwards into lower latitudes of ~25°S. Continued northern drift and thermal collapse of the northeastern passive margin led to a rapid marine transgression (Sharland et al., 2001). Palaeozoic clastic sedimentation ceased with the deposition of the late Permian Khuff carbonate rocks.

2.2. Stratigraphic framework of northern and central Saudi Arabia

Northern Saudi Arabian Palaeozoic stratigraphy underwent several re-definitions and revisions in the last 60 years (see Powers et al., 1966; Al-Laboun, 1993; Stump et al., 1995; Al-Laboun, 2010; SGS, 2013). This study follows the nomenclature established by Al-Laboun (2010) and the Saudi Geological Survey (SGS, 2013), with slight adjustments to the chronostratigraphy (Figure 3).

2.2.1. Saq Formation

The Saq Formation, originally defined by Thralls and Hasson (1956) and Steineke et al. (1958), is of (Middle) Cambrian to Middle Ordovician age, deposited between 520 Ma and 465 Ma during AP2 of Sharland et al. (2001). It is exposed in northern Arabia in a widening band along the eastern and northern margins of the Arabian Shield. The outcrop area stretches almost continuously from north of Riyadh to the Jordan border and beyond (Powers at al., 1966). Thickness increases toward the north, from only a few metres up to a maximum thickness of 850 m in Jordan (Quennell, 1951). The Saq Formation is of strikingly uniform lithology, consisting of dominantly poorly- to well-sorted and cross-bedded, mature quartz sandstone (Powers et al., 1966; own observations) (Figure 4a). Delfour et al. (1983) divided the Saq Formation into two members: the lower Risha Member and the upper Sajir Member. The Risha Member consists of medium- to coarse-grained, conglomeratic, massive to planar cross-bedded sandstones deposited in fining upward stacking patterns in a fluvial braided stream system (Hussian and Abdullatif, 2004; Hussain, 2007). Sedimentation then switched to a shallow marine near-shore environment in the Sajir Member, which is characterised by laminated and cross-bedded, fine- to medium-grained sandstone and siltstone. *Cruziana* and *Skolithos* ichnofacies have been observed (Powers et al., 1966; Hussain and Abdullatif, 2004). *Skolithos* ichnofacies is also reported from the Saq Formation equivalent in Jordan (Selley, 1972). Locally, sediments of the Saq Formation lie unconformably on Precambrian basement rocks. Powers et al. (1966) noted conglomeratic basal layers that contain reworked clasts from the underlying crystalline rocks, where the contact is exposed. However, this is not the case everywhere, as was observed during the field campaign in 2013. The Saq Formation is apparently conformably overlain by the basal graptolite-bearing shales of the Hanadir Member of the Qasim Formation and locally by the Permian Khuff Formation (Hussain and Abdullatif, 2004). Its Cambrian to Ordovician age mainly rests on the stratigraphic context; a few occurrences of *Cruziana* ichnofacies in shale lenses and Middle Cambrian trilobites were reported from Jordan (Powers et al., 1966). Parts of the Saq Formation are considered to be the equivalent of the southern Arabian Dibsiyah Formation (Figure 3). Although no direct transition between the two formations is exposed, the indicative *Skolithos* and *Cruziana* ichnofacies and the unconformable contact with basement rocks support this correlation. Further stratigraphic constraints are given by Middle to Late Darriwilian graptolites from the overlying Hanadir Member of the Qasim Formation.

2.2.2. Qasim Formation

The Qasim Formation was first introduced together with the Zarqa, Sarah, Uqlah, Qusaiba, Sharawra and Tawil formations by BRGM (1985) as the lower part of the former Tabuk Formation, which was discarded (Figure 3). Deposition of the Qasim Formation took place between 465 Ma and 445 Ma (AP2 of Sharland et al., 2001), from the Middle Ordovician until the onset of the Late Ordovician (Hirnantian) glaciation (Melvin, 2015). The formation is mostly exposed in an area north of the exposed Arabian Shield and west of the Nefud desert. Minor outcrops can be found east of the Arabian Shield, where the Qasim Formation conformably overlays the Saq Formation (Powers et al., 1966; Hussain and Abdullatif, 2004). Locally it rests unconformably on Precambrian basement (Figure 4b). Its combined total thickness is 261 m at the type locality and 358 m at reference sections in northern Saudi Arabia (SGS, 2013). Lithology of the succession has been described by Powers et al. (1966) as alternating cyclic deposits of thin-bedded, fine-grained sandstone to shale and thick-bedded, massive to cross-bedded sandstone. Those cyclic units were later recognised as the Hanadir ('lower shale' of Powers et al., 1966), Kahfah ('lower sandstone'), Ra'an ('middle shale' or 'upper siltstone') and Quwarah ('middle sandstone' or 'upper pre-Tawil sandstone') members (Powers et al., 1966; Vaslet, 1990; Stump et al., 1995). As the sudden change in lithology indicates, the depositional environment shifted from a continental to shallow

marine environment over to a more distal, deeper marine setting during the time of deposition of the Hanadir Member (Sharland et al., 2001). Subsequently, the system moved back again to the shallow marine environment of the sandy Kahfah Member. This cycle is then repeated with the Ra'an Shale and the Quwarah sandstone members. The fossil record supports this interpretation: The shaly Hanadir and Ra'an members contain graptolites (Powers et al., 1966), which are diagnostic for more open marine conditions during the Middle Ordovician. Shallower, high-energy conditions are indicated by the presence of *Skolithos* in the Kahfah Member (Powers et al., 1966). The Quwarah Member is devoid of diagnostic fossils, according to McGillivray and Husseini (1992), but Powers et al. (1966) reported *Skolithos* to be common in the upper pre-Tawil sandstone, which is treated as synonymous to the Quwarah Member due to its stratigraphic context. The basal thin-bedded and shaly Hanadir Member of the Qasim Formation conformably overlays the coarser, cross-bedded sandstones of the Saq Formation (Powers et al., 1966). It is noteworthy that the authors did find *Planolites* traces (Figure 5a) during their sampling campaign in northern Arabia, but did not find any obvious *Skolithos*. Since studied outcrops were close to the margin of the Arabian Shield, this may be caused by differences in depositional facies between Shield-proximal areas and the more distal parts of the Tabuk basin. Graptolites (Figure 5b) were encountered in the shaly Hanadir Member in an outcrop at the Sarah ridge (26°34'10.4''N / 43°22'02.7''E). They were identified as pendent didymograptids of Middle to Late Darriwilian age (J. Maletz, oral communication to G. Meinhold, 2013). Top contact is with the Zarqa and Sarah formations, which deeply incise into the underlying strata (Vaslet, 1990; McGillivray and Husseini, 1992; Sharland et al., 2001). The Qasim Formation has no direct equivalent in the Wajid area (Figure 3).

2.2.3. Sarah and Zarqa formations

For the purpose of this study the Sarah and Zarqa formations will be treated as one unit, since they are closely related (chrono-)stratigraphically and genetically (Senalp and Al-Laboun, 2000; Sharland et al., 2001; Al-Laboun, 2010). The term Zarqa Formation was first introduced by Vaslet et al. (1987) for glacial deposits in northern central Saudi Arabia. Clark-Lowes (1980) introduced the Sarah Member, which later got raised to formation status by Williams et al. (1987), to describe Upper Ordovician glaciogenic sediments in central and northern Saudi Arabia. The exact chronostratigraphic extent of the Sarah Formation, especially its upper boundary, is still in debate. Some workers assign a Late Ordovician (Ashgillian) to early Silurian (Early Llandoverian) age (445–440 Ma) to both formations, which coincides with the lower part of megasequence AP3 (McClure, 1978; Powell et al., 1994; Senalp and Al-Laboun, 2000; Sharland et al., 2001; Al-Laboun, 2010). Other authors (Al-Hajri, 1995; Sutcliffe et al., 2000; Clark-Lowes, 2005; Turner et al., 2005) put the top of the Sarah Formation at the Ordovician–Silurian boundary. Recent data gathered from the Qusaiba-1 shallow core hole support a Late Ordovician age for the uppermost parts of the Sarah Formation (Hints et al., 2015; Le Hérissé et al., 2015; Melvin, 2015; Paris et al., 2015a,b; Wellman et al., 2015), which will be applied in this study. Zarqa and Sarah outcrops can be found in central Saudi Arabia between Unayzah and Baqaa (Figure 2c) in a narrow, SE–NW trending band, more or less parallel to the margin of the Arabian Shield. Palaeovalleys extend perpendicularly east away from the Shield (Senalp and Al-Laboun, 2000; Al-Laboun, 2010). Thickness in the outcrop varies greatly and can reach up to 300 m (Senalp and Al-Laboun, 2000). This is observed in the subsurface as well, where thickness can range from 22.5 m (well data, Senalp and Al-Laboun, 2000) up to 650 m (seismic data, Sharland et al., 2001). According to Al-Laboun (2009), thickness at the type sections of the Zarqa and Sarah formations is 115 m and 81 m, respectively. The Zarqa Formation consists of typical glacial tillites and finer grained, micaceous sandstones, shales and clayey siltstones, with local soft-sediment deformation (Senalp and Al-Laboun, 2000; Sharland et al., 2001; Al-Laboun, 2010). Sediments of the Sarah Formation are generally comprised of fine- to medium-grained, trough and planar cross-bedded sandstones in fining-upward sequences, which form palaeovalley-fills (Al-Laboun, 2010; Al-Harbi and Khan, 2011).

In some places, tillites from the Sarah Formation have been reported at the base of palaeovalleys (Senalp and Al-Laboun, 2000). Other features indicative for glaciation reported from the Sarah/Zarqa formations are striated surfaces, dropstones, glaciated pavements, large erosional grooves, diamictites and drag-overturned folds (Senalp and Al-Laboun, 2000). Detailed lithological descriptions of the Upper Ordovician glaciogenics can be found in Senalp and Al-Laboun (2000), Clark-Lowes (2005) and Al-Harbi

and Khan (2011). The depositional environment is distinctly glacial, subglacial and proglacial. Tunnel valleys were incised by subglacial and subaqueous meltwater streams. Those were then afterwards filled with sediment during ice retreat (Sharland et al., 2001). Main characteristics of the tunnel valleys are low gradient walls as well as wide and deep valley floors (McGillivrey and Husseini, 1992; Stump and van der Eem, 1995). They can be traced in the subsurface, where they reach a depth from floor to top of valley wall of ~650 m (Stump et al., 1995; Sharland et al., 2001). They are decidedly deeper than their southern Saudi Arabian equivalents of the Sanamah Formation, for which a thickness of 80–150 m is assumed (Keller et al., 2011). Deposition of the Sarah Formation was not restricted to the tunnel valleys, but extended as 'spill-overs' laterally into outwash-plains (Sharland et al., 2001). Macrofossils are sparse in the Sarah/Zarqa formations. McClure (1978) report some *Skolithos* and *Cruziana* from the uppermost Sarah Formation, but otherwise the succession seems devoid of macrofossils. However, a recently drilled core reveals abundant and well preserved microfossils, including acritarchs, prasinophytes (green algae) and scolecodonts. They were used to improve the chrono- and biostratigraphy of the lower Palaeozoic units, allowing resolution at the stage level (Hints et al., 2015; Le Hérissé et al., 2015; Paris et al., 2015b; Wellman et al., 2015). The basal contact is erosive, as the tunnel valleys cut deeply into underlying strata (Figure 4c), in some places reaching the Sajir Member of the upper Saq Formation (Vaslet et al. 1990; Senalp and Al-Laboun, 2000; Sharland et al., 2001; Al-Harbi and Khan, 2011). There is clear evidence of sedimentary reworking of underlying strata in the Sarah Formation (Le Hérissé et al., 2015; Melvin, 2015). The Sarah/Zarqa sediments are unconformably overlain by the basal shale of the Qalibah Formation or the bioturbated, sandy Uqlah Formation (Senalp and Al-Laboun, 2000; Sharland et al., 2001; Al-Laboun, 2009; Al-Laboun, 2010; Melvin, 2015). Because of the similarities in glaciogenic origin, depositional environment and stratigraphic context, the Sanamah Formation from the Wajid area can be confidently assigned as the southern equivalent of the Sarah/Zarqa formations.

2.2.4. Qalibah Formation: Qusaiba Member

The Qusaiba Shale was first mentioned by Powers et al. (1966) as the Quşaybā' Member of the Tabuk Formation. The Qusaiba Shale was raised to formation rank by Janjou et al. (1996). As to this date there is no consensus whether to treat the Qusaiba (and the overlying Sharawra) as a formation or as a member of the Qalibah Group or Formation, respectively. Some authors are in favour of assigning a formation rank to the Qusaiba Shale (Janjou et al., 1996; Al-Laboun, 2009, 2010, 2011; Laboun, 2013) while the majority of recent literature prefers a status as a member of the Qalibah Formation (e.g., Senalp and Al-Laboun, 2000; Sharland et al., 2001; Abu-Ali, 2005; Al-Ajmi et al., 2015; Hints et al., 2015; Le Hérissé et al., 2015; Melvin, 2015; Paris et al., 2015a,b), which will also be followed in this study. An early Silurian age was recognised early (Powers et al., 1966). Sharland et al. (2001) put the Qusaiba Shale in the middle of megasequence AP3, at the transition from Middle to Late Llandovery. It spans the 'S10' maximum flooding surface (MFS), which dates to 440 Ma. Recent micropalaeontological research from three shallow core holes (Qusaiba-1, Baq'a-3, Baq'a-4) drilled in central Saudi Arabia and penetrating the lowermost Silurian helped to further constrain the chrono- and biostratigraphic range from Rhuddanian to Late Telychian (443.7 Ma to ~428 Ma) (Paris et al., 2015a). Paris et al. (2015a) also recognised a significant hiatus during most of the Rhuddanian and Lower Aeronian in the lower part of the Qusaiba-1 core, which probably represents a condensed sequence. The 'hot shale' at the base of the Qusaiba Member is of significant economic importance as a source rock for most Palaeozoic hydrocarbon reservoirs not only in Saudi Arabia (Bishop, 1995; Alsharhan and Nairn, 1997; Sharland et al., 2001), but in northern Africa as well where it corresponds to the 'hot shale' of the Tanezzuft Formation (Lüning et al., 2000; Meinhold et al., 2013a). It also serves as a good aquiclude to separate the lower and upper Palaeozoic aquifers (Edgell, 1997). Qusaiba outcrops in Saudi Arabia are confined to the central part of the Arabian Peninsula, where they can be found between the towns of Qusaiba and Baqaa, adjacent and parallel to outcrops of the Sarah/Zarqa formations (Lüning et al., 2000; Al-Laboun, 2010; Al-Laboun, 2011; Melvin, 2015) and west of Hail in the Tabuk basin (Al-Laboun, 2009). The Qusaiba Member is exposed at the surface in southern Saudi Arabia as well, although outcrops are not as widespread and well preserved, except for fresh road cuts near Hima, north of Najran (Stump and van der Eem, 1995; Keller et al., 2011; Al-Ajmi et al., 2015; own field observations). The 'hot shale' is well known from the subsurface through well logs and seismic lines (Evans et al., 1991), providing an excellent marker horizon. Thickness in central Saudi Arabia ranges between 83 m (Melvin, 2015) and

up to 256 m at the surface reference section (base at 27°51’23’’N / 38°33’57’’E, top at 28°05’57’’N / 38°22’26’’E; Lüning et al., 2000). Al-Laboun (2009) gives a thickness of 41 m at the type locality and 482 m at the reference locality, but does not provide coordinates. Surface lithology is described as an organic-rich marine shale with laminations and interbedded, rippled and ferruginous siltstones with micaceous sandstone at the top (Edgell, 1997; Lüning et al., 2000, Al-Laboun, 2009). The Qusaiba Member was deposited in an open marine, low-energy environment that developed during the large-scale transgression at the end of the Hirnantian glaciation (Lüning et al., 2000). A shallowing upward trend is observed towards the top (El-Khayal, 1987; Paris et al., 2015a). In accordance with its lithology and depositional environment, the Qusaiba Member is relatively fossil rich, both in macro- and microfossils, with prominent graptolites and trilobites, abundant palynomorphs, and bioturbation at the top (El-Khayal, 1987; Edgell, 1997; Le Hérissé et al., 2015; Melvin, 2015; Paris et al., 2015a). The contact with the underlying Sarah Formation is a marine flooding surface (El-Khayal, 1987; Senalp and Al-Laboun, 2000; Melvin, 2015). Al-Laboun (2009, 2011) describes the basal contact as unconformable but gives no description of its exact nature. Contact with the overlying Sharawra Member is gradational (Mahmoud et al., 1992).

2.2.5. Qalibah Formation: Sharawra Member

The Sharawra Formation was first introduced by Helal (1964), later discarded and again reinstated by BRGM (1985). As with the Qusaiba Member, there is currently no consensus whether to assign member or formation rank to the Sharawra deposits. This study follows the majority of recent authors and treats the Sharawra as the upper member of the Qalibah Formation. Its age has been firmly assigned as early to middle Silurian (Late Llandovery to Wenlock) by biostratigraphy (Al-Hajri and Paris, 1998). Together with the Qusaiba Member and the Tawil Formation, it forms the upper part of AP3 megasequence (Sharland et al., 2001). The Sharawra Member crops out in northern and central Saudi Arabia in the Tabuk and Widyan Basins (Figure 2c). Its thickness at the type section (28°02’18’’N; 37°59’26’’E to 28°11’51’’N; 38°00’00’’E) and reference section (28°14’47’’N; 37°15’55’’E to 28°24’42’’N; 37°16’42’’E) are 422 m and 510 m, respectively (Al-Laboun, 2009). The shales and micaceous siltstones and sandstone of the Sharawra Member (Figure 4d) were deposited in a shallow marine, prodeltaic environment on a broad and extensive epicontinental shelf with a low sloping angle (Al-Hajri and Paris, 1998; Al-Laboun, 2009, 2011). Al-Hajri and Paris (1998) described chitinozoans and acritarchs as well as abundant land plant spores. During fieldwork in spring 2013 trace fossils (burrows) and fragments of echinoderms (Figure 5c, d) were found. Contacts at bottom and top are both disconformable with the underlying shaly Qusaiba Member (Qusaiba Formation in Al-Laboun, 2009) and the overlying Tawil Formation, according to Al-Laboun (2009). However, at an outcrop west of the Qusaiba Depression (26°51'05.5"N; 43°34'42.3"E), basal contact was found to be conformable. Al-Hajri and Paris (1998) also reported the basal contact with the Qusaiba Member to be conformable. The Sharawra Member has not been found or described in outcrops from southern Saudi Arabia.

Figure 4: (a) Saq Fm. with large-scale trough cross-bedding, Highway 70. (b) Qasim Fm. unconformably overlying Precambrian basement near Hail. (c) Sarah Fm. cutting into the Qasim Fm. W of Al Qara. (d) Bioturbated fine-grained sandstone, Sharawra Mbr, W of the Qusaiba Depression. (e) Medium-grained, SiO_2-cemented sandstone of the Tawil Fm., W of Dawmut al Jandal. (f) Shales interbedded with fine- to medium-grained sandstone of the Subbat Mbr., Jauf Fm., Dawmut al Jandal. (g) Fine- to medium-grained sandstone with abundand ripples, Jubah Fm., W of Sakaka. (h) Well sorted, medium-grained sandstone of the Unayzah Fm., E of the Qusaiba Depression.

2.2.6. Tawil Formation

The Tawil sandstone was formally defined by Steineke et al. (1985) and was considered to be the uppermost member of the Tabuk Formation by Powers et al. (1966). When the Tabuk Formation was discarded in 1985, the former Tawil Member was raised to formation status. It is of late Silurian to Early Devonian age (McGillivray and Husseini, 1992; Laboun, 2013). The sequence stratigraphic position is in the middle of megasequence AP3, roughly bound by MFS S20 (~418 Ma) and D10 (~402 Ma) (Sharland et al., 2001). Outcrops can be found in central and northern Saudi Arabia. Reported thickness varies greatly between ~5 m (Al-Laboun, 2009), 85 m (Al-Harbi and Khan, 2008) and up to 200 m (Thralls and Hasson, 1956; Steineke et al., 1958; Powers et al., 1966; McGillivray and Husseini, 1992). The studied section of the Tawil Formation has a thickness of ~150 m near the town of Sakaka (Figure 2c). Lithology consists of cross-bedded and channelised, fine- to medium-grained sandstones (Figure 4e) interbedded with thin siltstones and shales (Al-Harbi and Khan, 2008). They were deposited in alternating shallow marine and fluvial braided environments, representing several transgressive-regressive cycles (McGillivray and Husseini, 1992; Konert et al., 2001; Laboun, 2013). Only a few fossils are described from the Tawil Formation. Powers et al. (1966) mentioned moulds of brachiopods and gastropods from Devonian sediments of the Tabuk Formation; its uppermost part is represented by the Tawil sandstone. Steemans et al. (2007) described miospores from earliest Devonian strata recovered from two boreholes in eastern Saudi Arabia. The Tawil Formation unconformably overlies the Sharawra Member of the Qalibah Formation at what is known as the 'pre-Tawil-Unconformity' (PTU, Wender et al., 1998). It is conformably overlain by sediments of the Jauf Formation (Al-Harbi and Khan, 2008; Laboun, 2013). As a consequence of its (litho-) stratigraphic context, the lowermost Khusayyayn Formation can be correlated to be the southern Saudi Arabian equivalent of the Tawil Formation.

2.2.7. Jauf Formation

The Jauf Formation was first named by E.L. Berg in 1944 for the town of Al Jawf (Powers et al., 1966) and formally introduced by Steineke et al. (1958) with the definition of a composite type section in the vicinity of Al Jawf. It is subdivided into five members (oldest to youngest): Sha'ibah, Qasr, Subbat, Hammamiyat and Murayr members. The age of the Jauf Formation has been well constrained by palynological studies to be Early Devonian (Late Pragian to latest Emsian) (Al-Ghazi, 2007; Breuer et al., 2015). It is positioned in the middle to upper part of megasequence AP3 and spans MFS D10 and D20 (Sharland et al., 2001). The Jauf Formation forms a significant non-associated gas reservoir in central Arabia (McGillivray and Husseini, 1992). Outcrops can be found in northern Saudi Arabia, at the type locality of Al Jawf, in and around Dawmut al Jandal and in the Wadi Murayr (Figure 2c). Formation thickness ranges between 158 m and 300 m in the outcrop at the type locality (Powers et al., 1966). The Jauf Formation consists mainly of varicoloured silty shales with various thin beds of limestone, dolomite, gypsum (Figure 4f) and rarely very thin beds of fine- to medium-grained sandstones (Powers et al., 1966; own observations). Its depositional environment ranges from shallow marine shelf conditions in northern Saudi Arabia, over a marginal marine to a continental delta and delta-front setting in central Arabia (Stump et al., 1995; Al-Ghazi, 2007). Reef and bioherm build-ups in the limestone layers indicate carbonate-platform facies (Meissner et al., 1989). Reported fossils are, among others: brachiopods (*Anathyri*s, *Lingula*, *Spirifer*), ostracods (*Bythocypris*, *Knoxiella*), various corals (*Cyaothophyllum*, *Favosites*), *Prototaxites*, fish remains, cephalopods (*Orthoceras*), tentaculites and crinoid stem fragments (Powers et al., 1966). A plethora of palynomorphs has been recovered from wells and core holes (Al-Ghazi, 2007; Breuer et al., 2015). The nature of its basal contact with the underlying Tawil Formation is presumably unconformable, though clear evidence is lacking (Powers et al., 1966; Breuer et al., 2015). Top contact with the overlying strata (Devonian Jubah and Cretaceous Aruma formations) is unconformable according to Powers et al. (1966), Al-Ghazi (2007) and Breuer et al. (2015). The upper part of the southern Arabian Khusayyayn Formation has been correlated with the (Lower) Jauf Formation on the grounds of Late Pragian to latest Emsian micro- and macrofossil assemblages (Stump et al., 1995; Al-Ajmi et al., 2015; Breuer et al., 2015).

2.2.8. Jubah Formation

The Jubah Formation was first introduced by Meissner et al. (1989) for Devonian sediments that conformably overlie the Jauf Formation in the area of Al Jubah. Like the Jauf Formation, its age is well constrained by palynomorphs to the Middle Devonian (Early Eifelian) to Late Devonian (Famennian) and possibly Mississippian (Early Tournaisian) (Al-Hajri et al., 1999; Clayton et al., 2000; Sharland et al., 2001). Deposition of the Jubah Formation took place across the sequence boundary of megasequences AP3 and AP4 (Sharland et al., 2001). Surface outcrops are situated around and between the towns of Al Jawf and Sakaka in northern Saudi Arabia. The formation is also well known from the subsurface in the northern part of Saudi Arabia (Breuer et al., 2007; Laboun, 2013). The thickness is not entirely certain, because the formation is not completely exposed, but it is estimated to be at least 220-340 m thick (Meissner et al., 1989). Thickness and regional extension of the Jubah Formation are highly variable. It was, like the other Devonian units, highly affected by uplift and erosion associated with the 'Hercynian Event' (McGillivray and Husseini, 1992; Sharland et al., 2001; Al-Ramadan et al., 2004; Laboun, 2013). Lithology of the Jubah Formation is dominated by fine- to medium-grained, well-sorted and thin to medium cross-bedded quartz sandstone (Figure 4g), which is interbedded with silty to sandy shales (Meissner et al., 1989; Wender et al., 1998). After the mixed carbonatic/clastic Jauf Formation, the system thus returned to fully siliciclastic deposition in a shallow marine to continental, probably deltaic-fluvial setting (Meissner et al., 1989; Sharland et al., 2001). Some macrofossils were reported from surface outcrops, such as Prototaxites and (fresh water) fish remains (Meissner et al., 1989). *Zoophycos* ichnofossils (Figure 5e) and plant remains were found during field work, but the poor preservation of the latter did not allow further identification (Figure 5f). The majority of biostratigraphic information comes from palynomorphs recovered from wells and shallow core holes (Breuer et al., 2007). The nature of contact with underlying strata is not entirely clear, depending on the authors: Meissner et al. (1989) and Al-Ramadan et al. (2004) report it as conformable whereas Powers et al. (1966), Al-Ghazi (2007) and Breuer et al. (2015) find the contact unconformable. The Jubah Formation is itself unconformably overlain by younger strata, in both outcrop and subsurface (Meissner et al., 1989; Laboun, 2013). The Jubah Formation has no equivalent in southern Saudi Arabia (Al-Ajmi et al., 2015).

2.2.9. Unayzah Formation

The term Unayzah was first introduced and later formally defined by Al-Laboun (1982, 1986). What was formerly known as the ‘basal Khuff clastics’, ‘Khuff sands’, ‘transition zone’ or ‘incised sands’ was now recognised as the Unayzah Formation. It is subdivided into 3 informal sequences (youngest to oldest): the Unayzah A, B and C members (McGillivray and Husseini, 1992; Sharland et al., 2001). Most authors agree on a Pennsylvanian (Moscovian to Gzhelian) to Middle Permian (Late Kungurian) age for the Unayzah Formation (Alsharhan, 1994; Senalp and Al-Duaiji, 1995; Sharland et al., 2001; Sharland et al., 2004; Stephenson, 2004; Melvin et al., 2010). Its upper and lower boundaries mark the extent of megasequence AP5 (Sharland et al., 2001; Sharland et al., 2004). The Unayzah Formation is the primary hydrocarbon reservoir rock in central Saudi Arabia. Hydrocarbons are sourced from the Silurian ‘hot shale’ of the Qusaiba Member (McGillivray and Husseini, 1992). Although mostly known from the subsurface, the Unayzah Formation crops out in a thin band east and south of the Qusayba Depression in central Arabia (Figure 2c) (Al-Laboun, 2010). Formation thickness generally increases towards the southeast (McGillivray and Husseini, 1992), though it varies greatly and is highly dependent on the palaeotopography of the Hercynian Unconformity (Ferguson and Chambers, 1991). In outcrop, the Unayzah Formation reaches a thickness between 8 m and 60 m (Senalp and Al-Duaiji, 1995; Al-Harbi and Khan, 2005; Khalifa, 2015). The formation consists of various conglomerates, fine- to coarse-grained and cross-bedded sandstones (Figure 4h), intercalations of siltstones and shales as well as caliches and nodular anhydrite (Alsharhan, 1994; Senalp and Al-Duaiji, 1995). The sediments of the lower Unayzah C and B members are results of a glaciofluvial to glaciolacustrine environment (Le Heron et al., 2009). The upper Unayzah A Member was deposited in an alluvial to fluvial environment dominated by braided and meandering streams. Downslope the system graded into playa lakes in an overall arid to semi-arid setting (McGillivray and Husseini, 1992; Senalp and Al-Duaiji, 1995). The predominantly terrestrial Unayzah Formation siliciclastics are mostly starved of fossils, including palynomorphs. This is especially true for outcrops, where most of the material is oxidised. The lack of fossils presents

challenges for precise dating and correlating (McGillivray and Husseini, 1992; Melvin et al., 2010). Palynomorphs have been recovered from wells and used to establish a palynological zonation (Stephenson, 2004; Melvin et al., 2010). The basal contact of the Unayzah Formation is erosional with various older sedimentary units as well as Precambrian basement rocks of the Arabian Shield. This erosional surface is known as the 'Hercynian Unconformity' or 'pre-Unayzah-Unconformity' (Sharland et al., 2001). Unayzah Formation sediments are unconformably overlain by the transgressing Khuff carbonate rocks at the 'pre-Khuff-Unconformity' (McGillivray and Husseini, 1992; Sharland et al., 2001). The equivalent of the Unayzah Formation in the Wajid outcrop area is the Juwayl Formation, which is correlated with the Unayzah C and B members (Melvin and Norton, 2013; Al-Ajmi et al., 2015).

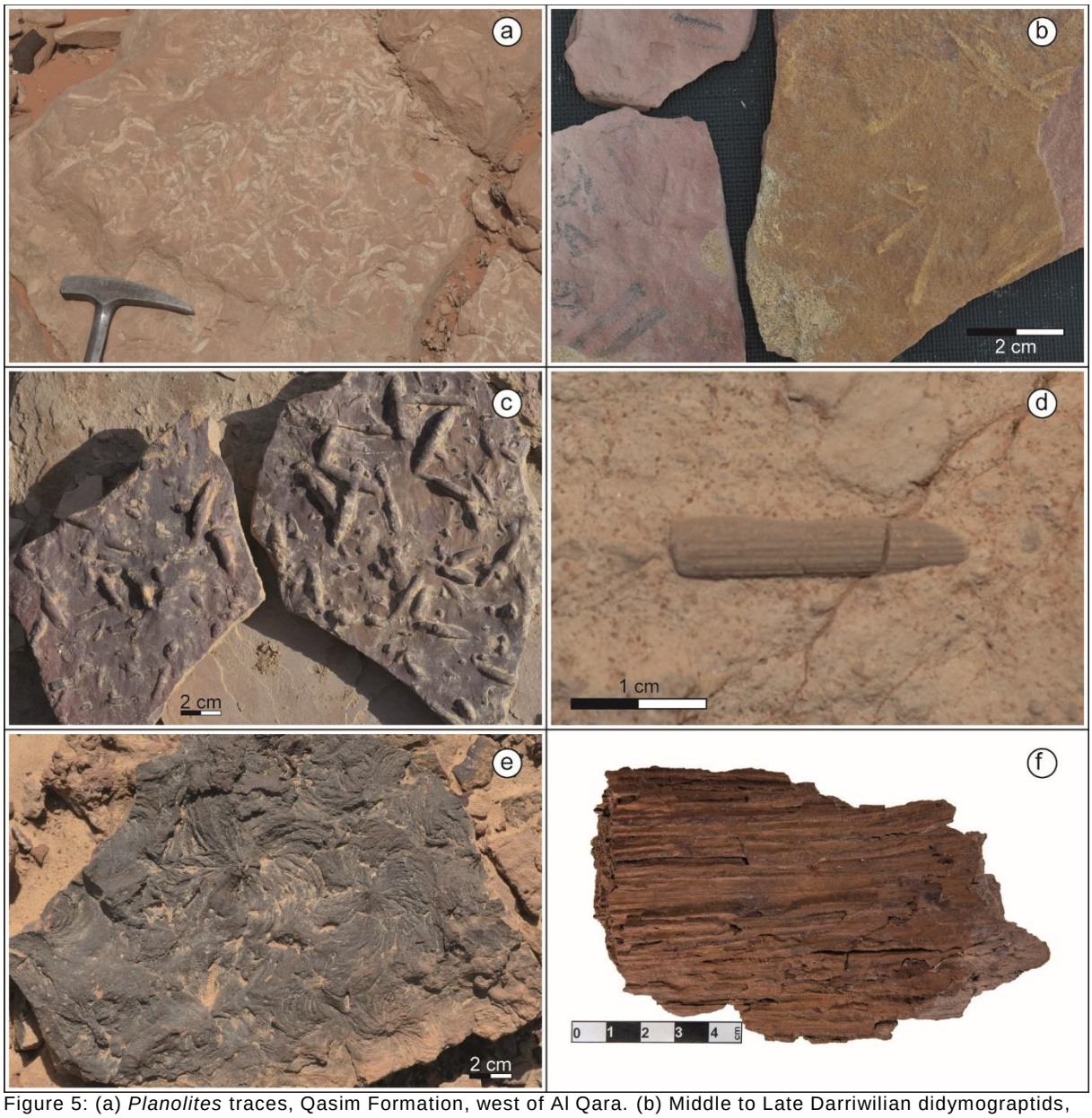

Figure 5: (a) *Planolites* traces, Qasim Formation, west of Al Qara. (b) Middle to Late Darriwilian didymograptids, Hanadir Member, Qasim Formation, Sarah Ridge. (c) & (d) Burrow traces and echinoderm fragments, Sharawra Member, Qalibah Formation, west of Qusaiba Depression. (e) & (f) *Zoophycos* and unidentified fossil wood, Jubah Formation, approximately 25 km north of Sakaka.

2.3. Stratigraphic framework of southern Saudi Arabia

Southern Saudi Arabian stratigraphy has a similar complicated history like its northern counterpart and also underwent several revisions since the early field works of Steineke et al. (1958) and others (see Powers et al., 1966; Kellogg et al., 1986; Evans et al., 1991; Stump and van der Eem, 1995; Al-Laboun, 2000b; Hussain et al., 2000; Al-Ajmi et al., 2015). The Wajid Formation with its four members (Dibsiyah, Sanamah, Khusayyayn and Juwayl) was first introduced by Kellogg et al. (1986), which has been regarded as an undivided unit before (Powers et al., 1966) and assigned a Cambrian–Ordovician age. Since the mid-90s, the southern Saudi Arabian Palaeozoic siliciclastics were referred to as the Wajid Group, when Stump and van der Eem (1995) raised the former Dibsiyah, Sanamah, Qalibah, Khusayyayn and Juwayl members to formation status. They also introduced the Qalibah Formation and Qusaiba Member. Although the nomenclature remained almost the same, the stratigraphic range of these units was repeatedly adjusted. This study follows the stratigraphy established by Al-Ajmi (2013) and Al-Ajmi et al. (2015) (Figure 3). Al-Ajmi (2013) revised and shortened the time intervals represented by each formation. By comparing sedimentary environments with modern analogues, sedimentation rates (on an order of magnitude-scale) can be estimated. Combined with preserved the thickness and some biostratigraphic control, Al-Ajmi (2013) achieved better estimates of the depositional time. He furthermore provides a detailed overview and history of research on the Wajid sandstone.

2.3.1. Dibsiyah Formation

The Dibsiyah Formation is the oldest formation of the Wajid Group and in the Wajid outcrop belt. Its age has been confidently determined to be Late Cambrian to Early Ordovician (megasequence AP2 of Sharland et al., 2001), despite the lack of good biostratigraphic indicators. The presence of *Skolithos* and *Cruziana* ichnofacies combined with the overlying Hirnantian glacial deposits help constrain the Dibsiyah Formation in time. It is most prominently exposed on the northern and western edge of the Wajid outcrop area, southeast of Wadi Ad Dawasir (Figure 2b), where it reaches a thickness between 160 m and 190 m (Al-Ajmi et al., 2015). Lithology consists of mature, medium- to coarse-grained sandstone and pebbly conglomerates, with a few intercalations of finer siliciclastics (Keller et al., 2011; Al-Ajmi et al., 2015). New research by Al-Ajmi et al. (2015) established a shallow marine depositional environment for the Dibsiyah Formation, rather than the partly fluvial setting suggested by Evans et al. (1991) and Stump and van der Eem (1995). Not many fossils are known from the Dibsiyah Formation, with the exception of some *Cruziana* tracks and spectacular *Skolithos* piperock (Figure 6a). The basal contact with the underlying Precambrian basement is not exposed in outcrop, but was encountered in several wells (GTZ/DCo, 2009), where it is represented by a thin weathering horizon. Top contact is erosional with the glaciogenic Sanamah Formation. The Dibsiyah Formation is the lateral equivalent of the Saq Formation of central and northern Saudi Arabia.

2.3.2. Sanamah Formation

The second oldest unit of the Wajid outcrop belt is the Sanamah Formation, though there are no biostratigraphically indicative fossils known from it. Its lithology and sedimentology clearly indicate a glacial influence, placing it in the context of the Hirnantian glaciation and making it the equivalent of other glacial deposits across northern Africa and Arabia, deposited at the beginning of megasequence AP3 (McClure, 1978; Ghienne and Deynoux, 1998; Sharland et al., 2001; Ghienne, 2003; Ghienne et al., 2003; Le Heron et al., 2004, 2005, 2009, 2010, 2013, 2015). Sanamah Formation outcrops can be found cutting into the underlying Dibsiyah Formation in the northern, northwestern and western Wajid area (Figure 2b). Formation thickness varies, but Keller et al. (2011) deduced a minimum formation thickness of 150 m. The lithological inventory of the Sanamah Formation comprises clast and matrix supported conglomerates, medium- to coarse-grained massive sandstones, siltstones and shales. Locally there is intensive Fe- and/or Mn-cementation (Figure 6b). Indicative features such as clasts with chatter marks, striations, fluted surfaces, depositional geometries and certain lithofacies associations support glaciogenic origin (Keller et al., 2011) (Figure 6c). The Sanamah Formation was deposited under polythermal conditions in three main glacial advances. Sub-glacial tunnel valleys deeply incised into the underlying Dibsiyah

Formation during initial ice-advance and were subsequently filled with sediment (Keller et al., 2011; Al-Ajmi, 2013). The main direction of ice-flow was toward the southeast, as evidenced by glacial striations and tunnel valleys, among others. Top contact is unconformable with the Khusayyayn Formation. The Upper Ordovician Zarqa and Sarah formations have repeatedly been interpreted as the central Arabian equivalent of the Sanamah Formation (Evans et al., 1991; Stump and van der Eem, 1995; Keller et al., 2011; Al-Ajmi et al., 2015).

2.3.3. Qalibah Formation: Qusaiba Member

The shaly Qusaiba Member of the Qalibah Formation known from northern Arabian outcrops and the subsurface also reach the Wajid area. Qalibah Formation outcrops are confined to a road cut west of Hima (Figure 6d), a narrow strip east of the town and a small depression southwest of Wadi Ad Dawasir (20°22'30.1''N; 44°31'39.5''E) (Figure 2b). Outcrop thickness is much reduced compared to northern Arabia, with a maximum of 6 m to 10 m. No fossils have yet been recovered from southern Qusaiba Member outcrops (Evans et al., 1991; Al-Ajmi et al., 2015). The Qusaiba Member rests unconformably on Precambrian basement, where the base is exposed. Top contact is sharp and unconformable with sandstones of the Khusayyayn Formation (Al-Ajmi et al., 2015).

2.3.4. Khusayyayn Formation

The Khusayyayn Formation has until recently been assigned an Early Devonian to Mississippian age (Evans et al., 1991; Stump and van der Eem, 1995; Al-Laboun, 2000a; Al-Husseini, 2004). Al-Ajmi (2013) and Al-Ajmi et al. (2015) constricted its depositional time to the Early Devonian (second half of megasequence AP3). They combined biostratigraphic information of Late Pragian to Emsian fish remains from the middle and upper Khusayyayn Formation with estimated sedimentation rates in the order of 10^{-1} m/ka to 10^{-2} m/ka. Outcrops of the Khusayyayn Formation dominate the Wajid area and can be found from Wadi Ad Dawasir in the north to Najran in the south (Figure 2b). No complete succession is exposed. According to Al-Ajmi et al. (2015), the most continuous Khusayyayn Formation succession is 55 m thick. They estimate an overall maximum thickness of 150 m from correlated outcrops. They could not confirm the thickness of 200 m given by Kellogg et al. (1986) and Stump and van der Eem (1995). The Khusayyayn Formation consists of a rather uniform succession of medium- to coarse-grained, partly conglomeratic, sandstones with large-scale cross-bedding and locally slumping structures (Figure 6e). Trace fossils, lithofacies association and architectural element interpretation reveal the shallow marine origin with a pronounced tidal regime of the Khusayyayn Formation (Al-Ajmi et al., 2008; Al-Ajmi et al., 2015). A fluvial to aeolian depositional environment, as proposed by Evans et al. (1991) and Stump and van der Eem (1995), is highly unlikely. Fossils are scarce in Khusayyayn Formation sediments with the exception of some fish remains, which are of biostratigraphic value, and some rare *Skolithos* ichnofacies (Evans et al., 1991; Forey et al., 1992; Al-Ajmi et al., 2015). The base of the Khusayyayn Formation usually rests unconformably on Precambrian basement, but in some outcrops it unconformably overlies the Sanamah Formation (Al-Ajmi et al., 2015). Where exposed, the top of the Khusayyayn Formation is marked by yet another regional unconformity with the overlying Juwayl Formation (Keller et al., 2011; Al-Ajmi et al., 2015). The regional equivalents of the Khusayyayn Formation are the upper Tawil and Jauf formations (Al-Ajmi et al., 2015).

2.3.5. Juwayl Formation

The youngest formation of the Wajid Group is the Middle Pennsylvanian to lower Permian Juwayl Formation. Its base marks the boundary between megasequences AP4 and AP5 (Sharland et al., 2001). The exact age of the Juwayl Formation is still debated by different authors (see Sharland et al., 2001; Keller et al., 2011; Al-Ajmi et al., 2015 and references therein). Outcrops in the northern Wajid area are known from two NW-SE trending belts and from the south-eastern Wajid at Bani Khatmah (McClure, 1980; Keller et al., 2011; Al-Ajmi et al., 2015) (Figure 2b). A succession west of Najran at Dahran al Janub has also been interpreted as Juwayl Formation by Al-Ajmi et al. (2015). They calculated a composite thickness of 125 m, which matches the thickness reported by McClure (1980). Lithology of the Juwayl Formation is quite diverse and consists of matrix-supported conglomerates, medium- to coarse-grained, massive to cross- and ripple-bedded sandstones as well as siltstones and shales (Figure 6f).

Prominent glaciogenic features are striated surfaces and clasts, dropstones, boulder pavements and large-scale soft-sediment deformation (Keller et al., 2011). Juwayl Formation sediments have been deposited in two distinct, glacio-fluvial settings: The two northern outcrop belts represent glacially cut valleys, possibly tunnel valleys (Al-Ajmi et al., 2015). In the southern Wajid area, the finer grained sediments have been interpreted as lake deposits from a periglacial lake, covering large parts of the southern Arabian Peninsula and extending into north-eastern Africa (Pollastro, 2003; Keller et al. 2011). The Juwayl Formation does not yield many fossils but early Permian palynomorphs have been described by McClure (1980) and Besems and Schuurmann (1987). South of Wadi Ad Dawasir, Juwayl Formation sediments cut erosively into the underlying Khusayyayn Formation, whereas the basal contact in the southern and eastern Wajid area seems to be a paraconformity. Top contact in the east is unconformable with the Permian Khuff Formation while in the south-east the Juwayl Formation is capped by the Jurassic unconformity (Al-Ajmi et al., 2015). The Juwayl Formation has been correlated to the Unayzah C and B members on the ground of lithostratigraphic similarities and palynological data (Melvin and Norton, 2013). An equivalent to the Unayzah A Member is not exposed/preserved in the Wajid outcrop area (Al-Ajmi et al., 2015).

Figure 6: (a) *Skolithos* piperock of the Dibsiyah Fm. at Jabal Nafla. (b) Intensive Fe-/Mn-cementation in the Sanamah Fm., Jabal Atheer. (c) Glacial striations striking ~150°, Sanamah Fm., SW of Wadi Ad Dawasir. (d) Khusayyayn Fm. Resting on the Qusaiba Mbr. of the Qalibah Fm., Hima/Nawan. (e) Slumping structures (black arrow) above planar cross-bedded sandstone (white arrow) in the Khusayyayn Fm., Jabal Abood. (f) Planar cross-bedded sandstone above (black arrow) laminated shales (white arrow) of the Juwayl Fm., Jabal Seab.

2.4. Provenance, chemostratigraphy and heavy mineral studies

The high maturity of Saudi Arabian Palaeozoic sandstones poses unique difficulties not only for stratigraphy, but also for provenance analysis and interpretation. Nevertheless, since the early 2000s there have been several studies concerning the provenance of those sediments, employing and combining standard techniques like petrographic, geochemical and heavy mineral analyses. While the Wajid Group has been studied previously, data from most of the Palaeozoic in central and northern Saudi Arabia are still lacking. So far, the majority of publications identified felsic igneous rocks from southern terrains, probably in Yemen, as the primary source for sediments of the Wajid Group (Babalola, 1999; Hussain et al., 2000; Hussain, 2001; Hussain et al., 2004; Wanas and Abdel-Maguid, 2006; Hussain, 2007; Knox et al., 2007). Secondary sources include metamorphic, metasedimentary and recycled sedimentary rocks, to varying degrees. A southerly provenance is supported by palaeocurrent data according to Babalola (1999), Hussain (2001) and Hussain et al. (2000). Yet, at least for the Wajid area a homogenous northward transport direction cannot be inferred for the entire Palaeozoic succession. Opposing (northwest to southeast) transport directions in the glaciogenic units of the Sanamah and Juwayl formations have been interpreted in recent studies (Hinderer et al., 2009; Keller et al., 2011; Al-Ajmi et al., 2015). They also indicated the ANS as a possible source area for the Juwayl Formation. Al-Harbi and Khan (2005, 2008, 2011) established the ANS as the primary source for sediments of the Sarah, Tawil and Unayzah formations in central and northern Saudi Arabia. In their studies they employed standard petrographic methods and tectonic discrimination diagrams of major elements in conjunction with palaeocurrent data. In contrast, Knox et al. (2010) identified a recycled sedimentary source to the south as the primary contributor for the Unayzah Formation by studying heavy mineral assemblages. All studies were concordant in assigning a passive margin and/or intracratonic depositional setting to Palaeozoic sandstones in both southern and northern/central Saudi Arabia.

Stratigraphic correlation of clastic successions by means of geochemical characteristics has been shown to yield promising results and is an increasingly important tool (Weibel et al., 2010). The idea behind chemostratigraphy is to use whole-rock geochemical changes as proxies for changes in provenance, weathering and thus palaeoclimate, depositional setting or other sedimentary features that enable stratigraphic correlations. This method has been successfully applied in low, medium and high accommodation fluvial and deltaic (Sabaou et al., 2009; Hildred et al., 2010 and references therein) as well as marine settings (Weibel et al., 2010). It can also be used to effectively correlate ‘barren’ (i.e. fossil-starved) sequences from drill cuttings (Pearce et al., 1999) and core samples (Friis et al., 2007). As whole-rock geochemistry of sandstones is dependent on their petrologic composition, problems may arise in highly mature successions. Through weathering, reworking and/or recycling the petrographic and therefore geochemical diversity of different sandstone units can be greatly altered and reduced. Reworking in this case refers to the re-mobilization of sediment during deposition, for instance by currents. Recycling means erosion of an older sedimentary succession. This usually leads ‘quartz dilution’, where SiO_2 becomes enriched and most other major and trace elements are depleted. Causes are feldspar dissolution and removal of clay minerals through sorting. Therefore, elements with low mobility and which are controlled by heavy mineral abundance have been shown to be better suited for geochemical correlations (Friis et al., 2007).

Despite the already mentioned difficulties in correlating Saudi Arabian Palaeozoic sandstones, so far only one publication (Hussain, 2007) dealt with a geochemical approach to stratigraphic correlation. This study was constrained to the lower Palaeozoic Lower Wajid Group and the Saq and Qasim formations. Although several workers utilised geochemical data in provenance studies, there has been no published effort to establish geochemical correlations for Palaeozoic sandstones from the Arabian Peninsula. Such correlations would be a powerful and useful tool, especially as the succession hosts both an important source rock and the primary hydrocarbon reservoir in central Saudi Arabia, in the form of the Silurian Qusaiba Shale and the Permian Unayzah Formation, respectively.

Standard heavy mineral analysis (SHMA, modal analysis) has been an important tool in provenance studies, both in ancient and recent sediments (Mange and Wright, 2007). So far several workers applied

SHMA to the Palaeozoic succession, but mostly concentrated their efforts on the Wajid outcrop belt of southern Saudi Arabia (Babalola, 1999; Hussain et al., 2000; Hussain, 2001; Hussain and Abdullatif, 2004; Hussain et al., 2004; Knox et al., 2007). They all noted the dominance of the ultra-stable fraction of zircon, tourmaline and rutile in the heavy mineral assemblage. Hussain (2001) interpreted this as the result of intensive weathering, whereas for Hussain et al. (2004) it is a clear indicator for sedimentary recycling. Babalola (1999), Hussain (2001), Hussain and Abdullatif (2004) as well as Hussain et al. (2004) identified acidic to intermediate igneous rocks in Yemen as the most likely source for the Wajid Group. According to them, other sources like metamorphic, mafic igneous and sedimentary rocks as well as the Arabian Shield to the west are only minor contributors. Knox et al. (2007) identified several distinct heavy mineral zones and significant changes in provenance signatures throughout the Wajid Group. They identified those changes between the Dibsiyah, Sanamah, Khusayyayn and Juwayl formations as well as within the Dibsiyah Formation. Furthermore they correlated the heavy mineral assemblage of the Juwayl Formation from the Wajid outcrop belt to the B and C members of the Unayzah Formation in central Saudi Arabia. Only a few studies have targeted the central and northern part of the country, with varying success (Powers et al., 1966; Hussain and Abdullatif, 2004; Knox et al., 2010).

Powers et al. (1966) conducted a pilot study to assess the potential of heavy mineral analysis. They report a dominant ultra-stable fraction from the Saq and overlying formations, which they interpreted as indicative for sedimentary recycling. Yet they also found mica (biotite and muscovite), which is surprising given their unstable nature during transport. Hussain and Abdullatif (2004) also report an abundance of the zircon, tourmaline and rutile from the Saq and Qasim formations, but were unable to use their heavy mineral data for correlations. Knox et al. (2010) on the other hand were successful in studying heavy mineral assemblages of the Unayzah Formation from wells. They identified two changes in provenance within the Unayzah Formation, dividing it into three different heavy mineral units. Those units largely correspond with the Unayzah A, B and C members. They also tentatively recognise the potential of heavy mineral analysis for regional correlations.

None of the above mentioned studies applied single-grain techniques, which is becoming an increasingly important tool in sedimentary provenance analysis (von Eynatten and Dunkl, 2012). While the sandstones from the Wajid area have been studied by several workers, data from the central and northern Saudi Arabian succession is still scarce.

This study intents to close the gap between the Wajid outcrop belt and the Palaeozoic successions in central and northern Saudi Arabia. It also means to reveal changes in sedimentary provenance in time by studying representative samples throughout the northern/central and southern successions, covering the entire Palaeozoic. While petrographic data are plentiful for both study areas in the literature (Hadley and Schmidt, 1974; Babalola, 1999; Hussain, 2001; Al-Ramadan et al., 2004; Al-Harbi and Khan, 2005; Knox et al., 2007; Al-Harbi and Khan, 2008, 2011), geochemical data, especially trace element data, are not. In order to provide a better understanding of their sedimentary provenance, tectonic setting and stratigraphic relationship, here the first comprehensive set of petrographic as well as major and trace element geochemical data of Cambrian through Permian sandstones from across the Arabian Peninsula is provided. A further goal is to link Saudi Arabian sandstones with other parts of the northern Gondwana margin, utilising both SHMA as well as single-grain techniques.

In recent years, several studies were published dealing with provenance and heavy mineral studies on the northern margin of Gondwana. Most of them feature U–Pb age dating of detrital zircons, but also touch upon SHMA. Avigad et al. (2003, 2005) and Kolodner et al. (2006) used SHMA and U–Pb dating of detrital zircons from Cambrian–Ordovician sandstones from southern Israel to deduce provenance and palaeoclimate. They found ubiquitous zircons with ages of 0.55–0.65 Ga, which were likely sourced from the nearby ANS. Three additional, pre-Neoproterozoic age populations were also identified. They are significantly smaller than the Neproterozoic population and are grouped around 0.9–1.1 Ga, 1.65–1.85 Ga and 2.45–2.7 Ga. Morag et al. (2011) utilised the corresponding Hf isotopic data to infer long-distance transport for Cambrian–Ordovician sediments. Weissbrod and Bogoch (2007) compiled heavy mineral data of Neoproterozoic to Mesozoic siliciclastic sediments from the northern margin of the ANS and provide a comprehensive review about heavy mineral studies in that area. They identified three

different heavy mineral assemblages: (1) an immature assemblage containing unstable phases in Neoproterozoic sediments; (2) a mature assemblage dominated by stable to ulstrastable phases sourced from the interior of Gondwana in lower Palaeozoic sediments; (3) a mature assemblage dominated by ultra-stable phases sourced from recycled sediments and distal basement in upper Palaeozoic to lower Mesozoic sediments. Assemblages (2) and (3) also received intermittent input from locally exposed basement of the ANS. Morton et al. (2011) and Meinhold et al. (2011, 2013b) studied heavy mineral assemblages and detrital zircon ages of Precambrian to Mesozoic siliciclastic sediments from the Murzuq basin, Libya, in order to reconstruct provenance, palaeogeography and stratigraphic correlations. Morton et al. (2011) identified three distinct provenance changes in the highly mature heavy mineral assemblages, which were dominated by ultra-stable phases. Meinhold et al. (2011, 2013b) identified similar age groups in detrital zircons from the Cambrian–Ordovician of southern Libya like those reported by Avigad et al. (2003, 2005) and Kolodner et al. (2006) from southern Israel. Furthermore, Meinhold et al. (2013b) used populations of zircons dated at ca. 1.0 Ga to test and support the hypothesis of a 'Gondwana super-fan system' by Squire et al. (2006). A provenance analysis employing detrital zircon U–Pb geochronology of Cambrian–Ordovician sandstones from the Algerian Sahara was conducted by Linnemann et al. (2011). They identified a range of several different cratons and terranes as sources areas, but excluded the ANS as a potential source. In their study concerning the provenance of recent Arabian desert sand, Garzanti et al. (2013) also analysed the heavy mineral assemblages and detrital zircon ages of two samples from Ordovician and Devonian units in northern Saudi Arabia. The assemblage they described consisted almost entirely of the ultra-stable heavy minerals zircon, tourmaline and rutile. Detrital zircon U–Pb ages are remarkably similar to those published by Avigad et al. (2003, 2005), Kolodner et al. (2006), Morton et al. (2011) and Meinhold et al. (2011, 2013b).

3. Provenance analysis

3.1. A short history of provenance analysis

The word provenance has its roots in the Latin verb *provenire*, which means 'to come forth' or 'to originate'. When talking about people, provenance means 'place of origin' or 'ancestry'. This definition incidentally is also quite fitting in a sedimentological context, since it encompasses not only the progenitor (the source rock) but the entire lineage (the processes involved in the generation of sedimentary rocks, e.g. weathering, transport/dispersal and diagenesis) as well. In geology and earth sciences, provenance usually is referred to as "*the area from which the constituent materials of a sedimentary rock or facies are derived*" (Bates and Jackson, 1987). In sedimentary petrology specifically, the term provenance (and in extension provenance analysis) is used in a wider sense, referring not only to the area of origin of a sediment but to "*all factors related to the production of sediment, with specific reference to the composition of the parent rocks as well as the physiography and climate of the source area from which sediment is derived*" (Weltje and von Eynatten, 2004).

Sedimentary provenance analysis originated more than 100 years ago in the late 19th century with the advent of microscope-assisted observations of accessory minerals in sands (Weltje and von Eynatten, 2004). Before 1870 investigations of accessory ('heavy') minerals were only descriptive. The first studies that tried to link recent river sediments to their source rock are from Ludwig (1874), Meunier (1877) and Michel Lévy (1878). A first attempt to apply provenance analysis to ancient sediments was made by Thürach (1884), while Retgers (1895) suggested the use of characteristic mineral phases to infer palaeocurrent directions. These first provenance studies on ancient sediments resorted to determine source rocks by qualitative analysis using single characteristic minerals and varieties.

The next major milestone was the introduction of quantitative methods by Fleet (1926), who suggested grain counting in order to estimate relative abundances of accessory minerals. The method proved highly popular and as a result, the early 20th century saw a 'boom' in heavy mineral studies. At the same time, framework minerals were thought to contain no significant provenance information (Solomon, 1932). Later in the 1930s and 1940s it became clear that the composition of heavy mineral assemblages in sandstones is not only dependant on source rock lithology, but that I can be significantly modified by hydrodynamic processes as well as diagenetic effects and weathering (Rubey, 1933; Pettijohn, 1941). These years also saw the proposal of sandstone classification schemes by P.D. Krynine and F.J. Pettijohn, which are still in use today (Klein, 1963; Okada, 1971). With these came a renewed interest in the study of the framework composition of clastic sediments. Furthermore Krynine (1941) already realised the connection between sandstone composition and tectonic setting. Although framework mineralogy was used in the 1950s and 1960s to infer source rock lithologies and weathering conditions of ancient sediments, many of these studies relied on insufficient evidence and did not consider modern analogues (Weltje and von Eynatten, 2004).

The next logical step was to establish clear rules and definitions to describe sandstone grains. These were provided by Gazzi (1966) and most notably Dickinson (1970). With these tools and the widespread acceptance of the theory of plate tectonics Dickinson then proceeded to demonstrate that sandstone composition is largely controlled by the tectonic setting – i.e. source rocks, relief, climate and transport conditions (Dickinson, 1970; Dickinson and Suczek, 1979; Dickinson et al., 1983). Advances in analytical techniques led to the use of whole-rock geochemical data in sedimentary provenance analysis. The major and trace element composition of sandstones is dependent on their mineralogical composition and has been used to infer provenance and tectonic setting (Bhatia, 1983; Bhatia and Crook, 1986; Roser and Korsch, 1986, 1988; Chandler, 1988; Verma and Armstrong-Altrin, 2013).

Geochemical indices using the major element composition of silicilastic sediments is furthermore used to infer weathering and consequently Palaeoclimate conditions. Among the most commonly employed indices are the chemical index of alteration (CIA) after Nesbitt and Young (1982) and the plagioclase

index of alteration (PIA) after Fedo et al. (1995). Weathering trends can be visualised in a ternary diagram of Al_2O_3, CaO^*+Na_2O and K_2O (A-CN-K; Nesbitt and Young, 1984). Source area weathering can also be quantified by petrographical methods: Pettijohn (1954) defined the mineralogical maturity index (MI) as the ratio of quartz to quartz+feldspar+lithic fragments.

Traditional petrographical and whole-rock geochemical methods as well as SHMA have in recent years increasingly come under critique (Armstrong-Altrin and Verma, 2005; Weltje, 2006; Garzanti et al., 2009; von Eynatten et al., 2012). Grain size and sorting effects have a great influence on the mineralogical and geochemical composition of siliciclastic sediments and can mask the provenance signal (von Eynatten et al., 2012). Errors in the interpretation of recent systems, statistical flaws in the original construction of discrimination fields and the use of unrepresentative data severely limit the usefulness of many traditional methods of provenance analysis (Armstrong-Altrin and Verma, 2005; Garzanti et al., 2009; von Eynatten and Dunkl, 2012; von Eynatten et al., 2012).

An alternative method to whole-rock and SHMA investigations are single-grain studies, which are becoming even more important (von Eynatten and Dunkl, 2012). This trend is certainly facilitated by the refinement and wider availability of analytical techniques to determine the chemical and isotopic composition of single mineral grains. The major advantage of this approach is that the effects of differential fractionation of the heavy mineral assemblage are negligible for grains from the same mineral phase (von Eynatten and Dunkl, 2012). Yet there are scenarios where some single-grain techniques may be insufficient and need to be used in conjunction with other methods to develop their full potential (von Eynatten and Dunkl, 2012). The integrated use of single-grain analysis with SHMA, whole-rock geochemistry and traditional sediment petrography promises to yield the best results in sedimentary provenance analysis.

3.2. Heavy minerals

Heavy mineral assemblages can be indicative for source rock lithology. Processes during transport, deposition and burial leave the relative abundances of heavy minerals largely unaffected, provided they share a similar hydraulic and diagenetic behaviour (Morton and Hallsworth, 1999). Yet intensive weathering, reworking or sedimentary recycling may severely reduce the variability within the heavy mineral assemblages of mature sandstones (see Table 1 for a comparison of the relative stabilites of some important heavy minerals). In such a case, examining the variability – for example crystal structure, internal layout or chemical composition – of single grains from the same mineral phase ('varietal studies') is an ideal complimentary technique. Consequently, standard heavy mineral analysis and varietal studies have been extensively used in a wide field of research – from high-resolution stratigraphic correlations, tectonic setting and provenance studies, mineral exploration to geoarchaeology and even forensic science (Mange and Wright, 2007; von Eynatten and Dunkl, 2012). Geochemical varietal studies are frequently conducted using a wide array of heavy minerals: garnet, chromite, tourmaline, pyroxenes, amphiboles, apatite as well as chloritoid, epidote, rutile and monazite, among others (Mange and Morton, 2007). To successfully conduct varietal studies the samples have to contain statistically significant amounts of the respective mineral. This is a fundamental challenge when studying highly mature siliciclastics with impoverished heavy mineral assemblages. A lot of the meta- and unstable phases are not preserved in sufficient numbers. The consequence is to target the ultra-stable fraction and/or any meta-stable or labile phase that occurs in acceptable quantity.

For this and other reasons, rutile and garnet were selected for single-grain geochemical analysis in this study. They both have variable chemical compositions, especially garnet, and their composition is provenance-dependant (Morton et al., 2004; Mange and Morton, 2007; Zack et al., 2004a; Meinhold et al., 2008; Meinhold, 2010; Triebold et al., 2012; Krippner et al., 2014). Furthermore rutile is part of the ultra-stable fraction and is present in sufficient abundance throughout the successions of both study areas. Garnet, although not as resistant and stable as rutile, occurs in upper Palaeozoic formations. Additionally the chemical composition of both can be measured in a non-destructive way utilising an electron-microprobe (EMP).

Table 1: Relative stability during burial diagenesis and in weathering profiles for some of the most important heavy minerals according different authors (modified after Morton and Hallsworth, 1999, 2007). C-amphibole=calcic amphibole, S-amphibole=sodic amphibole, S-pyroxene=sodic pyroxene.

Relative stability	Deep burial diagenesis	Weathering profiles						
	Morton and Hallsworth (2007)	Goldich (1938)	Dryden and Dryden (1946)	Piller (1951)	Weyl and Werner (1951)	Grimm (1973)	Lemcke et al. (1953)	Bateman and Catt (1985)
Most stable	Rtl, Anatase, Brookite, Zrc, Apt, Trm, Mzt, Spinel		Zircon	Zircon Trm		Zrc, Rtl Trm	Zrc, Rtl Trm	Zrc, Rtl Trm, Andalusite
					Ky	Andalusite, Ky	Stl	Ky, Stl
	Grt, Chloritoid		Sillimanite					Titanite
	Allanite		Monazite		Stl	Stl		
	Stl		Ky		Epd	Epd	Ky, Epd	
	S-amphibole		C-amphibole				C-amphibole	
	Ky		Staurolite					
	Titanite						Apt	
	Epd	Grt	Grt	Grt	Grt	Grt, Apt	Grt	Grt
	C-amphibole, Andalusite, Sillimanite	C-amphibole			C-amphibole	C-amphibole		
	S-pyroxene							Epd
	Opx, Cpx	Cpx	Opx			Cpx, Olivine		Cpx, Opx, C-amphibole
				Apt				Apt
Least stable	Olivine	Olivine						

3.2.1. Heavy mineral indices

Although a reliable provenance indicator under the right circumstances, the composition of heavy mineral assemblages from the same source rock can be altered and modified by many processes. Among those are: destruction of unstable grains by chemical weathering, hydraulic sorting during transport, sorting by grain size and diagenetic alteration (Morton and Hallsworth, 1999; Garzanti et al., 2008, 2009). These processes can affect a detrital heavy mineral assemblage in such a way that it no longer resembles the one from its source rock (Knox et al., 2007). Therefore results obtained by only studying percentage data can be unreliable. A remedy for the issue is the study of indices from heavy minerals of the same grain size, have similar hydraulic properties and are resistant to diagenetic alteration and weathering (Morton, 1985; Morton and Hallsworth, 1994, 1999; Knox et al., 2007). Indices used in this study include the zircon-tourmaline-rutile index (ZTR) (Hubert, 1962), the rutile:zircon index (RZi), the garnet:zircon index (GZi), the apatite:tourmaline index (ATi) and the staurolite:tourmaline index (STi) (Morton and Hallsworth, 1994, 1999) (Table 2).

The ZTR is a good maturity indicator. All three considered heavy minerals are highly stable, occur in a wide range of magmatic and metamorphic rocks and are largely unaffected by chemical weathering. This index is thus ideally suited to identify highly weathered, reworked or recycled sediments, though it has difficulties differentiating between reworking and recycling. As the ZTR describes the total share of zircon, tourmaline and rutile from the entire translucent heavy mineral fraction, its values are given as percentage.

The RZi is a reliable provenance indicator, as both heavy minerals are ultra-stable and are largely derived from distinctly different lithologies. Zircon mainly crystallises in granitic and other plutonic rocks, while rutile forms predominantly in middle to high grade metamorphic rocks (Mange and Maurer, 1992; Mange and Wright, 2007; Meinhold, 2010). The RZi can thus serve to determine the influence of primarily plutonic or metamorphic source rocks. If the source area contains older sedimentary rocks, the high stability of zircon and rutile can become problematic. Since ultra-stable heavy minerals tend to become enriched during recycling, the initial source rock signal may be overprinted.

The GZi is, like the RZi, a reliable provenance indicator, if garnet is present. Garnet, like rutile, is mainly derived from metamorphic rocks, but can also occur in magmatic rocks (Krippner et al., 2014). It is resistant to weathering, but can be dissolved in acidic groundwaters and during deep burial (Morton, 1987; Morton and Hallsworth, 1999; Knox et al., 2007).

The ATi can also be a provenance indicator, but is highly susceptible to weathering. Apatite is common in both magmatic and metamorphic rocks. Yet it is prone to dissolution, especially in humid conditions and under low relief (Morton and Hallsworth, 1999; Knox et al., 2007; Morton and Hallsworth, 2007). The ATi is therefore arguably better suited for studying weathering, especially during alluvial storage (Morton and Hallsworth, 1999). Additionally leeching from the outcrop, reworking and/or recycling may also lead to apatite-loss.

The STi is a good provenance indicator. Staurolite is commonly derived from low-grade metamorphic rocks like, gneisses, metapelites and schists. It is fairly resistant to weathering, but can be dissolved during deep burial (Morton et al., 2011). Features like serrated grain edges help to identify dissolution effects in staurolite assemblages.

Table 2: Overview of utilised heavy mineral indices (modified after Morton and Hallsworth, 1994).

Index	Index minerals	Calculation	Application
ZTR	zircon, tourmaline, rutile	100 x Σ(zircon + tourmaline + rutile) / Σtranslucents	maturity
RZi	rutile, zircon	100 x rutile / (rutile + zircon)	provenance
GZi	garnet, zircon	100 x garnet / (garnet + zircon)	provenance
ATi	apatite, tourmaline	100 x apatite / (apatite + zircon)	maturity, provenance
STi	staurolite, tourmaline	100 x staurolite / (staurolite + tourmaline)	provenance

3.2.2. Rutile

Rutile is a heavy mineral mainly consisting of titanium dioxide (TiO_2) and the main Ti-bearing phase in most rocks (>90% of whole-rock Ti content). Besides titanium, it is also an important carrier for high field strength elements and tungsten (Foley et al., 2000; Luvizotto et al., 2009; Meinhold, 2010). Additional minor components are V, Cr, Mo and Sn. Additionally, rutile can contain considerable amounts of Zr. Rutile is formed predominantly in medium- to high-grade metamorphic rocks, which are regarded as the primary source for detrital rutile. It also can be found in low-grade metamorphic rocks, quartz veins and in different igneous rocks (Meinhold, 2010). This variability coupled with its high chemical and physical stability make rutile a prime candidate for provenance studies. Electron microprobe analysis of single rutile grains to determine chemical composition has become a standard method of chemical geology and mineralogy as well as an increasingly important tool in sedimentary provenance analysis (Meinhold et al., 2008; Meinhold, 2010).

The trace element composition of rutile can give information about its source rock lithology and crystallisation temperatures. The Cr and Nb content of rutiles is supposed to reflect its host rock lithology. With this system, rutiles can be differentiated into 'mafic' and 'felsic' (called 'pelitic' by Triebold et al., 2012) origin. In order to achieve meaningful results, first the correct polymorph has to be identified (e.g. rutile, anatase or brookite). This can be done either with Raman spectroscopy, discriminant analysis of trace elements or optical microscopy, the latter which has been applied in this study. The concept of source lithology characterisation utilising the Cr-Nb system of rutile has first been proposed by Zack et al. (2004a) and then further refined by Triebold et al. (2007), Meinhold et al. (2008) and most recently by Triebold et al. (2012) with the following criteria:

$$x = 5 * (\mathrm{Nb_{ppm}} - 500) - \mathrm{Cr_{ppm}} \qquad \text{(equation 1)}$$

where mafic rutiles have x < 0 and felsic rutiles have a x > 0.

The Zr content of rutiles coexisting with zircon and quartz in their source rocks has been shown to be dependent on both temperature and pressure during crystallisation (Zack et al., 2004b; Zack and Luvizotto, 2006; Watson et al., 2006; Tomkins et al., 2007). This dependency can be used for Zr-in-rutile thermometry, if the pressure in the source rock can be estimated. This can be utilised in sedimentary provenance analysis to identify different source rocks through variances in rutile temperature populations. For this study, the Zr-in-rutile thermometer after Tomkins et al. (2007) has been used:

$$T\,[^{\circ}C] = \frac{83.9 + 0.14 * P}{0.1428 - R * \ln(\mathrm{Zr_{ppm}})} - 273 \qquad \text{(equation 2)}$$

with P = 10 kbar (as suggested by Triebold et al., 2012, for cases with unknown growth pressure) and the gas constant R = 0.0083144 kj/K. It gives similar results at 10 kbar like the thermometer of Watson et al. (2006). The maximum divergence of 8 K between both thermometers is well within their margins of error (± 20 °C).

3.2.3. Garnet

Garnets are a group of cubic, relatively stable heavy minerals with the general formula $X_3Y_2Si_3O_{12}$, where the X-position is usually occupied by divalent cations like Fe^{2+}, Ca^{2+}, Mg^{2+} or Mn^{2+} and trivalent cations like Al^{3+}, Fe^{3+} or Cr^{3+} commonly situated on the Y-position. The group has 14 principal end-members, of which pyrope ($Mg_3Al_2Si_3O_{12}$), almandine ($Fe_3Al_2Si_3O_{12}$), spessartine ($Mn_3Al_2Si_3O_{12}$), uvarovite ($Ca_3Cr_2Si_3O_{12}$), grossular ($Ca_3Al_2Si_3O_{12}$) and andradite ($Ca_3(Fe,Ti)_2Si_3O_{12}$) are the most common (Grew et al., 2013). The varied chemical composition of garnet, which is dependent on host rock lithology, and its occurrence in a wide range of metamorphic as well as igneous rocks, coupled with a relatively high stability make it suitable for provenance analysis (Krippner et al., 2014). Consequently, garnet has been utilised in provenance studies of sediments ranging from the Palaeozoic to the Holocene (Mange and Morton, 2007 and references therein).

3.2.4. Zircon

Zircon is a heavy mineral from the group of the nesosilicates with the formula $ZrSiO_4$ and the main bearer of Zr in most rocks. It furthermore contains a significant fraction of U, Th, Hf and REEs of the host rock (Poller et al., 2001; Hoskin and Schaltegger, 2003). During crystallisation from a melt, zircon incorporates radioactive uranium in its crystal structure. At the same time Pb, which is the decay product of U, is incompatible to the crystal structure of zircon and thus does not tend to get concentrated. Thus the initial Pb-content of zircon is low and all present Pb can be estimated to be radiogenic, making the U–Pb system in zircons very well suited to radiometric dating (von Eynatten and Dunkl, 2012). Zircon is highly stable and able to survive magmatic, metamorphic and erosional processes (Corfu et al., 2003), which make it an ideal candidate for varietal studies in the context of provenance analysis. Under certain, very high-grade metamorphic conditions in the upper amphibolite, eclogite and granulite facies, zircon can be alterated, re-crystallise or grow newly from fluids (Corfu et al., 2003; Chen et al., 2010).

The Th and U content of zircons, obtained for instance by LA-ICP-MS, can be used to distinguish between a metamorphic and a magmatic origin: Magmatic zircons have Th/U ratios between 0.2 and 1.5, whereas metamorphic zircons have much lower values, between 0.001 and 0.1 (Vavra et al., 1999; Hartmann et al., 2000; Corfu et al., 2003).

Another regularly employed technique to study zircon in single-grain analyses is cathodoluminescence (CL) imaging. It relies on an incident electron, emitted by the cathode, hitting a sample electron and exciting it into a higher energy state. After a brief time, the excited electron falls back on its previous energy state while emitting a photon of visible light, usually in the blue and yellow regions of the wavelength spectrum (Marshall, 1988; Corfu et al., 2003). The amount and exact wavelength of the emitted light is dependent on crystal structure chemistry (Corfu et al., 2003). U and possibly Hf are primarily responsible for repressing ('quenching') of the CL signal, while the concentration of REEs and Th exhibits no influence on the CL-brightness (Poller et al., 2001, Corfu et al., 2003). Therefore bright areas in CL images have lower U (and Hf) concentrations than fainter ones. This can be used to observe and visualise the internal structures of zircon grains and is vital as preparation for subsequent analyses, like U–Pb radiometric dating. Without the exact knowledge of a zircon's internal structure, meaningful measurements and conclusions are impossible for those techniques. A further application for CL images lies in interpreting magmatic and metamorphic events. This has been successfully done before, often in conjunction with other techniques like single-grain geochemistry and isotopic dating (e.g. Hanchar and Miller, 1993; Hanchar and Rudnick, 1995; Grant et al., 2009). Corfu et al. (2003) compiled a useful atlas of zircon textures, focussing heavily on internal structures revealed by CL and back-scattered electron imaging. With these imaging methods it is possible to identify distinct structural features that are diagnostic for certain magmatic or metamorphic events and conditions. This allows a classification of zircons into different morphotypes belonging to one of two groups with either predominantly magmatic or predominantly metamorphic features. For a description of morphotypes identified in this study see 5.6.3 (Zircon morphotypology), for example pictures see Figure 23.

Crystal habit and size can be used to classify zircons and to study their origin as well as the physical and chemical conditions of the melt during crystallisation. Pupin (1980) developed a diagram to identify

30 different zircon classes from granitic melts according to their crystal habitus. This was then later enhanced by Schermaier et al. (1992), who combined the Pupin-diagram with the granite classification scheme after Chappel and White (1974). Poldervaart (1955, 1956) and Hoppe (1963) used the elongation (ratio of length to width) to discern the origin of zircons. While these methods are cheap and can be applied with petrographic methods only, they are better suited for studying magmatic rocks. They are generally not applicable in palaeogeographic and provenance studies, since variability in size and shape is low due to rounding during transport, reworking and/or recycling (Poldervaart, 1955).

4. Methods and material

4.1. Sampling

Samples were collected during a field campaign in spring 2013. A total of 44 samples (identifiable by the prefix 'AB-SA'), covering the entire Palaeozoic succession in both study areas, have been obtained. For sample locations see Figure 2b), c), for exact GPS coordinates see Table 3. During earlier field campaigns between 2009 and 2010, a set of 17 samples has been collected from outcrops in the southern study area described in Al-Ajmi et al. (2015). The data were additionally used in our analysis and are presented in several graphs.

When selecting sediment samples, emphasis was put on fine- to medium-grained sandstones. Chosen samples are representative for their respective formations in most cases. Where possible they were taken from the lower, middle and upper part of each formation, in order to cover the entire stratigraphic range. Exceptions are units where the predominant and representative grain size would be unsuitable for heavy mineral analysis. Therefore, the samples from the Silurian Qusaiba Member of the Qalibah Formation and one sample from the Subbat Member of the Devonian Jauf Formation, which both are predominantly shaly, were taken from medium grained, sandy intercalations. Samples from the southern study area were mostly taken in the Wajid outcrop area south and southwest of Wadi Ad Dawasir (Figure 2b), from sections already described and logged by Keller et al. (2011) and Al-Ajmi et al. (2015). Three samples were taken near Hima, north of Najran (Figure 2b). The central and northern Arabian study area is geographically more extensive with most samples taken from the Buraida area, around Hail and from the vicinity of Sakaka (Figure 2c). Outcrops for sampling were chosen according to the 1963 USGS/Aramco geologic map of the Arabian Peninsula, El-Khayal (1987), Powers et al. (1966), Stump et al. (1995), Senalp and Al-Laboun (2000), Al-Ajmi (2005) and Al-Laboun (2009, 2010, 2011).

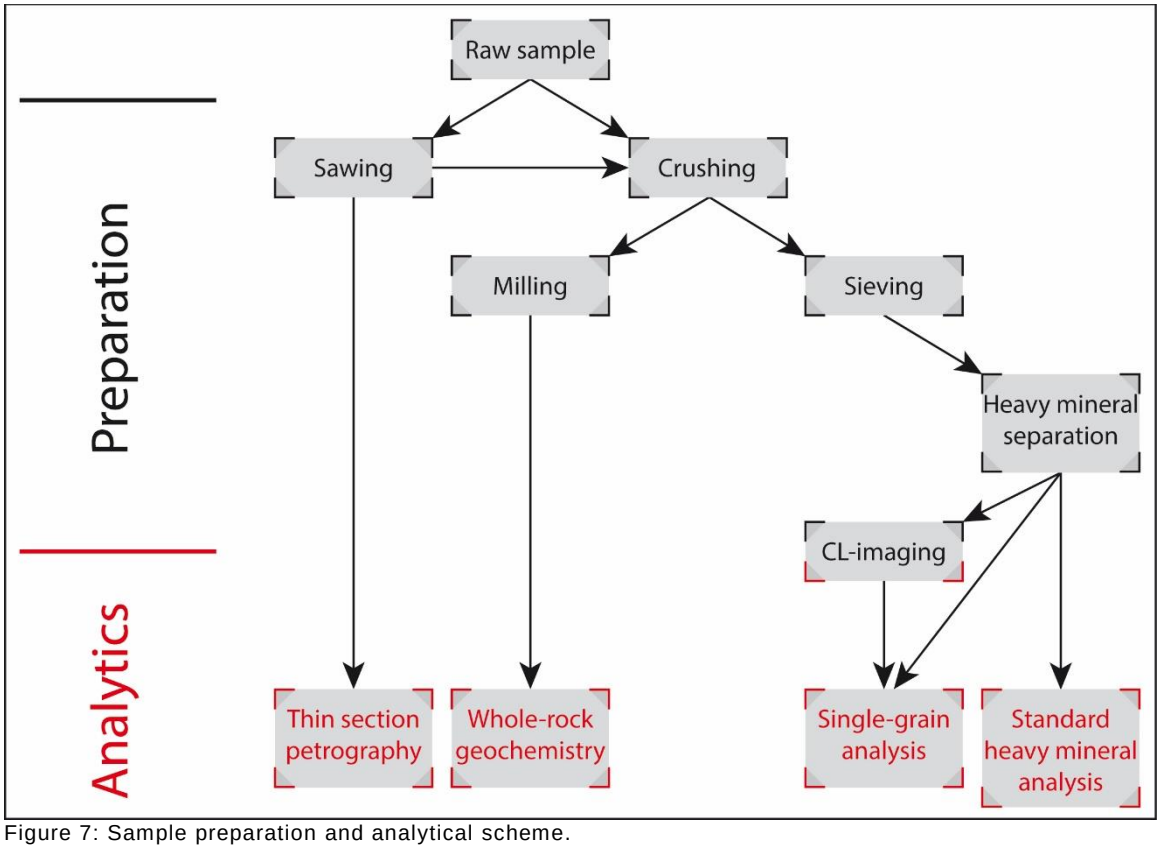

Figure 7: Sample preparation and analytical scheme.

4.2. Sample preparation

Sample preparation was performed at Darmstadt Technical University unless stated otherwise. The sample preparation procedure is illustrated in Figure 7. All samples were first cut with a rock saw to prepare thin section slices (Figure 8a), while half of the remaining material was then crushed by a jaw crusher. The remaining uncrushed half was retained as backup. Samples for geochemical analysis were ground in a vibratory disc mill with a tungsten carbide set for 5 minutes, ensuring a resulting grain size of <63 µm (Figure 8b). Samples for heavy mineral analysis were ground for 30 seconds in the vibratory disc mill to disintegrate the grain matrix without damaging the heavy minerals.

Figure 8: (a) Sawing of samples with a rock saw for thin section preparation and further disintegration. (b) Grinding of disintegrated sample for geochemical analysis in a vibratory disc mill with a tungsten carbide set to a grain size of <63 µm. (c) Dry sieving of disintegrated sample to separate 63–125 µm grain size fraction. (d) Density separation of heavy mineral fraction in a separator funnel filled with sodium polytungstate.

4.3. Petrography and standard heavy mineral analysis

Petrographic analysis was done using a petrographic microscope with an attached point counting stage. Mineralogical composition was determined by counting 300 points per thin section, including pore space and cement. Points were counted equidistantly along a series of traverses across the thin section using the Gazzi-Dickinson method (Gazzi, 1966; Dickinson, 1970; Weltje, 2002). Recorded components were: monocrystalline quartz with straight extinction (Qm), monocrystalline quartz with undulose extinction (Qmu), polycrastalline quartz (Qp), plagioclase feldspar (Plag), alkali feldspar (Afsp), lithic fragments (Lf), cement/pseudo matrix (Cem/PM) and pore space (Pore). Sorting and grain size classification was done by estimating the dominant, minimum and maximum grain-size fractions.

The 63–125 µm fraction was separated by dry-sieving (Figure 8c). Heavy minerals have been extracted in separation funnels by density separation with sodium polytungstate ($Na_6[H_2W_{12}O_{40}]$) with a density of 2.855 g/cm^3 (Figure 8d). Strewn slides were then prepared from a small amount of the heavy mineral residuum. In order to get statistically representative portion, the residuum was poured on a sheet of paper and repeatedly halved with a razor blade. Then the heavy minerals were mounted on a thin section slide with Epo-Tek 301 two-component resin and covered with a glass plate. SHMA was performed by counting under a petrographic microscope. First the ratio of translucent to opaque grains was determined by counting 200 grains per sample. In a second run, 300 translucent grains were counted to determine the abundance of translucent detrital heavy minerals. Where not enough translucent heavy minerals were available, all grains were counted. Mineral identification was done with the help of the excellent atlas of Mange and Maurer (1992). As counting method ribbon counting has been used. This technique involves randomly choosing bands ('ribbons') from the microscope slide and counting all grains within the band while mechanically moving the counting stage. The results obtained by ribbon counting are independent from grain size (Mange and Maurer, 1992).

Table 3: Palaeozoic sampling sites and outcrops with GPS coordinates. UT – Upper Tabuk; LT – Lower Tabuk; UW – Upper Wajid; LW – Lower Wajid. The Qusaiba and Sharawra members of the Qalibah Formation are listed under 'Formation' for convenience.

Sample #	Age	Stratigraphy	Lat	Long	Location
Tabuk area					
AB-SA120	Carbonif.-Permian	Unayzah Fm.	26°07'30.1"	43°59'11.7"	Buraida-Unayzah road
AB-SA129	Carbonif.-Permian	Unayzah Fm.	26°55'35.9"	43°34'39.8"	E of Qusaiba depression
AB-SA130	Carbonif.-Permian	Unayzah Fm.	26°55'35.5"	43°34'38.8"	E of Qusaiba depression
AB-SA150	Devonian	Jubah Fm.	29°58'14.2"	40°10'19.4"	W of Sakaka
AB-SA152	Devonian	Jubah Fm.	29°58'17.7"	40°10'21.0"	W of Sakaka
AB-SA153	Devonian	Jubah Fm.	29°58'18.4"	40°10'26.1"	W of Sakaka
AB-SA160/T	Devonian	Jauf Fm.	30°04'46.0"	39°55'52.0"	Wadi Murayr
AB-SA161	Devonian	Jauf Fm.	30°04'45.7"	39°55'55.4"	Wadi Murayr
AB-SA164	Devonian	Jauf Fm.	29°49'41.1"	39°53'00.9"	Dawmut al Jandal
AB-SA154	Devonian	Tawil Fm.	29°49'34.7"	39°32'10.8"	W of Dawmut al Jandal
AB-SA156	Devonian	Tawil Fm.	29°49'30.5"	39°32'16.4"	W of Dawmut al Jandal
AB-SA157	Devonian	Tawil Fm.	29°49'29.3"	39°32'17.0"	W of Dawmut al Jandal
AB-SA128	Silurian	Sharawra Mbr.	26°51'04.2"	43°34'40.9"	W of Qusaiba depression
AB-SA127	Silurian	Sharawra Mbr.	26°51'05.5"	43°34'42.3"	W of Qusaiba depression
AB-SA132/1	Late Ordovician	Zarqa Fm.	26°51'28.6"	43°21'22.2"	NW of Al Qara
AB-SA132/2	Late Ordovician	Zarqa Fm.	26°51'28.6"	43°21'22.2"	NW of Al Qara
AB-SA123/2	Late Ordovician	Sarah Fm.	26°23'02.4"	43°45'41.8"	W of Al Qara
AB-SA122/2	Late Ordovician	Sarah Fm.	26°23'03.8"	43°45'41.2"	W of Al Qara
AB-SA124	Ordovician	Qasim Fm.	26°23'25.1"	43°46'22.3"	W of Al Qara
AB-SA126	Ordovician	Qasim Fm.	26°34'10.4"	43°22'02.7"	Sarah ridge
AB-SA145	Ordovician	Qasim Fm.	27°43'14.2"	41°45'01.3"	N of Hail
AB-SA144/1	Ordovician	Qasim Fm.	27°40'09.0"	41°45'55.5"	Hail
AB-SA142/2	Ordovician	Qasim Fm.	27°40'57.1"	41°43'12.5"	N of Hail
AB-SA170	Cambr.-Ordov.	Saq Fm.	26°48'41.1"	39°29'04.2"	along Highway 70
AB-SA167	Cambr.-Ordov.	Saq Fm.	26°48'51.6"	38°31'03.6"	along Highway 70
AB-SA169	Cambr.-Ordov.	Saq Fm.	26°27'54.7"	39°14'46.3"	along Highway 15
Wajid area					
AB-SA98	Carbonif.-Permian	Juwayl Fm.	19°57'37.4"	44°44'59.0"	Jabal Seab
AB-SA80	Carbonif.-Permian	Juwayl Fm.	19°54'54.2"	44°38'59.2"	Jabal Blehan
AB-SA100	Carbonif.-Permian	Juwayl Fm.	19°57'37.1"	44°44'59.9"	Jabal Seab
AB-SA87	Devonian	Khusayyayn Fm.	20°04'50.6"	44°39'48.0"	Jabal Khusayyayn
AB-SA89	Devonian	Khusayyayn Fm.	20°04'52.2"	44°39'48.2"	Jabal Khusayyayn
AB-SA90	Devonian	Khusayyayn Fm.	20°04'53.9"	44°39'49.7"	Jabal Khusayyayn
AB-SA118	Devonian	Khusayyayn Fm.	18°10'21.8"	44°19'10.3"	Nawan
AB-SA32	Devonian	Khusayyayn Fm.	18°14'55.0"	44°27'34.0"	Hima
AB-SA115	Silurian	Qusaiba Mbr.	18°10'29.8"	44°19'11.0"	Nawan
AB-SA62	Late Ordovician	Sanamah Fm.	20°14'57.6"	44°17'13.8"	Jabal Atheer
AB-SA63	Late Ordovician	Sanamah Fm.	20°14'57.9"	44°17'12.7"	Jabal Atheer
AB-SA64	Late Ordovician	Sanamah Fm.	20°14'57.6"	44°17'12.2"	Jabal Atheer
AB-SA73	Late Ordovician	Sanamah Fm.	20°09'17.0"	44°09'53.9"	Jabal Nafla
AB-SA74	Cambr.-Ordov.	Dibsiyah Fm.	20°09'15.5"	44°09'53.3"	Jabal Nafla
AB-SA76	Cambr.-Ordov.	Dibsiyah Fm.	20°09'15.1"	44°09'51.8"	Jabal Nafla
AB-SA72	Cambr.-Ordov.	Dibsiyah Fm.	20°09'10.6"	44°09'45.3"	Jabal Nafla
AB-SA69	Cambr.-Ordov.	Dibsiyah Fm.	20°14'57.6"	44°17'06.3"	Jabal Atheer
AB-SA79	Cambr.-Ordov.	Dibsiyah Fm.	20°09'16.7"	44°09'34.4"	Jabal Nafla

4.4. Geochemical analysis

Most of the whole-rock geochemical analysis and preparation steps following grinding were carried out at the Geoscience Center at the University of Göttingen. Major element analysis was done using X-ray fluorescence spectrometry (XRF) on fusion tablets. Samples powder was mixed with Spectromelt® A 12 (Merck) and LiF and fused in platinum crucibles. Melting and quenching of the glass tablets was done fully automatic with a Breitländer autofluxer® plus fusion machine. The tablets were then measured with a PANalytical AXIOS Advanced sequential X-ray fluorescence spectrometer. Major element data of some samples were determined at the Institute for Geosciences at the University of Mainz following procedures described in Meinhold et al. (2007) (Table A3). For major element analysis the lower limit of detection is between 1% and 5% for samples analysed at the University of Göttingen and <2% for samples analysed at the University of Mainz.

Solution inductively coupled plasma mass spectrometry (ICP-MS) was used for trace element geochemistry. Analysis was carried out at the University of Göttingen. Sample powder (100±0.1 mg per sample) was dissolved by acid digestion with HF-HNO_3-HCl prior to analysis, using a PicoTrace® acid sample digestion system. The samples underwent a pre-reaction with 2 ml HNO_3 at 50°C over night. After cooling to room temperature, 3 ml HF (40%) and 3 ml $HClO_4$ (70% to 72%) were added and the samples heated to 150°C for 8 hours during the first pressure phase. In the subsequent evaporation phase the crucibles were heated to 180 °C and dried for 16 hours. Following cooling to room temperature, 10 ml H_2O (double de-ionised), 2 ml HNO_3 and 0.5 ml HCl were added and the samples heated to 150°C for 4 hours during the second pressure phase. After final cooling the samples were transferred into 100 ml volumetric flasks and 200 µl of an internal standard added. Samples, blanks and standards were analysed by a ThermoElectron VG PlasmaQuad 2 quadrupole ICP-MS. Based on co-processing the laboratory internal standards and the international standards as unknown samples, the 2σ error of the ICP-MS analysis was estimated to be ~5% for REEs, <20% for Nb and Ta, and <10% for all other trace elements (Wegener et al. 2011).

Statistical analyses have been done with the software PAST, version 3.07 (Hammer et al., 2001). Ternary plots have been created using the GeoChemical Data toolkit (GCDkit) for R, version 2.13.2 (Janoušek et al., 2006).

4.5. Single-grain analysis

From the lower and upper Palaeozoic successions of each study area, samples were randomly chosen for rutile varietal studies. Samples for garnet geochemical analysis were chosen for high abundance. Rutiles and garnets were hand-picked from the heavy mineral residuum under a binocular and placed on synthetic mounts. After polishing the mounts were cleaned and then coated with carbon by vapour deposition to ensure conductivity. Single-grain geochemical analyses of rutile and garnet were performed with a JEOL JXA 8900 RL EMP equipped with five wavelength dispersive spectrometers at the Geoscience Center at the University of Göttingen. Measuring conditions for rutile include a beam current of 80 nA and an accelerating voltage of 25 kV. The counting times per spot were 200 s for Nb, Al, Cr, Zr and V, 100 s for Sn, Si, Fe and W, and 15 s for Ti. Measuring conditions for garnet include a beam current of 20 nA and an accelerating voltage of 15 kV. The counting times per spot were 15 s for Si, Mg, Ca, Fe, and Al, and 30 s for Ti, Cr, and Mn. The JEOL JXA 8900 RL EMP was also utilised to capture CL images of zircon.

5. Results

5.1. Petrography

Sample lithology was determined using point-counting data plotted in a QFL diagram (Figure 9), petrographic parameters are presented in Table 4. Lithologies from both study areas are dominated by quartz arenites (Figure 10a, b), constituting over half of the analysed samples (50% of Tabuk samples, 67% of Wajid samples). Subarkose is the second most numerous lithology (31% of Tabuk samples, 17% of Wajid samples), with arkoses making up a minor fraction (19% of Tabuk samples, 11% of Wajid samples). The Sanamah Formation contains the only sublitharenite from both study areas. Pseudomatrix and cement are scarce to almost completely absent in most samples, with few exceptions (Figure 10c, d). Dominant grain size is affected by sampling bias and has been estimated in thin sections. Medium sand make up 77% of samples, fine sand 18% and coarse silt 5%. Sorting is poor (Figure 10e, f) to good with no discernible trends. Grains are subangular to rounded. Porosity ranges between approximately 5% and 20% and is highly variable within most formations. The Khusayyayn Formation from the Wajid area and the Unayzah and Jubah formations from the Tabuk area have rather uniform porosity distributions of 15% to 20%. Recorded minerals are predominantly quartz. Slightly less than half (46%) of the quartz grains from southern Saudi Arabia have undulatory extinction, between 47% are Qm with straight extinction. Qp content ranges between 2% and 17%. In contrast, the Permian Juwayl Formation has significantly more Qm (66%) than Qmu (27%). Sandstones from the Tabuk area have similar overall quartz composition, but the variability of the Qm/Qmu ratio within formations is higher than in the Wajid area. Feldspar content is low in most samples. Where feldspar is present, alkali-feldspars are usually more abundant than plagioclase. Striking exceptions are one sample from the Permian Juwayl Formation and the Silurian Qusaiba and Sharawra members. The sample from the Juwayl Formation (sample AB-SA98) contains two types of feldspar: the first being very weathered, the second is much fresher (Figure 10c, d). In thin sections encountered heavy minerals are dominated by zircon and rutile; some tourmaline and mica (muscovite, biotite and unidentified mica) were observed as well. Three samples show minor clinopyroxene and orthopyroxene.

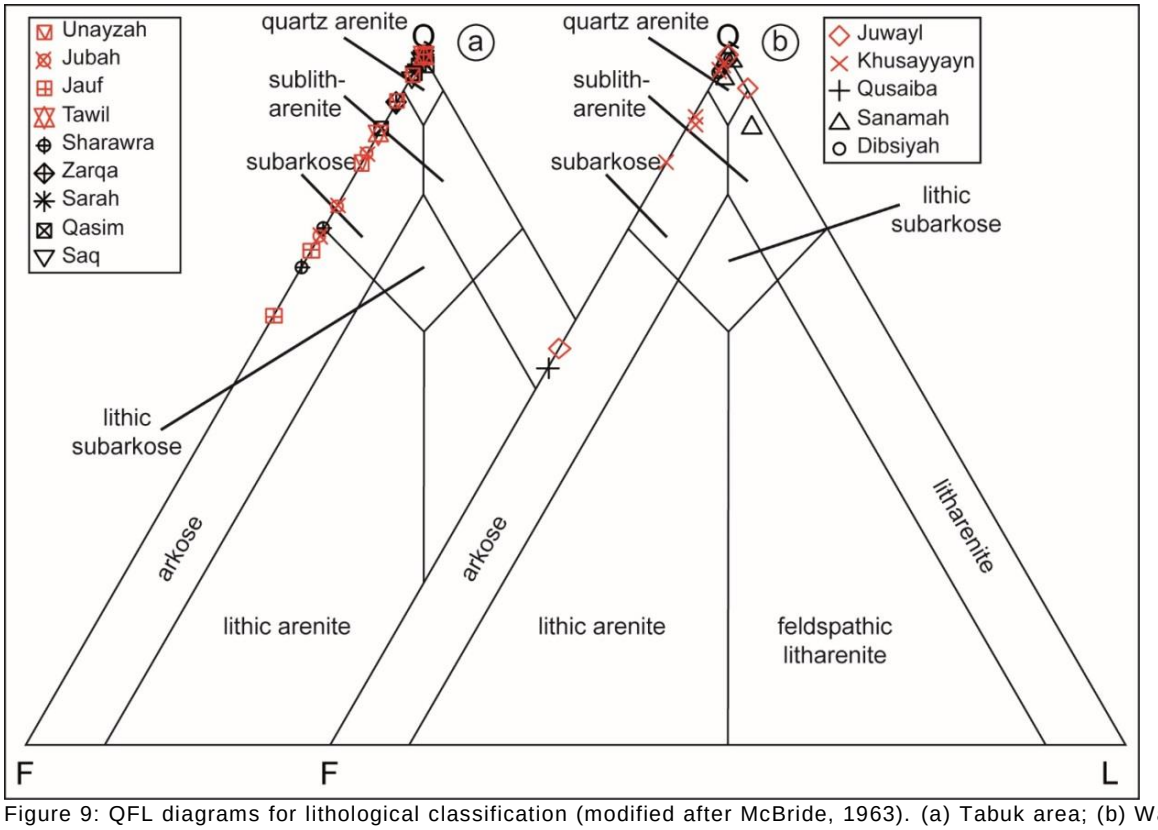

Figure 9: QFL diagrams for lithological classification (modified after McBride, 1963). (a) Tabuk area; (b) Wajid area.

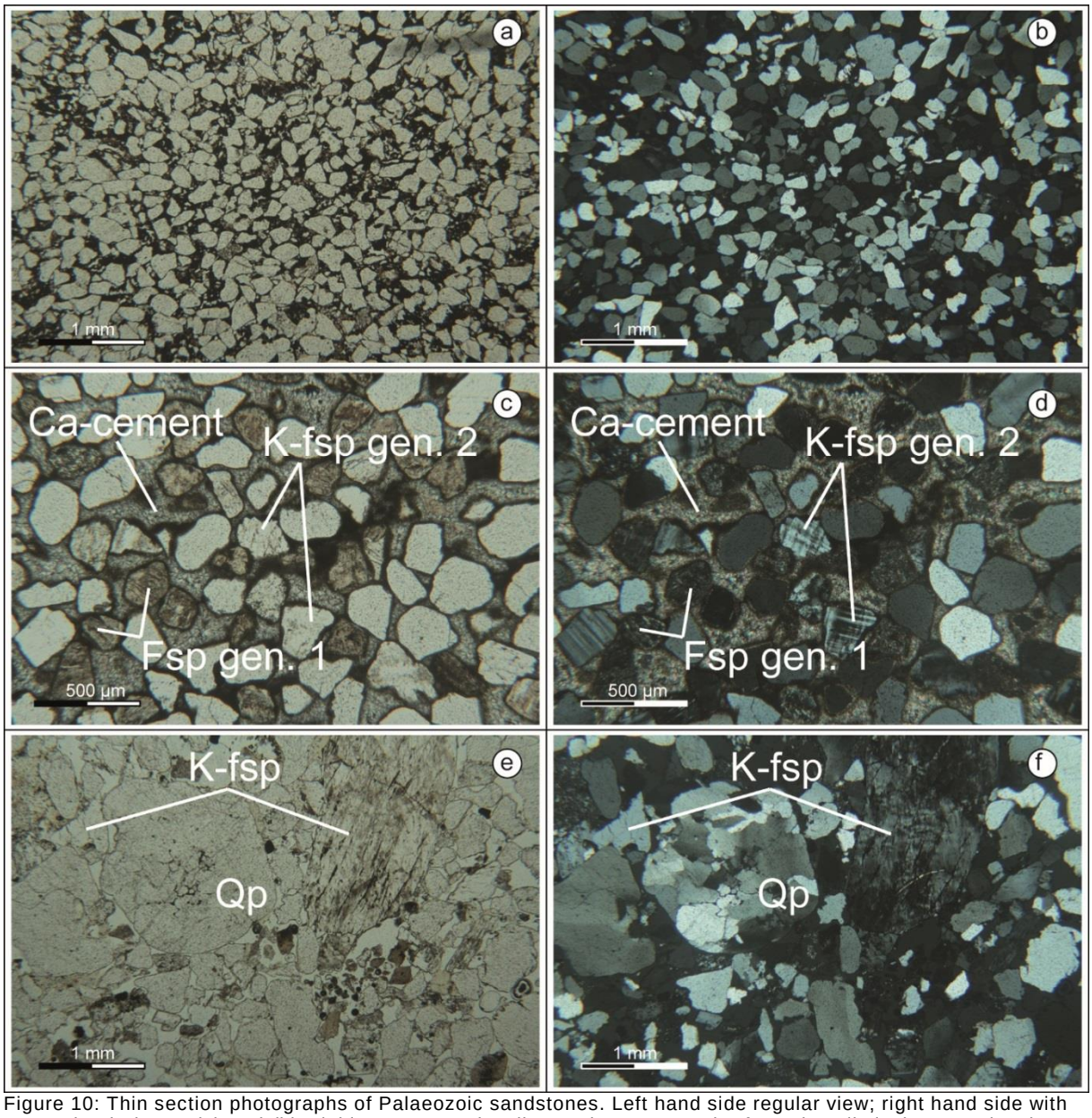

Figure 10: Thin section photographs of Palaeozoic sandstones. Left hand side regular view; right hand side with crossed polarisers. (a) and (b) Highly mature and well sorted quartz arenite from the Dibsiyah Formation (AB-SA79), typical for most of the Palaeozoic succession. (c) and (d) Arkose from the Juwayl Formation (AB-SA98) with strong calcitic cementation. 2 generations of feldspar are visible, displaying highly different degrees of weathering. (e) and (f) Poorly sorted subarkose from the Unayzah Formation (AB-SA120) with large grains of feldspar and Qp.

Table 4: Modal composition and framework mineralogy for Palaeozoic sandstones. Data was acquired by ribbon point counting of thin sections. Observed heavy minerals and accessories are listed under 'Accessories'; plus signs indicate abundance: + – present; ++ – abundant. bio – biotite; cpx – clinopyroxene; hbl – hornblende; olv – olivine; opx – orthopyroxene; px – pyroxene; rtl – rutile; trm – tourmaline; zrc – zircon; MI values are also given.

Sample	Formation	Classification	Qm	Qmu	Qp	Plag	Afsp	Lf	Pore	PMa+Cem	Total counts	Accessories	MI	GS	Sorting	Rounding
Tabuk area																
AB-SA 120	Unayzah	subarkose	84	65	33	10	22	0	53	33	300	+zrc, +rtl	0.85	mS	poor	subang.-rnd.
AB-SA 129	Unayzah	quartz arenite	91	107	2	6	0	0	79	15	300		0.97	mS	medium	subrnd.-rnd.
AB-SA 130	Unayzah	subarkose	66	155	5	13	3	0	52	6	300		0.93	mS	medium	subrnd.-rnd.
AB-SA 150	Jubah	subarkose	126	40	3	12	40	0	30	49	300	+rtl, +trm	0.76	fS	good	subang.-subroun.
AB-SA 152	Jubah	subarkose	131	64	3	10	23	0	58	11	300	+mica	0.86	mS	good	subang.-subrnd.
AB-SA 153	Jubah	arkose	133	42	1	2	54	0	46	22	300		0.76	mS	good	subang.-subrnd.
AB-SA 160/T	Jauf	arkose	74	72	2	10	64	0	28	50	300	+mica	0.67	fS	good	subang.-subrnd.
AB-SA 161	Jauf	arkose	83	75	5	8	39	0	39	51	300		0.78	mS	good	subang.-rnd.
AB-SA 164	Jauf	quartz arenite	90	75	13	0	0	0	5	117	300		1.00	mS	poor	rounded
AB-SA 154	Tawil	quartz arenite	200	80	11	0	0	0	9	0	300		1.00	mS	medium	subang.-subrnd.
AB-SA 156	Tawil	quartz arenite	79	115	1	0	0	0	54	51	300	++rtl, +zrc	1.00	mS	medium	subang.-rnd.
AB-SA 157	Tawil	subarkose	88	111	4	4	22	0	60	11	300	+zrc, +rtl	0.89	mS	medium	subrounded
AB-SA 128	Sharawra	arkose	56	77	3	53	7	0	22	56	300	+mica	0.69	cSi	good	subangular
AB-SA 127	Sharawra	arkose	74	62	1	41	5	0	23	58	300	+mica	0.75	cSi	good	subangular
AB-SA 132/2	Zarqa	subarkose	105	110	2	11	5	0	43	24	300	++zrc	0.93	fS	medium	subrounded
AB-SA 132/1	Zarqa	subarkose	93	56	1	9	2	0	10	129	300		0.93	fS	good	subangular
AB-SA 123/2	Sarah	quartz arenite	142	60	2	0	0	0	49	47	300		1.00	mS	poor	subang.-rnd.
AB-SA 122/2	Sarah	quartz arenite	99	94	17	2	1	0	76	11	300	+rtl, +zrc	0.99	fS	medium	subrnd.-rnd.
AB-SA 124	Qasim	quartz arenite	148	73	4	5	1	0	38	18	300	+mica	0.97	mS	good	subrounded
AB-SA 126	Qasim	subarkose	127	90	1	13	13	0	16	40	300	++zrc, +rtl	0.89	fS	good	subangular
AB-SA 145	Qasim	quartz arenite	93	94	36	1	0	2	45	29	300		0.99	mS	poor	subang.-rnd.
AB-SA 142/2	Qasim	quartz arenite	93	106	9	3	0	0	14	75	300		0.99	mS	poor	subang.-subrnd.
AB-SA 144/1	Qasim	quartz arenite	88	96	35	0	0	0	27	54	300	+rtl	1.00	mS	medium	subang.-subrnd.
AB-SA 170	Saq	quartz arenite	91	119	8	6	1	0	30	37	292		0.97	mS	medium	subrounded
AB-SA 167	Saq	quartz arenite	91	100	20	0	0	0	17	72	300	+rtl	1.00	mS	poor	subang.-subrnd.
AB-SA 169	Saq	quartz arenite	69	118	23	1	0	0	18	71	300		1.00	mS	medium	subang.-rnd.
Wajid area																
AB-SA 98	Juwayl	arkose	83	13	3	58	15	0	0	128	300		0.58	mS	good	subang.-subrnd.
AB-SA 80	Juwayl	quartz arenite	116	88	34	0	0	12	22	28	300	++zrc, +rtl,+ cpx, +titanite, +olv	0.95	mS	poor	subrnd.-rnd.
AB-SA 100	Juwayl	quartz arenite	127	59	11	0	0	0	62	41	300	++zrc	1.00	mS	medium	subrounded
AB-SA 87	Khusayyayn	subarkose	130	49	11	7	28	0	37	38	300	+mica, +zrc, +rtl	0.84	mS	good	subangular
AB-SA 89	Khusayyayn	subarkose	105	108	5	5	17	2	50	8	300	+rtl	0.90	mS	medium	subang.-subrnd.
AB-SA 90	Khusayyayn	subarkose	81	107	15	8	11	1	62	15	300	+mica, +opx, +zrc	0.91	mS	good	subang.-subrnd.
AB-SA 118	Khusayyayn	quartz arenite	67	121	39	5	0	0	51	17	300	+trm, +rtl	0.98	mS	medium	subrnd-well rnd.
AB-SA 32	Khusayyayn	quartz arenite	87	127	12	2	1	0	42	29	300	+mica	0.99	mS	medim	well rounded
AB-SA 115	Qusaiba	arkose	25	37	3	37	17	0	1	180	300		0.55	mS	poor	subangular
AB-SA 62	Sanamah	sublitharenite	74	96	28	1	4	18	58	21	300	+rtl, +zrc	0.90	mS	good	subrounded
AB-SA 63	Sanamah	quartz arenite	74	132	21	3	2	3	57	8	300	+zrc, +rtl, +bio	0.97	mS	poor	subrounded
AB-SA 64	Sanamah	quartz arenite	94	114	11	0	0	2	16	29	266	+px	0.99	mS	poor	subrounded
AB-SA 73	Sanamah	quartz arenite	75	135	5	0	0	0	50	35	300		1.00	fS	good	subang.-subrnd.
AB-SA 74	Dibsiyah	quartz arenite	95	132	10	6	0	0	47	10	300	+rtl, +zrc, +mica	0.98	mS	poor	subang.-subrnd.
AB-SA 76	Dibsiyah	quartz arenite	90	118	5	4	1	0	78	4	300	+zrc, +trm	0.98	mS	good	subangular
AB-SA 72	Dibsiyah	quartz arenite	123	34	24	0	1	0	10	59	300	++mica	0.99	mS	poor	subang.-subrnd.
AB-SA 69	Dibsiyah	quartz arenite	98	123	13	0	0	1	44	21	300	+bio, +zrc, +hbl, +mica	1.00	mS	poor	subrnd.-rnd.
AB-SA 79	Dibsiyah	quartz arenite	103	90	3	3	0	0	25	76	300		0.98	fS	good	subang.-subrnd.

5.2. Geochemistry

Due to the sample preparation procedure using a disc mill with a tungsten carbide set for grinding, the ground powder was contaminated with tungsten (W) and cobalt (Co). In consequence, these elements are not shown in any of the diagrams. Major and trace element concentrations of all analysed 44 samples are provided in Table A3 and Table A4 (annex). Note that some samples from both literature and this study show zero percent concentrations of some major elements (MgO, MnO, Na_2O, P_2O_5 and TiO_2). In order to allow calculation of the K_2O/Na_2O ratio and the discriminant functions of Verma and Armstrong-Altrin (2013), which rely on log ratios, those samples had these respective element concentrations set to 0.0001%. This allows the inclusion of those samples, but in the case of the K_2O/Na_2O ratio vs. SiO_2 diagram slightly exaggerates the 'vertical spread' of the sample population. However it has no influence on the behaviour of sample points near the field boundaries. Some samples revealed an intensive carbonatic cementation in thin section (Figure 10c, d). These samples have been excluded from most plots and calculations that include major elements, but are shown in Figures Figure 11 and Figure 12 for comparison.

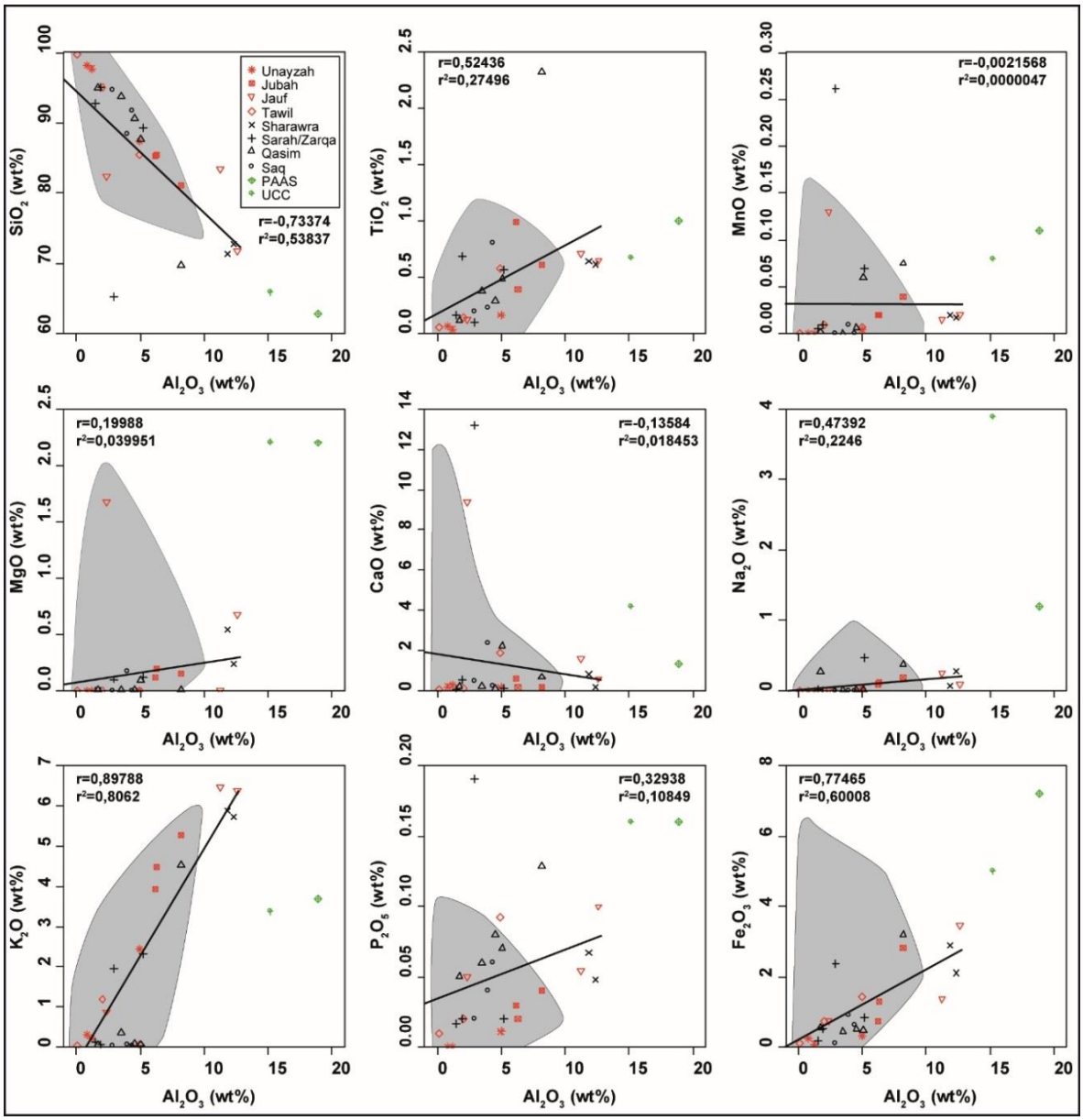

Figure 11: Major elements concentrations plotted against Al_2O_3 concentration for samples from the Tabuk area. Data for PAAS (from Taylor and McLennan, 1985) and UCC (from McLennan, 2001; Taylor and McLennan, 2009) were also plotted for comparison. The grey area represents the range of literature data (data from Al-Harbi and Khan, 2005, 2008, 2011; Hussain, 2007).

5.3. Major elements

Major element concentrations have been normalised against Al_2O_3 since Al can be regarded as immobile during weathering, diagenesis and metamorphic processes (Cardenas et al. 1996; Bauluz et al. 2000). Major oxides were plotted against Al_2O_3 in Figure 11 (Tabuk area) and Figure 12 (Wajid area). Values for the average Upper Continental Crust (UCC) and the Post-Archean Australian Shale (PAAS) after Taylor and McLennan (1985), McLennan (2001) and Taylor and McLennan (2009) have been added for comparison. Major element abundances reflect the lithologies and the high maturity of most analysed samples. SiO_2 concentrations are high (71.43% to 99.8%) in most sandstones. SiO_2/Al_2O_3 values are low in samples from the Qusaiba (5.69) and Sharawra members (5.89; 6.02) as well as three micaceous sandstones of the Dibsiyah (6.84) and Jauf (5.89; 6.02) formations. MgO and CaO show no correlation with Al_2O_3 and concentrations are low in most samples, well below the average UCC and PAAS. Three samples show high CaO/Al_2O_3 values (4 to 6.92), which is caused by strong calcitic cementation. Samples from the Wajid area are almost completely MgO-free, with one exception from the Qusaiba Member. Samples from the Tabuk area show low MgO concentrations. Elevated MgO abundances in samples from the Tawil Formation are due to intense dolomitic cementation. K_2O concentrations are well below the UCC and PAAS averages in samples from the Wajid area and only slightly elevated in the Khusayyayn Formation. The Qusaiba Member has a K_2O/Al_2O_3 value close to the UCC. In contrast, samples from the Jauf and Jubah formations from the Tabuk area show significantly higher K_2O concentrations. K_2O abundance in sandstones is mainly controlled by the presence of K-feldspar, K-mica and glauconite (Wedepohl, 1978). Elevated K_2O concentrations in the Jauf and Jubah formations reflect their modal composition, which is concordant to an increased abundance of K-feldspar in thin sections. The high K_2O concentration in the Qusaiba Member (3.48%) is probably primarily caused by clay minerals in the matrix, because the dominant feldspar is plagioclase. Na_2O is almost absent in most samples, but slightly more abundant in the Tabuk area. TiO_2 concentrations are very low in Wajid area samples. Concentrations in the Tabuk area are higher with a significantly larger spread and are linked to biotite and rutile. The extremely high TiO_2 content of sample AB-SA126 (2.33%; Qasim Formation) is caused by rutile from a heavy mineral placer deposit. The sample has correspondingly increased concentrations of trace elements (Zr, Th, Y, and REEs like La, Ce, Sm, Gd, Tb and Dy), which are indicative for other heavy minerals like zircon and monazite. TiO_2 from Juwayl Formation samples stems from Ti-rich augite. In samples from the Wajid area, SiO_2 shows a strong negative, TiO_2 and P_2O_5 a strong positive correlation with Al_2O_3. MgO, Na_2O, K_2O and Fe_2O_3 correlate weakly with Al_2O_3, while MnO and CaO exhibit no correlation. Samples from the Tabuk area display a strong negative correlation of Al_2O_3 with SiO_2, strong positive correlations with K_2O and Fe_2O_3 as well as weak positive correlations with TiO_2, Na_2O and P_2O_5. There is no correlation of Al_2O_3 and MnO, MgO and CaO. Strong positive correlations of K_2O, P_2O_5, Fe_2O_3 and TiO_2 with Al_2O_3 indicate association with micaceous/clay minerals. CaO and MgO show no or weak correlations and originate mainly from carbonatic cement (Das et al., 2006). Na_2O and K_2O concentrations and their ratios ($Na_2O/K_2O<1$) are consistent with the petrographic observation of alkali-feldspar as the dominant feldspar. Overall, the Wajid area samples show very similar major element abundances and are geochemically more mature (higher SiO_2 concentration) than samples from the Tabuk area. Major element concentrations except K_2O of samples from the Jauf and Jubah formations and SiO_2 are all lower than the average values for the UCC and PAAS, confirming the petrographic observation of high sediment maturity.

Table 5: Correlation matrix of selected major and trace elements. Major elements are given as oxides in weight-%, trace elements and ΣREEs in ppm. Correlation coefficients discussed in the text are highlighted; yellow – weak positive correlation, green – strong positive correlation.

	Cs	Rb	Ba	Sr	Th	U	Y	Zr	Hf	Nb	Ta	Sc	Cu	Ni	ΣREE	ΣLREE	ΣHREE	SiO_2	TiO_2	Al_2O_3	P_2O_5
Cs	1																				
Rb	0.93232	1																			
Ba	0.86352	0.91209	1																		
Sr	0.61864	0.60617	0.55408	1																	
Th	0.36228	0.46015	0.43494	0.33546	1																
U	0.33097	0.42794	0.40041	0.29145	0.94858	1															
Y	0.55845	0.60522	0.57368	0.46958	0.92004	0.87548	1														
Zr	0.36660	0.44927	0.43521	0.32806	0.97783	0.91141	0.90073	1													
Hf	0.35582	0.43734	0.42352	0.31952	0.97952	0.91455	0.90014	0.99968	1												
Nb	0.58689	0.67940	0.67520	0.47934	0.92105	0.86681	0.94144	0.89169	0.88887	1											
Ta	0.26179	0.40259	0.34021	0.17946	0.37850	0.33111	0.41276	0.30573	0.30684	0.48497	1										
Sc	0.68559	0.73975	0.61877	0.60709	0.72079	0.71391	0.83835	0.70373	0.69823	0.83112	0.48247	1									
Cu	-0.06862	-0.11852	0.01450	-0.23928	0.02449	0.01401	-0.06665	0.00875	0.01406	-0.03069	0.00794	-0.12299	1								
Ni	0.86509	0.73252	0.61946	0.47500	0.38430	0.40113	0.53928	0.38372	0.37829	0.52110	0.12938	0.68400	-0.01637	1							
ΣREE	0.41594	0.50616	0.47591	0.47457	0.96874	0.92353	0.93187	0.94085	0.94145	0.93751	0.38103	0.79036	-0.03696	0.41996	1						
ΣLREE	0.40776	0.49971	0.46970	0.47287	0.96805	0.92279	0.92688	0.93980	0.94047	0.93450	0.37907	0.78584	-0.03590	0.41270	0.99990	1					
ΣHREE	0.55954	0.61245	0.57872	0.48921	0.94417	0.90188	0.99295	0.92448	0.92375	0.95958	0.40437	0.84764	-0.05606	0.54541	0.96269	0.95885	1				
SiO_2	-0.66088	-0.60993	-0.58770	-0.71492	-0.31819	-0.30164	-0.49497	-0.29367	-0.28726	-0.45878	-0.11733	-0.60219	0.10990	-0.54374	-0.39147	-0.38588	-0.48538	1			
TiO_2	0.52043	0.62347	0.58986	0.41265	0.92540	0.85543	0.90161	0.93007	0.92505	0.94974	0.38237	0.77851	-0.09556	0.48353	0.90961	0.90711	0.92290	-0.37454	1		
Al_2O_3	0.77581	0.79077	0.73951	0.62127	0.30787	0.28023	0.51968	0.30277	0.29118	0.59880	0.26877	0.71954	-0.11640	0.61050	0.44296	0.43763	0.52970	-0.64649	0.53059	1	
P_2O_5	0.19558	0.25201	0.21427	0.39071	0.12920	0.12601	0.22370	0.16833	0.15784	0.24302	0.23030	0.36984	-0.31583	0.11841	0.22906	0.22868	0.22748	-0.20437	0.23926	0.36145	1

5.4. Trace elements

Selected trace element concentrations have been normalised against UCC values and are shown as spider plots in Figure 13 (Tabuk area) and Figure 14 (Wajid area). A correlation matrix of trace elements and some major oxides is provided in Table 5 (n=41).

5.4.1. Large-ion lithophile elements (LILE): Rb, Ba, Sr, Cs

LILEs are relatively mobile and incompatible elements and are thus enriched in the UCC compared to the mantle. Mean LILE concentrations of Wajid area samples are well below the values for the UCC. The Lower Wajid is especially depleted in Cs, Rb and Ba. The Silurian Qusaiba Member is less depleted in Cs and Rb compared to the Dibsiyah and Sanamah formations, and even enriched in Ba compared to the UCC. LILEs in the Khusayyayn and Juwayl formations are less depleted than in the Dibsiyah and Sanamah formations and samples show a large scatter. The Devonian Jauf and Jubah formations as well as the Silurian Sharawra Member from the Tabuk area show very little scatter and have approximately UCC concentrations of LILEs. The rest of the Tabuk samples show a large sample scatter and low LILE concentrations. Cs, Rb and Ba show a weak positive correlation with Al_2O_3 (Table 5). This may indicate phyllosilicates as a controlling factor of LILE concentrations (Etemad-Saeed et al., 2011). Variability and depletion of LILEs may be due to mobility during weathering, diagenesis and metamorphic processes (Wronkiewicz and Condie, 1987).

5.4.2. High field strength elements (HFSE): Th, U, Y, Zr, Hf, Nb, Ta

HFSEs are incompatible but immobile elements. They are enriched in felsic rather than mafic rocks (Bauluz et al., 2000). Due to their immobile nature they are regarded as provenance indicators (Taylor and McLennan, 1985). Zr and Hf behave similarly as is evidenced by their very high correlation coefficient (r=1.00; Table 5). Zr and Hf concentrations in rocks are mainly controlled by the heavy mineral zircon. This is supported by Zr/Hf ratios mostly between 35 and 40, similar to values reported for zircons by Murali et al. (1983). Furthermore, Zr shows strong positive correlations with REEs (r=0.94) suggesting that REEs are controlled by zircon abundances (Bauluz et al., 2000). The mean concentration of Zr in Wajid samples is depleted compared to the average UCC, except in the Dibsiyah Formation and the Qusaiba Member, which have approximately UCC Zr concentrations. In the Tabuk area, Zr is enriched except for the Saq, Tawil and Unayzah formations. One outlier sample from the Qasim Formation is highly enriched in Zr. This sample is probably from a heavy mineral placer deposit. Th and U concentrations are close to UCC values in both study areas, but are slightly depleted in both the Juwayl and Unayzah formations. Th and U exhibit a strong positive correlation between each other (r=0.95) and also towards Zr (r=0.98 and r=0.91, respectively), TiO_2 (r=0.93 and r=0.86, respectively) and REEs, which indicates that Th and U concentrations are controlled by heavy mineral abundances. Y has a lower concentration than the average UCC in southern Saudi Arabian samples, except for outliers from the Dibsiyah Formation and Juwayl Formation. In the Tabuk area, Y abundance is comparable to the UCC in the Sharawra Member and the Jauf, Jubah and Saq formations and in one outlier from the Qasim Formation. In the Satah, Zarqa, Tawil and Unayzah formations, Y is depleted in regards to the average UCC. Controlling phases for Y abundance are probably rutile and monazite rather than xenotime because of strong positive correlations with TiO_2 (r=0.90) and REEs (r=0.93) but a low correlation coefficient with P_2O_5 (r=0.49). Nb has a strong positive correlation with Y (r=0.94).

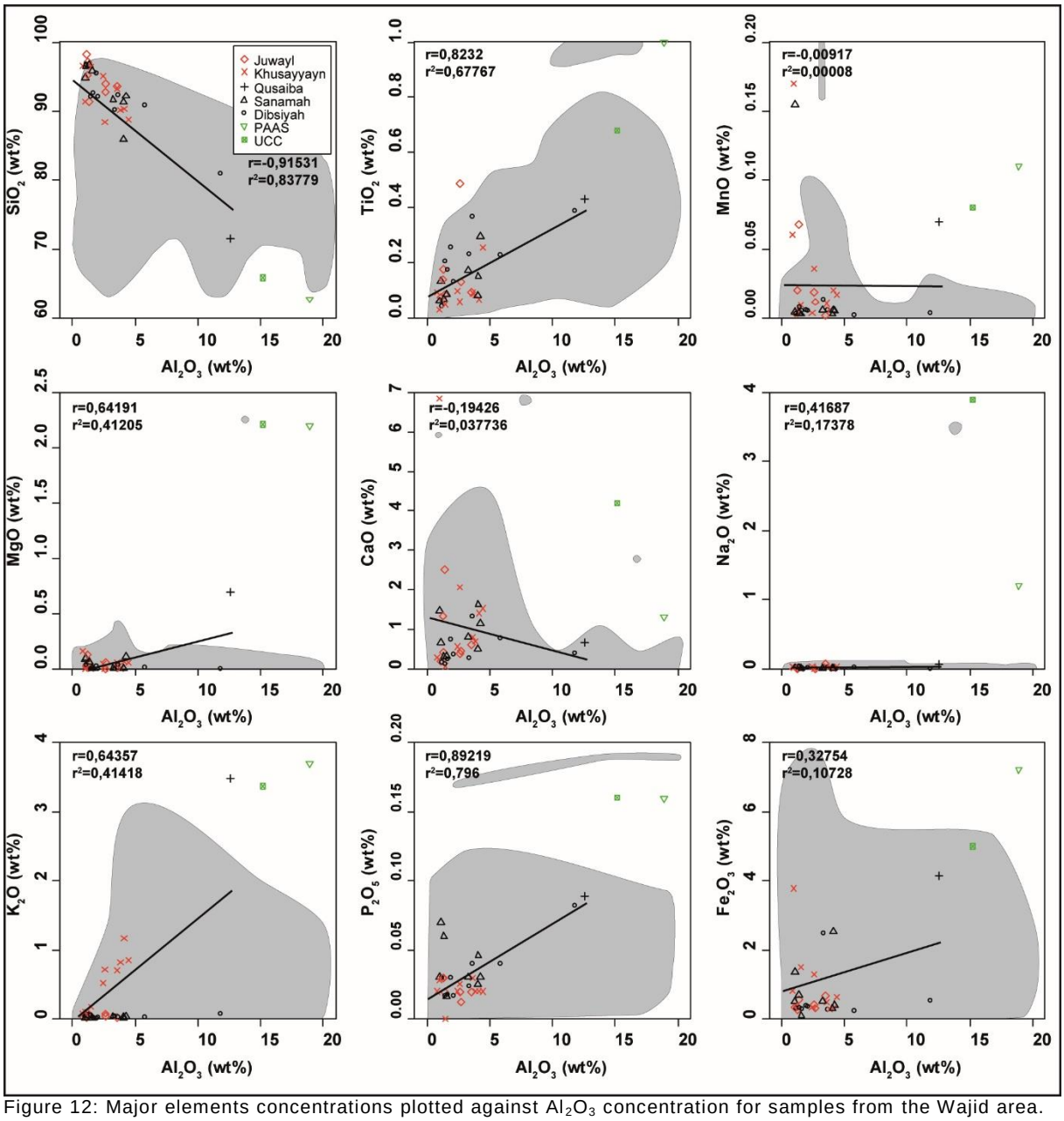

Figure 12: Major elements concentrations plotted against Al_2O_3 concentration for samples from the Wajid area. Data for PAAS (from Taylor and McLennan, 1985) and UCC (from McLennan, 2001; Taylor and McLennan, 2009) were also plotted for comparison. The grey area represents the range of literature data (from Hussain, 2001, 2007).

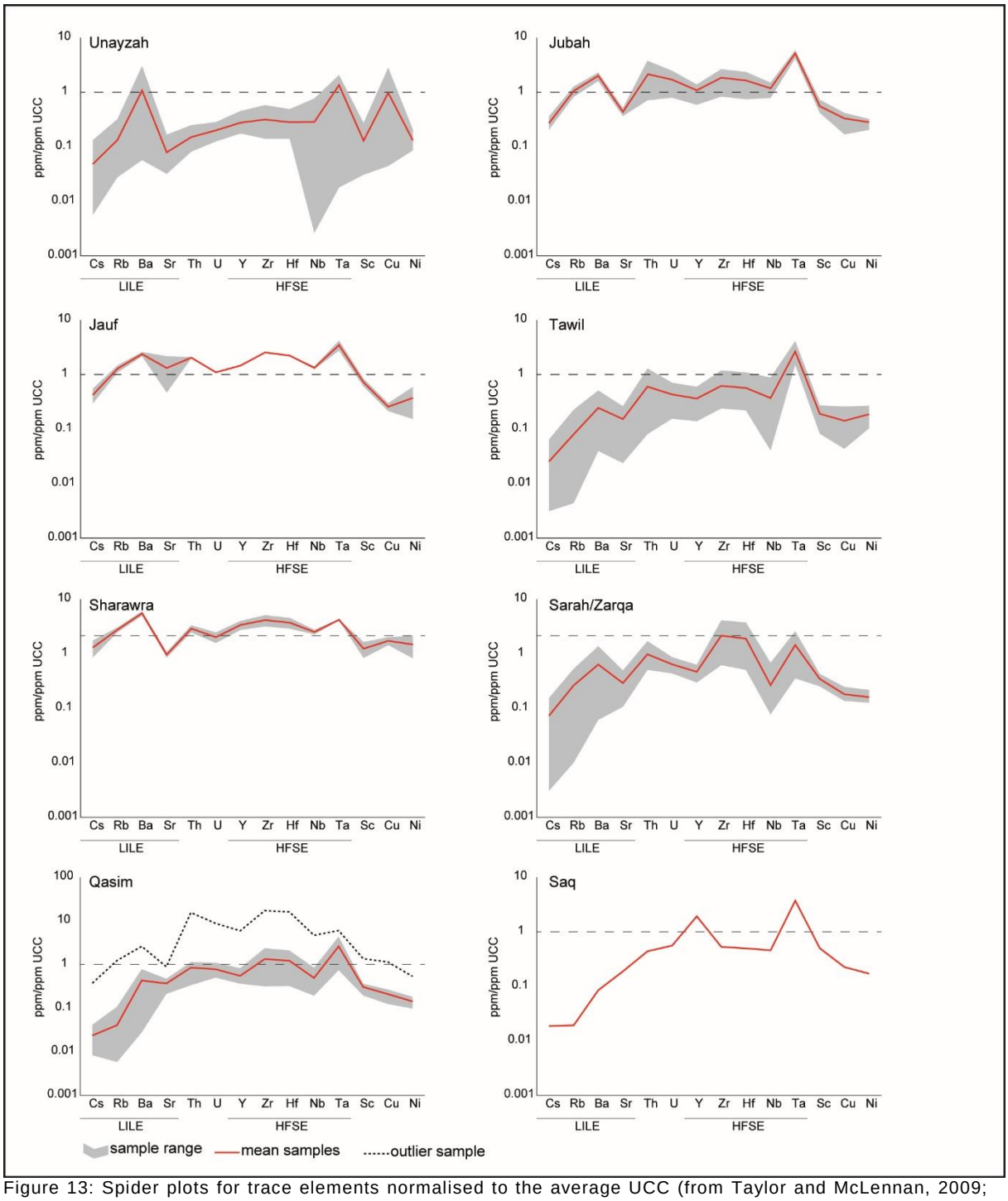

Figure 13: Spider plots for trace elements normalised to the average UCC (from Taylor and McLennan, 2009; McLennan, 2001) for samples from the Tabuk area. The solid red line represents the mean of samples, the dotted lines are outliers and the grey area represents the sample range without outliers.

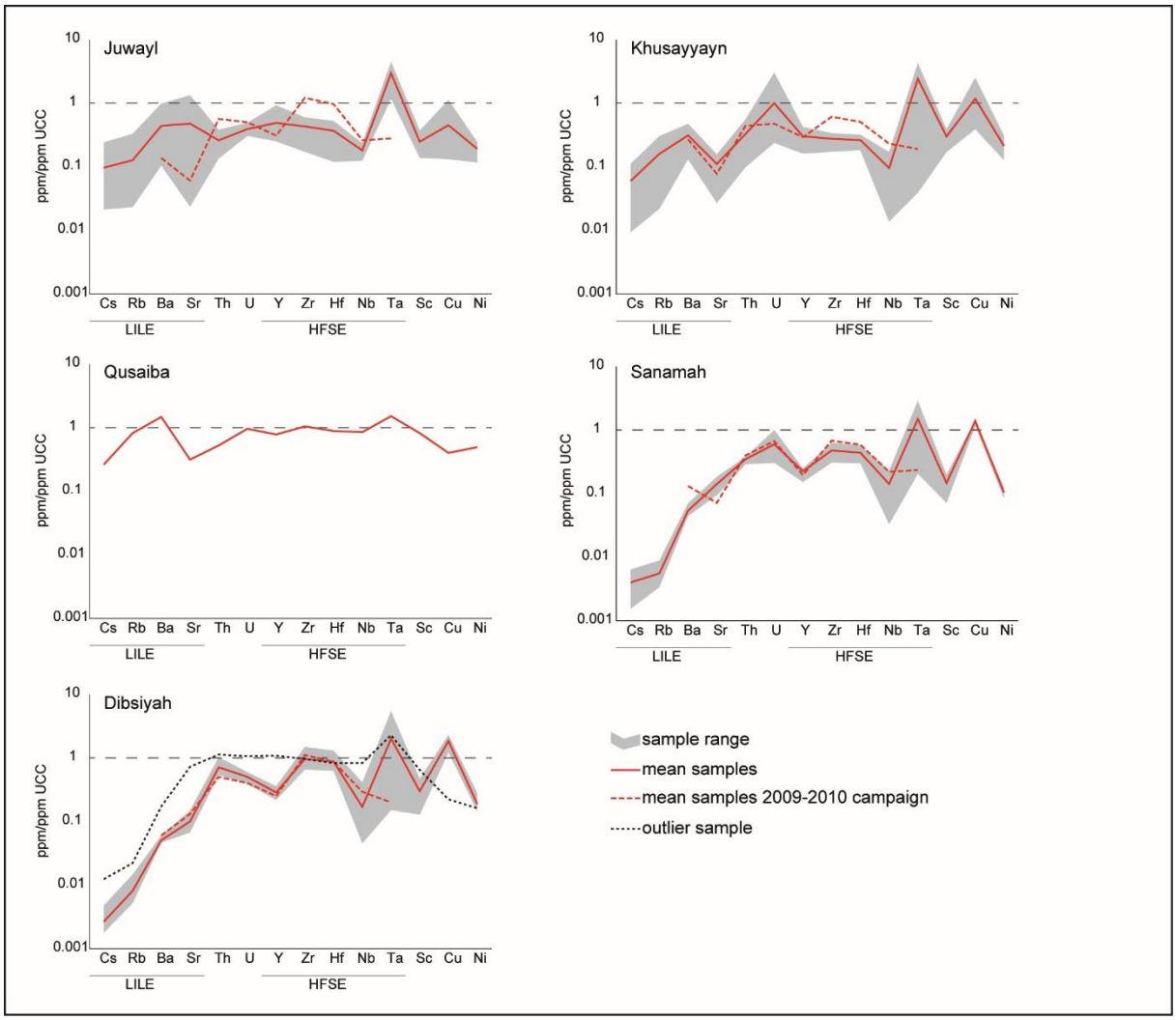

Figure 14: Spider plots for trace elements normalised to the average UCC (from Taylor and McLennan, 2009; McLennan, 2001) for samples from the Wajid area. The solid red line represents the mean of samples, the dotted lines are outliers, the dashed red line are samples from the 2009-2010 campaigns and the grey area represents the sample range without outliers.

5.4.3. Transition trace elements (TTE): Sc, Cu, Ni

Sc and Ni are depleted compared to the UCC in both study areas. Cu concentrations are comparable to the UCC in most samples from the Wajid and Tabuk areas, with the exception of the Silurian and Permian. No strong correlations between Cu and Ni and selected major elements have been observed. Sc correlates weakly positive with Al_2O_3 (r=0.72), TiO_2 (r=0.78), Zr (r=0.70) and the (heavy) REEs (r=0.79; r=0.85 for HREEs) (see Table 5). This may indicate phyllosilicates and heavy minerals as controlling factors for Sc concentrations (Etermad-Saeed et al., 2011).

5.4.4. Rare earth elements (REE): La, Ce, Pr, Nd, Sm, Eu, Gd, Tb, Dy, Ho, Er, Yb

The average total REE concentration (ΣREE) in Wajid sandstones is 46.87 ppm, much lower than the average PAAS (183.93 ppm) and UCC (145.72 ppm) concentrations. This is excluding two outlier samples – one from the Qusaiba Member (ΣREE=113.58 ppm) and one from the Dibsiyah Formation (ΣREE=367.19 ppm). In contrast, the Khusayyayn Formation hosts a sample with very low REE concentrations (ΣREE=15.88 ppm). ΣREE concentrations are higher in samples from the Tabuk area than in the Wajid area, with an average concentration of 124.76 ppm. The average value is excluding one outlier sample from the Qasim Formation, which is extremely enriched in REEs (ΣREE=1332.86 ppm). Two samples from the Tawil and Unayzah formations have very low total REE concentrations (ΣREE=18.85 ppm; ΣREE=27.17 ppm). REEs have been chondrite-normalised after McDonough and Sun (1995) and plotted in Figure 15 (Tabuk area) and Figure 16 (Wajid area).

CI-normalised REE patterns are similar to the PAAS and UCC with enriched LREEs, flat HREEs and a pronounced negative Eu anomaly. The latter was calculated according to McLennan (1989):

$$\frac{Eu}{Eu^*} = \frac{Eu_N}{(Sm_N * Gd_N)^{0.5}} \qquad \text{(equation 3)}$$

where the subscript N denotes chondrite-normalised values. In contrast, samples from the Sharawra Member as well as Sarah, Zarqa and Saq formations show 'rising' HREE patterns. Like other lanthanides, Eu is an incompatible element, but is preferentially incorporated into plagioclase. As a result, the average UCC exhibits Eu depletion through fractionation effects, leading to an Eu anomaly of Eu/Eu*=0.65. In samples from both study areas, the Eu anomaly is negative (Eu/Eu*<1), but more pronounced in the Tabuk area. There the mean and median Eu/Eu* is lower than the PAAS and UCC, whereas in samples from the Wajid area the Eu/Eu* values are slightly higher. The $(La/Yb)_c$ value, which describes the total slope of the CI-normalised REE trend, is lower than the UCC in most Upper Wajid samples and the Qusaiba Member, but higher in the Cambrian–Ordovician samples. It is also much more variable in the Tabuk area, where no clear distinction between formations could be established. The LREE slope, represented by the $(La/Sm)_c$ value, is lower than or close to values of the UCC in most Wajid samples. Only two samples from the Sanamah Formation show higher $(La/Sm)_c$ than the UCC. This is mirrored in the Tabuk area. HREE patterns, as delineated by $(Gd/Yb)_c$ values, are similar to the UCC in both study areas with no clearly discernible trends. A weak positive correlation between $(La/Sm)_c$ and P_2O_5 indicates the LREE abundances to be at least partially controlled by phosphates. Other controlling factors could not be ascertained, as there are no correlations between Eu/Eu*, $(La/Yb)_c$, $(La/Sm)_c$, $(Gd/Yb)_c$ and any other major element or Zr, Th and U (see Table 6).

Table 6: Correlation matrix of selected major elements, Zr, Th, U and selected REE-ratios. Major elements are given as oxides in weight-%, trace elements in ppm. Correlation of $(La/Sm)_c$ with P_2O_5 is highlighted.

	SiO_2	TiO_2	Al_2O_3	MnO	MgO	CaO	Na_2O	K_2O	P_2O_5	Fe_2O_3t	Zr	Th	U	Eu/Eu*	$(La/Yb)_c$	$(La/Sm)_c$	$(Gd/Yb)_c$
SiO_2	1																
TiO_2	-0.37454	1															
Al_2O_3	-0.64649	0.53059	1														
MnO	-0.55256	0.06304	0.03681	1													
MgO	-0.65801	-0.08815	0.09820	0.29307	1												
CaO	-0.61780	-0.16412	-0.06903	0.84475	0.62833	1											
Na_2O	-0.46546	0.54196	0.41289	0.20385	0.32396	0.08720	1										
K_2O	-0.59493	0.57534	0.79990	0.14980	0.10303	-0.00286	0.56754	1									
P_2O_5	-0.61210	0.46394	0.48576	0.56912	0.00384	0.42497	0.16538	0.34127	1								
Fe_2O_3t	-0.58288	0.39904	0.56170	0.49202	0.07856	0.25985	0.26587	0.56363	0.52621	1							
Zr	-0.29367	0.93007	0.30277	0.12049	-0.07070	-0.10444	0.49622	0.38160	0.40952	0.32184	1						
Th	-0.31819	0.92540	0.30787	0.13547	-0.05634	-0.07266	0.47889	0.39290	0.42563	0.34095	0.97783	1					
U	-0.30164	0.85543	0.28023	0.25957	-0.07082	0.00365	0.43418	0.35361	0.40076	0.47083	0.91141	0.94858	1				
Eu/Eu*	-0.18995	-0.41206	0.09646	0.13610	0.13320	0.21272	-0.08434	-0.00657	0.00366	-0.00066	-0.37076	-0.36542	-0.33188	1			
$(La/Yb)_c$	0.04259	0.09170	0.06128	0.06807	-0.25048	-0.02174	-0.14648	-0.10952	0.37084	-0.15064	0.08543	0.13852	0.08320	-0.02710	1		
$(La/Sm)_c$	-0.17093	0.13621	0.08360	0.30501	-0.23590	0.18180	0.00185	0.15544	0.54593	0.01052	0.12347	0.07448	-0.06722	0.04743	0.42341	1	
$(Gd/Yb)_c$	0.14592	-0.00302	-0.03619	-0.04468	-0.11415	-0.07055	-0.16736	-0.17426	0.04533	-0.14941	0.00822	0.08814	0.11499	-0.10429	0.79788	-0.11464	1

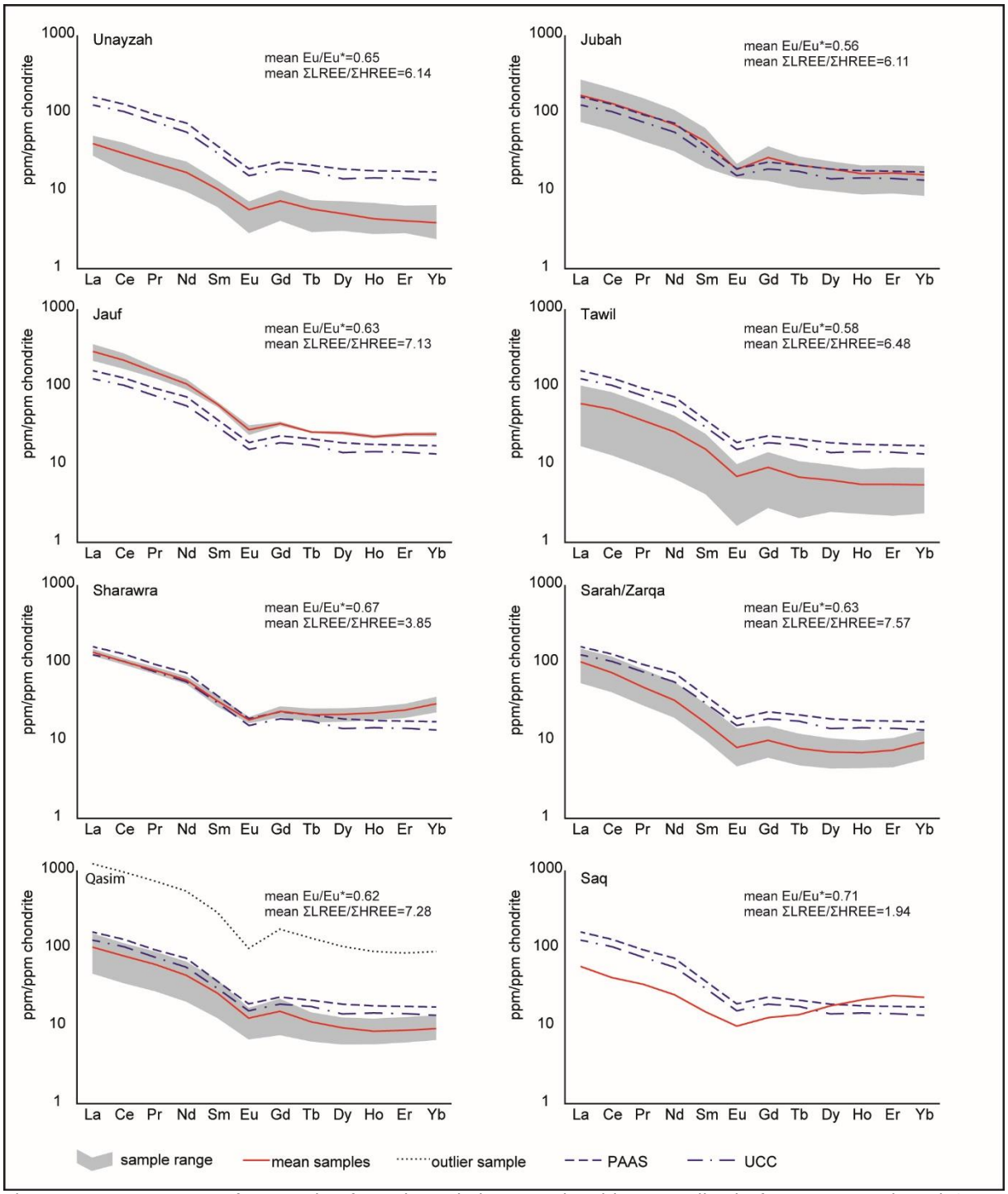

Figure 15: REE patterns for samples from the Tabuk area, chondrite-normalised after McDonough and Sun (1995). The solid red line represents the mean of samples, the dotted black line is an outlier and the grey area represents the sample range without outliers. Patterns for PAAS (blue dashed line; from Taylor and McLennan, 1985) and UCC (blue dashed and dotted line; from McLennan, 2001; Taylor and McLennan, 2009) have also been plotted for comparison.

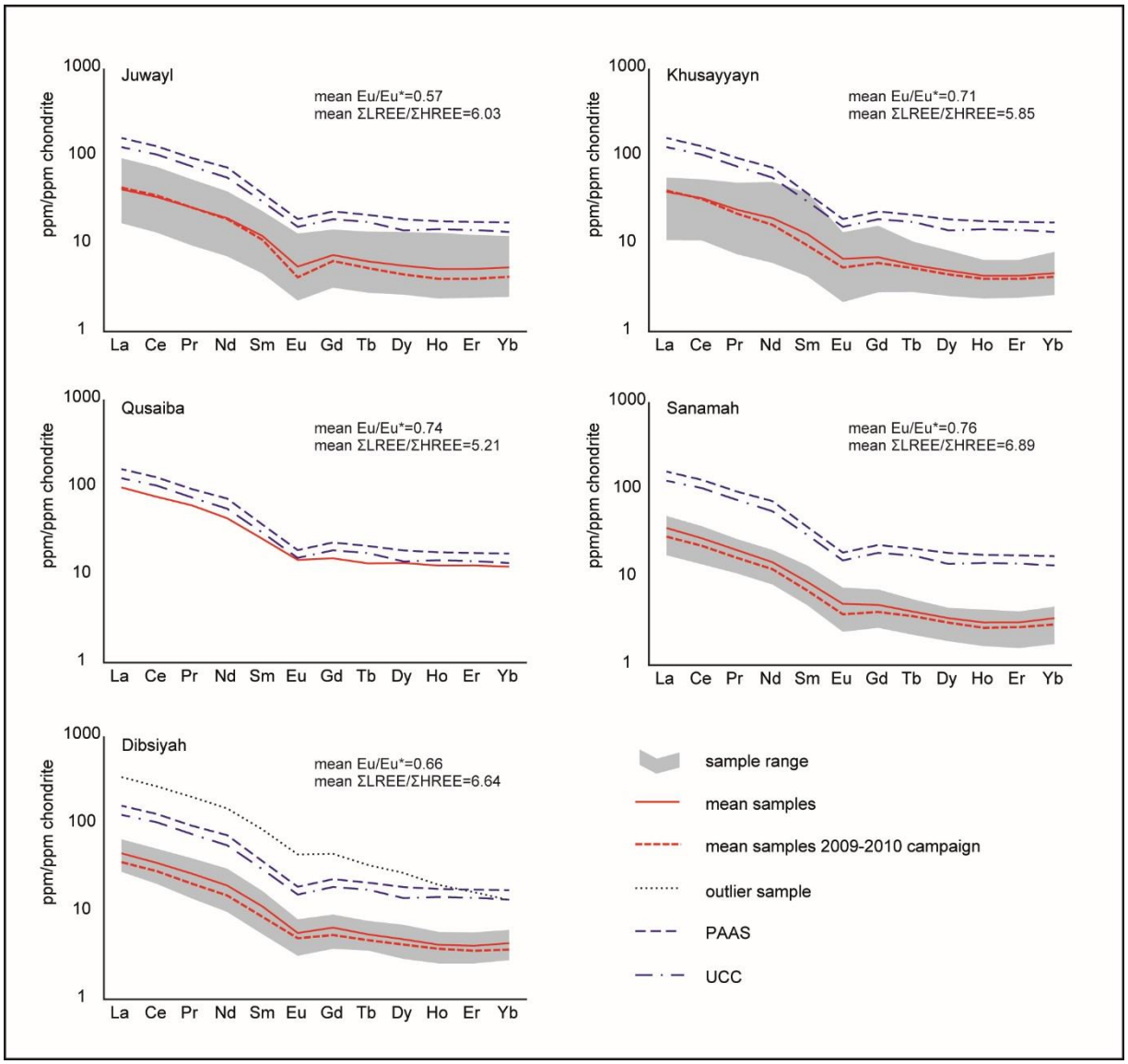

Figure 16: REE patterns for samples from the Wajid area, chondrite-normalised after McDonough and Sun (1995). The solid red line represents the mean of samples, the dotted black line is an outliers and the grey area represents the sample range (without the outlier). The dashed red line represents the mean of samples from the 2009-2010 field campaigns. Patterns for PAAS (blue dashed line; from Taylor and McLennan, 1985) and UCC (blue dashed and dotted line; from McLennan, 2001; Taylor and McLennan, 2009) have also been plotted for comparison.

5.5. Standard heavy mineral analysis

Results of SHMA are shown in Figure 17 and Table 7. They are presented as averages for each formation. From each the Unayzah Formation and Qusaiba Member only one sample was counted. The ratio of opaque phases to translucent heavy minerals is between 58% and 84%. Single samples have very high opaque amounts up to 97%. The heavy mineral suites of the Palaeozoic successions from both study areas are dominated by the ultra-stable set of zircon, tourmaline and rutile. Among the ultra-stables, zircon is the most abundant phase in most samples, followed by tourmaline, while rutile is the least abundant of the three. Mean zircon concentrations across formations are between 30% (Sharawra Member) and 62% (Sanamah Formation). Most of the encountered zircons were rounded (Figure 18a). Some euhedral zircons were observed, but they seemed to be evenly distributed throughout all formations (Figure 18b). Because most zircons were rounded, it was not possible to identify the zircon classes after Pupin (1980) or measure the elongation ratio after Poldervaart (1955, 1956) and Hoppe (1963). Zircons were mostly colourless with only very few having a slight yellowish tint. The second most abundant phase encountered is tourmaline with mean concentrations of 17% (Juwayl Formation) to 46% (Qasim Formation). Tourmaline was encountered as both rounded and prismatic grains (Figure 18d). Mean concentrations of rutile reach between 4% in the Juwayl Formation and a maximum of 12% in the Sarah and Zarqa formations. All rutiles were rounded and no prismatic grains were found (Figure 18c). Apatite is roughly equally distributed among all formations, never amounting to more than 8% average translucent grains. Two samples are a striking exception, both from the Wajid area: The single sample from the Qusaiba Member and one from the Khusayyayn Formation contain comparatively high amounts of apatite (17% and 26%, respectively). Apatite, when encountered, was always well rounded (Figure 18e, upper row).

Garnet occurs in significant amounts only in middle to upper Palaeozoic samples from the Tabuk area, from the Devonian Tawil Formation and younger. In the Wajid Group, garnet is less abundant. Only a couple of grains were found in all but one sample. Yet in this sample (AB-SA98) garnet was the dominant phase, amounting 54% of all translucent grains. Garnets appeared weathered, but still angular. No prismatic grains were observed (Figure 18f).

Staurolite appears mostly in the Juwayl and Khusayyayn formations of the Wajid area, where it reaches an average abundance of 10% and 8%, respectively. Staurolite is almost absent in samples of the Tabuk area. Only four formations (Saq, Sarah/Zarqa combined, Jubah and Unayzah) contain any at all and only the Unayzah sample in a significant amount (12%). Grains appear weathered but still sharply angular (Figure 18e, lower row), like the encountered garnet.

Other heavy minerals found in very small quantities encompass: monazite, kyanite, enstatite, epidote, tremolite, chromite, sphene and hornblende. They are rare and their combined share never exceeds 6.3% at the most, with the majority of samples containing between 0% and 3%.

The last encountered group of heavy minerals are altered grains. This class contains all translucent heavy minerals that are altered through overgrowths or diagenetic effects to the point where they could no longer be identified.

The different heavy mineral indices used in this study are shown in Table 2 and have been plotted in their inferred stratigraphical order in Figure 19.

What has to be considered when interpreting or searching for trends is the stratigraphic uncertainty. As stated before, correlations are difficult in the highly mature Palaeozoic succession of Saudi Arabia. While the samples have been arranged carefully, their exact order is by no means certain. Additionally the timescale between formations and samples varies significantly. All this can mask or create apparent trends in the data and has to be considered for interpretation.

Table 7: Heavy mineral composition and heavy mineral indices of Palaeozoic sandstones. LT=Lower Tabuk, UT= Upper Tabuk, LW=Lower Wajid, UW=Upper Wajid, Zrc=zircon, Trm=tourmaline, Rtl=rutile, Apt=apatite, Grt=garnet, Stl=staurolite, Alt=altered, Mzt=monazite, Ky=kyanite, En=enstatite, Epd=epidote, Trem=tremolite, Chr=chromite, Sph=sphene.

Sample	Formation	Area	Zrc	Trm	Rtl	Apt	Grt	Stl	Alt	Mzt	Ky	En	Epd	Trem	Chr	Sph	Total	Opq%	ZTR	RZi	GZi	ATi	STi
Tabuk area																							
AB-SA120	Unayzah	UT	59.67	16.33	5.33	1.33	3.67	12.00	1.67	0.00	0.00	0.00	0.00	0.00	0.00	0.00	300	86.50	81.33	8.21	5.79	7.55	42.35
AB-SA150	Jubah	UT	31.67	37.00	8.67	4.33	7.67	0.00	5.67	0.00	0.00	5.00	0.00	0.00	0.00	0.00	300	75.50	77.33	21.49	19.49	10.48	0.00
AB-SA152	Jubah	UT	60.33	16.33	10.33	4.33	4.33	3.33	1.00	0.00	0.00	0.00	0.00	0.00	0.00	0.00	300	67.00	87.00	14.62	6.70	20.97	16.95
AB-SA153	Jubah	UT	29.00	33.33	4.67	0.67	17.00	0.00	9.00	0.67	0.00	3.33	2.33	0.00	0.00	0.00	300	90.00	67.00	13.86	36.96	1.96	0.00
AB-SA160/T	Jauf	UT	45.67	42.67	11.33	0.00	0.00	0.00	0.00	0.33	0.00	0.00	0.00	0.00	0.00	0.00	300	56.00	99.67	19.88	0.00	0.00	0.00
AB-SA161	Jauf	UT	51.33	31.67	9.33	4.67	0.00	0.00	2.67	0.33	0.00	0.00	0.00	0.00	0.00	0.00	300	86.50	92.33	15.38	0.00	12.84	0.00
AB-SA164	Jauf	UT	50.67	19.00	13.00	1.67	14.67	0.00	1.00	0.00	0.00	0.00	0.00	0.00	0.00	0.00	300	47.00	82.67	20.42	22.45	8.06	0.00
AB-SA156	Tawil	UT	56.00	24.67	7.33	1.33	4.33	0.00	5.00	1.33	0.00	0.00	0.00	0.00	0.00	0.00	300	62.00	88.00	11.58	7.18	5.13	0.00
AB-SA157	Tawil	UT	46.00	42.33	9.33	0.33	0.00	0.00	0.67	1.33	0.00	0.00	0.00	0.00	0.00	0.00	300	42.00	97.67	16.87	0.00	0.78	0.00
AB-SA128	Sharawra	LT	7.33	24.00	2.33	4.33	0.33	0.00	61.00	0.67	0.00	0.00	0.00	0.00	0.00	0.00	300	65.00	33.67	24.14	4.35	15.29	0.00
AB-SA127	Sharawra	LT	51.96	28.47	13.52	3.56	1.07	0.00	0.00	1.42	0.00	0.00	0.00	0.00	0.00	0.00	281	80.00	93.95	20.65	2.01	11.11	0.00
AB-SA132/2	Zarqa	LT	42.33	33.67	19.67	0.33	0.00	0.00	2.33	1.67	0.00	0.00	0.00	0.00	0.00	0.00	300	32.00	95.67	31.72	0.00	0.98	0.00
AB-SA132/1	Zarqa	LT	53.44	22.75	14.29	5.29	4.23	0.00	0.00	0.00	0.00	0.00	0.00	0.00	0.00	0.00	189	97.50	90.48	21.09	7.34	18.87	0.00
AB-SA123/2	Sarah	LT	82.33	12.33	4.33	0.00	0.00	0.67	0.00	0.33	0.00	0.00	0.00	0.00	0.00	0.00	300	53.00	99.00	5.00	0.00	0.00	5.13
AB-SA122/2	Sarah	LT	62.00	25.00	8.00	0.00	0.00	1.00	1.00	1.00	0.00	0.00	0.00	0.00	0.00	2.00	300	49.00	95.00	11.43	0.00	0.00	3.85
AB-SA124	Qasim	LT	24.33	59.00	15.33	0.67	0.00	0.00	0.00	0.67	0.00	0.00	0.00	0.00	0.00	0.00	300	25.00	98.67	38.66	0.00	1.12	0.00
AB-SA126	Qasim	LT	23.33	63.00	11.33	0.33	0.00	0.00	1.33	0.67	0.00	0.00	0.00	0.00	0.00	0.00	300	44.50	97.67	32.69	0.00	0.53	0.00
AB-SA145	Qasim	LT	51.33	36.00	9.00	1.00	0.00	0.00	2.00	0.67	0.00	0.00	0.00	0.00	0.00	0.00	300	90.50	96.33	14.92	0.00	2.70	0.00
AB-SA142/2	Qasim	LT	48.00	30.33	16.00	0.00	0.00	0.00	4.00	1.67	0.00	0.00	0.00	0.00	0.00	0.00	300	58.50	94.33	25.00	0.00	0.00	0.00
AB-SA144/1	Qasim	LT	51.67	42.33	5.67	0.33	0.00	0.00	0.00	0.00	0.00	0.00	0.00	0.00	0.00	0.00	300	73.50	99.67	9.88	0.00	0.78	0.00
AB-SA170	Saq	LT	37.33	48.00	14.67	0.00	0.00	0.00	0.00	0.00	0.00	0.00	0.00	0.00	0.00	0.00	300	44.00	100.00	28.21	0.00	0.00	0.00
AB-SA167	Saq	LT	42.33	38.00	9.33	0.00	0.00	5.00	5.33	0.00	0.00	0.00	0.00	0.00	0.00	0.00	300	54.50	89.67	18.06	0.00	0.00	11.63
AB-SA169	Saq	LT	51.00	39.67	5.00	0.00	0.00	0.00	3.33	1.00	0.00	0.00	0.00	0.00	0.00	0.00	300	81.00	95.67	8.93	0.00	0.00	0.00
Wajid area																							
AB-SA98	Juwayl	UW	5.33	4.33	3.00	10.00	53.67	6.33	16.00	0.00	0.33	0.33	0.00	0.00	0.67	0.00	300	78.00	12.67	36.00	90.96	69.77	59.38
AB-SA80	Juwayl	UW	55.00	19.33	4.00	4.00	0.33	11.67	1.00	0.00	4.00	0.67	0.00	0.00	0.00	0.00	300	70.00	78.33	6.78	0.60	17.14	37.63
AB-SA100	Juwayl	UW	53.67	26.67	4.33	0.00	0.67	13.00	0.00	0.00	0.00	1.33	0.00	0.00	0.33	0.00	300	41.50	84.67	7.47	1.23	0.00	32.77
AB-SA87	Khusayyayr	UW	59.29	17.70	6.19	2.65	1.77	6.19	0.88	0.00	3.54	0.00	0.00	0.00	1.77	0.00	113	75.00	83.19	9.46	2.90	13.04	25.93
AB-SA89	Khusayyayr	UW	37.33	35.00	6.67	2.33	0.33	15.00	1.67	0.00	1.00	0.00	0.00	0.00	0.67	0.00	300	75.00	79.00	15.15	0.88	6.25	30.00
AB-SA90	Khusayyayr	UW	27.87	42.62	4.10	8.20	0.00	6.56	4.92	0.00	0.00	0.82	0.00	4.92	0.00	0.00	122	97.00	74.59	12.82	0.00	16.13	13.33
AB-SA118	Khusayyayr	UW	40.93	42.35	3.56	1.07	0.00	7.83	3.20	0.00	0.00	0.71	0.36	0.00	0.00	0.00	281	80.00	86.83	8.00	0.00	2.46	15.60
AB-SA32	Khusayyayr	UW	11.67	32.50	10.00	25.83	0.83	5.00	12.50	0.00	0.83	0.00	0.83	0.00	0.00	0.00	120	92.00	54.17	46.15	6.67	44.29	13.33
AB-SA115	Qusaiba	LW	7.33	8.33	0.33	17.00	1.00	0.00	66.00	0.00	0.00	0.00	0.00	0.00	0.00	0.00	300	96.00	16.00	4.35	12.00	67.11	0.00
AB-SA62	Sanamah	LW	69.67	14.67	8.00	5.33	0.00	0.00	0.00	2.00	0.00	0.00	0.00	0.00	0.00	0.00	300	71.50	92.33	10.30	0.00	26.67	0.00
AB-SA63	Sanamah	LW	56.67	29.00	5.33	4.00	0.00	4.33	0.67	0.00	0.00	0.00	0.00	0.00	0.00	0.00	300	48.50	91.00	8.60	0.00	12.12	13.00
AB-SA64	Sanamah	LW	60.67	22.33	11.00	1.00	0.33	0.00	3.33	1.33	0.00	0.00	0.00	0.00	0.00	0.00	300	53.00	94.00	15.35	0.55	4.29	0.00
AB-SA74	Dibsiyah	LW	81.00	9.33	8.67	0.67	0.33	0.00	0.00	0.00	0.00	0.00	0.00	0.00	0.00	0.00	300	64.50	99.00	9.67	0.41	6.67	0.00
AB-SA76	Dibsiyah	LW	62.67	24.00	7.00	3.67	0.00	2.00	0.33	0.00	0.00	0.00	0.00	0.00	0.33	0.00	300	56.00	93.67	10.05	0.00	13.25	7.69
AB-SA72	Dibsiyah	LW	35.67	42.00	13.67	0.67	0.00	0.33	6.67	1.00	0.00	0.00	0.00	0.00	0.00	0.00	300	57.50	91.33	27.70	0.00	1.56	0.79
AB-SA69	Dibsiyah	LW	56.07	24.30	14.49	1.87	0.00	0.00	2.80	0.47	0.00	0.00	0.00	0.00	0.00	0.00	214	71.50	94.86	20.53	0.00	7.14	0.00
AB-SA79	Dibsiyah	LW	63.67	26.33	7.67	1.00	0.00	0.67	0.33	0.00	0.00	0.00	0.00	0.00	0.33	0.00	300	79.00	97.67	10.75	0.00	3.66	2.47

5.5.1. Zircon-tourmaline-rutile index (ZTR)

The Cambrian–Ordovician sandstones of the Dibsiyah and Sanamah formations are distinguished by very high ZTR values, between 91% and 99%. These decrease markedly in younger units. Two drastic drops in ZTR content can be observed in the Qusaiba Member and Juwayl Formation. Whereas the very low value of the Silurian Qusaiba Member is due to high amounts of altered grains, the uppermost sample from the Juwayl Formation is dominated by garnet. The distributional pattern is similar in the Tabuk area: very high ZTR content in the Cambrian–Ordovician units (between 90% and 100%) and slightly less in later Palaeozoic formations. The difference though is not as prominent as in Wajid area. Another similarity is the very low ZTR value of the Silurian Sharawra Member. As with the Qusaiba Member, this is due to high amounts of altered grains. It is worth noting however that the second sample from the Sharawra Member has a very high ZTR content of 4%.

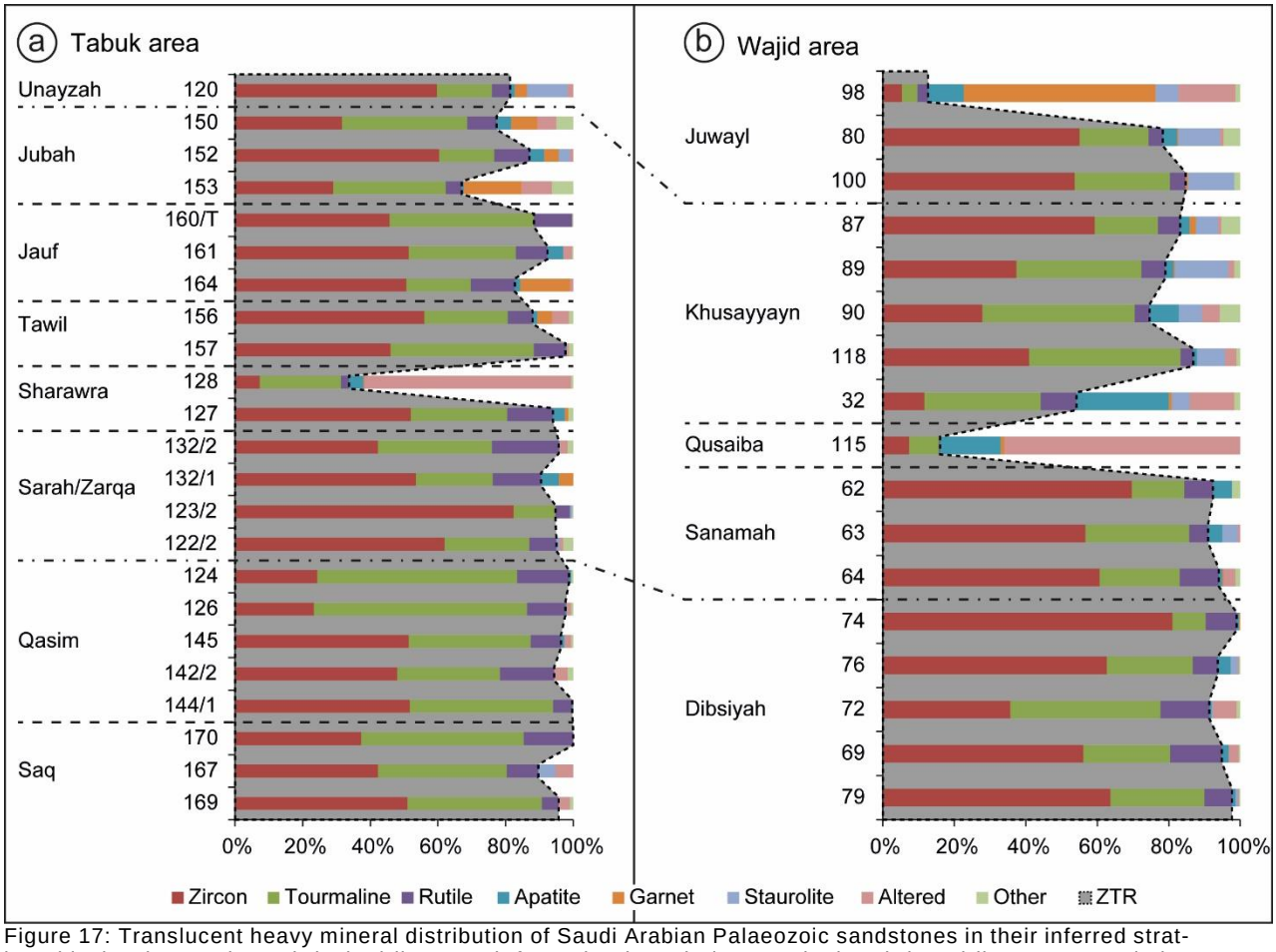

Figure 17: Translucent heavy mineral distribution of Saudi Arabian Palaeozoic sandstones in their inferred stratigraphical order. Horizontal dashed lines mark formation boundaries. Dashed and dotted lines are correlative nonconformities related to the Hirnantian and Carboniferous–Permian glaciations. Formation thickness is not to scale. Dotted, grey areas represent the ultra-stable ZTR fraction. 'Other' fraction contains: monazite, kyanite, enstatite, epidote, tremolite, chromite, sphene and hornblende. See text for further explanation. (a) Tabuk area; (b) Wajid area.

5.5.2. Rutile:zircon index (RZi)

The RZi shows no immediately recognisable trend throughout the stratigraphic successions of both study areas. It stays mainly in the range of <10 to 20 in the Wajid area, with two noticeable increases in the Khusayyayn and Juwayl formations. These are treated as outliers, as the other samples from those formations show a RZi similar to the remainder of southern Saudi Arabian samples. In the Tabuk area the RZi is overall a little higher, mostly between 10 and >20. Samples from the Qasim Formation have slightly elevated RZi values compared to the remainder of the Tabuk area.

5.5.3. Garnet:zircon index (GZi)

The GZi is very low in most of the Wajid Group. Only a dozen grains have been encountered throughout the succession. While the sample from the Qusaiba Member has a comparatively high GZi in regards to the rest of the Wajid samples, this is due to the very low zircon amount and not an increased garnet content. The youngest sample from the Juwayl Formation (AB-SA98) is a striking exception; 163 garnets were counted, resulting in a GZi of 91. In the Tabuk area a clear trend can be seen in the GZi: Lower Palaeozoic samples have a very low garnet and consequently low GZi. Upper Palaeozoic samples on the other hand have a significant garnet component, resulting in GZis of 5.8 to 37.

5.5.4. Apatite:tourmaline index (ATi)

The ATi in the Wajid area is generally below 20 but shows two distinct peaks. One centred on the Silurian Qusaiba Member, which has an ATi of 67.1. The second is found in the youngest Juwayl sample, which has an even higher ATi of 70. The Tabuk area does not display these spikes. Instead, there is a clear distinction between the Saq and Qasim formations and the remainder of the succession. While the former have a very low ATi or no apatite at all, the overlying units show values mostly between ~5 and ~20.

5.5.5. Staurolite:tourmaline index (STi)

The southern Saudi Arabian succession has a recognisable trend, increasing from very low values in the Cambrian–Ordovician and Silurian units up to almost 60 in the top sample from the Permian Juwayl formation. A marked increase of the STi appears between the Silurian Qusaiba Member and the Devonian Khusayyayn Formation. Samples from the Tabuk area do not exhibit this trend and have overall low staurolite content, with the exception of the single sample from the Permian Unayzah Formation.

5.5.6. Opaque phases

The percentage of opaque phases versus translucent heavy minerals has also been plotted (Figure 19). No clear trends were observed in both study areas, but there appears to be a minor distribution pattern in the Wajid succession. The mean opaque mineral content of the Dibsiyah, Sanamah and Juwayl formations is between 58% (Sanamah Formation) and 66% (Dibsiyah Formation). The Khusayyayn Formation and Qusaiba Member on the other hand have higher concentrations of 84% and 96%, respectively. The distribution of opaque heavy minerals in the Tabuk area is entirely erratic, with concentrations fluctuating between 25% and 98%.

5.5.7. Cross-plots

Knox et al. (2007) used cross-plots of heavy mineral indices to show provenance-related compositional groupings in samples from the Wajid Group. They were able to reveal compositional changes between formations and different compositional groups within the Juwayl Formation. However the groupings in the Juwayl Formation must be treated carefully, because the groups were arbitrarily chosen 'by hand'; no statistical treatment or analysis of the data was done. Heavy mineral indices from this study have been cross-plotted after Knox et al. (2007). The RZi has been chosen as the common reference index, as it is the most indicative index for changes in provenance and because sufficient counts of both zircon and rutile were obtained from all samples. However, these cross-plots did not yield informative results. No separation of stratigraphic units, groups or trends could be observed, except for single outlier samples. The plots are therefore not further considered in this study, but are presented as supplementary data (Figure A1, annex).

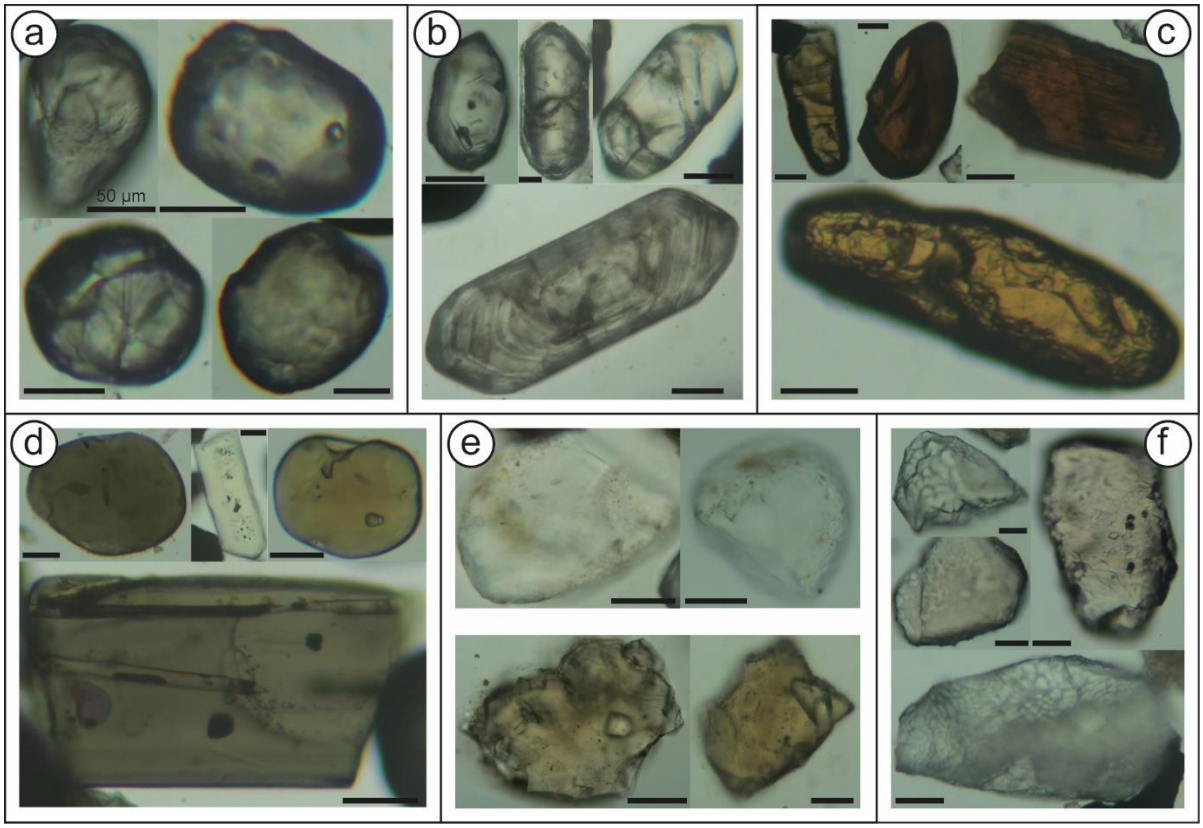

Figure 18: Photomicrographs of the most common heavy minerals. Black scale bars equal 50 µm. (a) Rounded zircon. (b) Euhedral zircons with fluid and mineral inclusions (upper row) and distinct zoning (bottom). (c) Rutile, upper right with distinct striation pattern. (d) Rounded and prismatic tourmaline, some with fluid and mineral inclusions (bottom). (e) Apatite (upper row) and staurolite (bottom row). (f) Garnet with distinct etch facets.

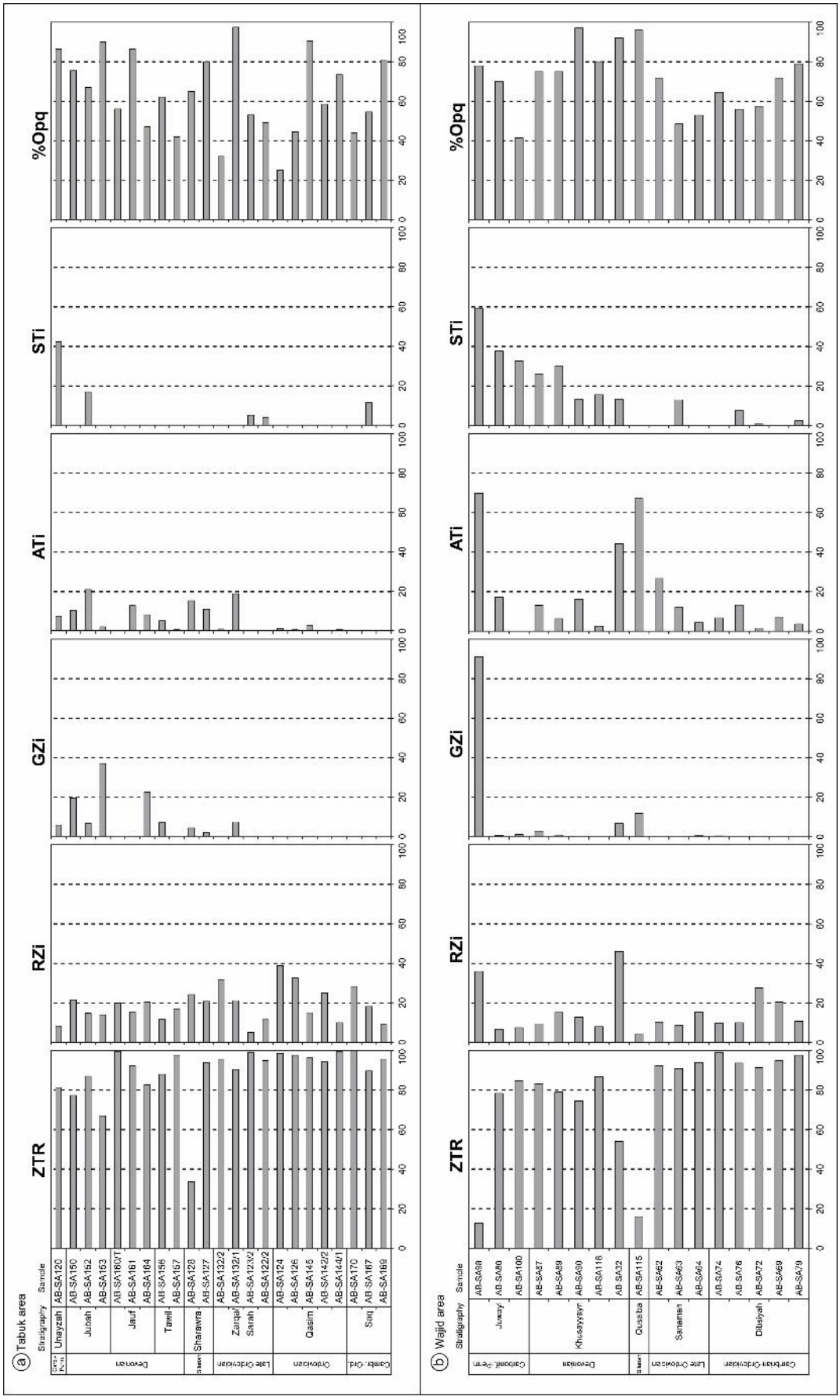

Figure 19: Different heavy mineral indices of samples from both study areas, plotted in their inferred stratigraphical succession. Formation thickness is not to scale. ZTR = zircon-tourmaline-rutile index; RZi = rutile:zircon index; GZi = garnet:zircon index; ATi = apatite:tourmaline index; STi = staurolite:tourmaline index; %Opq = percentage of opaque vs. translucent heavy minerals. See text for further explanation. (a) Tabuk area; (b) Wajid area.

5.6. Single-grain analysis

The mineral chemical data for rutile and garnet are provided as supplementary data (Table A5 and Table A6, annex).

5.6.1. Rutile chemistry

Results for rutile source rock classification are shown in Table 8 and in the inlays of Figure 20a and b. A total of 199 rutiles were measured from the upper and lower Palaeozoic successions of the Tabuk and Wajid areas. In the Tabuk area, rutiles from felsic source lithologies are dominant. From the Lower Tabuk, 53 rutiles were identified as felsic (73%) and 20 rutiles (27%) were identified as mafic. In the Upper Tabuk area, 45 rutiles were felsic (85%) and 8 were mafic (15%). In the Wajid area, mafic rutiles were more abundant than in the Tabuk area. In the Lower Wajid, 32 rutiles were identified as felsic (53%) and 28 rutiles (47%) as mafic (47%), while in the Upper Wajid 4 were felsic (31%) and 9 were mafic (69%).

Results for the Zr-in-rutile thermometry are shown as frequency histograms of in Figure 20. Each rutile has been assigned to a temperature population, with each population covering 50 °C. For example, the 600 °C population contains all rutiles between 600 °C and 649 °C.

From the Wajid Group a total of 72 rutiles yielded usable Zr concentrations (i.e. above detection limit of EMP): 31 from the Dibsiyah Formation, 28 from the Sanamah formation, 13 from the Juwayl Formation. Sandstones from the Tabuk area yielded a total of 123 suitable rutiles: 42 from the Saq Formation, 29 from the Qasim Formation, 52 from the Jubah Formation.

Distributions of temperature populations from both study areas are similar. Most rutiles (71.6%) fall into the 600 °C to 700 °C range. A minor population (20.1%) displays temperatures below 550 °C, while only a few (8.3%) show temperatures higher than 750 °C. Very high-grade (granulite-facies) rutiles were only encountered in the Saq Formation (Figure 20c; yellow box).

Table 8: Distribution of mafic and felsic rutiles in both study areas.

Formation	Study area	mafic	felsic	total
Tabuk area				
Jubah	Upper Tabuk	8	45	53
Qasim	Lower Tabuk	8	22	30
Saq	Lower Tabuk	12	31	43
Wajid area				
Juwayl	Upper Wajid	9	4	13
Sanamah	Lower Wajid	12	16	28
Dibsiyah	Lower Wajid	16	16	32

5.6.2. Garnet chemistry

Results of the garnet single-grain geochemical analysis are shown in the classification scheme after Mange and Morton (2007) (Figure 21a). Some garnets were measured at the core and rim. Plot points for rim measurements are shown as black symbols in Figure 21a and were not considered in further analyses. Average compositions for each formation are shown as yellow symbols. Average Garnet type distribution for the three studied formations is displayed as pie charts in Figure 21b, c and d. From the Jauf Formation only four garnets were measured in one sample. Half of them originate from high-grade metabasic rocks. Two (50%) are type Ci, two are type A (25%) and Bii (25%). From the Jubah Formation 50 garnets were measured in 3 samples. Amphibolite-facies type B garnets are dominant (78%). Three (6%) are type A, 12 (24%) are type Bi, 27 (54%) are type Bii, 7 (14%) are type Ci and 1 (2%) is of type Cii. The Juwayl Formation has a similar distribution like the Jubah Formation with dominant amphibolite-facies garnets, but a larger portion of high-grade metabasic rocks. Three (8%) garnets are of type A, 6 (17%) are type Bi, 16 (44%) are of type Bii, 10 (28%) are of type Ci and 1 (3%) is of type Cii. No type D garnets from Ca-rich metamorphic rocks were found in any of the samples.

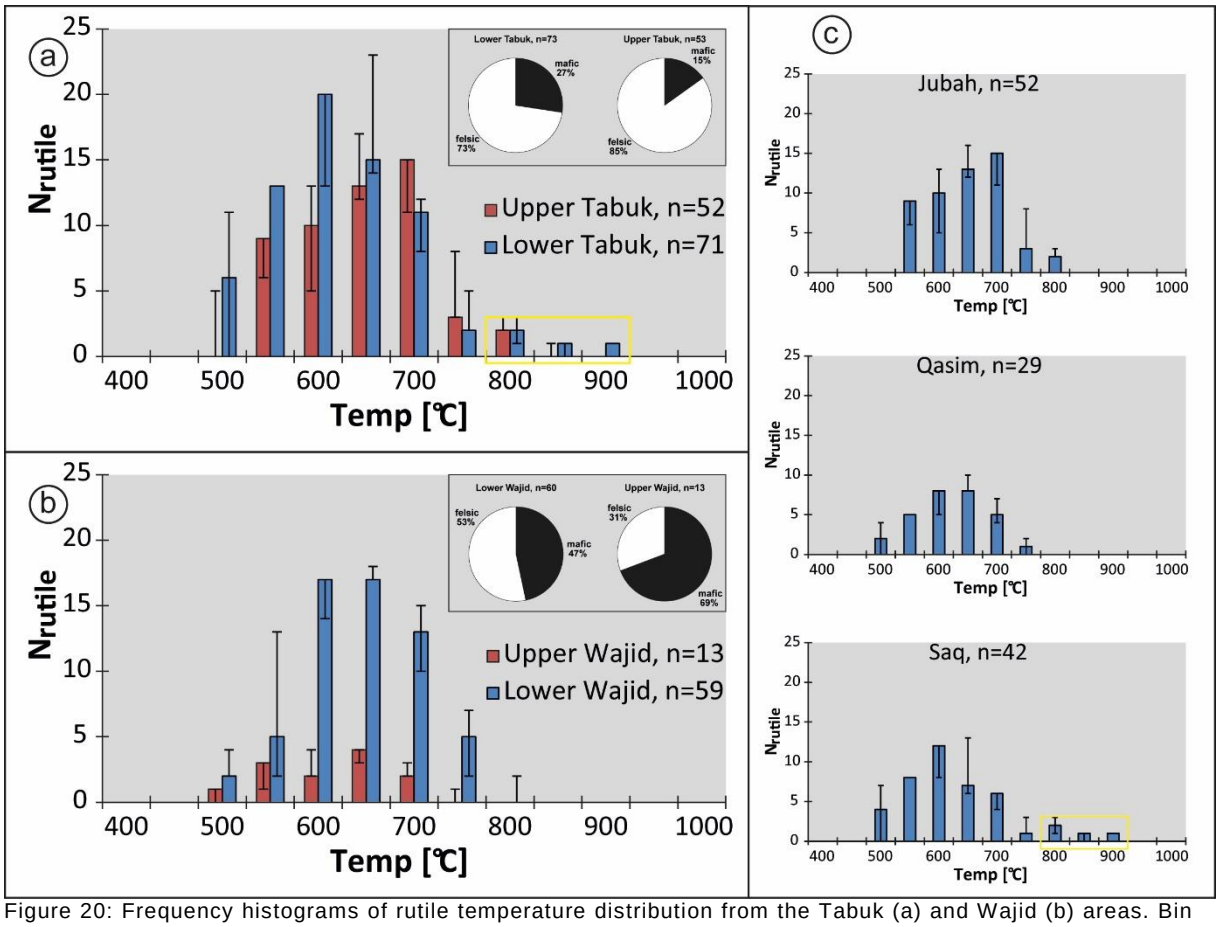

Figure 20: Frequency histograms of rutile temperature distribution from the Tabuk (a) and Wajid (b) areas. Bin width = 50 °C. (c) shows the data from (a) arrayed into formations. Temperatures have been calculated with the Zr-in-rutile thermometer after Tomkins et al. (2007), with P estimated at 10 kbar (see text for further explanation). Error bars are calculated for an error of T = 20 K. Note the distinct high-T population (≥800 °C; yellow box) in the Saq Formation of the Tabuk area. Inlays in (a) and (b) show the distribution of rutile source rock lithologies for lower and upper parts of the successions.

5.6.3. Zircon morphotypology

In total, 3,008 zircons from 26 samples (1,907 from the Tabuk area; 1,101 from the Wajid area) have been counted and assigned to morphotype classes, according to their internal structure. The morphotypes have been defined according to Corfu et al. (2003). Zircon internal structures were revealed by CL imaging of polished zircons. While counting and classifying the zircons, each grain was assigned to one morphotype class, according to their internal structure. Zircons that display features of two or more different morphotypes, e.g. regrowth features together with a convoluted interior, were assigned to the class with the most prominent feature. Grain fragments were treated like whole grains.

A total of seven different zircon morphotypes have been observed. The most abundant morphotype are regular, zoned zircons (Figure 22a). They are characterised by clearly visible zoning and the absence of large defects and any of the characterising features of the other morphotpyes. Undisturbed zoning is typical for primary magmatic growth (Corfu et al., 2003). Zoned zircons account for 38.1% (Lower Tabuk) to 46.3% (Upper Wajid) of all counted zircons. The second most abundant morphotype are zircons exhibiting regrowth features (Figure 22d) and encompass all grains that show large internal defects that have subsequently recrystallized ('healed') during late or post-magmatic cooling (Corfu et al., 2003). 'Healed' zircons make up 16.7% (Upper Wajid) to 19.7% (Upper Tabuk) of the total population. The third most frequent morphotype are zircons with xenocrystic cores and clearly zoned rims (Figure 22b). Xenocrystic cores are another typical feature of magmatic zircons (Corfu et al., 2003). They represent 10.6% (Lower Wajid) to 14.9% (Upper Wajid) of all grains. Zircons with xenocrystic cores but unzoned rims (Figure 22c) on the other hand are indicative for high-grade metamorphic conditions (Corfu et al., 2003). They are slightly less abundant than those with zoned rims, making up 5.1% (Lower Wajid) to 11.5% (Lower Tabuk). Similar abundances were observed for zircons with convoluted interior structures (Figure

22f, upper rows), representing from 5.6% (Upper Wajid) to 11.5% (Lower Tabuk) of the zircon population. Convoluted interiors have been designated as late magmatic features in this study, but they can also form under high-grade metamorphic conditions (Corfu et al., 2003). The second least frequent morphotype are unzoned ('homogenous') zircons, characterised by an absence or only faintly present zonation (Figure 22e). Homogenisation occurs under high-pressure conditions (Corfu et al., 2003). 6.4% (Lower Tabuk) to 8.7% (Upper Tabuk) of all zircons fall into this morphotype class. The least abundant morphotype are patchy zircons with highly deformed interior structures (Figure 22f, lower row), constituting only 2.2% (Lower Wajid) to 3.2% (Lower Tabuk) of the total population. Patchy interiors are another result of late to post-magmatic cooling (Corfu et al., 2003).

The distribution patterns of zircon morphotypes are similar in both study areas (Figure 23). The differences between the stratigraphic units and study areas are minute and no clear trends have been observed. Therefore, the data is only presented for the lower and upper parts of each study area and not for each formation. Magmatic morphotypes (zoned, xenocrystic cores with zoned rims, healed, convoluted, patchy) constitute the majority of the zircon populations, making up 82% and 81% of the Lower and Upper Tabuk area (Figure 23a, b) as well as 88% to 86% of the Lower and Upper Wajid area (Figure 23c, d), respectively. Metamorphic zircon morphotypes (xenocrystic core with unzoned rims, homogenous) constitute the remainder. The raw data for each sample is given in Table A1 (annex), percentages are given in Table A2 (annex).

While there are no striking discrepancies between formations and study areas, some minor tendencies are observable: The amount of zoned zircons seems to be more variable and slightly lower in samples from the Tabuk area (39.1%) than in those from the Wajid area (45.5%). At the same time, zircons with xenocrystic cores and unzoned rims are twice as abundant in the Tabuk area (11%) than in the Wajid area (5.5%). A common feature in both study areas seems to be an increased amount of zoned zircons in the Carboniferous–Permian formations (47% in the Unayzah Formation; 49.7% in the Juwayl Formation).

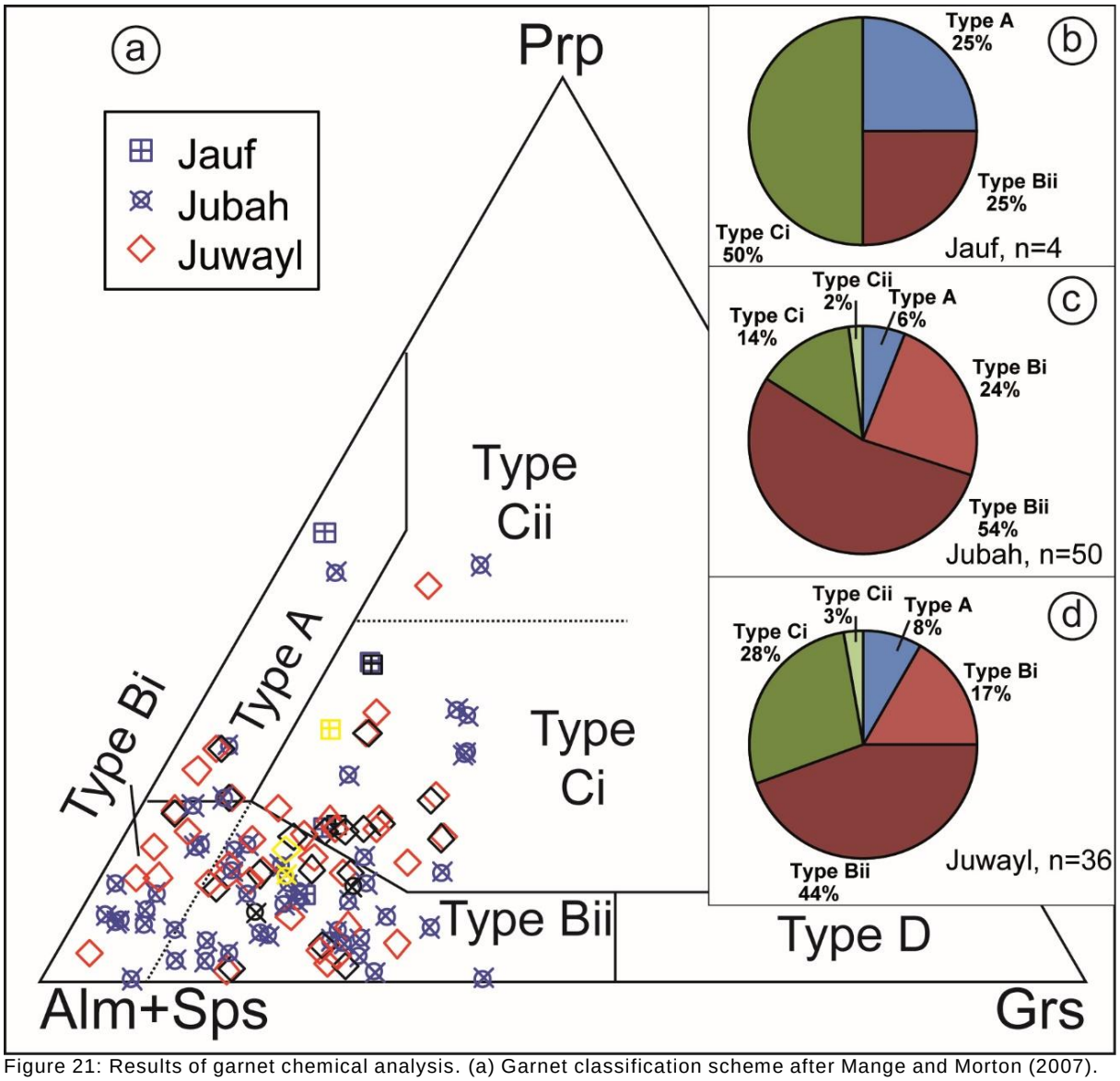

Figure 21: Results of garnet chemical analysis. (a) Garnet classification scheme after Mange and Morton (2007). The corners of the ternary diagram represent idealised garnet end members. Prp = pyrope, Alm = almandine, Sps = spessartine, Grs = grossular. A – sourced from granulite facies metasediments, charnockites or intermediate to acidic deeper crust rocks; Bi – from intermediate to acidic igneous rocks ; Bii – from amphibolite-facies metasediments; Ci – from high-grade metamafic rocks; Cii – from ultramafic rocks with high Mg; D – from Ca-rich metamorphites like metasomatic rocks (skarns), very low-grade metabasic rocks or ultra-high temperature calc-silicate granulites. Black symbols are values from garnet rims, yellow symbols are average compositions for each formation. (b), (c) and (d) Percentage distribution of garnet types in the Jauf, Jubah and Juwayl formations, respectively.

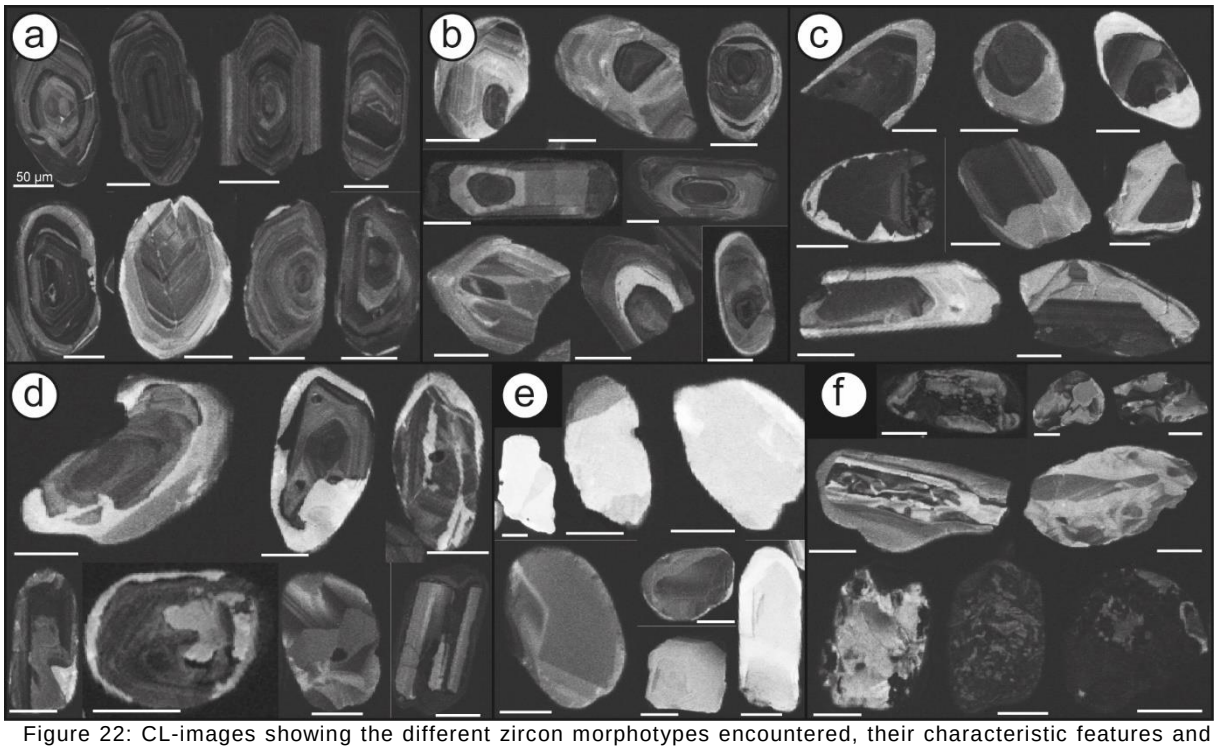

Figure 22: CL-images showing the different zircon morphotypes encountered, their characteristic features and internal structures. (a) Zoned zircons; (b) zircons with xenocrystic cores and zoned rims; (c) zircons with xenocrystic cores and unzoned rims; (d) zircons with prominent regrowth features ('healed zircons'); (e) unzoned ('homogenous') zircons; (f) zircons with convoluted (upper rows) and patchy (lower row) internal structure. White scale bars equal 50 µm.

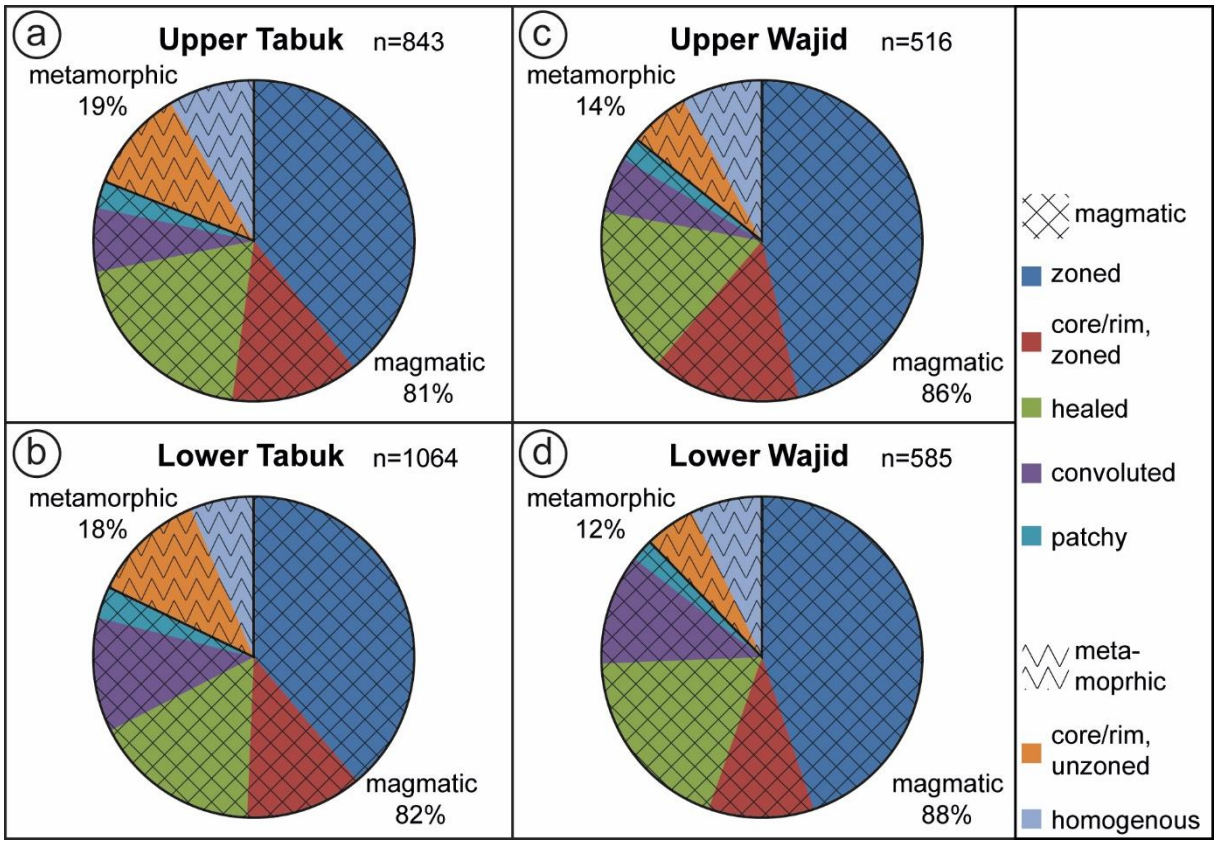

Figure 23: Results of the zircon morphotype classification. Quartered signature represents predominantly magmatic morphotypes, wavy signature represents predominantly metamorphic morphotypes. (a) & (b) Tabuk area; (c) & (d) Wajid area.

6. Discussion

6.1. Source area weathering

During transport and deposition, sediments undergo changes in their mineralogical and consequently in their major element composition, compared to their source rocks. For example quartz, and thus SiO_2, tend to become enriched. Feldspars on the other hand break down, leading to the removal of Na_2O, K_2O and CaO (Fedo et al., 1995). The (geochemical) composition of sedimentary rocks is controlled by a complex interplay of various factors, like provenance, weathering, fractionation, sorting and diagenesis, which in their turn are dependent on aspects such as tectonic setting and climate (Bhatia, 1983; Johnsson, 1993). At the extreme end of this process stand highly mature quartz arenites, which are composed of 90% or more detrital quartz, with only small amounts of feldspar or lithic fragments. They are the result of intensive chemical weathering, reworking and/or sedimentary recycling. Weathering and climate have a profound impact on the composition and maturity of siliciclastic sediments (Chandler, 1988). The amount and influence of source area weathering has to be taken into account in order to correctly interpret the provenance of Saudi Arabian Palaeozoic succession, as it is dominated by quartz arenites.

A vast variety of different chemical weathering indices have been used to estimate and quantify weathering of rocks (Fedo et al., 1995; Duzgoren-Aydin et al., 2002). Among those, the CIA of Nesbitt and Young (1982) is the most widely accepted und utilised tool to describe weathering in siliciclastic sediments (Bahlburg and Dobrzinski, 2011). It is a measure of Al_2O_3 versus labile oxides and defined as:

$$CIA = \frac{Al_2O_3}{(Al_2O_3 + CaO^* + Na_2O + K_2O)} * 100 \qquad \text{(equation 4)}$$

where CaO* represents the Ca of silicates only. Samples with carbonatic matrix have not been taken into account. CaO was low in all considered samples. Consequently, CaO* was regarded equal to CaO. All element oxides are in molar proportions. Lower values equal low weathering; higher values equal more intense weathering. Some typical values and end members are 100 for kaolinite, 50 for unaltered albite, anorthite and K-feldspar, 0 for diopside. Average CIA ranges for fresh common rocks are 30 to 45 for basalt, 45 to 55 for granites and granodiorites and 75 to 85 for the average shale (Nesbitt and Young, 1982). As feldspar is chemically weathered, Na^+, K^+ and Ca^{2+} are mobilised and removed from the system by soil solutions (Fedo et al., 1995). Consequently, the immobile Al_2O_3 remains, increasing the CIA. Since feldspar makes up the bulk of labile material in the continental crust, the CIA is thus a measure of feldspar alteration into clay minerals (Fedo et al., 1995; Akarish and El-Gohary, 2008). Problems may occur when transport and sorting effects lead to fractionation of grain sizes. Sorting tends to concentrate Al-rich clays in the mud fractions and feldspars and quartz in the sand fraction (Nesbitt et al., 1996). When comparing different successions and/or different depositional environments, it is important to consider similar grain sizes (Bahlburg and Dobrzinski, 2011). This mechanical effect still requires chemical weathering beforehand. Physical weathering alone has little impact on the CIA. Nesbitt and Young (1996) found no evidence that mechanical weathering (abrasion) causes increased comminution of feldspars in regards to quartz and has thus little influence on the CIA. They further argue that quartz arenites cannot be produced by comminution alone and need chemical weathering. When interpreting CIA values one also has to take recycling into account. Recycled sediments may have undergone several fractionation and sorting events. This can potentially lead to CIA values that are not representative for the weathering processes and climate in the source area, but may reflect weathering in an older sedimentary basin (Huntsman-Mapila et al., 2009).
CIA values in the Wajid area range from 33.2 (equivalent to unweathered basalt) in the Juwayl Formation up to 93.8 (highly weathered) in the Dibsiyah Formation. Mean values for each formation are shown in Table 9 and range from 58.2 (Khusayyayn Formation) to 77.1 (Dibsiyah Formation). Those values are lower than expected given the mineralogical maturity of the samples.

In the Tabuk area the CIA for samples is between 42.2 (equivalent to unaltered granite) in the Tawil Formation and 91.2 (highly weathered) in the Saq Formation. Mean values for the individual formations in the Tabuk area have a similar range like their southern counterparts, between 54.7 (Jubah Formation) and 83.6 (Saq Formation) (see Table 9).
Samples from the lower Palaeozoic (Lower Wajid/Tabuk; Cambrian and Ordovician) in both study areas differ substantially in their CIA from those of late Palaeozoic age (Upper Wajid/Tabuk; Devonian to Permian). The mean values of Cambrian–Ordovician units are significantly higher than those of younger units (see Table 9). This trend can be observed in both study areas. For this comparison the Silurian units have been excluded, since their petrological parameters and depositional setting are not comparable to the other formations.
Higher CIA values for samples from the Saq, Qasim, Zarqa and Sarah formations from the Tabuk area and the Dibsiyah and Sanamah formations from the Wajid area indicate moderate to intense weathering and/or sediment recycling in the source area. The relatively low CIA of the remaining formations would suggest low weathering conditions and/or mixing of fresh, unweathered material with recycled sediments.

A second, similar chemical weathering index is the plagioclase index of alteration (PIA) of Fedo et al. (1995). It is defined as:

$$PIA = \frac{Al_2O_3 - K_2O}{Al_2O_3 + CaO^* + Na_2O - K_2O} * 100 \qquad \text{(equation 5)}$$

in molar proportions and where CaO* represents the Ca of silicates only. CaO was considered to be equal to CaO* (for explanation see CIA).
CIA and PIA correlate strongly positive (r=0.84; n=39) and have mostly comparable values (see Table 9). Noticeable differences in between CIA and PIA occur in the Qusaiba and Sharawra members as well as Tawil, Jauf, Jubah and Unayzah formations of the Tabuk area. The exact cause could not be determined with the current data set.

A third way to quantify source area weathering utilising petrographical data is the MI (Pettijohn, 1954). It is expressed as the ratio of quartz to quartz + feldspar + lithic fragments. Mean values for all formations are shown in Table 9. Sandstones from the Wajid area have high to very high values for the MI, ranging from a minimum of 0.84 (Khusayyayn Formation) to the maximum of 1.00 in several samples from different formations. The mean values from the Wajid area are uniformly high, indicating a very high mineralogical maturity. Only the sample from the Qusaiba Member has a significantly lower MI value of 0.55. The bulk of the Tabuk area samples show high to very high mineralogical maturity as well. Several samples from throughout the succession have an MI of 1.00. In contrast to the Wajid area, the Sharawra Member from the Tabuk area exhibits a mean MI of 0.72, which is distinctly more mature than the Qusaiba Member from the Wajid area. The most mineralogically immature unit in the Tabuk area is the Jauf Formation, which has a mean MI of 0.73. Very high MI values are explained by (meta-) sedimentary recycling by Bhatia and Crook (1986). MI values for the present data set do correlate with neither the CIA (r=0.34) nor the PIA (r=-0.05). This suggests that the controlling factors for both the CIA and PIA are not found in the framework grains, but in the matrix and cement of the sandstones, which are not considered in the MI. Consequently, sorting and diagenetic effects have a much higher impact on the CIA and PIA and they do not correctly reflect chemical weathering.

Table 9: Mean values of different weathering indices for Palaeozoic formations from the Tabuk and Wajid areas.

Formation	Area	n	mean CIA	mean PIA	mean MI
Tabuk area					
Unayzah	Upper Tabuk	3	60.1	70.9	0.92
Jubah	Upper Tabuk	3	54.7	73.1	0.79
Jauf	Upper Tabuk	2	56.6	69.6	0.73
Tawil	Upper Tabuk	3	53.2	60.4	0.96
Sharawra Mbr.	Lower Tabuk	2	62	83.6	0.72
Sarah/Zarqa	Lower Tabuk	3	70.5	77.6	0.97
Qasim	Lower Tabuk	5	70.5	74.3	0.97
Saq	Lower Tabuk	2	83.6	84.1	0.99
Wajid area					
Juwayl	Upper Wajid	2	54.2	54.4	0.98
Khusayyayn	Upper Wajid	4	58.6	61.6	0.91
Qusaiba Mbr.	Lower Wajid	1	71.4	87.3	0.55
Sanamah	Lower Wajid	4	70.1	70.4	0.97
Dibsiyah	Lower Wajid	5	83	84	0.99
	Upper Tabuk	11	57.2	59.2	0.93
	Lower Tabuk	12	77.3	78	0.98
	Upper Wajid	6	56.1	68.4	0.86
	Lower Wajid	10	73.1	77.3	0.97

The ternary A-CN-K diagram can be used to determine weathering trends (Nesbitt and Young, 1984). Additionally, it may be used to deduce the source rock composition of a weathering product (Fedo et al., 1995). Coincidentally the 'height' above the CN-K line of the triangle corresponds to the CIA. Samples from the Wajid Group uniformly plot very close to the A-CN side of the triangle, leaning more towards the A apex (Figure 24b). Striking exceptions are the samples from the Devonian Khusayyayn Formation, which plot more towards the K apex. Results from this study are in accordance with literature data from Hussain (2001), Babalola et al. (2003) and Hussain (2007) (grey area in Figure 24 represents range of literature data). This is a surprising observation, since plagioclase breaks down much more easily than K-feldspar. Consequentially one would expect highly weathered and mature sandstones to plot near the A-K line and the A apex. Samples from the Tabuk area show a much wider spread in the A-CN-K diagram than those from the Wajid area (Figure 24a). Roughly half of the samples, mainly those from lower Palaeozoic units, plot near the CN-A line. The other half – mainly samples from the Devonian Jauf and Jubah formations – plot toward the A-K line of the diagram, near the composition of idealised biotite. This distribution has also been observed in the Wajid area, albeit much less pronounced. A possible explanation could be a change in the weathering regime, a change in provenance, or both during Devonian times. This distributional pattern may then have been amplified by sorting effects during transport, since the sampling points for the Devonian sandstones from the Tabuk area are significantly farther away from the potential source areas than any of the other formations (Figure 2c).

There are several possible reasons for unexpectedly low CIA and PIA values and sample point distribution in the A-CN-K diagram. Diagenetic effects may have altered the initial CaO, Na_2O and K_2O distribution after sedimentation and burial through smectite addition and/or illite and muscovite removal by pore waters. In the present case, significant smectite addition is unlikely. CaO and Na_2O concentrations are very low and thin section petrography revealed low cementation and matrix content in most samples (see Table 4). Another influencing factor may be the high SiO_2 content of the sandstones. Since SiO_2 makes up 80% to 90% of the whole rock and Al_2O_3 making up the bulk of the remainder, small changes in the CaO, Na_2O and K_2O concentrations have a large impact on the CIA, PIA and A-CN-K diagram. The third and most likely factor is sorting. In their paper, Nesbitt and Young (1982) looked only at very fine grained sediments (lutites), which are enriched in clay minerals and thus ideally suited to preserve the weathering signal determined with both the CIA and PIA. Coarser material, like the sandstones from this study, might be deposited without the accompanying clay fraction. This effectively leads to Al_2O_3 depletion as the clay minerals are washed out and deposited further downstream (Nesbitt et al., 1996). The CIA and PIA of the remaining coarser fraction are consequently lower and no longer directly reflect weathering processes in the source area. Thus, the depositional setting has a profound impact on the

CIA and PIA. Grain size and sorting effects must be taken into consideration when trying to interpret geochemical weathering indices like the CIA and PIA (Bahlburg and Dobrzinski, 2011).
In their original paper, Nesbitt and Young (1982) used the CIA to differentiate between glacial and non-glacial sediments from the early Proterozoic and to reconstruct climate change from whole-rock geochemistry. If applied in the right conditions, the CIA is a powerful tool for climate reconstruction throughout Earth history (Bahlburg and Dobrzinski, 2011). The presented data set unfortunately seems unsuitable in this regard. Although grain size variations were kept minimal by carefully selecting samples, the material is too coarse to successfully utilise the CIA for palaeoclimate reconstruction. Al_2O_3 concentrations in the studied samples are predominantly controlled by the rate of clay mineral removal and thus sorting, not by the rate of feldspar weathering. This effectively means that the influence of sorting is strong enough to mask the climate signal. This can clearly be seen in the data: Due to a prevalence of physical weathering over chemical weathering in cold climates, glaciogenic units should exhibit lower (average) CIA values than those of non-glacial origin (Bahlburg and Dobrzinski, 2011). This was not observed in this study. The glaciogenic units in both study areas (Zarqa, Sarah and Unayzah formations in the Tabuk area; Sanamah and Juwayl formations in the Wajid area) have all higher mean values than the non-glacial Devonian formations (Table 9). Without regarding sorting effects, this would falsely indicate more intensive weathering and hence warmer, more humid conditions in the Hirnantian and Permian units. In this case sorting effects clearly mask the climate signal. Consequently, it is not possible to draw conclusions about source area weathering and climate conditions from the usual weathering indices with the presented data set.

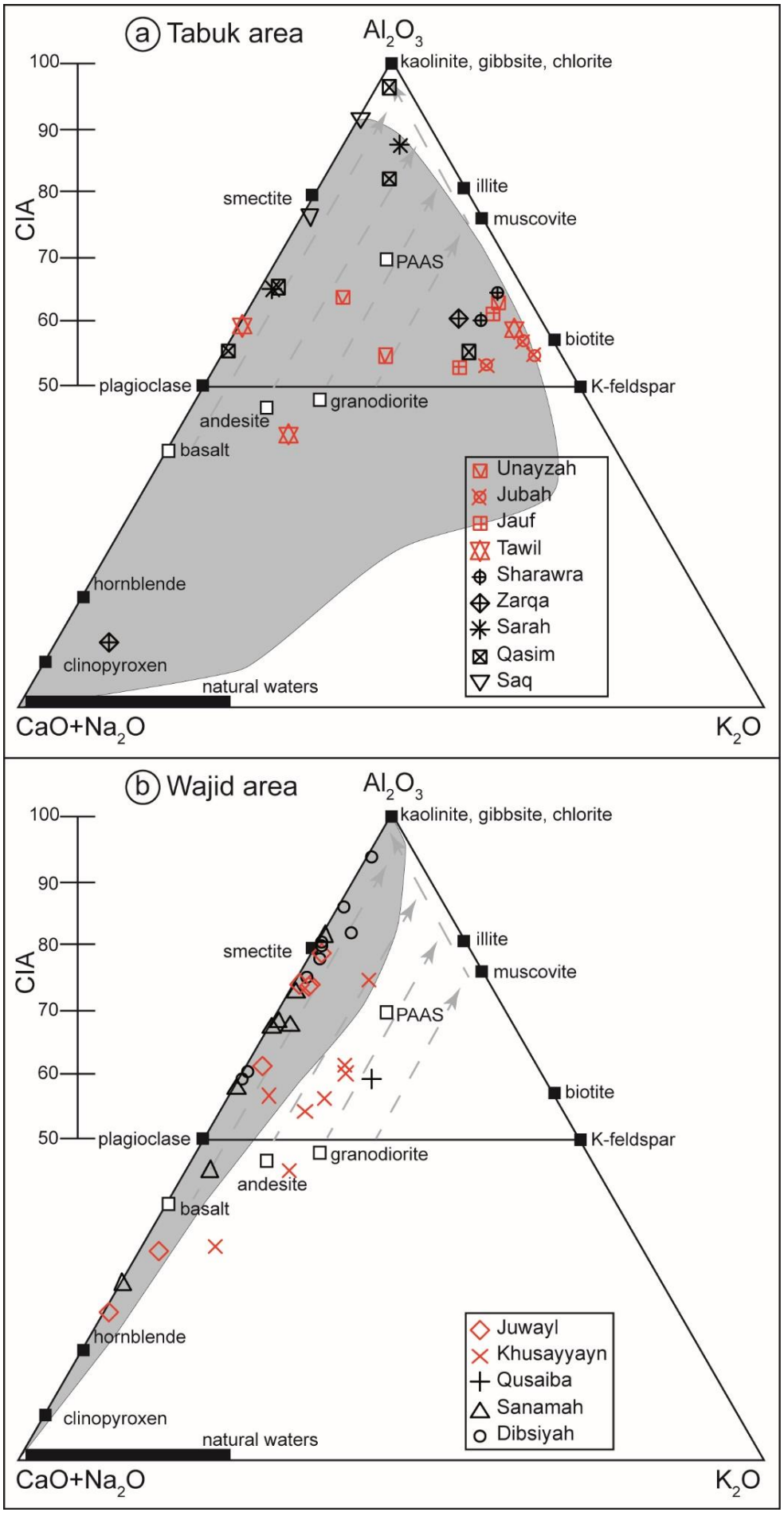

Figure 24: A-CN-K diagram, modified after Nesbitt and Young (1984), showing idealized weathering trends for some common magmatic rocks. Blue symbols are mean values of formations. (a) Tabuk area; the grey area represents range of literature data (from Al-Harbi and Khan, 2005, 2008, 2011; Hussain, 2007). (b) Wajid area; the grey area represents range of literature data (from Hussain, 2001, 2007).

6.2. Sedimentary recycling

Apart from the aforementioned problems, one fundamental flaw with all three weathering indices (CIA, PIA and MI) as well as the A-CN-K ternary diagram remains: they fail to distinguish heavy weathering from sedimentary recycling. Petrographical and textural maturity of the studied samples (=high quartz content, low feldspar and lithic fragments) suggest sediment recycling. A possible source, at least for southern Saudi Arabian sediments, has been suggested by Hussain et al. (2004). They consider, among several Neoproterozoic terranes, the 'infra-Cambrian' Ghabar Group in Yemen to be a source for recycled sandstones of the Wajid area. A geochemical approach to identify sediment recycling has been presented by McLennan et al. (1993). They used ratios of Th/Sc vs. Zr/Sc to identify sedimentary recycling trends in modern turbidite sands. Sc has been used to normalise for its uniform abundance in most minerals. The Th/Sc ratio is mainly governed by compositional variances in the source rock, whereas the Zr/Sc ratio is related to the zircon content of siliciclastics. Recycling of clastic sediments usually leads to an increase in maturity and zircon enrichment and thus to increased Zr/Sc ratios (McLennan et al., 1993). Ideal recycling trends are flat and progress along the x-axis of the diagram. In the presented data set, no overall recycling trend has been observed: Most samples plot together in a point cloud, regardless of stratigraphic position (Figure 25a). For a clear recycling signal, a much flatter trend line would have been expected. Furthermore, older samples would be expected to have overall lower Zr/Sc ratios than younger ones. This is an argument against a lower Palaeozoic source for later Palaeozoic sediments and intensive, continuous recycling of older sandstones. Subordinate recycling trends within single stratigraphic units could not be proven either. Each formation has been checked for recycling trends (plots not shown), without correlations between Zr/Sc ratio and stratigraphic position. Therefore, based on whole-rock geochemistry, there is no evidence for subordinate recycling trends within stratigraphic units. In fact the opposite seems to be the case for sandstones from the Wajid area: Samples from the Khusayyayn and Juwayl formations have comparatively low Th/Sc and Zr/Sc ratios. They plot together in a separate group to the lower left of all other samples, close to UCC composition (Figure 25a). Samples from the Tabuk area do not show this separation. One possible explanation is an influx of fresh material – possibly from the nearby Arabian Shield – in the Wajid area, which did not reach the northern Arabian basin. A second possibility is simply regional variation. Both explanations hint to a change in the provenance of the Khusayyayn and Juwayl formations.

Considering the Arabian Shield as the main source for Palaeozoic sandstones (Babalola, 1999; Hussain, 2001; Hussain et al., 2004; Al-Harbi and Khan, 2005, 2008, 2011; Wanas and Abdel-Maguid, 2006; Knox et al., 2007) leads to further difficulties in interpreting the Th/Sc vs. Zr/Sc diagram. In Figure 25b some typical basement rocks of the Arabian Shield (from Jackson et al., 1984; Stuckless et al., 1985, 1986; Jackson and Douche, 1986; Leo, 1986; Ramsay et al., 1986; and own samples) are plotted together with Palaeozoic sediments (Figure 25). The selected basement samples represent potential source rocks for the Palaeozoic sandstones and cover a wide area of the Arabian Shield. They can thus be considered 'end members' of a hypothetical mixing process. Some of those end members from certain regions, like the samples from the northeastern and central Arabian Shield, plot closely together (Figure 25b). Others, like basement rocks from the eastern and southeastern Shield, show no trends and a wide spread across the diagram (Figure 25b). Some points plot in the same position as the sediment samples. This is true even for high Zr/Sc and moderate Th/Sc values, which are interpreted by McLennan et al. (1993) to indicate sedimentary recycling. Because of the wide spread of basement samples in the diagram, it is possible to explain high Zr/Sc values of sediments not only by sedimentary recycling but also with mixing of different basement rocks. Contrary to the suggestion of McLennan et al. (1993), the Zr/Sc ratios of Saudi Arabian Palaeozoic sandstones seem not only to be controlled by sedimentary processes, but also have significant dependence on the source rocks as well. While insufficient to make conclusions about sediment recycling, the Th/Sc vs. Zr/Sc plot nevertheless can help to differentiate samples from the Wajid and Tabuk areas. When compared, samples from the present study and literature data (grey area, Figure 25a) differ significantly. There is almost no overlap between the two data sets. The data from Hussain (2007), representing samples from the Saq and Qasim formations as well as from the not further differentiated Wajid Group, show much lower Zr/Sc ratios and partially higher Th/Sc ratios. Furthermore, the variability of the Th/Sc ratio is much higher than that of the Zr/Sc

ratio, resulting in a ‘vertical spread’ rather than a ‘horizontal spread’. Hence this data set exhibits even less evidence for sedimentary recycling. A possible explanation for the differences may be regional variability. The sample points in northern and southern Saudi Arabia of Hussain (2007) differ significantly – in the order of several hundred kilometres – from this study. This disparity between geographically different sandstones of the same age and formations gives even more emphasize on source area composition and mixing – in contrast to sediment recycling – as the dominant factors for Th/Sc and Zr/Sc ratios in the case of Saudi Arabian Palaeozoic sandstones.

Trace element geochemistry, especially Th, Zr and Sc concentrations, of Saudi Arabian Palaeozoic sandstones show no evidence of a significant input from a recycled sedimentary source. Instead, variances in those element abundances can be explained by mixing of different magmatic source rocks from the ANS. The mineralogical maturity of the analysed samples is very high, which has been attributed to be the result of sedimentary recycling by Bhatia and Crook (1986). Yet it can also be explained by intensive weathering and reworking. Modal composition is not only dependent on provenance, but also modified by weathering, fractionation, sorting, chemical alteration as well as diagenetic effects (Weltje, 2004; Weltje and von Eynatten, 2004) and thus unable to differentiate recycling from reworking. Although intensive source area weathering is not indicated by both the CIA and PIA, it cannot be refuted either. The chemical weathering indices have been shown to be highly sensitive to grain size and sorting effects (Nesbitt et al., 1996; Bahlburg and Dobrzinski, 2011). Clay mineral removal can lead to unexpectedly low CIA and PIA values, regardless of weathering. Essentially, the highly mature Palaeozoic sandstones from the Arabian Peninsula are first cycle sediments.

Evidence for the presence of first cycle quartz arenites on the northern Gondwana passive margin were presented by Avigad et al. (2005). They studied Cambrian sandstones from the Elat area of southern Israel, which can be correlated to the northern Saudi Arabian Saq and Qasim formations. Detrital zircon ages reveal only a short time lag between consolidation of the magmatic source and deposition of detritus. This time lag has not been long enough to allow sedimentary recycling. Hence the maturity of those sandstones is a result of intensive source area weathering coupled with low sedimentation rates. Further similar detrital zircon ages are also reported from Cambrian–Ordovician sandstones from Israel and Jordan (Kolodner et al., 2006). Adjacent to the northern ANS and south of the Elat, lower Palaeozoic sandstones from the eastern Sinai Peninsula have been interpreted to be first cycle sediments as well (Akarish and El-Gohary, 2008).

In Saudi Arabia, Babalola (1999) concluded a first cycle provenance from intermediate to felsic source terranes in Yemen for sandstones from the Wajid area, utilising petrographical and geochemical methods as well as heavy mineral analysis. Wanas and Abdel-Maguid (2006) arrived at the same results for lower Palaeozoic Wajid sediments near the border to Yemen. Al-Harbi and Khan (2005) studied quartz arenites of the Unayzah Formation using petrographic and geochemical techniques. They argued that reworking during deposition, not recycling, is mainly responsible for the maturity of the sandstones. Similar, albeit not identical conclusions are presented by Al-Harbi and Khan (2008, 2011) for the Tawil and Sarah formations of central and northern Saudi Arabia. They identify, apart from granitic and metasedimentary rocks, polycyclic sediments as part of the source for these units, but also mention extensive reworking. Their conclusions fit well to the data set presented in this study. In contrast, by studying heavy mineral assemblages of the Wajid sandstone, Hussain et al. (2004) infer a mix of Neoproterozoic basement and ‘infra-Cambrian’ sediments from Yemen as source for Palaeozoic sediments in southern Arabia. They completely disregard the exposed terranes of the ANS to the north and west as significant sources. Similarly, Meinhold et al. (2011) presented evidence from detrital zircons for a possible recycling of Neoproterozoic sediments in Palaeozoic sandstones of southern Libya.

It is evident, that the question of sedimentary recycling is far from solved and that further studies are required. Considering the presented data set, the most likely explanation for the high mineralogical maturity of the samples and the lack of apparent recycling trends in the geochemical data seems to be a mixture of compositional variation of source rocks and reworking during deposition. The issue of sedimentary recycling cannot be unequivocally solved at this point.

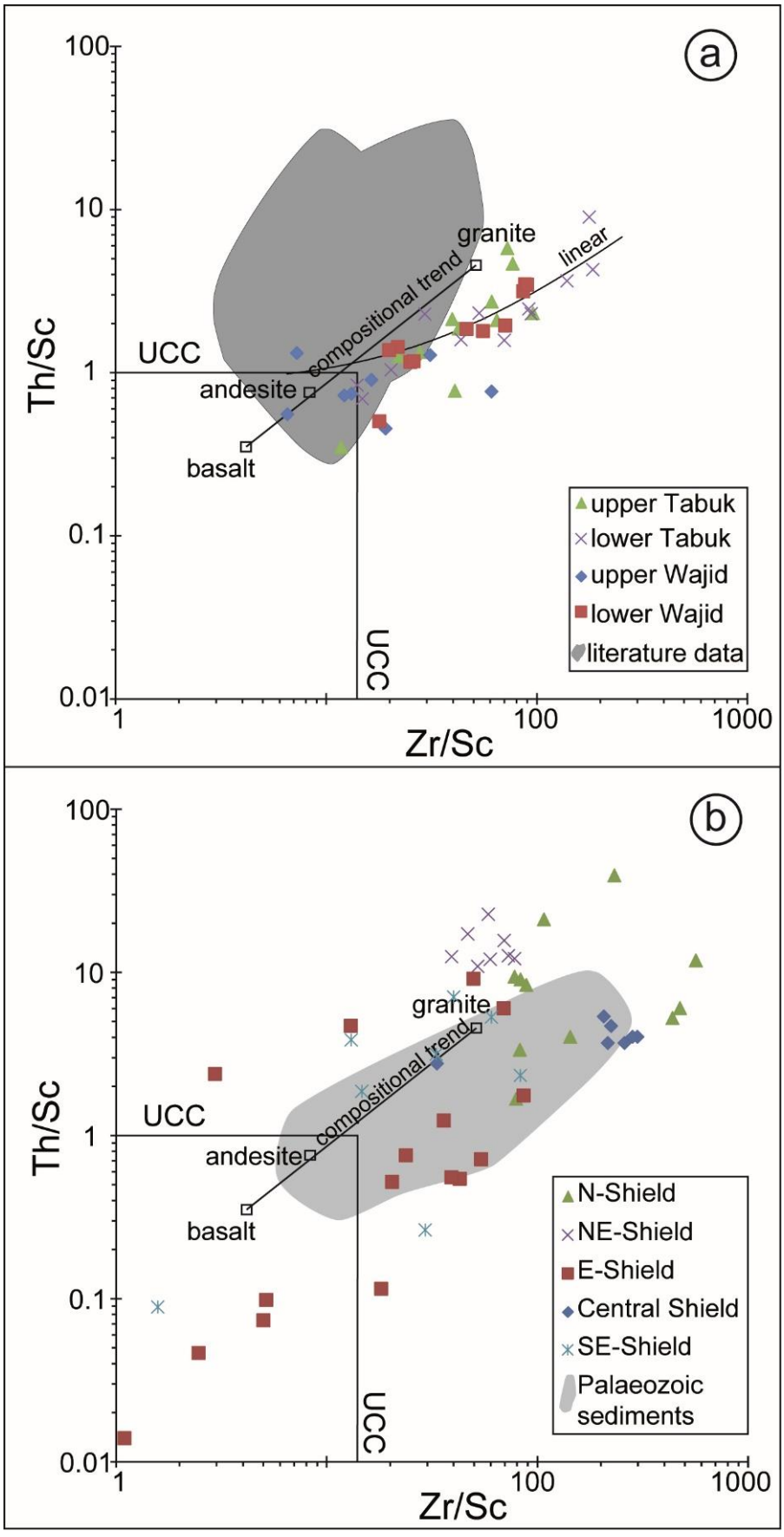

Figure 25: Th/Sc vs. Zr/Sc plot (modified after McLennan et al., 1993) showing zircon enrichment interpreted as sedimentary recycling. UCC (from McLennan, 2001; Taylor and McLennan, 2009) and an idealized compositional trend (from Mongelli et al., 2006) have been plotted for comparison. (a) Data from Palaeozoic sediments; dark grey area represents literature data (from Hussain, 2007). (b) Data from selected basement rocks of the Arabian Shield (from Jackson et al., 1984; Stuckless et al., 1985, 1986; Jackson and Douche, 1986; Leo, 1986; Ramsay et al., 1986; and own samples); light grey area represents Palaeozoic sediments

6.3. Tectonic setting

The chemical composition of sedimentary rocks can give some clues not only about reworking, recycling and weathering conditions, but also on the tectonic setting of their depositional basin. For this purpose, geochemical discrimination diagrams have been developed and used for decades (e.g. Bhatia 1983; Bhatia and Crook 1986; Roser and Korsch 1986; Roser and Korsch 1988; Verma and Armstrong-Altrin 2013). In the past, this approach has been applied to parts of the Arabian Palaeozoic stratigraphic succession (Hussain, 2001; Al-Harbi and Khan, 2005, 2008, 2011; Wanas and Abdel-Maguid, 2006). They uniformly assign a passive margin/intracratonic depositional setting for various Palaeozoic sandstones of the Arabian Platform. This is largely confirmed by the major element, trace element and petrographical data presented in this study.

The geochemical approach to deduce the tectonic setting by studying the major element composition of sedimentary rocks is not without pitfalls. One of those pitfalls is a strong grain size control on sediment composition, which limits the usefulness of whole-rock geochemical analysis in sedimentary provenance studies (von Eynatten et al., 2012). Armstrong-Altrin and Verma (2005) evaluated six common tectonic setting discrimination diagrams proposed by Bhatia (1983) and Roser and Korsch (1986). They compiled an extensive database of geochemical data of Miocene to recent sands and sandstones from three different, known tectonic settings: (1) passive margin (PM), (2) active continental margin (ACM) as well as (3) ocean island arc (OIA). This data set was then used to test the six discrimination diagrams. Success rates varied greatly but were better for the diagram of Roser and Korsch (1986), which managed to correctly discriminate 32% to 62% of the samples, depending on the respective field. It worked best for passive margin and active continental margin settings, but was most unreliable for ocean island arcs. The major element plots and discriminant function diagram of Bhatia (1983) fared even worse, successfully discriminating only 0% to 58% of the samples. It is noteworthy that most of the discrimination fields in the plots of Bhatia (1983) had a success rate of 25% or lower. Only the ocean island arc field of the Al_2O_3/SiO_2 vs. $MgO+Fe_2O_3$ plot managed 58% success when using averaged values from the sample sites. The diagrams after Bhatia (1983) are therefore not further considered in this study. Although the diagram of Roser and Korsch (1986) worked better, the maximum success rate of 62% is still somewhat unsatisfactory and lower than that for the petrographical 'Dickinson model' after Dickinson and Suczek (1979) and Dickinson et al. (1983). Yet when applied with the necessary caution and combined with other techniques, it can still be a useful tool for the interpretation of major element compositional data. Roser and Korsch (1986) used the K_2O/Na_2O ratio vs. SiO_2 concentration in order to discern three different tectonic settings. Generally, as tectonic settings change from ocean island arc to active continental margin to passive margin, derived sediments become enriched in stable phases like quartz and depleted in labile minerals, like feldspars. This leads to increasing SiO_2 concentrations and decreasing K_2O/Na_2O ratios, among others (Bhatia, 1983; Roser and Korsch, 1986, 1988; Huntsman-Mapila et al., 2009). Samples from both study areas have SiO_2, K_2O and Na_2O concentrations typical for sediments deposited on a passive margin or in an intracratonic basin (Figure 27a, b). This is in accordance with literature data (grey area in Figure 27a) and b) and the established tectonic model of the Arabian Peninsula (Sharland et al., 2001). A passive margin or intracratonic setting can also be inferred from the high petrographical and geochemical maturity of the samples (Schwab, 1978; Weltje et al., 1998). Few (7 in total) samples of undifferentiated Wajid sandstone from Hussain (2001) and Babalola et al. (2003) show unexpectedly low SiO_2 concentrations (between 20% and 60%) and/or low K_2O/Na_2O ratios. They thus plot in the active margin and oceanic arc fields. These seven samples are treated as outliers, because Babalola et al. (2003) specifically studied iron-rich horizons ('ironstones'). Therefore outlying samples cannot be regarded as representative for the entire succession. Hussain (2001) unfortunately provides no further explanation for outlying samples.

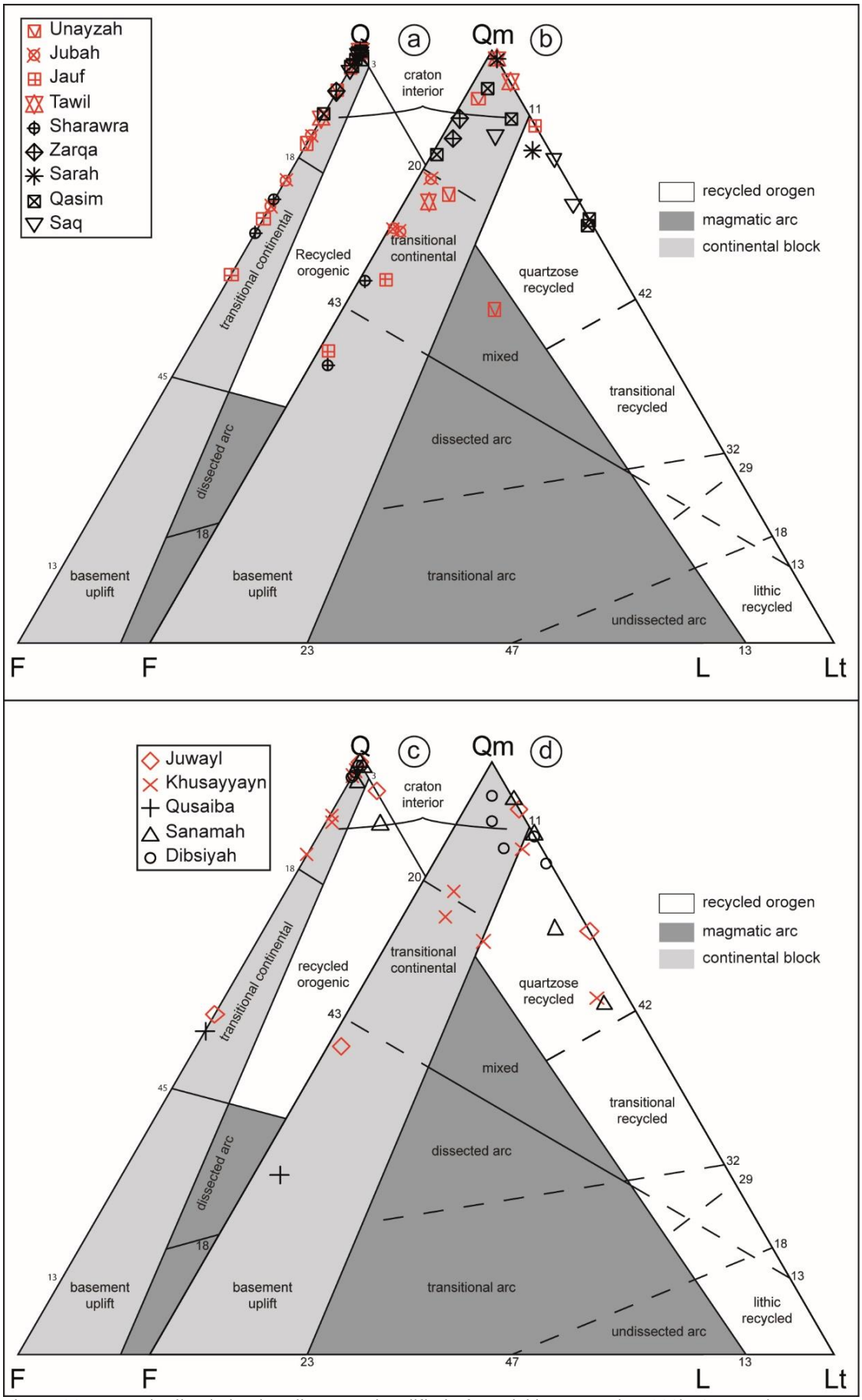

Figure 26: Tectonic discrimination diagrams (modified after Dickinson et al., 1983). Q – total quartzose grains including monocrystalline (Qm) and polycrystalline (Qp) quartz; F – total feldspar; L – total lithic fragments; Qm – monocrystalline quartz only; Lt – total lithic fragments including Qp. (a) & (b) Tabuk area; (c) & (d) Wajid area.

Table 10: Calculations of discriminant functions for tectonic discrimination diagrams of Roser and Korsch (1988) and Verma and Armstrong-Altrin (2013) for high silica rocks (63% – 95% SiO_2).

Roser and Korsch (1988)	
DF1	$(-1.773*TiO_2)+(0.607*Al_2O_3)+(0.76*Fe_2O_3t)+(1.5*MgO)+(0.616*CaO)+(0.509*Na_2O)+(-1.224*K_2O)-9.09$
DF2	$(0.445*TiO_2)+(0.07*Al_2O_3)+(-0.25*Fe_2O_3t)+(-1.142*MgO)+(0.438*CaO)+(1.475*Na_2O)+(1.426*K_2O)-6.861$
Verma and Armstrong-Altrin (2013)	
DF1	$(-0.263*\ln(TiO_2/SiO_2))+(0.604*\ln(Al_2O_3/SiO_2))+(-1.725*\ln(Fe_2O_3t/SiO_2))+(0.66*\ln(MnO/SiO_2))+(2.191*\ln(MgO/SiO_2))+(0.144*\ln(CaO/SiO_2))+(-1.304*\ln(Na_2O/SiO_2))+(0.054*\ln(K_2O/SiO_2))+(-0.330*\ln(P_2O_5/SiO_2))+1.588$
DF2	$(-1.196*\ln(TiO_2/SiO_2))+(1.064*\ln(Al_2O_3/SiO_2))+(0.303*\ln(Fe_2O_3t/SiO_2))+(0.436*\ln(MnO/SiO_2))+(0.838*\ln(MgO/SiO_2))+(-0.407*\ln(CaO/SiO_2))+(1.021*\ln(Na_2O/SiO_2))+(-1.706*\ln(K_2O/SiO_2))+(-0.126*\ln(P_2O_5/SiO_2))-1.068$

Verma and Armstrong-Altrin (2013) proposed new discrimination function-based diagrams to discern the tectonic setting of siliciclastic sediments, utilising major elements (SiO_2, TiO_2, Al_2O_3, Fe_2O_3, MnO, MgO, CaO, Na_2O, K_2O and P_2O_5; see Table 10 for calculation of discriminant functions). They introduced two sets of diagrams, optimized for either low silica (35% to 63% SiO_2) or high silica rocks (63% to 95% SiO_2). Both sets were successfully tested on Neogene-Quaternary as well as Precambrian sediments (success rates of 75% to 100%). Three different tectonic settings were considered: Continental and ocean island arcs ('Arc'-field), continental collision ('Col'-field) and continental rifting leading to the development of passive margins and intracratonic basins ('Rift'-field) (Figure 28). Results from this study and literature data are shown in Figure 28. Samples with elevated CaO due to calcitic cementation were not considered. Most of the samples fall into the rift-field, which fits well to the passive margin/intracratonic setting suggested by the diagrams of Roser and Korsch (1986). Yet the sample population shows a larger spread. Out of 21 sandstone samples from the Tabuk area, 6 plot close to the border of and within the collisional field. Unlike samples from the Sarah and Zarqa formations from this study, samples from the Sarah Formation from Al-Harbi and Khan (2011) plot entirely in the collisional field. Sandstones from the Wajid area cluster more closely together in the rift-field, which is largely in accordance with literature data. Significant discrepancies exist between the presented data set and the samples analysed by ActLabs (grey symbols, Figure 28b). Those samples concentrate around the rift-collisional field boundary and in the collisional field. The main differences between the two analytical sets seem to be SiO_2 concentrations, which were higher in the samples analysed by ActLabs. This is surprising, since samples from both analytical sets came partly from the same outcrops and have comparable lithologies. The geochemical differences therefore probably stem from differences in sample preparation and especially analytical methods: The samples from this study have been analysed with XRF while the ActLabs samples have been analysed with ICP. Although the majority of analysed samples are identified as of rift-/passive margin/intracratonic basin setting, the larger spread of the data compared to the diagram of Roser and Korsch (1986) is striking. The likely explanation is an increased sensitivity to source rock composition and provenance. The signal from sediments deposited in a different tectonic setting than that of their source rocks may be overprinted by the source signal ('provenance signal') in some cases (Verma and Armstrong-Altrin, 2013). While the intracratonic setting of the Arabian Platform is prevalent, some samples display a collisional signal, linked to the final stages of the Pan-African Orogeny in the late Neoproterozoic. Fresh material from the Arabian Shield might have been able to carry this tectonic signature into the basin and preserve it. This theory explains the collisional setting of Sarah samples from Al-Harbi and Khan (2011). Although these authors inferred a predominantly sedimentary to metasedimentary source from petrographical observations and the diagrams of Roser and Korsch (1986, 1988), they also mention a possible granitic source. The new discrimination diagram of Verma and Armstrong-Altrin (2013) is arguably better suited to reflect the initial tectonic source signal over weathering and recycling. This is further confirmed by samples from the Sanamah and Juwayl formations from the 2009–2010 field campaigns and analysed by ActLabs, which also plot in the collisional field (Figure 28b, grey symbols). During glacial periods, Neoproterozoic basement of the Pan-African Orogen apparently constituted a significant source for Palaeozoic sandstones.

A predominantly intracratonic setting, mixed with an older collisional signal can also be inferred from REE concentrations. In the two study areas both mean negative Eu anomaly (0.49 to 0.76) and mean ΣLREE/ΣHREE (5.21 to 7.57) (Figure 15, Figure 16) fall between idealised values for intracratonic and continental island arc settings, according to Bhatia (1985).

As already mentioned, mature quartz arenites can be the result of either repeated sedimentary recycling or intensive weathering and reworking during deposition. Passive margins and intracratonic basins are usually characterised by low sedimentation rates and strong weathering. This leaves sufficient time to produce highly mature, first cycle quartz arenites through reworking (Schwab, 1978; Weltje et al., 1998), without necessitating sedimentary recycling, contrary to the claims of Suttner et al. (1981).

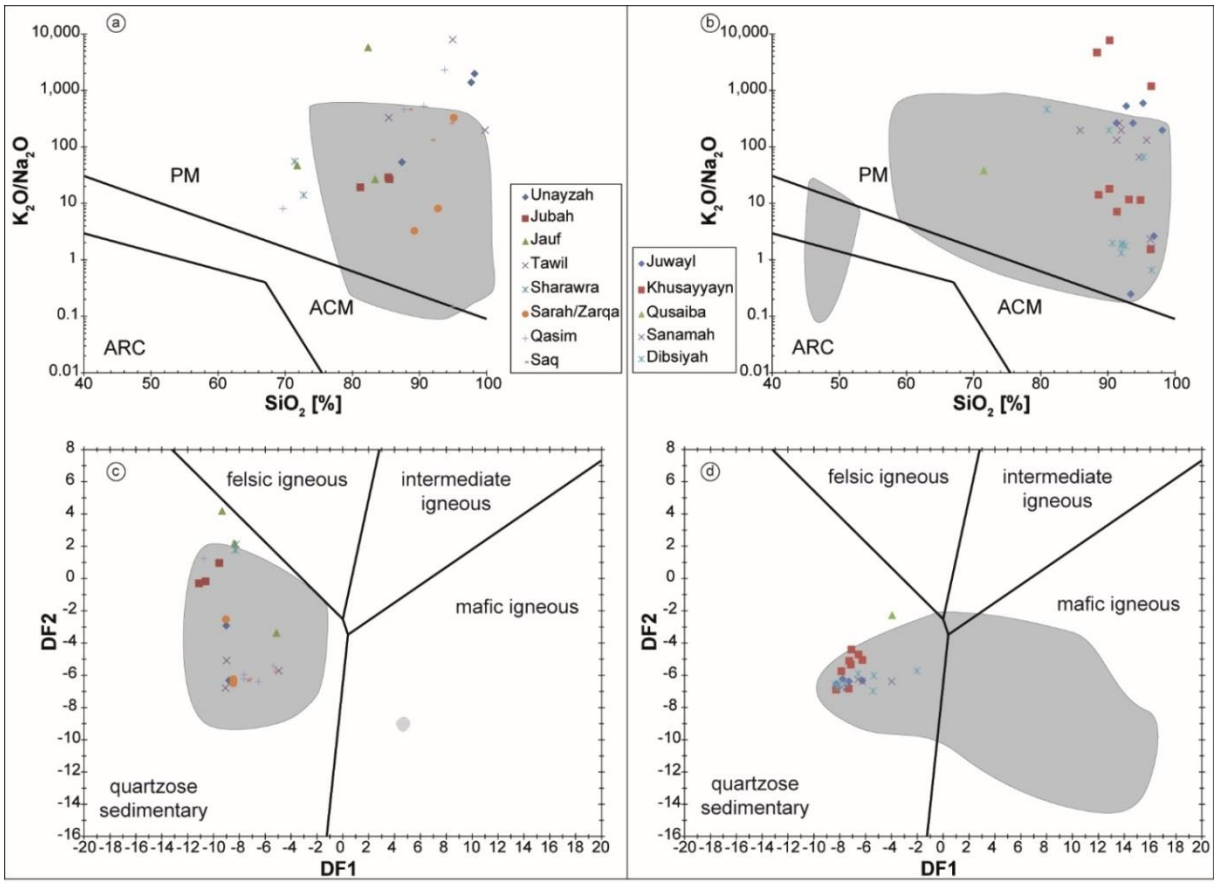

Figure 27: Tectonic setting discrimination diagrams after Roser and Korsch (1986) (a & b) and provenance discrimination diagram after Roser and Korsch (1988) (c & d) for the Tabuk (left side) and Wajid (right side) areas. See Table 10 for calculations of the discriminant functions. PM **–** passive margin, ACM **–** active continental margin, ARC **–** ocean island arc. Grey area represents literature data (from Hussain, 2001; Babalola et al., 2003; Al-Harbi and Khan, 2005, 2008, 2011).

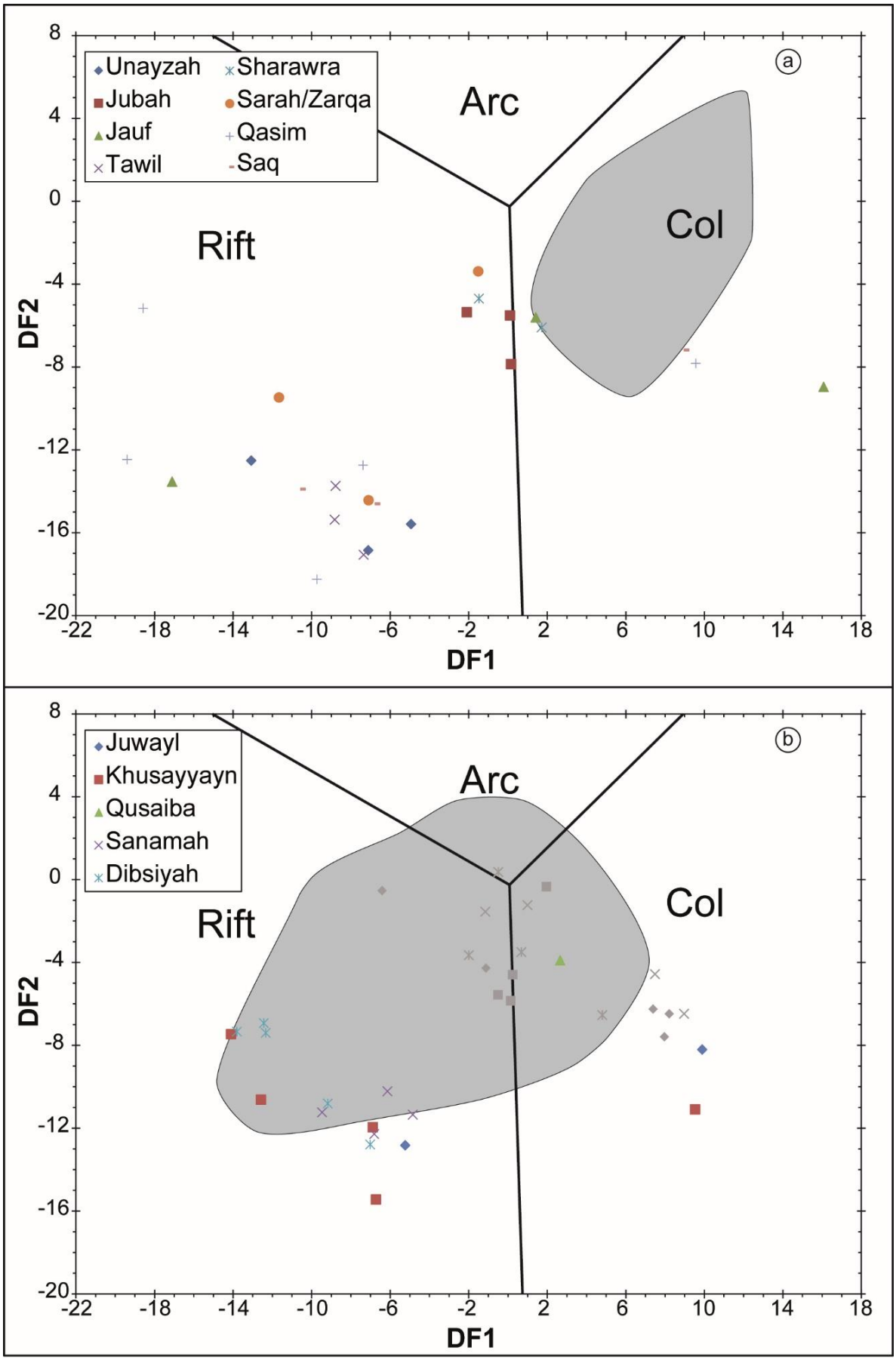

Figure 28: Tectonic setting discrimination diagrams after Verma and Armstrong-Altrin (2013). (a) Tabuk area; (b) Wajid area. Grey area represents range of literature data (from Hussain, 2001; Babalola et al., 2003; Al-Harbi and Khan, 2011); grey symbols in (b) are Wajid samples from the 2009–2010 field campaigns. See Table 10 for calculations of the discriminant functions.

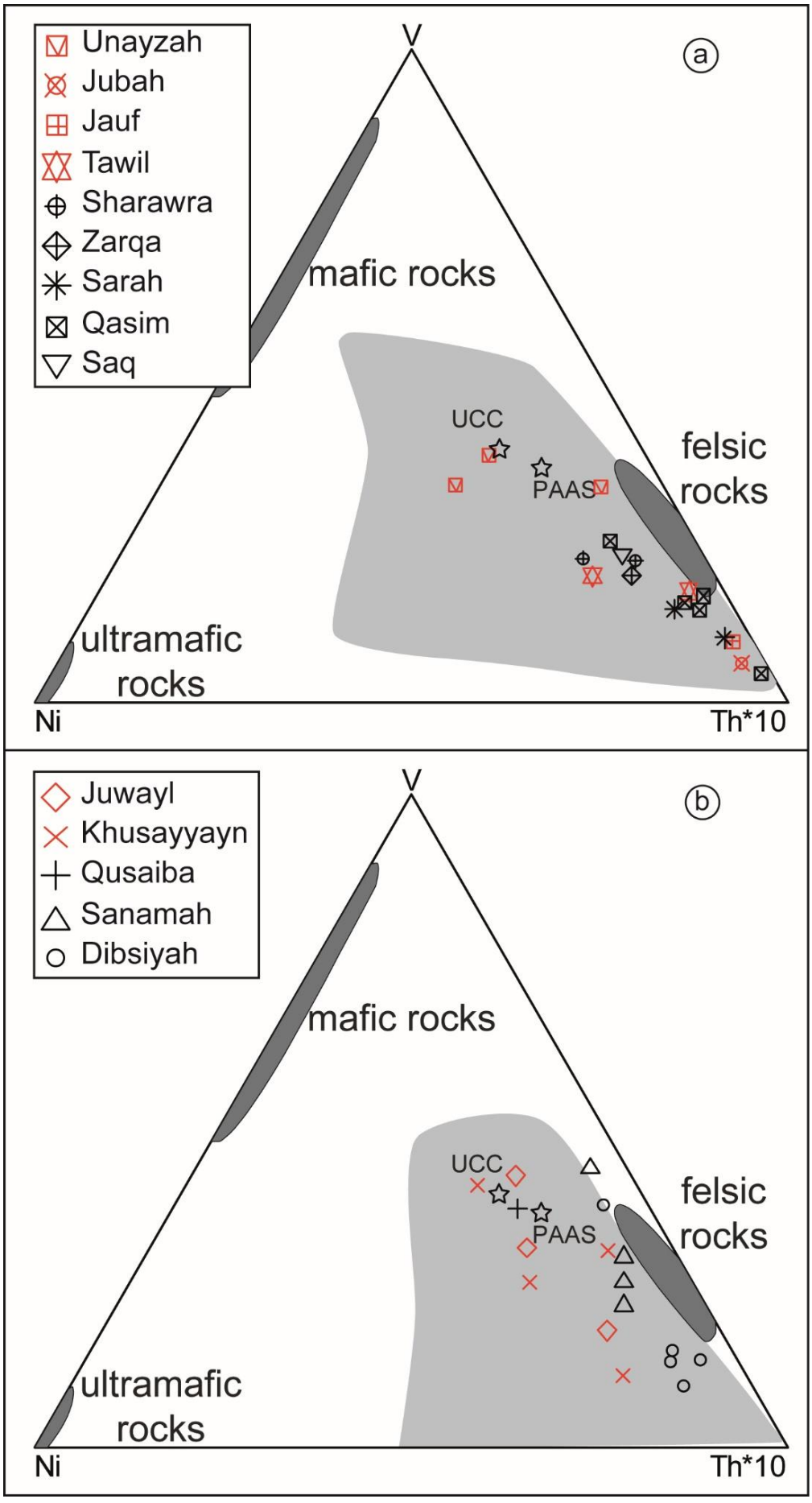

Figure 29: Ternary Ni-V-Th*10 diagram for source rock discrimination (modified after Bracciali et al. (2007). (a) Tabuk area; (b) Wajid area. Light grey area represents literature data (from Hussain, 2001; Al-Harbi and Khan, 2011). Dark grey areas represent idealised source rock end-members. PAAS (from Taylor and McLennan, 1985; McLennan, 2001) and UCC (from Rudnick and Gao, 2003) have

6.4. Provenance

Not only the tectonic setting of the sedimentary basin, but also the type of source rocks supplying the detritus can be deduced by studying the petrography as well as major and trace element composition of sediments.

Dickinson and Suczek (1979) and Dickinson et al. (1983) used detrital framework modes of sandstone suites to deduce tectonic setting and provenance. Ternary diagrams of quartz (Q), feldspar (F) and lithic fragments (L) as well as monocrystalline quartz (Qm), feldspar (F) and lithic fragments including polycrystalline quartz (Lt) are subdivided into tectonic provenance fields. When dealing with quartz-rich sandstones, the QmFLt diagram is better suited to differentiate recycled orogenic provenance settings, since chert grains and quartzose lithic fragments are indistinguishable in the QFL plot. As the sedimentary suites of both study areas are dominated by quartz-rich sediments, the results from the QmFLt diagram have been chosen in this study. Figure 26 shows detrital mode distribution in both diagrams for the Tabuk (a, b) and Wajid (c, d) areas. Samples from the Tabuk area plot mostly in the continental block fields. Only 6 samples can be interpreted to be of recycled orogenic provenance. A craton interior (intracratonic) and quartzose recycled provenance seems to be prevalent in samples from the Saq and Qasim formations, while younger sediments fall also into the transitional continental and even the basement uplift fields (Figure 26b). A similar distribution pattern can be observed for samples from the Wajid area (Figure 26d). A transition from an intracratonic setting to a back-arc in northern Arabia towards the end of the Devonian (Figure 3) could not be identified from detrital mode data. However results from QFL and QmFLt analyses must be treated with prudence. Problems with quartz-rich sands derived from craton interior and recycled orogenic provenance were already recognised by Dickinson et al. (1983). The 'Dickinson model' has been reviewed and challenged in recent years (e.g. Weltje, 2002, 2004, 2006; Weltje and von Eynatten 2004). QFL and QmFLt plots have a success rate of only 75% and do not deal adequately with sands of mixed provenance (Weltje, 2006). Some of the main issues are that detrital modes are not insensitive to fractionation (Weltje, 2004) and they are further modified during generation and dispersal by weathering, abrasion, sorting, chemical alteration as well as after burial by diagenetic effects (Weltje and von Eynatten, 2004). These processes are in turn, at least partly, independent from provenance and tectonic setting. Results obtained from the 'Dickinson model' must be supplemented by other techniques (von Eynatten and Dunkl, 2012).

Roser and Korsch (1988) introduced two diagrams to determine sedimentary provenance and source rock composition. They are discriminant function based and optimized for sediments with and without a significant biogenic fraction, respectively. As there were no bioclasts observed in thin section, the latter one will be applied in this study. The diagram differentiates four source rock types: felsic igneous (acidic plutonic and volcanic detritus), intermediate igneous (andesitic detritus), mafic igneous (basaltic and subordinate andesitic detritus) and quartzose sedimentary (recycled detritus). The first three groups are interpreted as first cycle sources, while the quartzose sedimentary is polycyclic. Samples with intensive carbonate cementation have not been considered in the plot. All analysed samples fall firmly in the quartzose sedimentary field (Figure 27c, d). This suggests either a significant contribution from recycled sediments or intensive reworking and weathering. The plotting range of samples in the quartzose sedimentary field is much tighter for samples from the Wajid area, while samples from the Tabuk area show a larger spread. This may again be due to regional variation and greater differences in depositional facies in the northern study area. Looking at published data (from Hussain, 2001, 2007; Al-Harbi and Khan, 2005, 2008, 2011), the opposite trend becomes apparent: Sandstones from the Tabuk area are grouped together, while samples from the Wajid area – especially those from Hussain (2001) – show a large spread into the mafic igneous field (grey area, Figure 27d). The most likely explanation is that of non-representative outliers. Out of the 74 measured samples, 34 show extremely increased Fe_2O_3 (up to 29%), CaO (up to 42.4%) and Al_2O_3 (up to 33.2%) concentrations. Unfortunately Hussain (2001) gives no explanation regarding those extreme values. Likely causes for elevated CaO and Fe_2O_3 concentrations are calcitic and Fe-cementation, according to own field observations. Abundant Fe-cementation has been observed in some lower Palaeozoic outcrops (Figure 6b) and carbonate cementation is known

from thin sections. As diagenetic features, elevated Fe and Ca concentrations are skewing the provenance signal. The source of high Al_2O_3 concentrations cannot be determined with certainty. Possible causes are clay mineral accumulations or micaceous intercalations. All 34 outlier samples are treated as unrepresentative of the succession and their mafic igneous provenance signal is not considered meaningful. Discrimination diagrams utilising major elements can be useful in determining the provenance of Saudi Arabian Palaeozoic sandstones, yet samples have to be carefully selected. Diagenetic overprints, like strong Fe-cementation in Cambrian–Ordovician units, carbonate cementation or clay mineral accumulation can mask or distort the original source rock signal. Major element composition is furthermore largely dependent on framework mineralogy and thus ill-suited to differentiate reworking and strong weathering from recycling, especially in highly mature quartz arenites.

Trace elements are arguably better suited to determine the source rocks of a sedimentary suite (McLennan et al., 1993; Bracciali et al., 2007). A ternary plot of Ni-V-Th*10 can be used to discern between three source rock 'end-members': ultramafic, mafic and felsic rocks (Bracciali et al., 2007). Unsurprisingly, all samples from both study areas have felsic source rock signatures (Figure 29). A noticeable stratigraphic grouping can be seen in samples from the Wajid area. Samples from the Dibsiyah and Sanamah formations tend to cluster towards the idealised felsic composition. Samples from the Khusayyayn and Juwayl formations are more spread out and seem to have more mafic input (Figure 29b). This trend is not apparent in the Tabuk area (Figure 29a). Literature data (from Hussain, 2001; Al-Harbi and Khan, 2011) show a significant spread. Especially data from the Sarah Formation indicate a significant mafic and ultramafic input. This again points to a relic signal from the Neoproterozoic Arabian Shield and fits their collisional setting in the diagram of Verma and Armstrong-Altrin (2013).

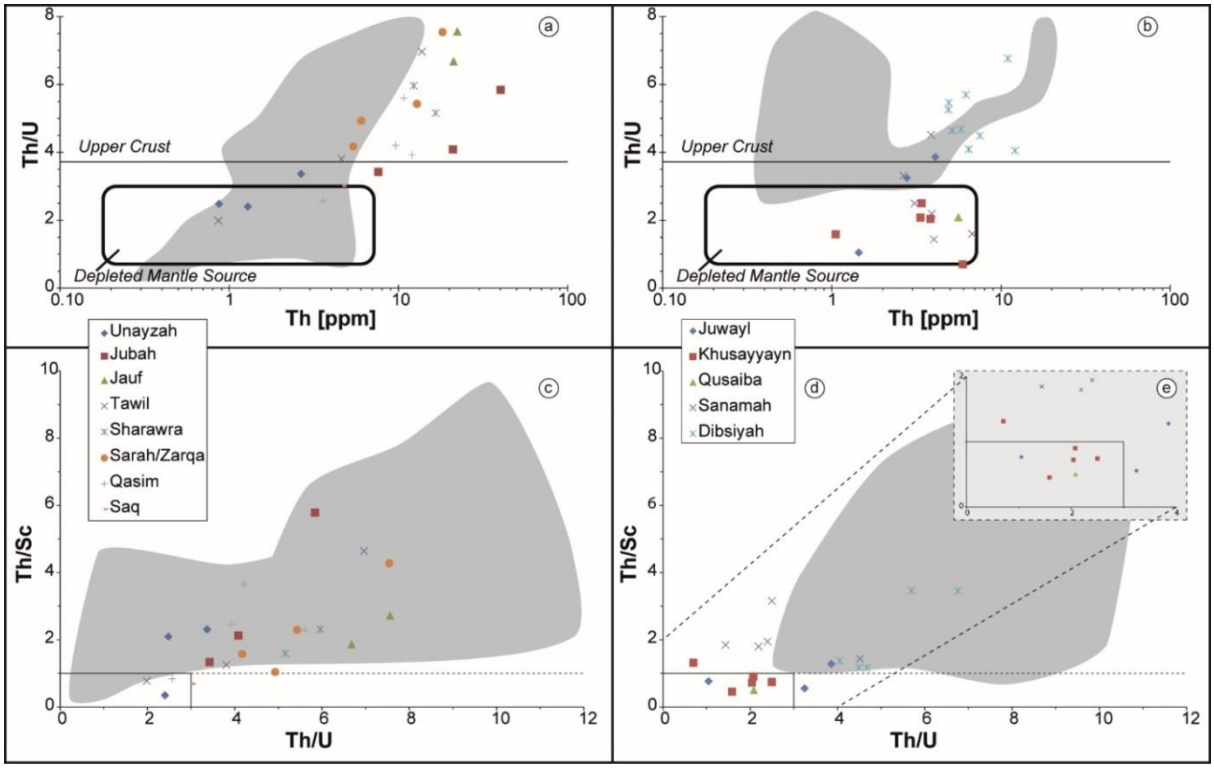

Figure 30: (a) and (b): Plots of Th/U vs. Th (modified after McLennan et al., 1993) for the Tabuk and Wajid areas, respectively. See text for explanation. Grey area represents range of literature data (from Hussain, 2007). (c) and (d): Plots of Th/Sc vs. Th/U for the Tabuk and Wajid areas, respectively. See text for explanation. Grey area represents range of literature data (from Hussain, 2007) Dotted vertical line represents Th/Sc ratio of 1.0. Small box delineates idealised composition of sediments derived from island or continental arcs. (e) Enlarged detail of (d).

McLennan et al. (1993) published several geochemical criteria for discerning tectonic setting and provenance using trace elements. Among them are εNd, Eu/Eu*, Th/Sc and Th/U. They can be used to discern five different provenance types: old upper continental crust (OUC), recycled sedimentary (RS), young undifferentiated arc (YUA), young differentiated arc (YDA) and 'exotic components'. YUA and YDA provenance types correspond to the arc setting, but cannot differentiate further between continental and island arcs. Likewise the OUC and RS provenance types represent the combined collisional and passive margin settings, without differentiating them. 'Exotic components' are any provenance signals at odds with the predominant setting, for example caused by allochthonous terranes. For further detailed descriptions of the five provenance types see McLennan et al. (1993). While these criteria can give valuable clues for sedimentary provenance analysis, they have to be interpreted with care, because they were compiled from modern turbiditic sediments only. The data are therefore not necessarily representative for different grain sizes, depositional facies and climate conditions. With those limitations in mind, trace element ratios can still be useful tools in the study of Saudi Arabian Palaeozoic sandstone provenance. When plotted in a Th/U vs. Th diagram (Figure 30a, b), some samples show a distinct separation. Most of the sandstones from the Tabuk area and those from the Dibsiyah Formation of the Wajid area have Th/U ratios similar or higher than the average UCC. This is further evidence for an intracratonic setting. In contrast, the Sanamah and Khusayyayn formations show a noticeable grouping significantly below UCC values, with U and Th concentrations typical for a 'depleted mantle source'. While high Th/U ratios point to either an OUC source or sedimentary recycling and reworking, low Th/U ratios are indicative for (fresh) material derived from volcanic arcs. Also characteristic for arc-sourced sediments are Th concentrations lower than those of Sc. Whereas the Sanamah Formation exhibits Th and Sc concentrations typical for intracratonic sediments, Th/Sc ratios in the Khusayyayn Formation are predominantly around or lower than one (Figure 30d, e). Possible sources for this detritus are Neoproterozoic juvenile arc terranes that form the core of the ANS (Johnson et al. 2011), which is in accordance with an increased mafic input inferred by Ni, V and Th abundances. A similar distribution in sandstones from the Tabuk area has not been observed (Figure 30a, c). As discussed above, an influx of fresh material, possibly coupled with some minor regional variations in provenance seems likely for the Khusayyayn Formation. Evidence for that are a lower CIA, Th/Sc, Zr/Sc and a marginally lower MI than in other samples from the Wajid area. This influx was confined to the Wajid area and did not reach the sampling sites for the Tawil, Jauf and Jubah formations in the Tabuk area.

6.5. Chemostratigraphy

Highly mature quartz arenites present a unique challenge for stratigraphic correlations, especially when the successions lack fossils. The loss of compositional variety that leads to the creation of quartz arenites also leads to loss of information as rocks become more homogenous. In barren sandstones, where biostratigraphic techniques are limited, different means of correlating rock units are needed. One possible solution is correlation aided by lithostratigraphy, which is stratigraphy based on lithology, lithofacies and type of contacts between strata. Yet lithostratigraphy can be unreliable in subsurface or across large basins as lithofacies change. Another approach is to use changes on the whole-rock geochemistry of sediments as proxies for changes in provenance, weathering (and thus palaeoclimate), depositional setting or other sedimentary features that enable stratigraphic correlations. The major advantages of this method are that it is not as sensitive to sorting effects, especially when considering the immobile trace elements, and it can easily be used with drill-cuttings (Pearce et al., 1999). Although chemostratigraphy is a powerful and increasingly popular tool to correlate barren successions, so far it only has seen limited use in the Palaeozoic of Saudi Arabia. Only one publication (Hussain, 2007) used geochemistry of 50 major and trace elements to correlate lower Palaeozoic sandstones from the Arabian Peninsula. In this study, graphical plots of element compositions or ratios did not yield meaningful results or trends and thus were unable to differentiate between the studied units. Better results were obtained with statistical methods. By performing cluster- and factor-analyses, Hussain (2007) was able to identify significant overlap between samples from the Saq Formation and the Lower Wajid, but only minor overlap between the Qasim Formation and the Lower Wajid. He concluded that all sandstones were deposited in the same basin, but that the Lower Wajid and Saq sandstones were more closely related. This study proves that a geochemical approach can be successfully employed to discern Saudi Arabian Palaeozoic sandstones, but is unfortunately limited to the lowest part of the succession.

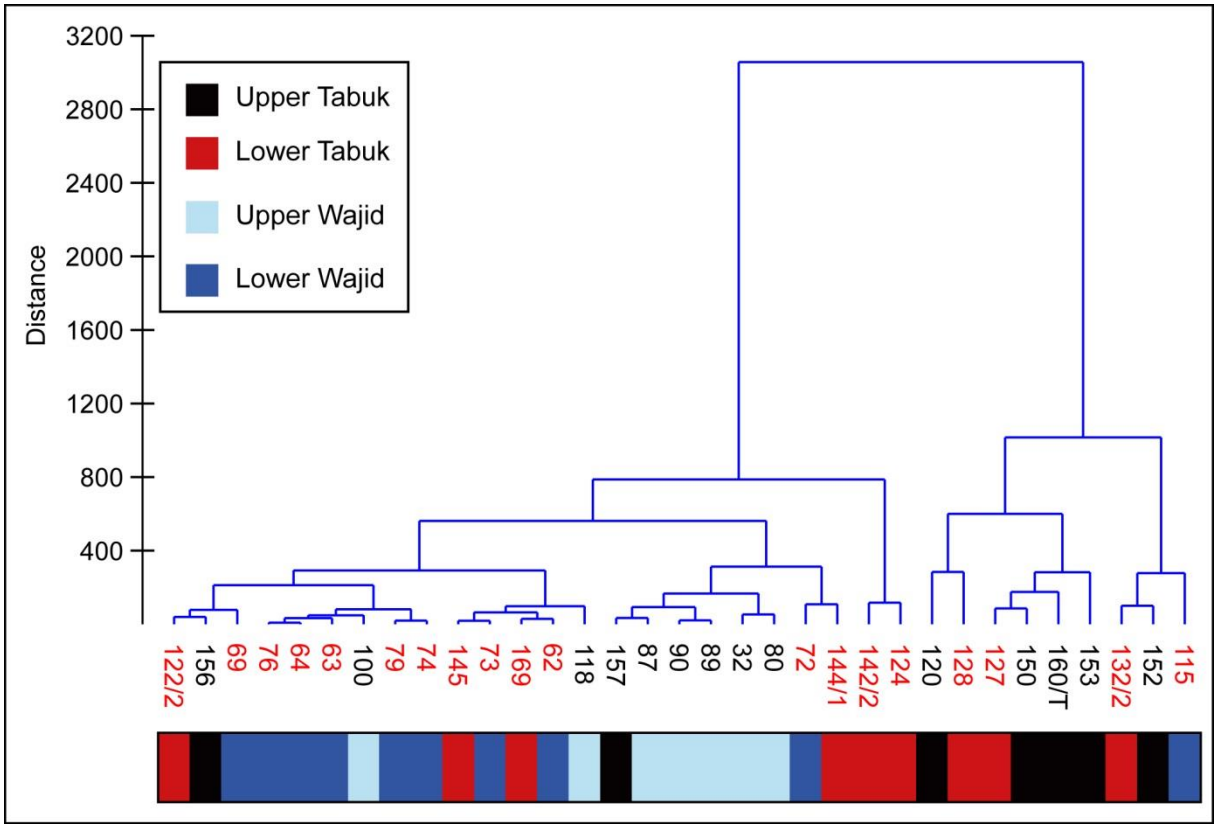

Figure 31: Cluster dendrogram showing association of samples from both study areas. Samples are on the x-axis. Upper Wajid samples cluster closely together in the centre of the dendrogram. Samples from the Lower Wajid, Lower and Upper Tabuk samples also show some clustering.

In the data set presented here as well as in literature data, possible geochemical markers from some discrimination diagrams are tentatively identified. When only considering the samples from the 2013

field campaign, the plot of Th/Sc vs Zr/Sc (Figure 25a) shows a clear grouping of Upper Wajid samples. The Khusayyayn and Juwayl formations seem to be characterised by low Th/Sc and Zr/Sc ratios. Other samples from the Wajid outcrop belt as well as from the Tabuk area displayed higher ratios. Similarly, sample from the Upper Wajid seem to have slightly more mafic and ultramafic input than those from the Lower Wajid, according to the diagram of Bracciali et al. (2007) (Figure 29). While this was not confirmed by our samples for the Tabuk area, literature data from the Sarah Formation (from Al-Harbi and Khan, 2011) display a distinct mafic signal that clearly separates them from the remaining samples from the Tabuk area. The same separation can also be seen in the distinct collisional setting for those samples in the tectonic discrimination diagram of Verma and Armstrong-Altrin (2013) (grey area, Figure 28a).

While the aforementioned criteria may be used as geochemical markers, the 'manual' selection of elements or ratios is too arbitrary and so a statistical approach is needed. One such approach is cluster analysis, which is a multivariate analysis tool to statistically organize large data sets in significant groups or 'clusters' of increasing similarity. Included in the cluster analysis as variables were the concentrations of all measured major and trace elements. As a consequence of the inclusion of major element data, samples with extensive cementation were excluded. The samples from the 2009–2010 field campaigns, analysed by ActLabs, were not considered, because several trace element concentrations were not measured. A first step was to determine and remove potential outliers with the 'single linkage' method. The cluster analysis was then performed using 'Ward's method'; the results are shown as a cluster dendrogram in Figure 31. Each study area divided into a lower part (containing Cambrian through Silurian units) and upper part (containing Devonian through Permian units). Samples from the Lower Wajid (dark blue, Figure 31) tend to cluster in the left side of the dendrogram, while samples from the Upper Wajid (light blue, Figure 31) cluster in the centre. Samples from the Tabuk area (red and black) tend to concentrate on the right hand side of the dendrogram (Figure 31). They do not cluster as closely together and the separation between the Lower and Upper Tabuk areas is not as clear as between the Lower and Upper Wajid areas. Although some overlap exists, this grouping points to a higher degree of homogeneity within Lower and Upper Wajid area samples and a clear distinction from the Tabuk area. The clustering pattern is also in accordance with the observations from Th/Sc vs. Zr/Sc plot (Figure 25a).

Another useful tool of multivariate analysis of large data sets is principal component analysis (PCA). It creates uncorrelated variables, called principal components (PCs), from a data set of (possibly) correlated variables. The first principal component has the highest influence on sample variance and is usually displayed on the x-axis of a biplot. The second PC (usually displayed on the y-axis) accounts for second highest variance, the third PC for the third highest and so on. The goal is to identify the principal directions in which the data varies. The sample range and considered variables for the PCA were the same as for the cluster analysis. A correlation matrix was used, since the data set contains different units of measurement. Results of the PCA are plotted as biplot in Figure 32a and b. PC 1 (x-axis) is responsible for 54.3% of the total variance, PC 2 (y-axis) accounts for 8.9% of the variance (Figure 32c). The green vectors in Figure 32b represent the influence of each variable on principal components one and two. Vectors with similar orientation correlate with each other; vectors with opposite directions correlate negatively. Vectors that are offset by 90° are independent from each other. Similarly, the more aligned a vector is with an axis, the more it correlates with that principal component. The length of the vector represents that components influence on the variance along that axis. Another measure of a variable's influence on a principal component is its correlation value: the higher the absolute value or modulus, the higher the influence on the principal component.

PC 1 has a lot of influential variables with correlation values >0.5, including SiO_2 (negative), TiO_2, Al_2O_3, MgO, K_2O, P_2O_5, Fe_2O_3t, Li, Sc, Ni, Ga, Y, Zr, Nb, Sb, Rb, Sr, Cs, Ba, REEs, Lu, Hf, Tl, Pb, Bi, Th and U. PC 2 on the other hand has only five variables with correlation values >0.5: MgO, Fe_2O_3t, Li, Zn and Mo. The remained of variables exert only minor influence on the total variance. Figure 32b shows a good negative correlation of SiO_2 with Fe_2O_3t and MgO as well as weaker a negative correlation with CaO, MnO and K_2O. This is unsurprising and reflects the degree of sandstone maturity and matrix content. SiO_2 shows no significant correlation with Al_2O_3, P_2O_5 and Na_2O. TiO_2, REEs, Zr, Hf and Th do not correlate with neither of the other major elements. This indicates their abundance is not controlled by framework grains or matrix, but rather by heavy minerals like zircon and rutile. The high number of variables significantly influencing PC 1, and therefore total variance, creates difficulties for the interpretation of the PCA and the controlling factors of the principal components. Nevertheless the sample distribution in the scatter plots shows a clear distinction between the two study areas along the x-axis (PC 1). The Wajid area samples cluster closely together on the left side of the plot (grey areas, Figure 32b), while the Tabuk area samples are much more spread out. The variance of the samples from the Wajid area seems mainly dependant on PC 2 (y-axis).

In order to facilitate interpretation of the plots and to enhance the apparent trend within the Wajid area samples, the PCA has been repeated several times with reduced sets of variables (not all plots shown). The process started with all significant (correlation value >0.5) variables for PC 1 and PC 2 and was repeated with a decreasing number of variables. Throughout the process, the general trend and appearance of the biplot did not change significantly, but the separation between samples from the Lower and Upper Wajid increased. The final iteration is shown in Figure 33. Significant variables include: SiO_2, TiO_2, Al_2O_3, MgO, K_2O, Fe_2O_3t, Li, Zn, Y, Zr, Nb, Rb, Sr, Ba, Lu, Hf, Th, U. REE distributions are represented with the variables ΣREE, ΣLREE/ΣHREE and Eu/Eu*. CIA values have also been included. PC 1 is responsible for 52.3%, PC 2 for 14.6% of the total variance. The subordinate trend within the samples from the Wajid areas separating the Dibsiyah and Sanamah formations (red dots, Figure 33b) from the Khusayyayn and Juwayl formations (black dots, Figure 33b) along the y-axis, is clearly visible.
PC 1 is mainly controlled by major elements without Fe_2O_3t, plus Y, Nb, Rb, Ba and Lu. PC 2 is mainly controlled by Zr, Hf, Th and Eu/Eu*. Nb and Y abundances are primarily controlled by heavy minerals, especially rutile and monazite. Rutile however exerts only minor control on the total variance, as can be inferred from the TiO_2 concentrations, which do not correlate with either PC 1 or PC 2. This non-correlation is also apparent with Zr and Hf concentrations, suggesting zircon abundances do not vary much throughout both successions. Likewise, clay minerals do not vary much as well, as is demonstrated by the non-correlation of Al_2O_3 with PC 1 and PC 2. Both the CIA and Eu/Eu* are linked to the abundance of plagioclase. They are thus influenced by weathering and susceptible to sorting effects. Whilst Lower and Upper Wajid area samples show a clear separation, it may be strongly dependant on facies variability rather than representing changes in provenance or climate. Nevertheless, cluster and principal component analyses were clearly able to discern between different stratigraphic units and study areas. Chemostratigraphy evidently has the potential to characterise and correlate Palaeozoic sandstones from Saudi Arabia. Yet due to the small sample size, this data set can only be considered as a pilot study. To identify and develop robust geochemical markers a larger, statistically more significant database needs to be established.

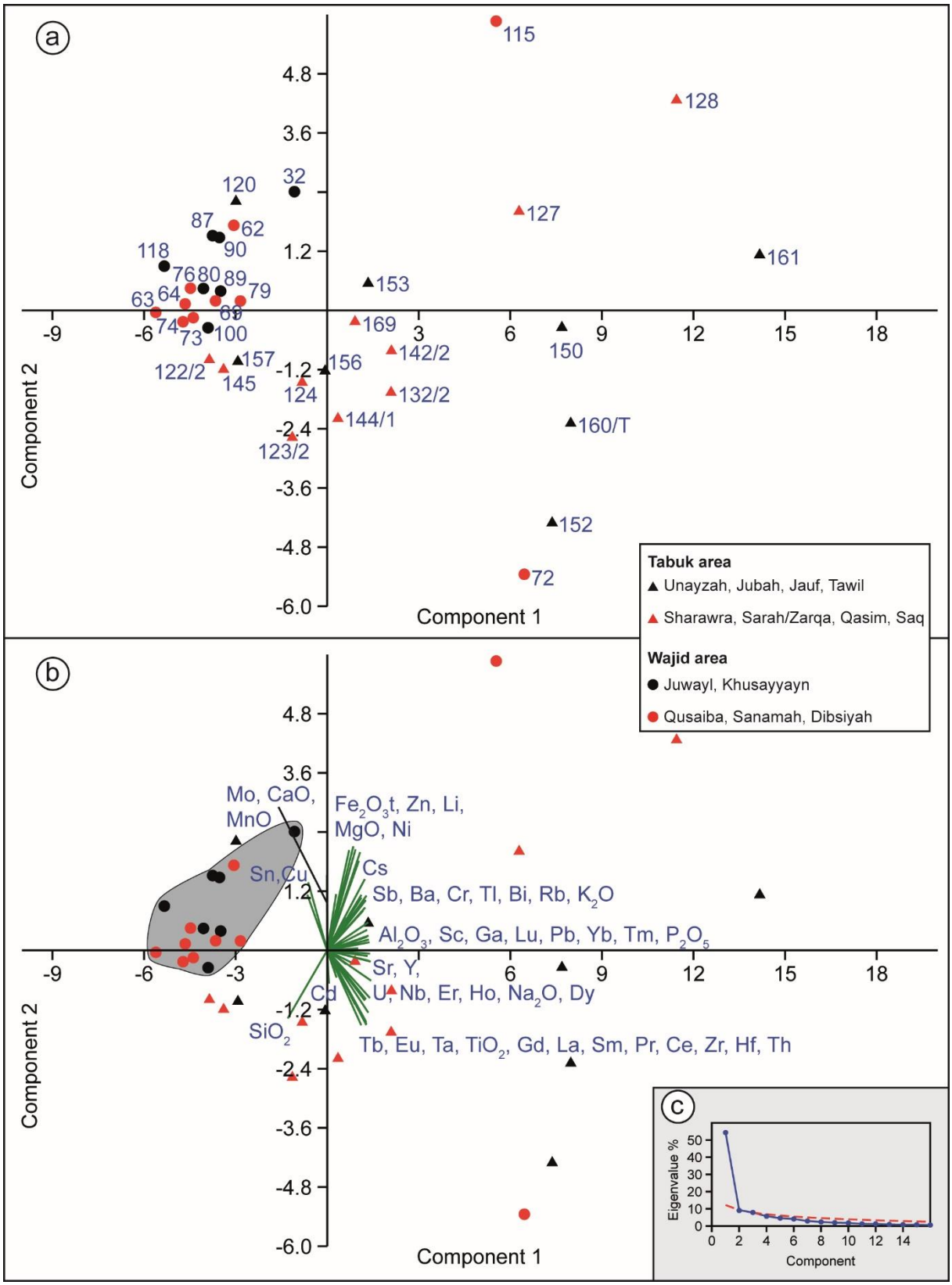

Figure 32: Scatter plot of the two most significant components of a principal component analysis (PCA). Different symbols and colours represent samples from upper and lower successions from both study areas. The first two principal components accounted for 63.2% of the total variance of the data set. (a) Arrangement of samples; (b) biplot of variables; grey area represents range Wajid area samples without outliers; (c) scree plot of principal components vs. eigenvalues.

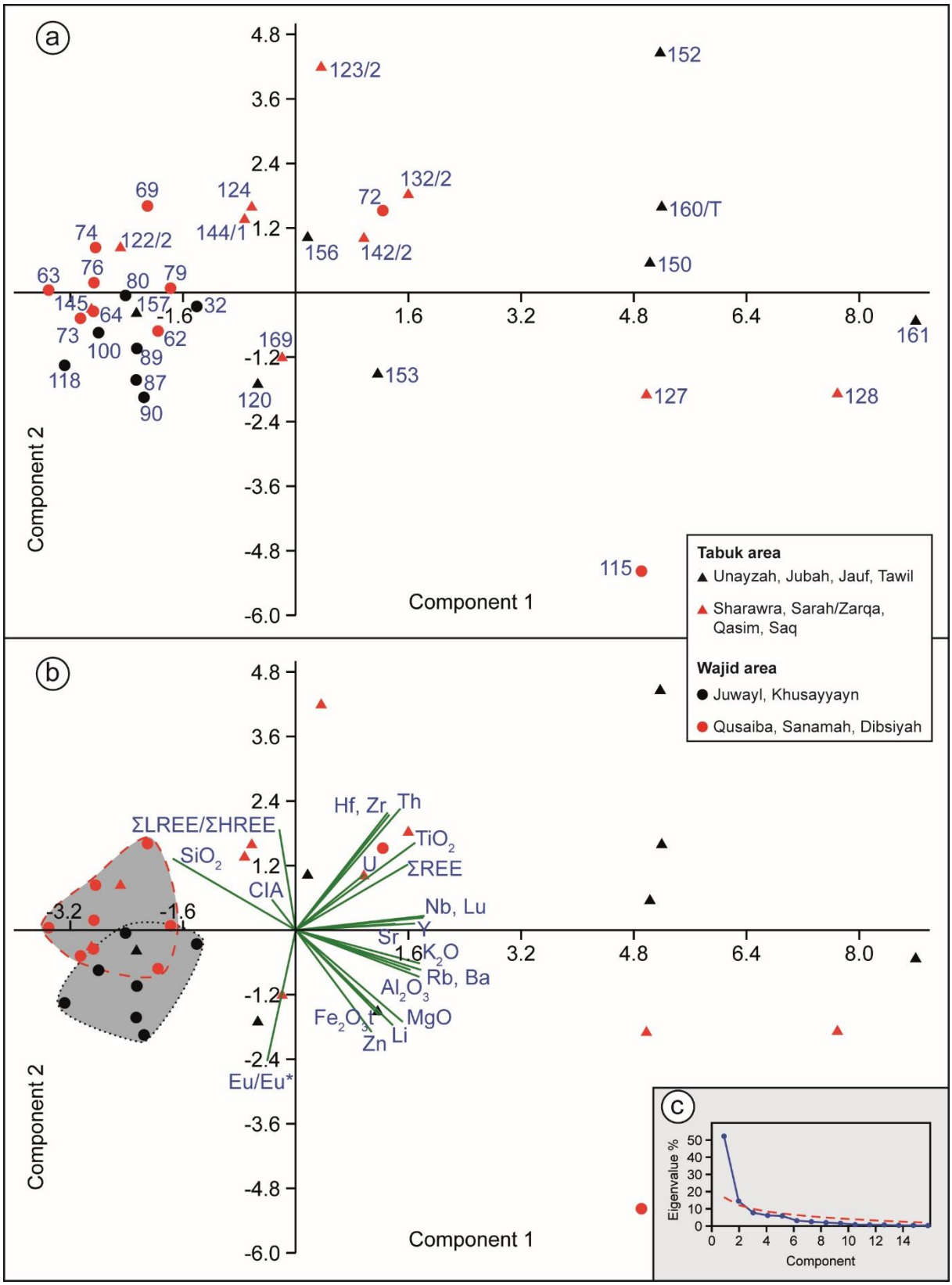

Figure 33: Scatter plot of the PCA with a reduced data set. The first two principal components accounted for 67.1% of the total variance of the data set. (a) Arrangement of samples; (b) biplot of variables; black dotted area represents range of Upper Wajid samples; red dashed area represents range of Lower Wajid samples without outliers; (c) scree plot of principal components vs. eigenvalues.

6.6. Standard heavy mineral analysis

The heavy mineral assemblages of the studied samples are typical for highly mature sandstones. Dominant fractions are the ultra-stable minerals zircon, tourmaline and rutile, which are heavily resistant to weathering and diagenesis. Less stable heavy minerals, like apatite, staurolite and garnet make up only a fraction of the total assemblage, while metastable and unstable minerals are almost completely absent. This distribution can be the result of several processes: a primary source signal from acidic igneous rocks, recycling of older sedimentary rocks, heavy weathering in the source area, reworking during deposition, dissolution after burial or any combination of those, through removal of less stable phases. The abundance of ultra-stable minerals alone gives no evidence which process was responsible and is in itself not a reliable provenance indicator, without further considering depositional facies, palaeoclimate and tectonics.

The presence of prismatic zircon and hypidiomorph tourmaline throughout the successions of both study areas most likely indicates that some detritus was freshly derived from an intermediate to felsic volcanic source (Morton et al., 1992). This would hint to a mixed recycled sedimentary and igneous provenance, under the assumption that the rounded zircon and tourmaline grains were derived from recycled sediments. Another explanation would be alluvial storage (Morton and Hallsworth, 1999) and/or constant reworking during deposition, accompanied by regular influxes of fresh material. In this scenario, the prismatic grains would represent the ‘latest batch’ of fresh detritus which consequently did not undergo much reworking before burial.

The ZTR index of Devonian-Carboniferous samples decreases compared to Cambrian–Ordovician sandstones (Figure 19). Consequently, the latter units cannot have been the sole source for the upper Palaeozoic successions. At least some input from freshly exposed basement is required to introduce the less stable heavy mineral phases. According to Avigad et al. (2005) the impoverished heavy mineral assemblage of the Cambrian–Ordovician sandstones is the result of extreme weathering coupled with low sedimentation rates. Hirnantian samples from both study areas (Sarah, Zarqa and Sanamah formations) exhibit very high ZTR values as well (Figure 19). Their depositional setting in a glacial context under cold conditions did allow for neither strong chemical weathering nor reworking during deposition. The high ZTR content must therefore largely be the result of sedimentary recycling. Similar values for the ATi from Hirnantian and Cambrian–Ordovician samples further support recycling over weathering. The slightly higher RZi values encountered in the Tabuk area hint to a somewhat higher contribution of metamorphic rocks compared to the Wajid area (Figure 19).
An increased contribution from metamorphic sources in the Devonian-Carboniferous is implied by the steady increase of the STi in the Wajid area from the Devonian onwards. The RZi and STi patterns do not fit very well in samples from the Tabuk area. While an increased RZi compared to Wajid samples indicates a higher metamorphic input, Tabuk samples are almost devoid of staurolite (Figure 19). Since the RZi is a more reliable provenance indicator, the absence of staurolite in the Tabuk area is probably either caused by dissolution or fractionation during transport.

Apatite is exceptionally resistant during burial diagenesis but highly susceptible to chemical weathering under surface conditions, especially in humid climates (Morton and Hallsworth, 2007). The comparatively low abundance of apatite and consequently low ATi encountered in most samples reinforces weathering and/or recycling rather than dissolution after burial as the main reason for their depleted heavy mineral assemblages. Knox et al. (2007) argued convincingly that ATi values are an original feature and not the result of Quaternary weathering. The very low ATi of lower Palaeozoic Tabuk samples compared to the corresponding Wajid succession is striking (Figure 19). While this could be a genuine provenance signal pointing to a recycled sedimentary source, it is more likely the result of intensive weathering (Morton and Hallsworth, 1999). This of course begets the question as to why the Tabuk area experienced increased weathering during the early Palaeozoic compared to the Wajid area. Localised climate differences seem improbable. Further transport and/or prolonged alluvial storage are apparently better explanations. This indicates the contribution of a common, southerly source of the lower Palaeozoic successions from both study areas: Sediments deposited in the Tabuk area would

have experienced longer transport and thus increased weathering, resulting in lower ATi values, than the corresponding sediments deposited in the Wajid area. Potential southerly source areas are situated in central and eastern Afria and include the Irumide and Mozambique belts (Meinhold et al., 2013b).

As discussed below (see 4.2), there arise problems with the rutile distribution in this model. Specifically the absence of high-grade rutile in the Dibsiyah Formation and significant differences in rutile source lithologies between the study areas do not support a common source. The detritus of the lower Palaeozoic in both study areas was derived from distinct sources within the ANS, but the Saq and Qasim sediments experienced stronger weathering, probably caused by longer transport and/or alluvial storage. Hence, circumstances of different source areas and prolonged transport both are unclear so far. The high GZi in sample AB-SA98 is probably a real provenance signal, since it is accompanied by high RZi, ATi and STi, which together indicate a large contribution from a nearby fresh metamorphic source and weak weathering conditions. This fits well with the glaciogenic depositional model of the Juwayl Formation.

Whether the low GZi/absence of garnet in lower Palaeozoic units in both study areas is a real provenance signal or due to post-depositional modification has to be carefully evaluated. Intrastratal dissolution could have removed the garnets from the older units during burial. This is well known from other deep sedimentary basins (Morton and Hallsworth, 2007). In the presented case, there is evidence for diagenetic dissolution of garnet. Slight etch markings and corrosion textures, which are indicative signs for beginning diagenetic dissolution, have been observed in this study (Figure 18f). Knox et al. (2010) report dissolution features on some garnets from wells penetrating the Unayzah Formation in central Saudi Arabia. In more deeply buried successions garnet is entirely absent, which Knox et al. (2010) attributed at least partly to burial dissolution. The absence of garnets in older sediments is problematic to bring in accordance with the abundance of garnet-bearing rocks in and around the ANS (Stacey and Agar, 1985; du Bray, 1988; Kröner et al., 1991; Ghebreab, 1999; Woldehaimanot, 2001; Fritz et al., 2002; Wahed et al., 2006; Al-Saleh, 2012).

On the other hand, Knox et al. (2007) explicitly mention the absence of dissolution features on garnets from the Wajid area and consider their samples unaffected by diagenetic dissolution. Staurolite, which is less stable than garnet during deep burial, is still present in some of the older, underlying Palaeozoic formations from this study and is also reported by Knox et al. (2007). It is possible that the Wajid area was probably never buried deeply enough to dissolve all garnet, given its position at the rim of the Arabian Shield and the low sedimentation rates in an intracratonic basin. Paris et al. (2015a, b) recovered well preserved microfossil assemblages from Upper Ordovician and lower Silurian subsurface samples. Similarly, Melvin (2015) did not report any dissolution features in his descriptions of Upper Ordovician and lower Silurian cores, but instead mentions well preserved trace fossils. The sample from the Juwayl Formation (AB-SA98) is strongly cemented and retains fresh K-feldspar unaffected by diagenetic dissolution (Figure 10c, d). While not as prominent as in the Juwayl sample, the samples from the Jubah Formation still contain significant K-feldspar (Figure 9; Table 4). K-feldspar removal by dissolution is a common pattern in sedimentary basins during deeper burial, between 1.5 and 4.5 km (Glasmann, 1992; Wilkinson et al., 2001). The etch markings and dissolution features observed on garnets in those samples are therefore not necessarily related to the deep burial of the Palaeozoic sediments. They could have been inherited from a previous diagenetic event, if a recycled (meta-) sedimentary source is assumed. Garnet dissolution through surface weathering has been excluded for the Juwayl Formation by Knox et al. (2007).

Whether the absence of garnets in the older units is a provenance feature or a result of intrastratal dissolution could not be answered with confidence. Regional variation of diagenetic conditions may also play a significant role. Although there is evidence for both cases, it is tentatively assumed that the presence of garnet in the younger Palaeozoic formations is a genuine provenance signal. In this context, the importance of petrographic observations in conjunction with heavy mineral studies is stressed.

The general composition of heavy mineral assemblages with a high ZTR fraction and few other meta- and unstable minerals is also observed in several other studies of the Palaeozoic of northern Gondwana (Powers et al., 1966; Hussain et al., 2004; Knox et al., 2007; Weissbrod and Bogoch, 2007; Morton et al., 2011; Garzanti et al., 2013). Yet in detail those studies differ significantly from each other and from this study. Powers et al. (1966) observed mica (biotite and muscovite) in Palaeozoic sandstones from northern Saudi Arabia. Noteworthy mica content has not been reported from any of the other mentioned publications. Unfortunately, no percentages are given for the observed heavy minerals. The presence of biotite and muscovite in lower and upper Palaeozoic sandstones is surprising, since mica breaks down relatively easy during chemical weathering and mechanical abrasion. This is even more dubious as Powers et al. (1966) infer a recycled sedimentary provenance for the Palaeozoic sandstones. They also observed a remarkably impoverished heavy mineral assemblage for the Saq Formation compared to that of the Tawil Formation, which is in accordance with this study. Hussain et al. (2004) also observed high ZTR abundances in samples from the southern Wajid area. Contrasting to this study, they also reported minor occurrences of hornblende, epidote and kyanite, but a complete lack of apatite. While some kyanite and epidote was observed in this study, it was to a much lesser degree. Hornblende was not present at all in the analysed samples. Hussain et al. (2004) interpreted this assemblage as derived from a mix of Neoproterozoic basement terranes and the 'Infracambrian' Ghabar Group in Yemen. They explicitly excluded the Arabian Shield as a significant source. It is noteworthy that they only studied the 125–250 µm grain-size fraction. Their results may therefore not necessarily be comparable to others since there is a grain-size dependence of heavy mineral composition (e.g., Garzanti et al., 2009; Krippner et al., 2015). The strong control of heavy mineral assemblages by hydraulic sorting related to grain size is well known (Garzanti et al., 2009). Krippner et al. (2015) demonstrated significant variances in the heavy mineral assemblages of different grain size fractions from the same sample. They attributed grain size-dependant variability to different grain sizes of certain mineral phases in the host rocks and not to hydraulic sorting. Krippner et al. (2015) observed a decrease of apatite and an increase of green calic amphibole towards the coarse tail of their size distribution (125 µm). This helps to explain the presence of hornblende and the complete absence of apatite in the coarser grain-size fractions of Hussain et al. (2004).

The compositional variations reported by Knox et al. (2007) in their study of Wajid Group sandstones have not been encountered to the same amount in the presented data set. Key differences are the lack of monazite and hornblende compared to the samples of Knox et al. (2007). They found hornblende in minor concentrations (0.1% to 7.5%) in almost every sample, with two samples having strongly elevated concentrations (23.8% in a sample from the Khusayyayn Formation; 43.9% in a sample from the Juwayl Formation). Monazite is likewise present in almost every sample of Knox et al. (2007), though they did not observe strongly elevated concentrations. Instead, monazite concentrations range from 0.3% to 8.7%. Yet the general composition and compositional trend are similar to this study: a dominant ZTR fraction and a decrease of ultra-stable minerals towards younger strata. A drop of the RZi has been observed in this study as well, albeit not at the Sanamah-Dibsiyah boundary, but within the Dibsiyah Formation. This is mirrored to some degree in the Tabuk area. Although the RZi generally behaves twitchy, there is a significant drop between the Qasim and Sarah formations (Figure 19). Also similar to the data set of Knox et al. (2007) is the STi, which shows a significant increase in the Khusayyayn and Juwayl formations' strata compared to older samples from the Wajid area (Figure 19).

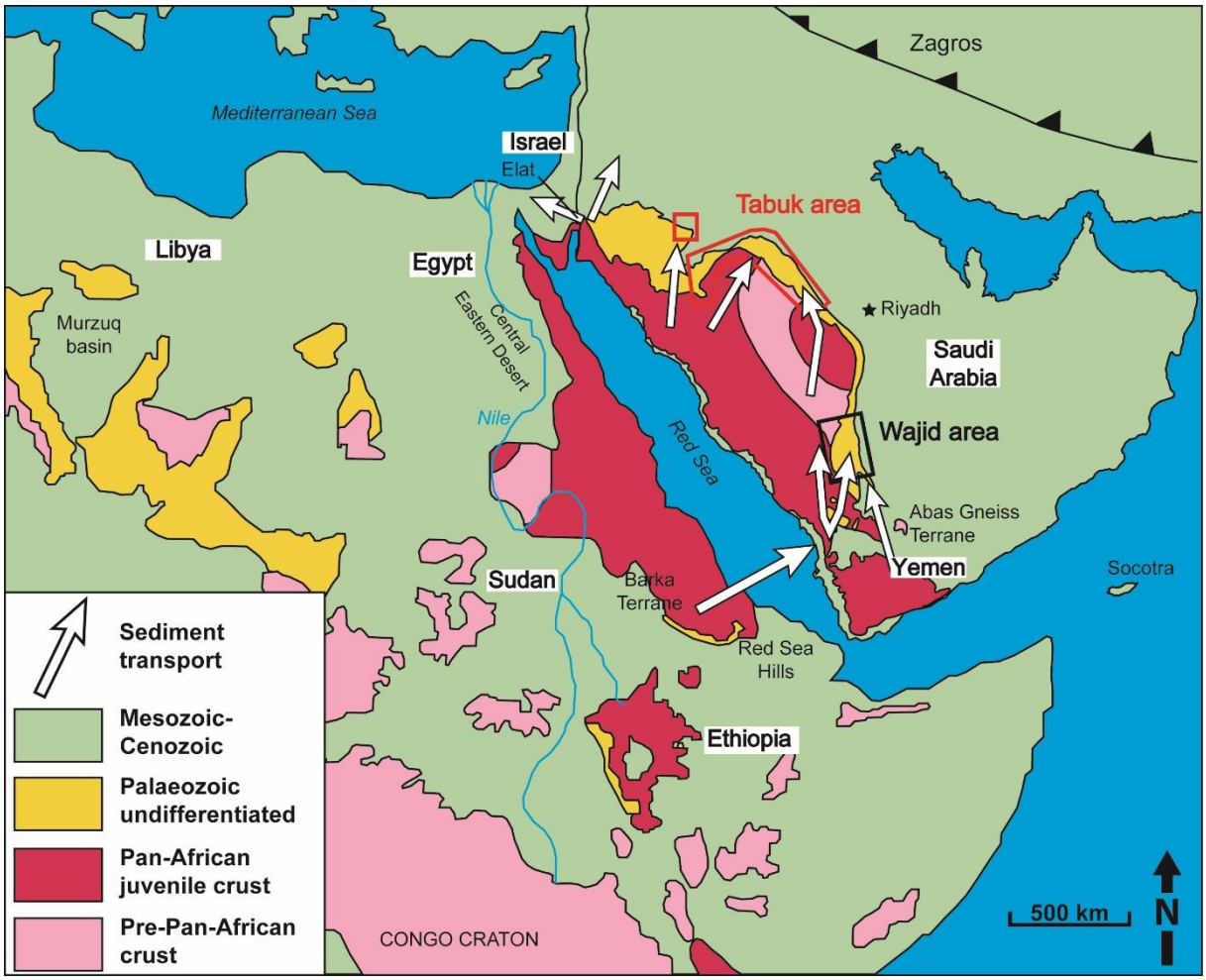

Figure 34: Sketch map of the Arabian Peninsula and surrounding areas (modified after Powers, 1968; Avigad et al., 2005; Meinhold et al., 2013b). White arrows show implicated sediment transport directions.

Weissbrod and Bogoch (2007) compiled heavy mineral data for, among others, Palaeozoic sandstones from the northern margin of the ANS (Figure 34). The cited assemblages are again largely concordant with the results from Saudi Arabia. Cambrian–Ordovician sandstones from southern Israel and southern Jordan as well as Cambrian and Carboniferous sandstones from west central Sinai are dominated by ultra-stable heavy minerals and have consistently high ZTR values. Yet again differences appear in the accessory fractions of less stable minerals. Staurolite is reported from the Cambrian to Silurian from southern Jordan. In contrast, Tabuk samples are poor in staurolite (Figure 19a). The Late Ordovician and Silurian in southern Jordan also feature significant garnet. Likewise the abundance of apatite from the Cambrian of southern west central Sinai and southern Israel does not match Saudi Arabian assemblages. They interpreted the heavy mineral assemblages of Cambrian–Ordovician sandstones as first-cycle detritus derived from the interior of Gondwana and transported over long distances, including extensive alluvial storage. In contrast, upper Palaeozoic sandstones are thought to be mainly sourced from recycled, lower Palaeozoic sediments. This interpretation does not fit completely with the data from Saudi Arabia. The reduction of ZTR values in later Palaeozoic units requires the input of at least some detritus derived from fresh basement outcrops, particularly regarding the greatly impoverished heavy mineral assemblages of lower Palaeozoic sandstones.

Knox et al. (2010) used SHMA and heavy mineral indices (ATi, RZi, GZi, monazite:zircon index [MZi], chrome-spinel:zircon index [CZi], pink zircon index [pZi], euhedral zircon index [eZi]) to correlate sandstones of the Unayzah Formation between wells in central Saudi Arabia. They identified and characterised four principal heavy mineral units (UNZ1A, UNZ1B, UNZ2, UNZ3), largely corresponding to the established lithological subdivision of the Unayzah Formation reservoir. UNZ1A and B correspond to the Unayzah A Member and the 'un-named middle Unayzah Member', UNZ2 to the Unayzah B Member and UNZ3 to the Unayzah C Member (Knox et al., 2010). Furthermore, they recognised the influence of

local sand influx and placer deposits and the problems associated with interpreting them. Unfortunately, they do not provide raw data, i.e. heavy mineral counts, only chosen heavy mineral indices. Assigning a single surface sample from this study to one of the heavy mineral zones of Knox et al. (2010) is difficult: They rely heavily on trends to characterise the zones and employ indices not recorded in this study (monazite-zircon index, euhedral zircon index) and only studied sub-surface samples. Furthermore, they did not consider staurolite and garnet or the corresponding indices (STi and GZi). According to Knox et al. (2010), those minerals are heavily affected by burial dissolution and are absent in deeper parts of the wells. With these caveats in mind, sample AB-SA120 can tentatively assigned to the UNZ1B heavy mineral unit, because of low values for the RZi and ATi and the absence of monazite (Figure 17a, Figure 19a). According to this characterisation, the outcrop sample belongs to either the 'un-named middle Unayzah Member' or the Unayzah A Member. This fits to field observations. Although the outcrop of sample AB-SA120 was small and in a bad condition, lithology and geographic position fit to the uppermost Unayzah Formation (Unayzah A Member) at the type locality in the town of Unayzah (Senalp and Al-Duaiji, 1995; Khalifa, 2015).

Compared with data from Palaeozoic sandstones of the eastern Murzuq Basin, Libya (Figure 34), the presented data set again shows general similarity, but differs in detail (Morton et al., 2011). The heavy mineral assemblage from the Murzuq Basin is largely impoverished, with a dominating ultra-stable fraction. Also similar is the occurrence of garnet in later Palaeozoic samples. Contrary to the observations from the Wajid and Tabuk areas is the continuously high ZTR in Devonian samples, indicating either a recycled sedimentary source or stronger weathering/longer transport than in Saudi Arabia. Morton et al. (2011) were also able to observe significant changes and trends in the RZi, which they used to identify distinct provenance events. These trends are not seen in the samples from the Tabuk and Wajid areas. At this point it cannot be answered whether this is due to a generally more uniform provenance source or a result of lower sample density. Morton et al. (2011) took more than twice as many samples from a comparable stratigraphic range. Furthermore, some of the Libyan sandstones contain up to 7% monazite and some formations have abundant clinopyroxene. Both of those heavy minerals are nearly absent in this data set. The high GZi in the Silurian Tanezzuft Formation is another feature not recorded in Silurian samples from Saudi Arabia.

Garzanti et al. (2013) published the heavy mineral assemblages of two samples from the lower Palaeozoic of the Tabuk area: they consist virtually entirely out of the ZTR fraction plus anatase.

The very high amount of opaque phases observed in this study is also reported by Hussain et al. (2004) as well as Weissbrod and Bogoch (2007). This indicates selective decomposition of meta- and unstable minerals mainly through weathering rather than burial dissolution (Hussain et al., 2004; Van Loon and Mange, 2007)

The high GZi of sample AB-SA98 raises the issue of placer deposits and sampling points. While most certainly a genuine provenance signal, the extremely high garnet content of the sample is curious, since such high garnet contents have not been reported by other workers. Furthermore, it is not replicated by the other two Juwayl samples and must be considered a placer deposit. Likewise while an increase in staurolite content and the STi was observed in this study, it did not reach the same scale as reported by Knox et al. (2007), although they sampled the same outcrop area. There seems to be a certain amount of bias involved during sampling. Consequently placer deposits can have a significant impact, especially if the sample density is low.

All cited studies confirmed the ultra-stable zircon, tourmaline and rutile as the main constituents of the heavy mineral assemblages of Palaeozoic sandstones from the northern Gondwana margin. Yet the variance in the assemblages is surprising. Especially metastable and labile phases are affected, both the total count data as well as indices using them. These include garnet, staurolite, monazite, hornblende, epidote and their respective heavy mineral indices. There are several explanations and factors responsible for these variances: I) real regional and stratigraphic variance, i.e. provenance and weathering signals; II) sampling bias and placer deposits; III) differences in sample preparation and counting methods, i.e. systematic errors; IV) operator bias and/or misidentification. Factor III) Includes differences

in analysed grain sizes and sample treatment before counting. Especially the analysed grain size fraction can have a large impact on the result of the SHMA (Mange and Maurer, 1992; Krippner et al., 2015). Mange and Maurer (1992) stress that "*for correlation, on either a local or a regional scale, only similar grain sizes and similarly treated and analysed heavy mineral suites should be used*". The various methods of mechanical disaggregation (crushing, grinding, percussion mortar) have different tendencies to damage and/or remove specific heavy minerals. Some counting methods, like 'line counting', are grain size sensitive and can introduce further systematic errors (Mange and Maurer, 1992). The method used for separation (i.e. funnel separation, centrifugal separation, panning) can also impact the heavy mineral distribution and yield (Kellmann, 2014; Anna Lewin, personal communication, 2016). Factors III) and IV) are only relevant when the results from several studies are compared. Sample preparation and counting methods usually do not change within one study. Similarly, the error introduced by grain misidentification should be constant (within a reasonable range) for the same operator. Factor IV) is especially troubling, since it is hard to reconstruct or estimate and heavily dependant on the operator. While, for example, zircon is easy to identify in a strewn slide, other heavy minerals can easily be misidentified, especially when poorly preserved. Apatite may be overlooked or mistaken for sillimanite or poorly preserved kyanite; staurolite may be confused with tourmaline. Colourless tourmaline appears similar to sillimanite and andalusite, while very darkly coloured tourmaline may look opaque. Deeply coloured rutile can appear opaque. If its characteristic surface stains and pitting are absent, monazite can be misidentified as zircon. SHMA with ‘manual’ mineral identification by different operators clearly has its limits, at the very least in the presented case.

6.7. Rutile varietal studies

The bulk of the rutile populations in both study areas are in the low- to medium-temperature range. Potential sources for these rutiles are abundant in the nearby ANS and include medium-grade metamorphic and metasedimentary rocks as well as igneous rocks. The small population of high-T rutiles from the Saq Formation require a high-grade metamorphic source. Yet granulite-facies rocks are scarce in the ANS and are known only from small exposures in the eastern Afif Terrane of Saudi Arabia and the Barka Terrane in north-eastern Sudan (Johnson and Woldehaimanot, 2003; Figure 34). The nearest exposed granulitic rocks outside of the ANS are the granulite-facies gneisses of the Abas Gneiss Terrane and from Socotra Island, Yemen (Wahed et al., 2006; Denèle et al., 2012; Figure 34) as well as granulites from the Mozambique Belt and from south-eastern Sudan (Stern and Dawoud, 1991; Figure 34). A southerly provenance (in present-day orientation) of high-grade rutiles is problematic and seems unlikely. They were only found in the northern study area. If the source area was to the south, the Dibsiyah Formation of the Wajid area would be expected to also contain a significant, if not larger, population. The fact that no high-T rutiles were found in the Wajid area makes the few exhumed granulite-facies rocks in the central and northern ANS the most likely source. Evidence that they were exposed in ancient times is given by the sub-Murdama unconformity in the eastern Afif Terrane. There, the Late Proterozoic Murdama Group unconformably overlies granulites, which were extensively eroded (Johnson and Woldehaimanot, 2003). The presence of high-grade rutiles in the Saq Formation and their lack in the overlying Qasim Formation suggest a slight change in provenance. Such a change has also been observed by Hussain (2007). This was most likely a regional shift within the ANS rather than a large scale change in provenance. Progressive unroofing seems an unlikely cause for the change in rutile chemistry. This would result in an increase of high-grade rutiles in younger stratigraphic levels, which was not observed. The occurrence of very few (2) high-grade rutiles in the Devonian Jubah Formation hints at either a reactivation of the original granulitic source or at some degree of recycling of Saq sediments. Regional variance can also be seen in the source lithologies of detrital rutile assemblages. Rutiles from the Tabuk area have predominantly felsic source lithologies, while the Wajid area displays a larger mafic input. Although mafic and ultra-mafic complexes are scarce in the Arabian Shield and constitute only 1% of its currently exposed surface area (Johnson et al., 2004), they are a potential sources for mafic rutiles. Examples are ultra-mafic complexes in the Midyan Terrane (Jackson et al., 1984) and mafic volcanic rocks from the Hali basin in the Asir Terrane (Johnson et al., 2013). Potential bimodal sources are present as well, for instance in the central Hijaz Terrane (Jackson et al., 1984) or in several volcanosedimentary basins (Murdama, Jibalah and Hibshi basins) in the Afif Terrane (Johnson et al., 2013). Detrital rutile has repeatedly been employed as a valuable tool in provenance studies: Zack et al. (2002, 2004a, 2004b) identified the potential of rutile varietal studies for sedimentary provenance analysis. In their provenance study, Meinhold et al. (2008) used geochemical data of detrital rutile from Early Triassic sandstones from Chios Island, Greece. Morton and Chenery (2009) utilised rutile data as provenance tracers and to characterise Jurassic to Palaeocene sandstones from the Norwegian Sea. At the northern margin of Gondwana, Morton et al. (2011) identified provenance changes in Palaeozoic sandstones from the Murzuq and Kufra basins in Libya with the help of rutile single-grain geochemical studies. While the presented study can only be considered a pilot study due to the restricted sample size, varietal studies on detrital rutiles have shown to be a powerful tool in provenance studies of north Gondwanan Palaeozoic sandstones.

6.8. Garnet varietal studies

As Krippner et al. (2014) have recently shown, host rock identification using major element discrimination diagrams for garnet is feasible, but imprecise. According to them, the plot after Mange and Morton (2007), which is used in this study, has proven to contain significant overlap of different garnet host lithologies. This is partly because of the nature of the diagram, which uses solid lines as field boundaries and partly because of real overlap of specific garnet suites (Krippner et al., 2014). Bearing that in mind, garnet discrimination diagrams can still prove useful when handled with care.

The distribution patterns of garnet host rock lithologies from the Jauf Formation cannot be evaluated in a meaningful way, since the sample population was extremely small, containing only four garnet grains. This sample size is unfortunately insufficient to compare with the other formations or to draw conclusions about provenance. The garnet distribution patterns from both the Devonian Jubah Formation and the Carboniferous–Permian Juwayl Formation are remarkably similar (Figure 21c, d), despite being separated both regionally and stratigraphically (Figure 2, Figure 3). The discrimination diagram after Mange and Morton (2007) suggests mainly amphibolite facies metasedimentary and metaigneous source rock lithologies, with a smaller contribution from intermedit to acidic igneous rocks (Figure 21b–d). The main difference between the garnet populations of the two formations are the respective amounts of type Ci (high-grade metamafic) and type Bii (amphibolite-facies metasedimentary) garnets: The Jubah Formation contains less type Ci (14%) and more type Bii (54%) garnets than the Juwayl Formation (28% type Ci, 44% type Bii). This is most probably not a genuine provenance signal. It must rather be attributed to the nature of the diagram and the fact that a lot of garnets plot close to the discrimination line between the Ci and Bii fields (Figure 21a). The average compositions (median points of the garnet populations) of the Jubah and Juwayl formations plot closely together, in the Bii field. There is no significant difference between the median points of their garnet populations (Figure 21a, yellow symbols). The peri- and proglacial Juwayl Formation is expected to be more influenced by local garnet sources, owing to a shorter transport distance and less opportunities for mixing and homogenisation of detritus. In contrast, the fluvial-deltaic to shallow marine Jubah Formation should display a more homogenised garnet population, covering a wider catchment area. A possible explanation for the similarity is that the detritus of both formations is largely derived from an already homogenised (meta-) sedimentary source, for instance Precambrian garnet-bearing (meta-) sediments (Ghebreab, 1999; Woldehaimanot, 2001; Fritz et al., 2002). Sedimentary recycling of older Palaeozoic sediments is only a reasonable possibility when the absence of garnet in those units is assumed to be a later, diagenetic feature.

Potential garnet-bearing rocks are abundant in and around the ANS. Within the ANS they include garnet-sillimanite gneiss and granites from the southern Afif Terrain (Stacey and Agar, 1985; du Bray, 1988), garnet-biotite paraschists from the Kirsh gneiss dome (Al-Saleh, 2012) and granites from the Khida Terrane (du Bray, 1988, and own observations). Proximal to the ANS lies the garnet-bearing Abas Gneiss Terrane in Yemen (Wahed et al., 2006; Figure 34). While sources for (felsic) igneous and metaigneous garnets are aplenty within the ANS and in its near vicinity, potential host rocks for metasedimentary and metamafic garnets are scarcer. Possible candidates are metapelites from the Central Eastern Desert in Egypt (Fritz et al., 2002), metavolcanics from the southern Red Sea Hills in Sudan (Kröner et al., 1991) and amphibolite-facies gneisses and metasediments from eastern and central Eritrea (Ghebreab, 1999; Woldehaimanot, 2001; Figure 34). Various metasedimentary and metaigneous rocks (including metabasites) from the Elat area in southern Israel (Cosca et al., 1999; Figure 34) could also serve as source, but are not in accordance with the northward sediment transport direction commonly inferred in the literature (Babalola, 1999; Hussain et al., 2000, 2004; Hussain, 2001; Wanas and Abdel-Maguid, 2006; Knox et al., 2007).

The presence of Type A garnets in all garnet-bearing formations is interesting. They are most likely derived from granulite-facies metasedimentary rocks (Morton et al., 2004; Mange and Morton, 2007; Krippner et al., 2014). Yet such high-grade metasediments are rare in the ANS. They are known from the Barka Terrane in Eritrea, but no garnet has been reported from there (Johnson and Woldehaimanot, 2003). Significant sources for granulite-facies metasedimentary garnets are located more distally, in the

Mozambique Belt and Sudan (Stern and Dawoud, 1991). While long-distance transport could explain the similar garnet distribution patterns of the Jubah and Juwayl formations, it is at odds with the glaciogenic origin and sedimentological architecture of the latter, containing what are probably tunnel valleys (Keller et al. 2011). They imply shorter transport distances and suggest a proximal source within the ANS and/or Yemen. Other possible host lithologies for Type A garnets are intermediate to acidic deeper crust rocks and charnockites (Mange and Morton, 2007), yet these are also not prevalent within the ANS.

A potential proximal source for Type A garnets can be found in the Abas Gneiss Terrane in Yemen. This terrane contains garnet-bearing, granulite-facies paragneisses (Wahed et al., 2006). Although it is a potential candidate for granulite-facies detritus in the upper Palaeozoic, it is unlikely to have supplied the high-T rutiles encountered in the Saq Formation of the Tabuk area. If the Abas Terrane was an active source during the early Palaeozoic, there should be at least some traces of high-grade minerals (granulite-facies garnet or rutile) in the Dibsiyah Formation of the Wajid area.

While a definite answer cannot be given at this point, a proximal source, probably to the south in Yemen, is the most likely cause for the presence of Type A garnets in the Jauf, Jubah and Juwayl formations, but did most likely not supply the granulite-facies rutiles of the Saq Formation.

The most likely explanation for the similarity of the garnet populations from the Jubah and Juwayl formations is a common provenance, dominated by detritus sourced in or proximal to the ANS. Whether this includes recycled lower Palaeozoic sediments could not be answered with confidence, as already discussed in 6.6 (Standard heavy mineral analysis).

6.9. Zircon morphotypology

A special feature in sedimentary environments is the potentially wide range of source lithologies from where detrital zircons can originate. Identifying characteristic (internal) structures linked to specific magmatic or metamorphic conditions with cathodoluminescence opens the possibility to potentially distinguish between detrital zircon suites from different source areas (Hanchar and Miller, 1993; Götze et al., 1999; Richter et al., 2003). In the Tabuk and Wajid areas, seven different zircon morphotypes have been identified after Corfu et al. (2003): five magmatic (zoned, xenocrystic cores with zoned rims, healed, convoluted, patchy) and two metamorphic (xenocrystic core with unzoned rims, homogenous) morphotypes (Figure 22). A further differentiation of the metamorphic morphotypes according to their protoliths in metasedimentary or metaigneous was not possible. The distribution patterns of zircon morphotypes in from both study areas are remarkably similar: Magmatic dominate over metamorphic morphotypes; zoned zircons are by far the most abundand morphotype (Figure 23).

The similarity between the zircon morphotype populations in both study areas (Figure 23) hints to a common provenance. The dominance of magmatic morphotypes (81% to 88%) and only minor abundance of metamorphic morphotypes (12% to 19%) further suggest a source area dominated by magmatic or low-grade metamorphic rocks. The small discrepancies in the abundance of zoned zircons between the Tabuk area (39%) and the Wajid area (46%) could be interpreted as a provenance signal, but the differences are too small to draw conclusions with confidence. The same applies to the apparent increase of zoned zircons in the Carboniferous–Permian Unayzah and Juwayl formations (Table A1, Table A2, annex). While these changes in the zircon morphotype compositions could be linked to a shift in provenance, the variation and sample size is too small to be reasonably certain. This is confirmed by statistical testing of the data. Statistical tests were performed with the software PAST, version 3.07 (Hammer et al., 2001). The data was first log-transformed to achieve normality. Then F- and t-tests were performed. The F-test ($F=1.4194$; $p=0.68141$) indicated that there is no difference between the variances of zircon morphotypes in both study areas. The unpaired t-test ($t=1.4363$; $p=0.17647$) indicated that there is no significant difference between the zircon morphotype distributions in the Tabuk and Wajid areas.

Although zircon textures revealed by CL images are regularly employed in studies concerning the magmatic and metamorphic history in rocks (e.g. Hanchar and Miller, 1993; Hanchar and Rudnick, 1995; Grant et al., 2009), there exist some pitfalls with this approach when applied to detrital zircons. The principal of assigning magmatic and metamorphic morphotypes is problematic. Firstly, diagnostic features are not always easily identifiable, which leads to uncertainties in the assigning of morphotypes. For instance, convoluted and patchy interior structures can look similar. Secondly, some of the diagnostic structures are ambiguous and can be formed under both magmatic and high-grade metamorphic conditions (Corfu et al., 2003). Thirdly, the strict definition of morphotypes is also problematic, since only the most prominent feature is counted and grains are assigned one morphotpye only, although they may show characteristics of several different morphotypes. This leads to a certain amount of operator bias that is hard to evaluate, but which may greatly influence the resulting distributions.

As stated earlier, the characterisation schemes after Pupin (1980) and Schermaier et al. (1992) as well as the elongation-method after Poldervaart (1955, 1956) and Hoppe (1963) were not applied in this study. Most of the encountered zircons were too rounded or mere fragments and thus unsuitable for these classification schemes.

6.10. An integrated approach to provenance analysis

Statistical treatment of data and multivariate analyses (cluster analysis, PCA) have proven to be useful and necessary when evaluating large data sets. Here this approach is applied to integrate different techniques in provenance analysis in order to better identify reliable provenance indicators. The PCA involved provenance sensitive variables from suitable methods: petrographic observations, geochemistry and SHMA. Results from single-grain analyses could not be considered, because the sample density was insufficient. The chosen variables need to reflect provenance changes and are ideally unaffected by sorting, diagenetic or weathering effects. They should also display marked changes between different formations and/or study areas. Considering these requirements, the following variables have been selected: abundance of quartz relative to total Q+F+L ('Q%'), the heavy mineral indices ZTR, ATi, GZi, RZi, STi, the concentrations of Al_2O_3, TiO_2, Zn, Li, Ba, Rb, Sr, Nb, the total concentration of REEs (ΣREE), the element ratios of Zr/Sc, Th/Sc, Ni/Th, ΣLREE/ΣHREE, ΣLREE/ΣHREE and Eu/Eu*. While most of these variables are reliable provenance indicators, some are not unambiguous. The heavy mineral indices GZi and STi are potentially modified by burial diagenesis, while the ATi can be modified by weathering. The concentrations of Al_2O_3, Ba and Rb are tied to phyllosilicates and therefore sensitive to grain size and sorting effects. The relative abundance of quartz is, as previously shown, sensitive to weathering and sorting. The resulting PCA does therefore not only reflect provenance, but a variety of factors influencing sandstone petrogenesis.
Results of the PCA are shown in Figure 35. PC 1 is responsible for 35.8%, PC 2 for 21.8% of the total variance. PC 1 is mainly influenced by the concentrations of Al_2O_3, Nb, Rb and Q%, indicating a strong control by grain size and sorting effects. Q% and the ZTR are directly tied to and reflect the maturity of the sediments. Al_2O_3, Ba, and Rb concentrations are linked to phyllosilicates and correlate negatively with the maturity indicators (ZTR, Q%). PC 2 is mainly influenced by the concentrations of TiO_2, the ZTR, the ratios of Th/Sc, Zr/Sc, Ni/Th and ΣLREE/ΣHREE. These variables reflect the abundance of zircon, rutile and other heavy minerals and the degree of fresh input from (mafic) basement. Especially the variables RZi and TiO_2 reflect the abundance of rutile. They both correlate negatively with the STi. The STi is an indicator for input from a metamorphic source, but does not have large correlation values with either principal component.

The biplot shows a clear separation and grouping of samples from the Wajid area (red and black dots, Figure 35). Samples from the Upper Wajid (black dots) cluster in the lower left part of the biplot. They are characterised by increased STi and Ni/Th and are depleted of rutile. Lower Wajid samples (red dots) on the other hand are strongly influenced by Q% and the ZTR, and depleted of Al_2O_3, Ba and Rb. This reflects the higher maturity Lower Wajid compared with Upper Wajid samples, which is in accordance with petrographic observations. The plot does not give further evidence whether the higher maturity is a provenance signal (meaning recycling), reflects intensive weathering or is due to sorting effects. The distribution of Wajid area samples is in accordance with an influx of fresh basement material during the late Palaeozoic implicated by the Th/Sc vs. Zr/Sc plot (Figure 25). Results for Tabuk area samples (red and black triangles, Figure 35) are inconclusive. A minor trend towards high maturity of Lower Tabuk samples (red triangles) can tentatively be assumed. Tabuk area samples are strung out along the x-axis of the plot. The variance of these samples is largely controlled by PC 1 and therefore likely the result of sorting effects.

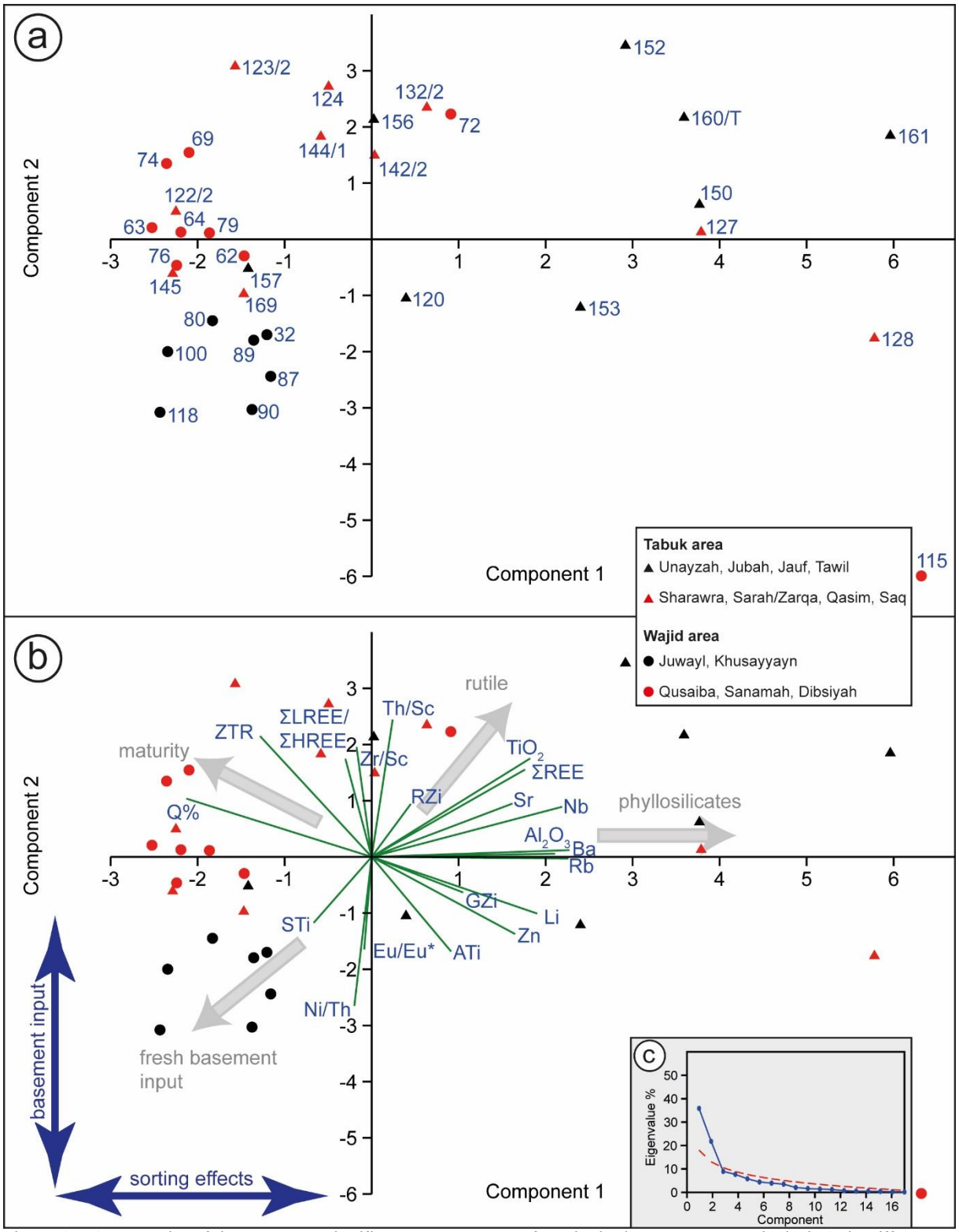

Figure 35: Scatter plot of the two most significant components of a principal component analysis (PCA). Different symbols and colours represent samples from upper and lower successions from both study areas. The first two principal components accounted for 57.6% of the total variance of the data set. (a) Arrangement of samples; (b) biplot of variables; grey arrows indicate controlling factors; (c) scree plot of principal components vs. eigenvalues.

As already shown, traditional methods alone (petrographic discrimination [after Dickinson et al., 1983], geochemical discrimination diagrams, other geochemical criteria [after McLennan et al., 1993]) are insufficient to determine the provenance of quartz-rich Palaeozoic sandstones. Yet they can provide a broad framework that then needs to be supplemented with additional techniques, like SHMA and single-grain methods (Morton and Hallsworth, 1999; von Eynatten and Dunkl, 2012). Their main advantages are their low cost, they are easy to perform and provide quick results. Consequently, the most effective approach is to supplement more generalist methods, which can generate a lot of data quickly and cheaply but can give ambiguous results, with more reliable yet expensive and laborious techniques. The resulting simplified stratigraphic scheme of provenance sensitive parameters from different methods enabled the confident identification of four changes in provenance, termed 'provenance events' (PEs) (Figure 36).

PE 1 occurred at the base of the Qasim Formation. Evidence are high-T rutiles in the Saq Formation, which are absent in samples from the overlying Qasim Formation. Further indicators are an increase of Th/Sc and Th/U in samples of the Qasim Formation. This event was likely local and resctricted to the Tabuk area, but final evidence for this is missing. In the Wajid area, no direct equivalent of the Qasim Formation has been preserved, which could have recorded the provenance event.

PE 2 is observed in both study areas, at the base of the Hirnantian glaciogenic units (Sanamah, Sarah and Zarqa Formation) and marks a change from a first-cycle source to recycled sediments. They have similarly high maturity and ZTR values (>90) as the Cambrian–Ordovician (Dibsiyah, Saq, Qasim) formations, requiring either intensive chemical weathering or sedimentary recycling. Avigad et al. (2005) convincingly showed that the quartz-rich Cambrian–Ordovician sandstones of northern Gondwana are first-cycle sediments, resulting from intensive weathering. Palaeoclimate conditions during Hirnantian times did not favour strong chemical weathering. The resulting high maturity of those sediments must therefore be the result of recycling from older material. This is supported by ATi values similar to the Cambrian–Ordovician sandstones. The ATi is very susceptible to chemical weathering in warm, humid climates and the low ATi values of the Hirnantian sandstones must therefore be inherited. With additional literature data (marked ‡, Figure 36) and samples from the 2009–2010 field campaigns (marked †, Figure 36), a collisional signal in the Sanamah, Sarah and Zarqa formations, has been identified in the tectonic setting discrimination diagrams after Verma and Armstrong-Altrin (2013) (Figure 28). While the 'Rift' (meaning intracratonic) signal of the other Palaeozoic formations reflects the tectonic setting of the depositional basin, the collisional signal is linked to the final stages of the Pan-African Orogeny and thus indicates at least some contribution from Neoproterozoic basement. Interestingly, the Sanamah Formation is the only unit from the Wajid area that is characterised by a distinct quartzose recycled tectonic setting in the diagram of Dickinson et al. (1983) (Figure 26d).

The low ZTR in the Silurian units (<20 in the Qusaiba Member; <70 in the Sharawra Member) and the high ATi (>60) in the Qusaiba Member are most likely due to sorting effects, because the samples were taken from sandy intercalations in shales and siltstones. No single grain data is available from these units. The different heavy mineral assemblages in the Qusaiba and Sharawra members can therefore not be interpreted as provenance events.

PE 3 marks a provenance change at the base of the Khusayyayn and Jauf formations. In the Tabuk area, PE 3 is chiefly indicated by the appearance of garnet and increased GZi values at the top of the Tawil Formation and the base of the Jauf Formation, respectively. The Jubah Formation has an even higher amount of felsic rutiles (85%) than the Lower Tabuk (73%). Whether this change happened in the Late Devonian or coincides with PE 3 could not be determined, because no rutiles from the Tawil and Jauf formations were analysed.
In the Wajid area, the later Palaeozoic sandstones have much lower Th/Sc ratios (<1 to ~1) than the early Palaeozoic formations. This indicates input of fresh detritus from a nearby basement source (McLennan et al., 1993). Further evidence is found in the heavy mineral indices ZTR and STi. The ZTR, while still high (~80), is significantly lower in the Juwayl and Khusayyayn formations than in the Dibsiyah and Sanamah formations. Increasing values for the STi from the base of the Khusayyayn Formation on upward hint at shift to source area more dominated by metamorphic rocks. It is important to keep in mind that the scarcity of staurolite in the Lower Wajid and the Tabuk area could also be at least partly attributed to intrastratal dissolution.

A fourth change in provenance, PE 4, occurs at the base of the Juwayl Formation. It is also is tentatively assumed for the Unayzah Formation, but here the data is scarce and more evidence is needed to identify the provenance event with confidence.
The Juwayl Formation from the Wajid area is, in contrast to the underlying Khusayyayn Formation, characterised by Th/Sc values ~1, Th/U values comparable to the UCC and a very pronounced negative Eu anomaly (Eu/Eu*=0.57). Samples also exhibit increased values for STi and ATi. In the diagram after Verma and Armstrong-Altrin (2013) (Figure 28b), a strong collisional signal, probably related to the Pan-African orogeny, is visible in samples from the 2009–2010 field campaigns (marked †, Figure 36), similar to the Sanamah Formation. One sample from the Juwayl Formation (AB-SA98) contains very high amounts of garnet (GZi >80; ZTR <20) and significant apatite (ATi >60). Because of its peri- to proglacial depositional environment (Hinderer et al., 2009; Keller et al., 2011) the abundance of apatite can be attributed to palaeoclimatic conditions unfavourable for apatite removal through chemical weathering. The appearance of garnet is likely a genuine provenance feature. While the Juwayl Formation is characterised by dominantly mafic rutiles (69%), this may be the result of the very small sample size of only 13 analysed rutiles.
The Unayzah Formation from the Tabuk area shows distinct differences from the underlying Devonian formations in many provenance sensitive geochemical markers: It is strongly depleted in LILEs (Figure 13), has very variable Th/Sc values and lower Th/U than the average UCC. However, more reliable single grain data is unavailable data from SHMA only from one sample. Hence there is not enough evidence to confidently identify a provenance event in the Unayzah Formation.

Besides provenance changes through time, there are also differences in provenance sensitive factors between the two study areas. The most predomiant differences are revealed by rutile varietal studies: The high-T rutiles, which mark PE 1 in the Tabuk area, have not been found in samples from the Wajid area. Furthermore, rutiles from the Tabuk area were predominantly sourced from felsic source rocks, whereas the Wajid area contains many more rutiles from mafic sources. Interestingly, the distribution patterns of garnet host rock lithologies from both study areas are very similar and do not reflect the differences seen in the rutile distributions. Distribution patterns of zircon morphotypes obtained with cathodoluminescence are also remarkably similar. This however may be due to fundamental problems of the method. PE 2 is marked in the Wajid area with higher values for ATi and STi, which is not as pronounced in sandstones from the Tabuk area. Lastly, the decreased Th/Sc and Th/U values, which mark PE 3 in the Wajid area, are not observed in the Tabuk area.

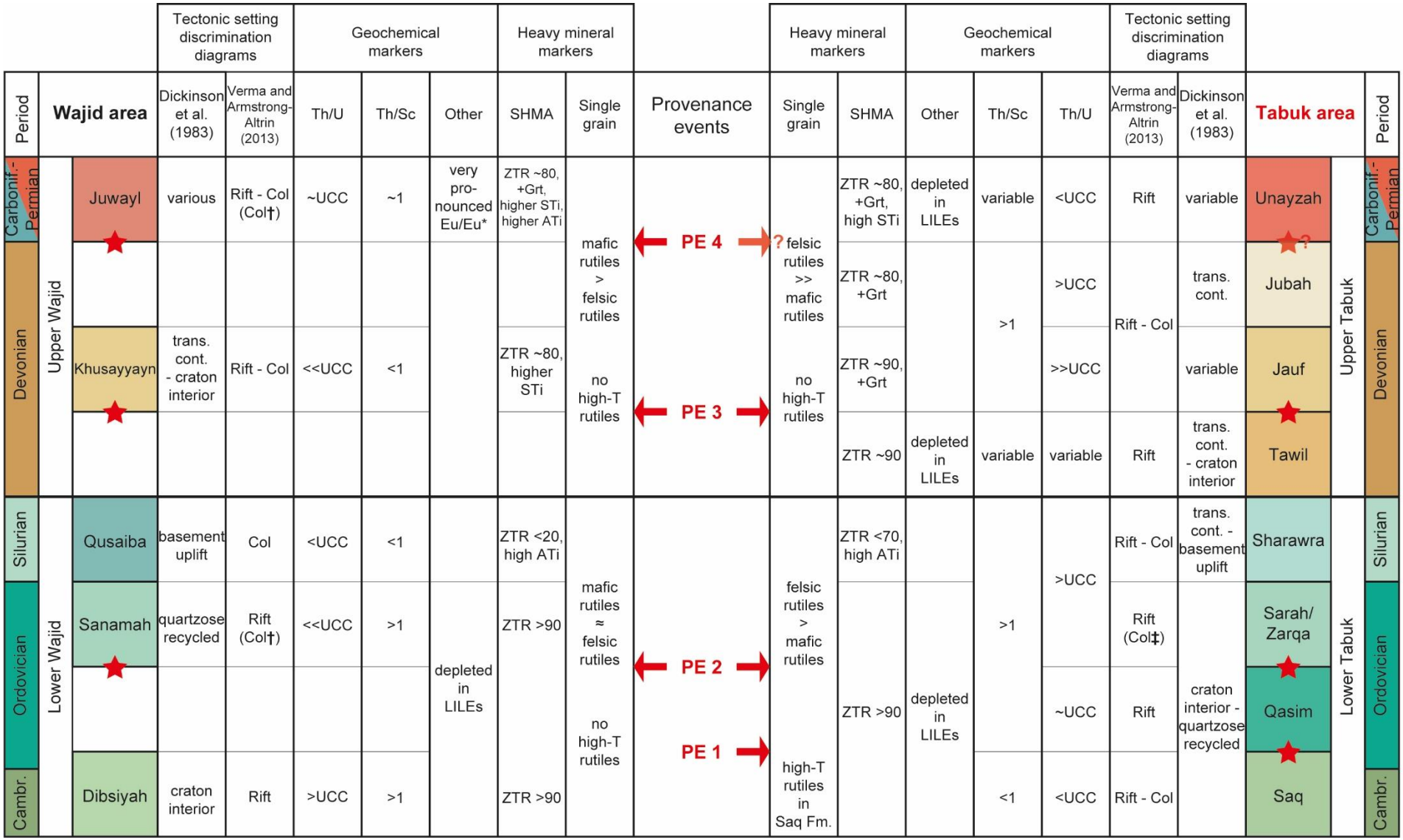

Figure 36: Compilation and comparison of provenance sensitive parameters of different methods used to identify and correlate 4 provenance events (PEs, red arrows/stars) in the Tabuk (right) and Wajid (left) areas. Stratigraphic columns not to scale. †=samples from the 2009–2010 field campaigns; ‡=samples from Al-Harbi and Khan (2011); Cambr.=Cambrian; Carbonif.=Carboniferous; trans. cont.=transitional continental; +=present; <<=much lower; >>=much higher.

7. The Khida Terrane: A closer look at a potential source for Palaeozoic sandstones in southern Saudi Arabia

7.1. Geological setting

Formation of the Arabian-Nubian Shield (ANS) took place over a period of ~300 Ma, from the break-up of Rodinia to the final amalgamation of Gondwana. The ANS consists of several Neoproterozoic arc terranes that formed in the closing Mozambique Ocean between ~780 Ma and 600 Ma (Johnson, 2014). Orogenic activity and shield evolution in the ANS ceased by ~550 Ma with the development of a passive margin (Johnson and Woldehaimanot, 2003; Johnson et al., 2011). The ANS represents the northern continuation of the East African Orogen.

While the exact dates of the events leading to the amalgamation of Gondwana are still under debate (e.g. Meert and Van Der Voo, 1997; Johnson and Woldehaimanot, 2003; Meert, 2003; Stern et al., 2010; Stern and Johnson, 2010; Johnson et al., 2011; Johnson, 2014), a rough timeline is given in Table 11.

Table 11: Simplified timeline of the events leading to the assembly of Gondwana. 1) Agar (1987); 2) Johnson and Woldehaimanot (2003); 3) Stern et al. (2010); 4) Johnson et al. (2011); 5) Johnson (2014).

Time [Ma]	Events	References
570–550	End of deformation, magamtism and orogenic activity; final assembly of Gondwana	3); 4)
580	Collision of arcs with Saharan Metacraton and full assembly of ANS	4); 5)
630–615	End of arc accretion; beginning of amalgamation of East and West Gondwana	3); 5)
640–630	Beginning of Najd movement	1); 5)
680–640	Nabitah orogenic cycle	4); 5)
780	Beginning of arc accretion	2); 5)
870	Start of subduction in the Mozambique Ocean	2); 5)

Within the Neoproterozoic predominantly oceanic island arc terranes of the ANS lies an enigmatic block of continental crust, which also contains Palaeoproterozoic gneiss, granite and anorthosite (Stoeser et al., 2001; Johnson and Kattan, 2008). The presence of Archean crust is inferred by Nd model ages (Stoeser and Frost, 2006). This unit is commonly known as the Khida Terrane, sometimes referred to as the Khida sub-terrane, Khida microplate and Khida basement (Stoeser and Frost, 2006). It is situated at the southeastern margin of the ANS as part of the Afif composite terrane, between approximately 21°00’ – 22°00’ N and 43°30’ – 45°00’ E (Figure 37a). The Khida Terrane can be differentiated from other ANS rocks by its older εNd initial ratios, Palaeoproterozoic Nd model ages, elevated Pb isotopes and Sr initial ratios as well as Palaeo- to Neoproterozoic U–Pb zircon ages (Johnson and Kattan, 2012). Three major deformation phases (D1, D2, D3; Thieme, 1988) are recognizable in this terrane. D2 and D3 are correlatable throughout the Arabian Shield. The oldest deformation phase (D1) is unrelated to younger Arabian Shield tectonics. Tectonic activities of the D1 phase are not well defined in time; but they must have taken place after ~1,630 Ma (Thieme, 1988). The second phase (D2) correlates with the Nabitah (formerly named Hijaz) orogenic cycle (Brown and Coleman, 1972), which was active between 680 Ma and 640 Ma (Stoeser and Stacey, 1988). The D2 phase has been largely overprinted by the later D3 phase. This youngest deformation phase culminated in and was part of the Najd orogeny (Agar, 1987). The Najd orogeny began between 640–630 Ma, shortly after the end of the Nabitah orogenic cycle (Agar, 1987; Johnson, 2014) and lasted until at least ~573 Ma (Johnson et al., 2011).

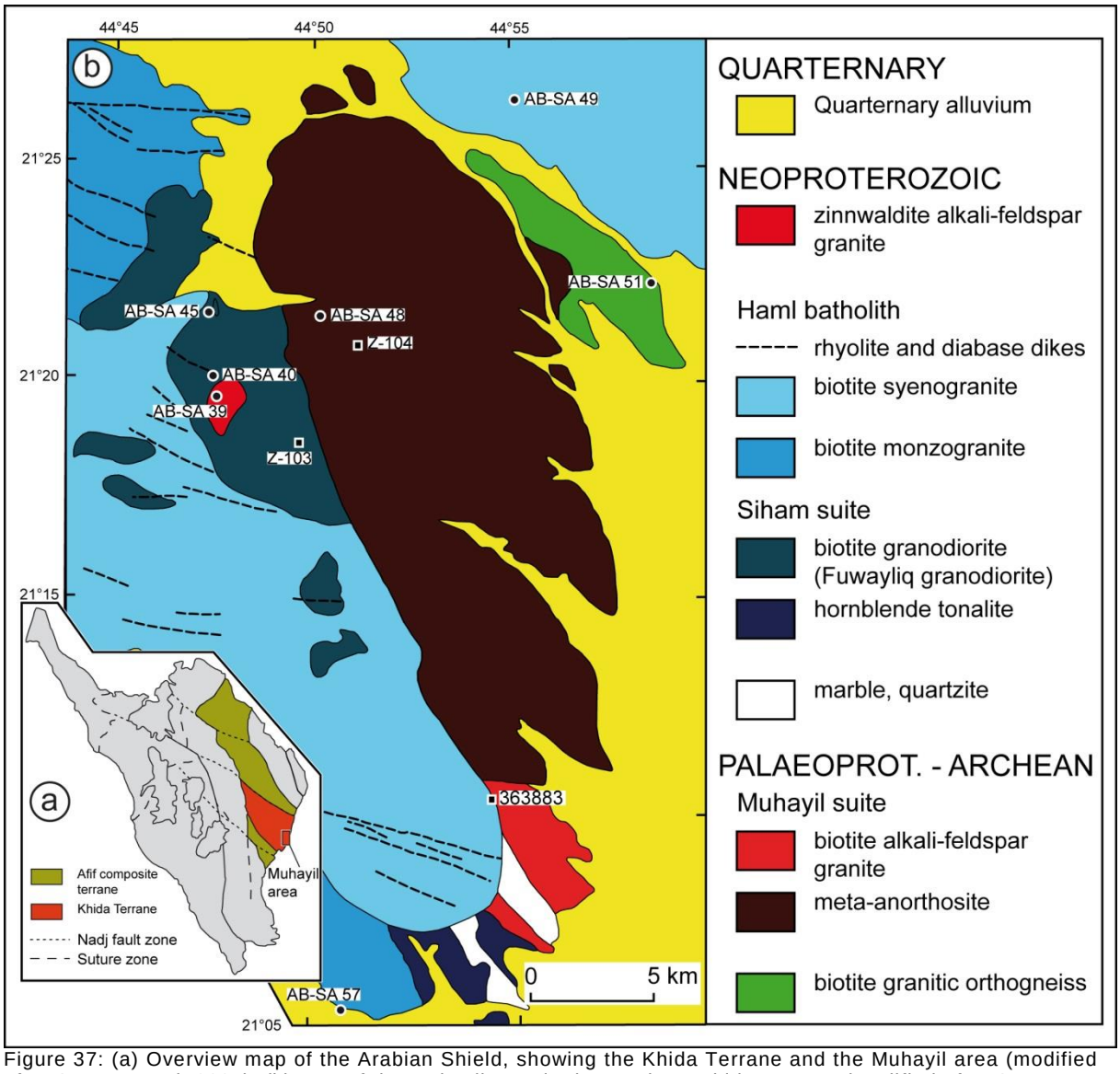

Figure 37: (a) Overview map of the Arabian Shield, showing the Khida Terrane and the Muhayil area (modified after Stoeser et al. 2001). (b) Map of the Muhayil area in the southern Khida Terrane (modified after Stoeser et al., 2001), showing sample locations from literature (squares) and this study (circles).

The total expanse of the Khida Terrane is yet unknown since it disappears under a cover of Phanerozoic sediments toward the south, but it is suspected to extent south into Yemen. This assumption is supported by magnetic anomaly maps and the lithological similarities between the Khida Terrane and the Abas and Al Mahfid terranes (Johnson, 2014).

Most exposed rocks in the Khida Terrane are Cryogenian arc assemblages and granites (Johnson et al., 2011). Granitic plutons constitute approximately 75% of the rocks underlying the Jabal Kihda quadrangle, but intermediate, mafic and ultramafic rocks are also present (Thieme, 1988). Age relationships between the different intursions are not yet entirely understood and rest mainly on the influence of the three major deformation phases (D1, D2 and D3). The Surayhah complex is the oldest intrusive suite and affected by D1 deformation. It crops out in the northern half of the map quadrangle and consists of diorites, granodiorites and gabbros (Thieme, 1988). Hajizah and Damar complexes as well as the Siham suite are pre- and syn-D2 intrusive rocks. The Hajizah complex crops out in the southwestern corner of the quadrangle and comprises 'granitic to granodioritic gneiss and amphibolite' (Thieme, 1988). The intermediate to mafic Damar complex is exposed in the southern and central part of the quadrangle and consists of and 'intermediate to mafic series of rocks (Thieme, 1988). The Siham suite is a suite of associated biotite-granodiorite and hornblende tonalite from the Muhayil area (Stoeser et al., 2001; Figure 37b). Calc-alkaline granite plutons of the NW trending Haml batholith are the youngest Precambrian

intrusive rocks; voluminous amounts of calc-alkaline granite which intruded in many plutons during the Najd orogenic cycle (Thieme, 1988)

The Khida Terrane also contains various sedimentary and volcaniclastic rocks of Neoproterozoic age. They include marbles, quartzites, cherts, pelitic schists, siltstones, tuffaceous sandstones, quartz arenites and conglomerates (Thieme, 1988; Stoeser et al., 2001). Metamorphic grades vary from low-grade metamorphism in sediments of the Bani Ghayy group, to middle and upper greenschist facies in the Siham Group, and amphibolite facies rocks are known from the Tays Formation (Thieme, 1988). These metasediments could have acted as a potential sediment source for the Palaeozoic sandstones.
The 'pelitic' and quartzofeldspathic schist and gneiss of the Tays Formation are the oldest metasediments in the Jabal Khida quadrangle. They are affected by D1 deformation and are closely associated to the Surayhah complex (Thieme, 1988). The Siham Group consists of three formations in the Jabal Khida quadrangle: the Hijar, Duraybah and Musammah formations. The Hijar and Duraybah formations are of predominantly volcanogenic origin, while the Musammah Formation is of mixed volcanogenic, siliciclastic and carbonatic composition (Thieme, 1988). The Siham Group was affected by the D2 deformation phase and is associated with the Hajizah and Damar complexes and the Siham suite (Thieme, 1988; Stoeser et al., 2001). Sediments of the Bani Ghayy Group crop out in the west and southwest of the quadrangle and are only weakly affected by D3 metamorphism. The Bhani Ghayy Group encompasses the Juqjuq and Arfan formations. The Juqjuq Formation consists of volcanogenic sediments; the Arfan Formation is of mixed volcaniclastic and siliciclastic origin.

The Muhayil area within the Khida Terrane is of special interest. It contains Palaeoproterozoic granitoids, which are the oldest exposed rocks in Saudi Arabia (Agar et al., 1992; Whitehouse et al., 2001). It is also the area within the Khida Terrane for which the only reliable and published age data is available (Table 12). Furthermore, it is relatively easy to access from Wadi Ad Dawasir. The Muhayil area is located at the south-eastern margin of the Khida outcrop area, between approximately 21°05' – 21°30' N and 44°45' – 44°60' E (Figure 2a; Figure 37b).

7.2. Previous studies

While the ANS has been studied intensively (e.g. Stoeser and Camp, 1985; Nehlig et al., 2002; Johnson and Woldehaimanot, 2003; Johnson and Kattan, 2008; Johnson et al., 2011; Fritz et al., 2013; and references therein), the Khida Terrane is underrepresented in recent publications and research. Furthermore, many publications are hard to come by and are not easily accessible online (e.g. unpublished reports).

The area was systematically mapped for the first time by Whitlow (1966). Subsequent studies during the 1980s focussed on economic aspects (e.g. Bishop, 1982; Howes, 1982; Ramsay, 1982; du Bray, 1983; Jackson and Al Yazidi, 1985) as well as preliminary geochronologic research (Kröner et al., 1979; Stacey et al., 1980; Kellogg and Beckmann, 1982; Darbyshire et al., 1983). Stacey and Hedge (1984) were the first to publish Palaeoproterozoic U–Pb zircon ages, together with feldspar common Pb as well as whole-rock Sm–Nd and Rb–Sr isotopic data. They studied a single sample (Z-103) from the Muhayl area in the southeastern Khida Terrane (Figure 37b) and concluded that the granodiorite was emplaced at ~1,630 Ma. Stacey and Agar (1985) performed U–Pb geochronology on detrital zircons from metasediments (paragneisses) from the Zalm region in the central Arabian Shield. One sample from the northwestern margin of the Khida Terrane yielded a discordant age of 1,830 Ma. Newer studies on other pre-Siham sediments from the Khida Terrane yielded several age populations, the youngest being ~800 Ma (Agar et al., 1992), contradicting a ~1.8 Ga depositional age (Whitehouse et al., 2001).

In two extended abstracts, Stoeser et al. (2001) and Whitehouse et al. (2001) revisited the Khida Terrane and presented new data. Stoeser et al. (2001) re-evaluated the petrology of several intrusive rocks, gneisses and metasediments in the Muhayil area using thin section petrography. They classified the 'Muhayil charnockite' of Agar et al. (1992) as a biotite-rich, quartz-poor alkali-feldspar granite, not a true charnockite. They also provide an updated geological map of the area. Whitehouse et al. (2001) redated the sample of the Muhayil biotite alkali-feldspar granite (sample 363883, Figure 37b), previously interpreted to be 1,660 ± 97 Ma old by Agar et al. (1992). The studies of Whitehouse et al. (2001) resulted in an age of 1,660 ± 10 Ma, confirming and further constraining the previously published age. They furthermore present a new intrusion age of the Fuwayliq granodiorite (sample Z-103, Figure 37b) of ~750 Ma, which was previously thought to have intruded at ~1.7 Ga (Stacey and Hedge, 1984). Stoeser et al. (2001) and Whitehouse et al. (2001) furthermore infer a pre-Siham age (~800 Ma) for metasediments in the Muhayil area and elsewhere in the Khida Terrane. This interpretation rests on plutons of the Siham suite intruding the metasediments in the Muhayil area and on ages published by Agar et al. (1992). Unfortunately Stoeser et al. (2001) and Whitehouse et al. (2001) do not provide any new data from the metasediments themselves. Stoeser and Frost (2006) used Nd, Pb, Sr and O isotopic data, both own and from literature, to characterise different ANS terranes, including samples from the Khida Terrane. They concluded that both eastern and western arc terranes in the ANS are of oceanic affinity. The Khida Terrane on the other hand is the only one underlain by Proterozoic to Archean continental crust.

The few published data so far, are insufficent to further define the history of this enigmatic terrane and its relation to the other ANS terranes. Furthermore, a lot of the age data provided by Stern et al. (2010, appendix) is stated as personal communication while most of the data in Johnson and Kattan (2008, page 10) is hard to reconstruct and cannot be found in the cited sources (see also Table 12). Of all the published U–Pb ages only the two datings by Whitehouse et al. (2001) for the Muhayil granite (1660 ± 10 Ma) and the Fuwayliq granodiorite (~750 Ma) can be seen as reliable. All other published U–Pb ages are either obsolete or are hard to reconstruct from the cited sources. Sm–Nd model ages for Khida rocks on the other hand are quite robust and date between ~1.3–2.5 Ga (Stacey and Hedge, 1984; Agar et al., 1992).

Table 12: Published ages for Khida Terrane rocks. imp = ion microprobe; n/a = not available.

Sample	Unit	Assigned age [Ma]	Method	Source	Reliability
363883	Muhayil granite	1660 ± 10	U-Pb (imp)	Whitehouse et al., 2001	good
363883	Muhayil granite	1660 ± 97	U-Pb (imp)	Agar et al., 1992	obsolete
363402	Kabid Formation	~1830	U-Pb	Stacey and Agar, 1985	obsolete
Z-103	Fuwayliq granodiorite	~1630	U-Pb (imp)	Stacey and Hedge, 1984	obsolete, re-dated
		~750	U-Pb (imp)	Whitehouse et al., 2001	good
99KD-080	S. Libab felsic gneiss	1860	SIMS/SHRIMP	Stern et al., 2010 (Stoeser writ. comm., 2001)	poor, unpublished
99KD-041	Muhayil pluton	1676	SIMS/SHRIMP	Stern et al., 2010 (Stoeser writ. comm., 2001)	poor, unpublished
99KD-038	Muhayil granite	1668	SIMS/SHRIMP	Stern et al., 2010 (Stoeser writ. comm., 2001)	poor, unpublished
99KD-078	N. Libab granite gneiss	851	SIMS/SHRIMP	Stern et al., 2010 (Stoeser writ. comm., 2001)	poor, unpublished
99KD-013	Fuwayliq granodiorite	755	SIMS/SHRIMP	Stern et al., 2010 (Stoeser writ. comm., 2001)	poor, unpublished
363401	Kabid gneiss	663	SIMS/SHRIMP	Stern et al., 2010 (Stoeser writ. comm., 2001)	poor, unpublished
99KD-092	Soroya gneiss	642	SIMS/SHRIMP	Stern et al., 2010 (Stoeser writ. comm., 2001)	poor, unpublished
363865	Fajirah gneiss	<808	n/a	Johnson and Kattan, 2008	poor, not found in cited source
363878	Surayah gneiss	642 ± 8	n/a	Johnson and Kattan, 2008	poor, not found in cited source
363867	Kabid Formation	~800	n/a	Johnson and Kattan, 2008	poor, not found in cited source
80	S. Libab gneiss	>1860 ± 25	n/a	Johnson and Kattan, 2008	poor, not found in cited source
363402	Kabid Formation (paragneiss)	~800	n/a	Johnson and Kattan, 2008	poor, not found in cited source
41	Muhayil granite	1675 ± 11	n/a	Johnson and Kattan, 2008	poor, not found in cited source
38	Muhayil granite	1668 ± 10	n/a	Johnson and Kattan, 2008	poor, not found in cited source

7.3. Geology of the Muhayil area

The Muhayil area is an outcrop area at the south-eastern margin of the known extent of the Khida Terrane (Figure 37a). It is comprised of various metasedimentary and intrusive rocks, some of them also metamorphic. The Muhayil suite contains some of the oldest rocks in the Khida Terrane, including the oldest yet dated rock of Saudi Arabia (1,660 ± 10 Ma obtained from zircons of the Muhayil granite by Whitehouse et al., 2001). It is a 'coarse-grained biotite-rich quartz-poor weakly orbicular meta-alkali-feldspar granite' (Stoeser et al., 2001; 'Muhayil charnockite' of Agar et al., 1992). According to the map after Stoeser et al. (2001) (Figure 37b), it is exposed at the south-eastern margin of the Muhayil outcrop area. Unfortunately, during field work in 2013 exposures of this granite at the indicated location were not discovered and no samples were recovered. Adjacent lies a large outcrop area of the Muhayil anorthosite (sample Z-104 of Whitehouse et al., 2001; Figure 37b), which is a 'medium to coarse-grained meta-leuco-gabbro' (Stoeser et al., 2001) that contains large (up to 10 cm) plagioclase laths. Metamorphic amphibole has replaced all primary mafic minerals (Stoeser et al., 2001). This anorthosite is thought to be cogenetic with the biotite alkali-feldspar granite. Sm-Nd and feldspar Pb isotopic data suggest the presence of an early Palaeoproterozoic component (Whitehouse et al., 2001). The biotite alkali-feldspar granite and the meta-anorthosite are supposed to belong to a single anorthosite-alkali suite. This is the first such suite to be reported from the ANS (Stoeser et al., 2001). A potentially older unit of biotite granitic orthogneiss is reported by Stoeser et al. (2001) from the northeast of the outcrop area. Their argument for an older age of this orthogneiss is the lack of similar deformation in rocks of the Muhayil suite. Consequently the orthogneiss may represent an event of high-grade regional metamorphism prior to the emplacement of the Muhayil suite rocks. So far no data has been published from this orthogneiss to verify its age. During field investigations the extensive outcrop areas as indicated by the map of Stoeser et al. (2001) (Figure 37b) could not be located and only some small outcrops of weakly metamorphosed granite (sample AB-SA51) were encountered in the area. It is uncertain whether these metagranites correspond to the orthogneiss described by Stoeser et al. (2001).

Various metasediments can be found throughout the Muhayil outcrop area. They consist of marbles and quartzites (meta-psammites sensu lato) of probably early Siham age or older. They are intruded by plutonitic rocks of the Siham suite. This necessitates a minimum age that is younger than the Siham Group, which was emplaced at ~750 Ma (Stoeser et al., 2001). Other pre-Siham metasediments in the Khida Terrane have a depositional age of ~800 Ma (Whitehouse et al., 2001) and are possibly cogenetic with the metasediments from the Muhayil area.

The Siham suite is a suite of Neoproterozoic intermediate to felsic plutonitic rocks, consisting of the Fuwayliq biotite granodiorite (~750 Ma; Whitehouse et al., 2001) and a biotite-hornblende tonalite (Stoeser et al., 2001). They dated zircon cores of ~1.7 Ga from this unit, which they interpreted as remnants of a late Palaeoproterozoic source. The next younger unit is the Haml batholith, which was emplaced between 649 ± 4 Ma (Agar et al., 1992) and 609 ± 11 Ma (Stuckless and Futa, 1987). It is regionally extensive and consists of two complexes: The Samim complex is an assemblage of monzogranites and granodiorites, which in some places show weak traces of the D3 deformation phase. It is intruded by the post-tectonic Himarah complex, which comprises numerous diapiric granites, syenogranites and alkali-feldspar granites (Thieme, 1988). The youngest Precambrian unit exposed in the Muhayil area is a zinnwaldite alkali-feldspar granite, which is part of the Usayran Member (Thieme, 1988). It was first described by du Bray (1983) and du Bray and Stoeser (1983) as the 'Mahail granodiorite'. Du Bray (1983) identified it as a quartz-rich granodiorite that is extremely depleted in all granitophile elements, containing primary muscovite and almandine-spessartine garnet. Neither du Bray (1983), du Bray and Stoeser (1983) nor Thieme (1988) did identify any mica as zinnwaldite. Stoeser et al. (2001) first mentioned this type of mica in their geological map but they did not in the explanatory notes.

7.4. Methodology

Seven samples of basement metasediments and igneous rocks were collected from the Muhayil are of the Khida Terrane during the field campaign in 2013. Sample locations are given in Figure 37b, GPS coordinates are provided in Table 13. Sample preparation followed the same procedure used for sedimentary rocks (see Chapter 4.2). Major element concentrations of samples AB-SA39, AB-SA45, AB-SA 48 and AB-SA49 were measured with XRF at the University of Göttingen. Major element concentrations of samples AB-SA40, AB-SA51 and AB-SA57 were measured with XRF at the University of Mainz. Trace element concentrations were measured with ICP-MS at the University of Göttingen. The same analytical precisions as given in chapter 4.4 (Geochemical analysis) apply. Modal composition of the samples was determined by point-counting thin sections after the Gazzi-Dickinson method. 300 grains were counted per thin section. Recorded components were: monocrystalline quartz with straight extinction (Qm), monocrystalline quartz with undulose extinction (Qmu), polycrystalline quartz (Qp), plagioclase feldspar (Plag), alkali-feldspar (Afsp), microcline, orthoclase, muscovite, biotite and zinnwaldite.

Geotectonic plots, classifications and CIPW norms were calculated using GCDkit 3.0 plugin for R 2.13.2 (Janoušek et al., 2006).

Table 13: GPS coordinates and short description of samples from the Khida Terrane, including the lithological descriptions of Stoeser et al. (2001).

Sample #	Lithology (acc. To Stoeser et al. 2001)	Latitude	Longitude	Colour	Remarks
AB-SA39	zinnwaldite alkali-feldspar granite	21°19'16.4''	44°47'35.1''	grey to beige	contains garnet grains
AB-SA40	Fuwayliq biotite granodiorite	21°20'39.2''	44°47'29.0''	grey	contains veins of coarse pegmatitic Fsp-Qtz-Bio-Granite
AB-SA45	Silham meta-sediment	21°22'03.8''	44°47'28.3''	green to light brown	bedding mm to 1/2 cm; striking 32/70
AB-SA48	meta-anorthosite (Muhayil suite)	21°21'54.8''	44°51'18.5''	grey to reddish brown	
AB-SA49	granite	21°27'02.0''	44°55'11.3''	reddish brown to pink	strongly weathered, fine grained
AB-SA51	biotite granitic orthogneiss	21°22'19.7''	44°57'46.4''	grey	
AB-SA57	granite	21°05'19.9''	44°51'10.3''	grey	fine grained

7.5. Results

7.5.1. Petrography

Results of petrographical analyses (point-counting) for plutonic rocks are plotted in the QAPF (quartz, alkali-feldspar, plagioclase, feldspathoid) diagram after Streckeisen (1974) (Figure 38a) and summarised in Table 14.

Thin section petrography on the alkali-feldspar monzogranite (sample AB-SA39) revealed pale mica. According to Stoeser et al. (2001), this pale mica is preliminarily identified as zinnwaldite. This assumption, however, needs to be confirmed by other analytical methods, since zinnwaldite is hard to identify in thin section. Additional geochemical (whole-rock and/or single-grain) analyses are required to identify zinnwaldite with confidence. Another uncommon feature of this particular monzogranite is the presence of garnet (Figure 39a, b). The garnet grains range in size from approximately 0.2–0.5 mm and are of undisputedly magmatic origin, since they are idiomorphic and the sample shows no signs of metamorphic impact.

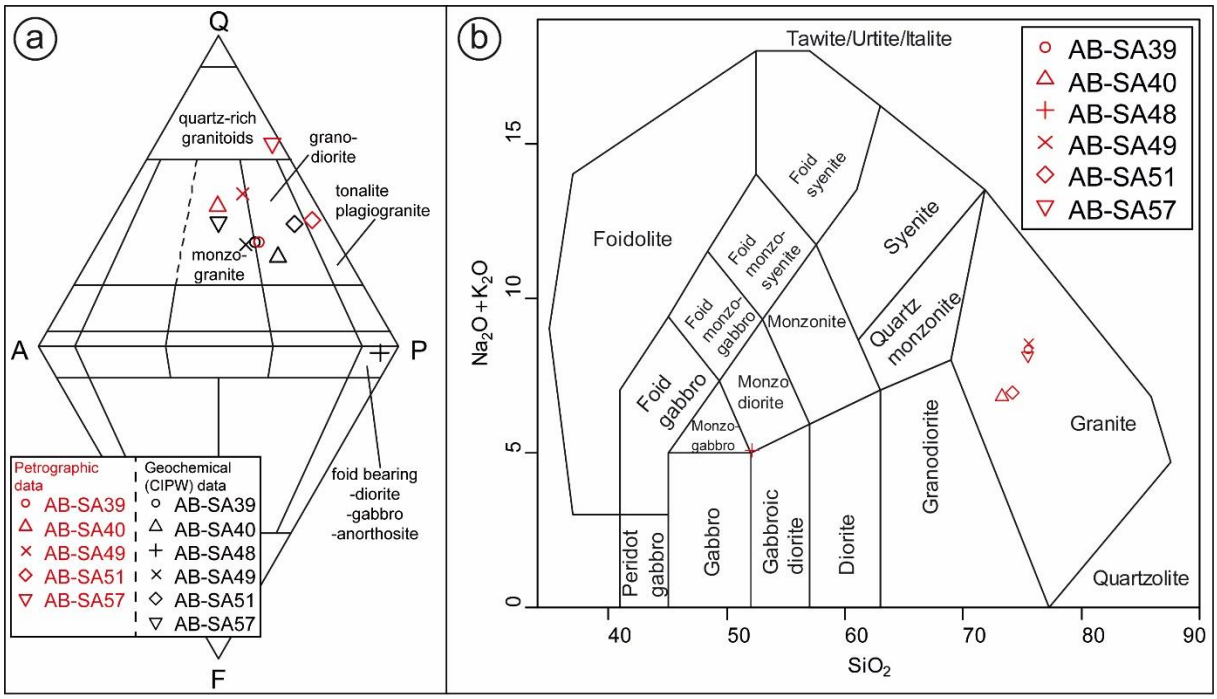

Figure 38: (a) QAPF classification diagram after Streckeisen (1974); red symbols represent petrographical data (point-counting), black symbols represent geochemical data (CIPW). (b) TAS classification diagram after Middlemost (1994).

Table 14: Summarised results of different petrographic and geochemical classification schemes for samples from the Khida Terrane.

Sample	Classification			
	petrographic	CIPW	TAS	Stoeser et al. (2001)
AB-SA 39	granodiorite	monzogranite	granite	granite
AB-SA 40	monzogranite	granodiorite	granite	granodiorite
AB-SA 48	-	foid bearing anorthosite	monzodiorite	meta-anorthosite
AB-SA 49	monzogranite	monzogranite	granite	syenogranite
AB-SA 51	tonalite	granodiorite	granite	granitic orthogneiss
AB-SA 57	quartz-rich granitoid	monzogranite	granite	monzogranite

The sampled metasediment (AB-SA45) is a quartzite (meta-psammite sensu lato) with alternating thin- and coarse-grained layers of several mm thickness (Figure 39c, d). Bedding is visible in outcrop. Thin section petrography revealed significant amounts of Cr-spinel.

Sample AB-SA51 (granitic orthogneiss of Stoeser et al., 2001) has a tonalitic composition according to petrographic analysis (Table 14, Figure 38a). Obvious signs for metamorphism like foliations or other metamorphic textures were not visible in the small outcrop. However signs of tectonic stress like quartz with undulose extinction and altered feldspars are clearly visible in thin section (Figure 39e, f). We therefore decided to follow the classification of Stoeser et al. (2001).

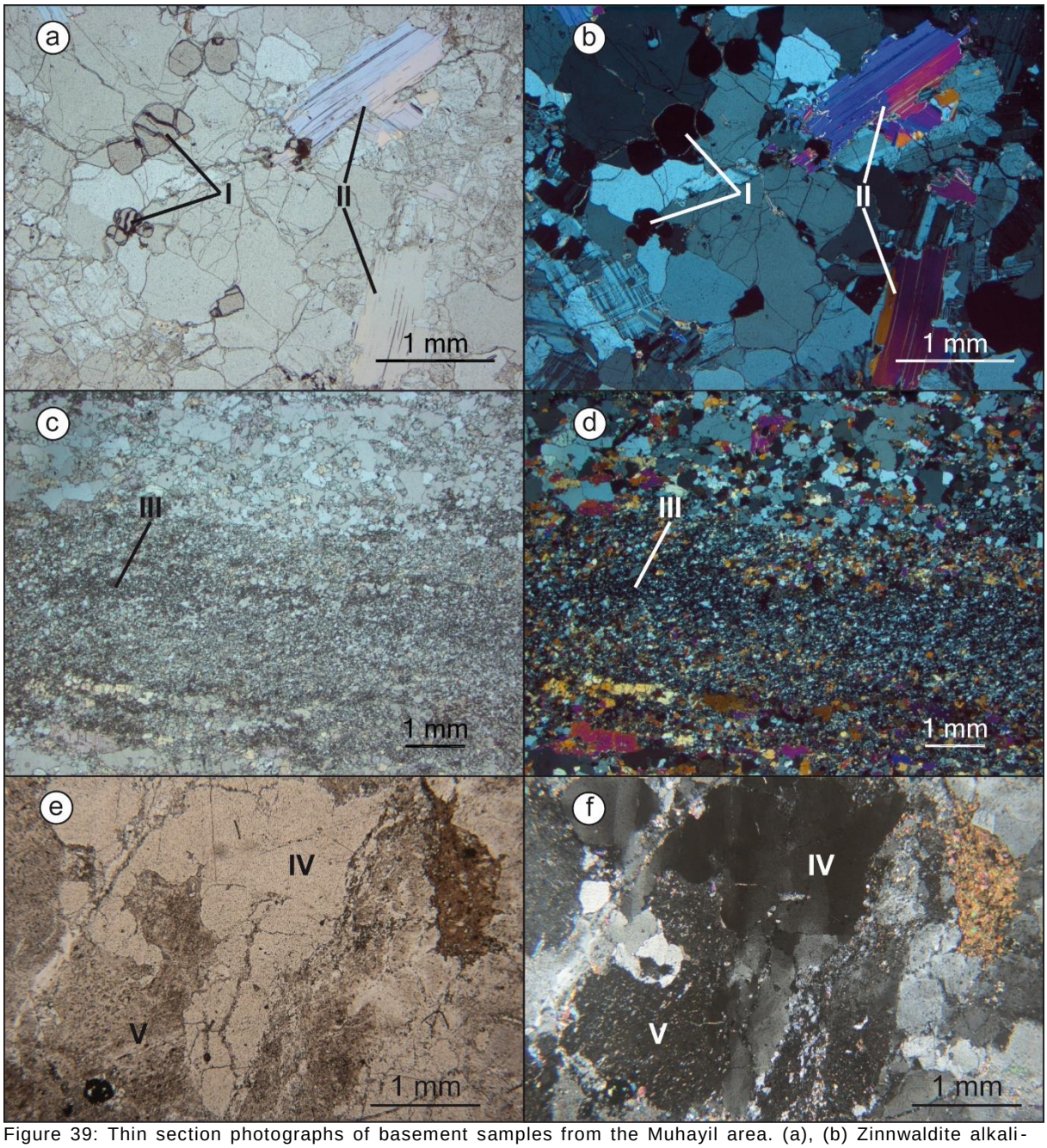

Figure 39: Thin section photographs of basement samples from the Muhayil area. (a), (b) Zinnwaldite alkali-feldspar granite (sample AB-SA39), containing idiomorphic magmatic garnet (I) and zinnwaldite mica (II). (c), (d) Meta-psammite (sample AB-SA45) with mm-scale layers, containing Cr-spinel (III). (e), (f) Biotite granitic orthogneiss (sample AB-SA51) containing quartz with undulose extinction (IV) and altered feldspar (V).

7.5.2. Geochemistry

Major and trace element composition of all basement samples are provided as supplementary data in Table A7 (annex).

Geochemical classification schemes are widely used to describe igneous rocks and are often preferred to petrographical modal analysis (Middlemost, 1994; Frost et al., 2001). Among the most common are the CIPW norm proposed by Cross et al. (1902) and the TAS diagram (Middlemost, 1994). The CIPW norm was calculated according to Hutchison (1974, 1975). Results have been plotted in the QAPF diagram (Figure 38a) and are also given in Table 14. Results for the TAS (total alkali versus silica) classification are shown in Figure 38b and Table 14.

The various petrographical and geochemical classification schemes yielded different results (Table 14). Geochemical classification schemes are more reliable than petrographic modal analysis (Middlemost, 1994). The TAS classification has proven to be less useful, since all igneous samples but one are classified as granite. Consequently, the classification after the CIPW norm is used. Where CIPW results from this study differ from the classification of Stoeser et al. (2001) the former is used, unless stated otherwise.

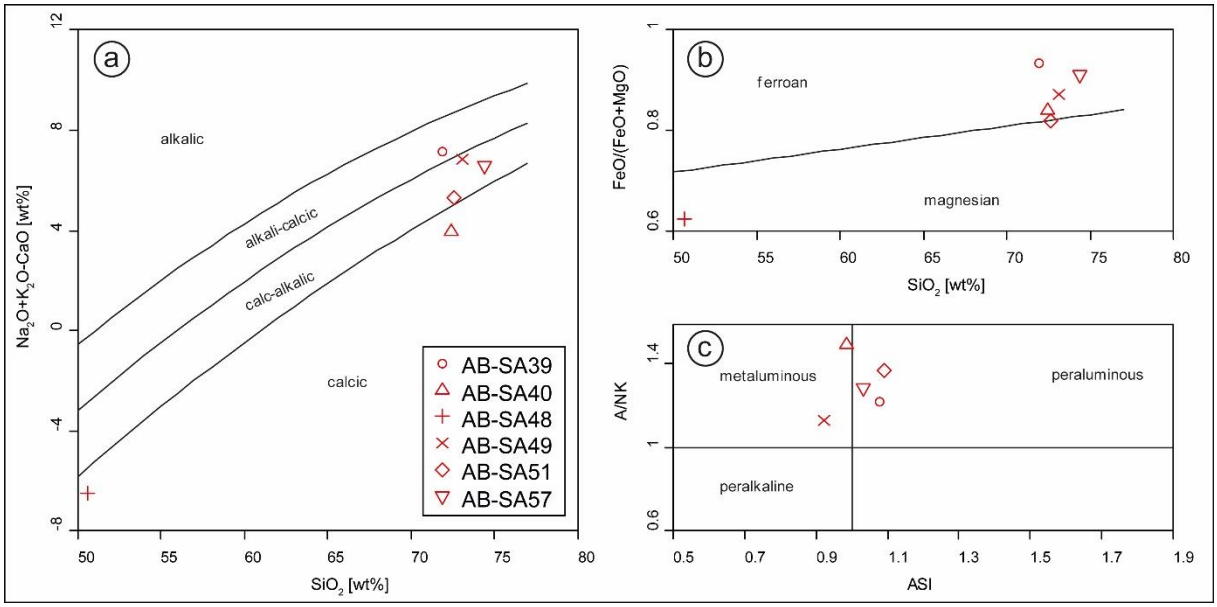

Figure 40: Results of the geochemical characterisation scheme for granitic rocks after Frost et al. (2001). (a) MALI; (b) Fe*; (c) ASI.

Frost et al. (2001) proposed additional criteria for the characterisation of granitic rocks: the Fe* ($FeO^{tot}/[FeO^{tot}/MgO]$), the modified alkali-lime index (MALI; Na_2O+K_2O-CaO) and the aluminium saturation index (ASI; molecular ratio of Al/[Ca-1.67*P+Na+K]). Results for the Khida Terrane rocks are summarised in Figure 40 and Table 15.

Table 15: Results of the geochemical characterisation scheme for granitic rocks after Frost et al. (2001).

Sample	Fe*	MALI	ASI
AB-SA39	0.93 ferroan	7.14 alkali-calcic	1.08 peraluminous
AB-SA40	0.84 ferroan	3.95 calcic	0.99 metaluminous
AB-SA48	0.62 magnesian	-6.52 calcic	0.98 metaluminous
AB-SA49	0.87 ferroan	6.85 calc-alkalic	0.92 metaluminous
AB-SA51	0.82 magnesian	5.207 calc-alkalic	1.09 peraluminous
AB-SA57	0.91 ferroan	6.58 calc-alkalic	1.03 peraluminous

REE concentrations have been chondrite-normalised after McDonough and Sun (1995) and are plotted in Figure 41. Eu anomalies (Eu/Eu*) have been calculated according to equation 3 and are also shown in Figure 41. Samples AB-SA40, AB-SA45 and AB-SA49 display the typical pattern for the UCC and have pronounced negative Eu anomalies (Eu/Eu*<1). Samples AB-SA51 and AB-SA57 have less pronounced Eu anomalies (Eu/Eu*=0.73 and Eu/Eu*=0.88, respectively) and 'falling' HREE trends. Sample AB-SA39 (alkali-feldspar monzogranite) has a much 'flatter' LREE pattern compared to the UCC and an extremely pronounced negative Eu anomaly (Eu/Eu*=0.01). Sample AB-SA48 (meta-anorthosite of Stoeser et al., 2001) is depleted in REEs compared to the UCC, but has an extremely pronounced positive Eu anomaly (Eu/Eu*=17.28).

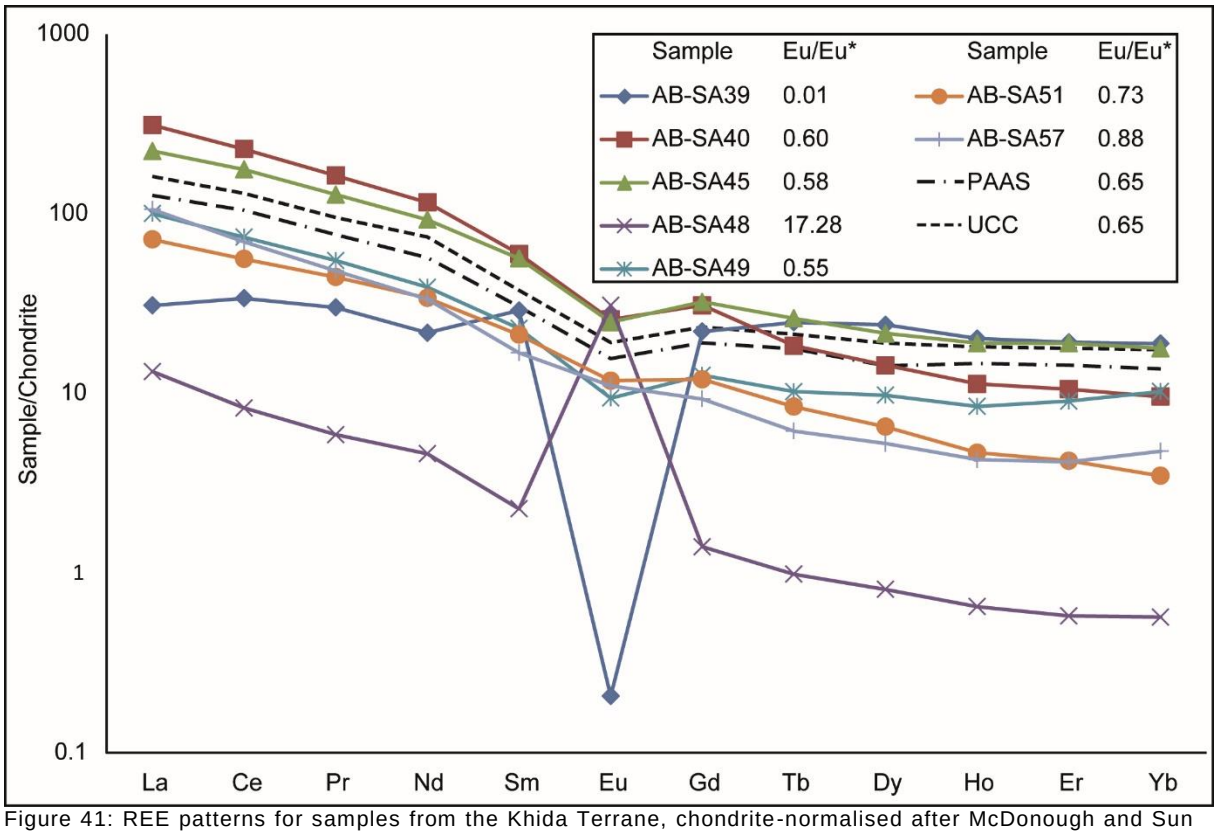

Figure 41: REE patterns for samples from the Khida Terrane, chondrite-normalised after McDonough and Sun (1995). PAAS (from Taylor and McLennan, 1985) and UCC from (McLennan, 2001; Taylor and McLennan, 2009) are plotted for comparison.

7.6. Discussion

Geochemical data have been used for a long time to infer tectonic setting of magmatic rocks, yet only a few are suitable for acid rocks (Verma et al., 2013). The discrimination diagrams proposed by Pearce et al. (1984) utilise trace element concentrations of Rb, Y, Yb, Nb, and Ta to discern the tectonic settings of granitic rocks. Although they are widely used, they have recently been re-evaluated and criticized: They have problems distinguishing between volcanic-arc and collisional settings, have overlapping fields for within-plate and ocean-ridge granitoids, partly use a mobile element (Rb) and treat compositional data statistically wrong (Verma et al., 2012; Verma et al., 2013). Furthermore, the diagrams proposed by Pearce et al. (1984) were based on Phanerozoic rocks and cannot easily be applied to Precambrian intrusions (Pearce et al., 1984). There are similar issues with the geochemical diagram of Harris et al. (1986), which uses Rb, Hf and Ta concentrations to characterise collision-zone magmatism. Additionally the diagram of Harris et al. (1986) is only applicable for continent-continent collisions and unsuitable to determine an unknown setting. Verma et al. (2013) proposed three new sets of 5 discrimination diagrams each to discriminate the tectonic setting of acid (SiO_2>63%) rocks. They are based on natural log-ratio transformed major and trace element concentrations and were successfully tested on Phanerozoic and Precambrian rocks. The first set of diagrams utilise major elements only. The second set of diagrams utilises a combination of immobile major and trace elements. The third set of diagrams utilises immobile trace elements only. In this study, the third set of diagrams utilising trace elements only was preferred, which showed a success rate of 60% to 96% (Verma et al., 2013). The first and second set require readjusted major element data using the SINCLAS software (Verma et al., 2002), which was unavailable.

The diagrams proposed by Verma et al. (2013) work only for acidic magmas with a SiO_2 content >63%. Sample AB-SA48 (anorthosite) has a SiO_2 content of 50.6% (Table A7). Verma and Agrawal (2011) proposed a set of five discrimination diagrams for basic and ultrabasic (<52% SiO_2) rocks. However they also require readjusted major element concentrations. Consequently, the tectonic setting of sample AB-SA48 could not be discriminated using the newly proposed diagrams. Employing the whole set of five diagrams, four different tectonic settings can be distinguished: Island arc (IA), continental arc (CA), collision (Col) as well as continental rift and ocean island combined (CR+OI). Within the set of five plots, the IA-CR+OI-Col diagram (Figure 42d) delivers the best results in most cases, although it cannot identify the CA setting (Verma et al., 2013). To discriminate a potential CA setting, the IA-CA-CR+OI plot (Figure 42b) is best suited (Verma et al., 2013). Results for the samples from the Khida Terrane are shown in Figure 42 and are intriguing: Samples AB-SA39, AB-SA40, AB-SA49 and AB-SA57 consistently plot in the Col-fields, while sample AB-SA51 consistently plots in the CA-field. The collisional setting of the alkali-feldspar monzogranite (AB-SA39) is likely related to the final assembly of the ANS or the amalgamation of Gondwana, since it is the supposedly youngest Precambrian unit in the Khida Terrane. The Haml batholith (samples AB-SA49, 57) was emplaced between 649 and 609 Ma (Stuckless and Futa, 1987; Agar et al., 1992), at the end of arc accretion and the beginning of the amalgamation of East and West Gondwana (Table 11). The collisional setting of samples AB-SA49 and AB-SA57 therefore are likely related to the beginning of the amalgamation of Gondwana. The apparent collisional setting of sample AB-SA40 is more enigmatic. The Fuwayliq granodiorite was emplaced at ~750 Ma (Whitehouse et al., 2001), during arc accretion in the Mozambique Ocean (Table 11). An arc signature would be expected for this granodiorite, if it originated in this setting. According to Whitehouse et al. (2001), the Fuwayliq granodiorite has a late Palaeoproterozoic source and was reworked during the Neoproterozoic. This is supported by the presence of highly evolved Type III Pb isotopes in feldspars and zircons containing Palaeoproterozoic cores with Neoproterozoic rims (Stacey and Hedge, 1984; Whitehouse et al., 2001; Johnson, 2014). The collisional signal of AB-SA40 may therefore be unrelated to arc accretion in the Mozambique Ocean, but rather be inherited from an older source. The continental arc signal of sample AB-SA51 (granitic orthogneiss) could be due to metamorphic alteration. Alternatively, the CA setting may represent a still older tectonic situation. According to Stoeser et al. (2001), the orthogneiss is potentially older than the Muhayil suite. To resolve this issue, further age data are needed.

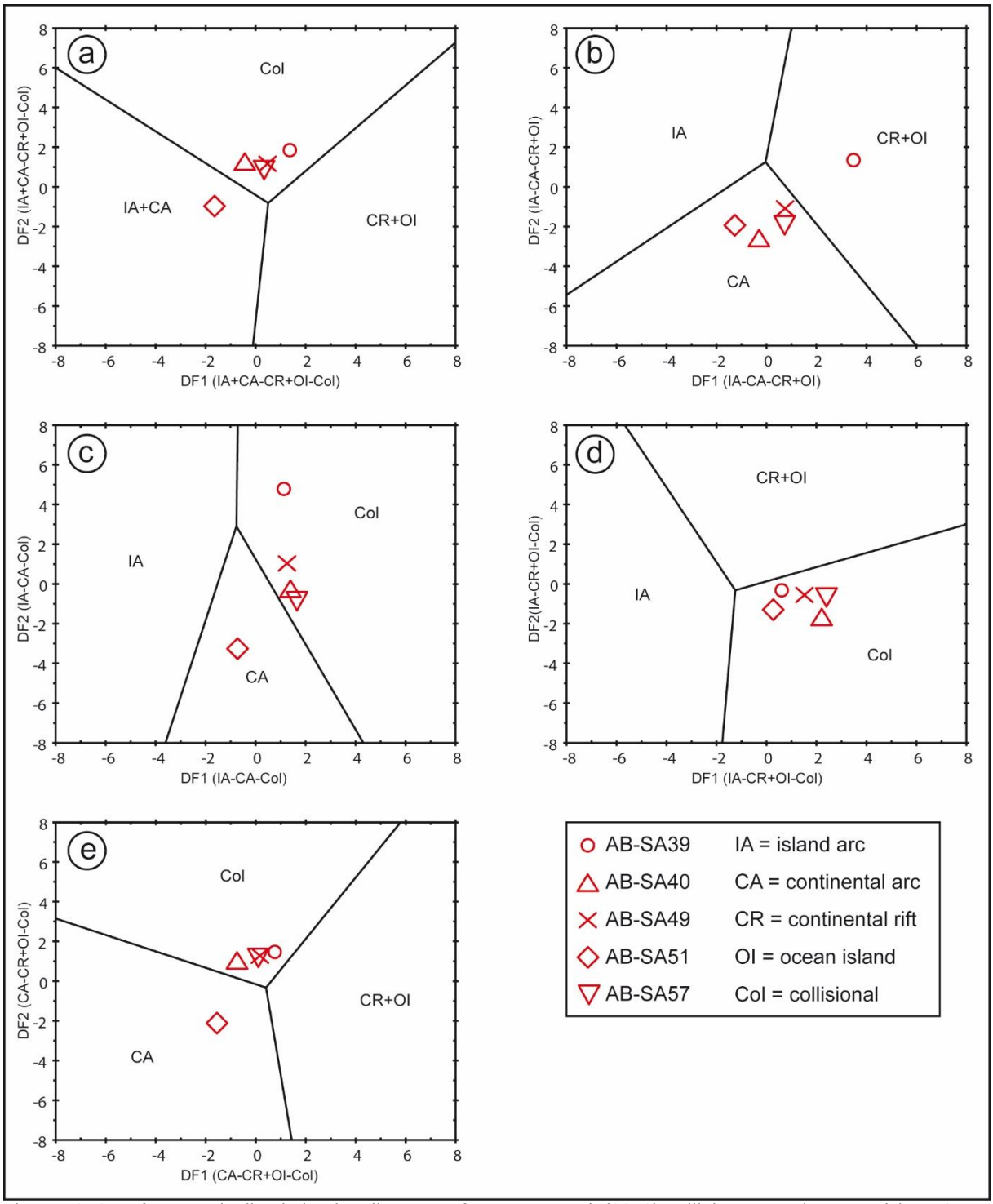

Figure 42: Set of 5 tectonic discrimination diagrams after Verma et al. (2013), utilising trace elements. (a) IA+CA-CR+OI-Col; (b) IA-CA-CR+OI; (c) IA-CA-Col; (d) IA-CR+OI-Col; (e) CA-CR+OI-Col. Calculations for discriminant functions are given in Table 16.

The REE concentrations of Khida Terrane samples mostly follow typical UCC distribution (Figure 41). Yet there are two striking exceptions. The extremely pronounced negative Eu anomaly (Eu/Eu*=0.01; Figure 41) of sample AB-SA39 is surprising, since plagioclase is present in significant amount (Figure 38a) and Eu is usually enriched in plagioclase. One possible explanation is a magma source already depleted in Eu (i.e., high fractionation). Another possibility is a plagioclase-rich source, where Eu was retained in the restite during melt generation. Sample AB-SA39 is additionally strongly depleted in Sr compared to the UCC (plot not shown). Sr tends to be concentrated in plagioclase (Drake and Weill, 1975). This supports the hypothesis of a plagioclase-rich source, although a high degree of fractionation

and extremely negative Eu/Eu* are also characteristic for other alkali-feldspar granites in the ANS (Johnson et al., 2011). The second unusual REE pattern belongs to sample AB-SA48: The meta-anorthosite has a very pronounced positive Eu/Eu*, which is expected because of the high plagioclase content (Figure 38a). High plagioclase concentrations can be achieved by fractionation of a basaltic magma (removal of mafic phases) or by plagioclase accumulation prior to emplacement.

Sample AB-SA39 is of special interest because of its unusual mineralogical composition, containing magmatic garnet and probably zinnwaldite. The geochemical composition of sample AB-SA39 supports the assumption that the pale mica observed in thin section is indeed zinnwaldite: zinnwaldite is a Li-mica ($KLiFe^{2+}Al[AlSi_3]O_{10}[F,OH]_2$) and often associated with tin ore deposits (Anthony et al., 2015). Since sample AB-SA39 has elevated Sn (9.9 ppm) and highly elevated Li (114.86 ppm) concentrations, there is strong evidence for the presence of zinnwaldite. For absolute certainty single-grain chemical analysis on thin sections are necessary.
Sample AB-SA39 is furthermore interesting for provenance analysis, since the magmatic garnets contained in the Muhayil granite are a possible source for the Type Bi garnet population in upper Palaeozoic sediments of the Juwayl Formation of the Wajid area. Primary igneous garnets are an uncommon accessory mineral in granitoid rocks (du Bray, 1988). They form only under very specific conditions: They crystallise during partial melting in the restite phase or precipitate under low-pressure conditions from a highly fractionated, peraluminous melt (Krippner et al., 2014; and references therein). Du Bray (1988) has reported other occurrences of small peraluminous plutons in the ANS, including the zinnwaldite alkali-feldspar monzogranite from the Khida Terrane (named 'Mahail granodiorite' by du Bray, 1988).

Siliciclastic metasediments (Thieme, 1988; Stoeser et al., 2001; own observations) from the Khida Terrane are a possible source for recycled, highly mature Palaeozoic sandstones of the Wajid area. The elevated Cr concentration of sample AB-SA45 (708 ppm) is in accordance with petrographical observations and the presence of significant amounts of Cr-spinel. While prevalent in the sampled metasediments, Cr-spinel is absent in Palaeozoic sandstones from the Tabuk area. However Cr-spinel has been encountered in minor concentrations in some samples from the Wajid area (Table 7). This could indicate the Khida Terrane to be a potential source of detrital Cr-spinel in sediments from the Wajid area, yet it presents no conclusive evidence. Other potential source rocks for Cr-spinel such as ophiolitic rocks, for instance, are abundant in the ANS (Johnson et al., 2013).

Table 16: Calculations of discriminant functions for tectonic discrimination diagrams of Verma et al. (2013) utilising trace element concentrations in ppm for for acidic magmas with a SiO_2 content >63%.

IA+CA-CR+Ol-Col (Fig. 39a)	
DF1	(-4.99*ln(La/Yb))+(7.81*ln(Ce/Yb))+(-4.33*ln(Sm/Yb))+(0.82*ln(Nb/Yb))+(0.063*ln(Th/Yb))+(0.64*ln(Y/Yb))+(-0.57*ln(Zr/Yb))-9.50
DF2	(2.32*ln(La/Yb))+(-3.62*ln(Ce/Yb)+(2.62*ln(Sm/Yb))+(0.25*ln(Nb/Yb))+(0.84*ln(Th/Yb))+(-1.14*ln(Y/Yb))+(-1.27*ln(Zr/Yb))+10.25
IA-CA-CR+Ol (Fig. 39b)	
DF1	(-5.21*ln(La/Yb))+(6.62*ln(Ce/Yb))+(-3.63*ln(Sm/Yb))+(1.69*ln(Nb/Yb))+(0.33*ln(Th/Yb))+(1.56*ln(Y/Yb))+(-0.49*ln(Zr/Yb))-9.61
DF2	(-3.72*ln(La/Yb))+(4.79*ln(Ce/Yb))+(-2.68*ln(Sm/Yb))+(0.16*ln(Nb/Yb))+(-0.50*ln(Th/Yb))+(1.04*ln(Y/Yb))+(-0.34*ln(Zr/Yb))-4.93
IA-CA-Col (Fig. 39c)	
DF1	(-0.047*ln(La/Yb))+(1.08*ln(Ce/Yb))+(-0.96*ln(Sm/Yb))+(0.84*ln(Nb/Yb))+(0.59*ln(Th/Yb))+(-0.88*ln(Zr/Yb))-0.73
DF2	(-4.07*ln(La/Yb))+(4.74*ln(Ce/Yb))+(-0.077*ln(Sm/Yb))+(-0.23*ln(Nb/Yb))+(0.77*ln(Th/Yb))+(-2.49*LN(Zr/Yb))+5.1
IA-CR+Ol-Col (Fig. 39d)	
DF1	(0.26*ln(La/Yb))+(1.05*ln(Ce/Yb))+(-1.00*ln(Sm/Yb))+(0.90*ln(Nb/Yb))+(0.54*ln(Th/Yb))+(0.089*ln(Y/Yb))+(-0.62*ln(Zr/Yb))-2.91
DF2	(-5.36*ln(La/Yb))+(8.41*ln(Ce/Yb))+(-5.37*ln(Sm/Yb))+(0.48*ln(Nb/Yb))+(-0.41*ln(Th/Yb))+(1.12*ln(Y/Yb))+(0.37*ln(Zr/Yb))-13.95
CA-CR+Ol-Col (Fig. 39e)	
DF1	(-5.41*ln(La/Yb))+(8.44*ln(Ce/Yb))+(-4.78*ln(Sm/Yb))+(0.78*ln(Nb/Yb))+(-0.079*ln(Th/Yb))+(0.64*ln(Y/Yb))+(-0.26*ln(Zr/Yb))-11.34
DF2	(1.68*ln(La/Yb))+(-1.73*ln(Ce/Yb))+(0.52*ln(Sm/Yb))+(0.84*ln(Nb/Yb))+(1.04*ln(Th/Yb))+(-0.98*ln(Y/Yb))+(-1.41*ln(Zr/Yb))+6.09

7.7. Summary and outlook

Most analysed samples (AB-SA39, AB-SA40, AB-SA49 and AB-SA57) from the Khida Terrane display a collisional geochemical signature in the tectonic discrimination diagrams of Verma et al. (2013). The Haml batholith (samples AB-SA49, AB-SA57) and the zinnwaldite alkali-feldspar monzogranite (sample AB-SA39) are likely related to the beginning and final phases of the amalgamation of Gondwana, respectively. The collisional setting of the Fuwayliq granodiorite (sample AB-SA40) is unrelated to arc accretion in the Mozambique Ocean and likely represents the influence of an older, reworked Palaeoproterozoic source. The apparent continental arc setting of the granitic orthogneiss (sample AB-SA51) could either be the result of chemical modification due to metamorphism or represents an older (i.e. inherited) tectonic setting.

The light mica in alkali-feldspar monzogranite (sample AB-SA39) is most likely zinnwaldite. The highly pronounced negative Eu anomaly caused by high fractionation and/or has an already plagioclase-rich source. Primary igneous garnets in this granite are a possible source for Type Bi garnets in upper Palaeozoic sediments from the Wajid area. Also siliciclastic metasediments in the Khida Terrane are a potential source for recycled sandstones from the Wajid area.

Petrographic and whole-rock geochemical analysis revealed new information about the arguably most enigmatic terrane of the ANS. Yet many issues remain unresolved. There is still a lack of reliable and robust geochronologic data for the Khida Terrane. The next logical step should be U–Pb isotopic dating of zircons. In conjunction with the plethora of temporal data already available from the remainder of the ANS, new, robust ages from the Khida Terrane would help to better understand its complex history and relationship with the ANS. Further insights into the evolution and cooling history could also be gathered with fission track dating. Zircon U–Pb and fission track ages might also help to answer the question when the basement of the Khida Terrane was exposed at the earth's surface to be a potential source area for Palaeozoic sediments. Additionally, further single-grain (EMP) analysis on thin sections of sample AB-SA39 (alkali-feldspar monzogranite) should be conducted to study the primary igneous garnets and confirm the presence of zinnwaldite.

8. Conclusions and outlook

Palaeozoic sandstones of southern, central and northern Saudi Arabia are dominated by quartz arenites. The main goal of this study was to identify the source areas and their change through time of these highly mature clastic successions. Of particular interest were the effects of the two major Palaeozoic glaciations on sediment transport, distribution and provenance. While it was not possible to pinpoint the exact geographic source area, several changes in provenance were identified. Some of those provenance changes are clearly linked to the Hirnantian and Carboniferous–Permian glaciations, which significantly impacted source areas and sediment dispersal.
A further aim was to identify potential petrographic, geochemical and heavy mineral markers with which to correlate different sandstone units from the two study areas. This was successful to a limited extent. It became evident that in order to develop robust markers, a much larger data base is needed. Heavy mineral data was used to link and compare Saudi Arabian Palaeozoic clastic sediments with adjacent counterparts in northern Gondwana.

The Arabian Shield as a source area was likely a large, though not the sole, contributor throughout most of the Palaeozoic. Various tectonic setting discrimination diagrams and trace element geochemistry suggest deposition of the sediments in an intracratonic basin, which developed adjacent to the ANS after the final amalgamation of Gondwana. Trace element geochemistry, especially concentrations of Th, Sc, Zr, Ni and V, indicate the Neoproterozoic basement of the nearby ANS as the most likely source for the detritus. A significant contribution of the ANS can also be seen in the collisional setting of the Sanamah, Juwayl, Sarah and Zarqa formations, which were deposited in a glaciogenic context. These collisional signals are interpreted to be relics from the last stages of the amalgamation of Gondwana, which were carried over by glaciogenic sediments. The higher mineralogical and geochemical maturity of lower Palaeozoic samples from both study areas and the decreasing maturity towards younger strata necessitate input from fresh basement rocks nearby. This is backed up by an increase in diversity of upper Palaeozoic heavy mineral assemblages. Although most encountered heavy minerals were rounded, some euhedral zircon and tourmaline grains indicate short transport distances. Potential source rocks for encountered heavy minerals are abundand in the ANS and its vicinity. Garnets from the glaciogenic Juwayl Formation, for instance, were probably derived from a proximal source. High-grade metamorphic garnets in non-glaciogenic units on the other hand could have been sourced from further away, like the Mozambique Belt or Sudan. Similarly, high-T rutiles from the Saq Formation require high-grade, granulite-facies source rocks, which are scarce in the ANS.

The effects of source area weathering were not possible to assess with geochemical methods. Weathering indices like the CIA and PIA showed highly variable and unrealistic values. Both indices are too dependant on grain size and susceptible to sorting effects and thus do not accurately reflect weathering conditions during deposition of the studied sandstones. Heavy mineral indices, like the ZTR and ATi, were better suited but also struggle to discern intensive weathering from reworking during deposition and sedimentary recycling. The very low ATi values in the lower Palaeozoic of the Tabuk area require increased weathering, compared to the Dibsiyah Formation from the Wajid area. This is likely not related to different climatic conditions, but rather caused by longer transport distances and/or alluvial storage.

Petrographical and geochemical data present some evidence for recycling of older sedimentary rocks. A significant contribution of recycled sediments in the Sanamah, Sarah and Zarqa formations was proven with standard heavy mineral analysis, used in conjunction with petrographic and field observations. Very high ZTR values in climatic conditions unfavourable for strong weathering require a recycled sedimentary source. This is supported by similar ATi values in Hirnantian as well as older samples.

Petrographic observations proved unsuitable for correlations between the two study areas. Geochemical analysis of trace elements revealed some potential markers for the characterisation of barren units, like variances in the ratios of Th/Sc, Zr/Sc and Th/U as well as V-Ni-Th concentrations. Yet these variables were not consistent enough throughout both successions to be used for correlations. Better results were

achieved with multivariate cluster and principal component analyses of major and trace element concentrations. These statistical approaches to the handling of large data sets allowed differentiating between the two study areas as well as separate lower and upper Palaeozoic units in the Wajid area. However the sample size was too small to allow the development of robust chemostratigraphic markers. While the geochemical approach has shown clear potential, a much larger data set is needed to clearly characterise and correlate individual formations.

While the principal heavy mineral composition of Saudi Arabian Palaeozoic sediments is similar to those from other parts of the northern Gondwana margin, they differ significantly in detail. All exhibit high ZTR values but vary considerably in their accessories. While this certainly reflects regional variations in provenance, other factors like differences in sample preparation, operator and sampling bias can have a large impact and are hard to estimate.

Single-grain ('varietal') studies of heavy minerals, especially rutile, delivered good results and showed great potential for further provenance studies in the area. They enabled the identification of provenance changes through time as well as regional variations between study areas. Moreover, rutile chemistry provided clues for long-range transport of some of the lower Palaeozoic sediments.
Following regional variance in rutile source lithologies could be identified: The Tabuk area contains predominantly felsic rutiles, while the Wajid area has a greater mafic input. The bulk of rutiles in both study areas were formed under low- to medium-temperature conditions. Potential sources for these rutiles are abundant in the nearby ANS. The Cambrian–Ordovician Saq Formation contains high-grade, granulite-facies rutiles, which are absent in the overlying Qasim Formation. They occur again in the Devonian Jubah Formation and have not been observed at all in the Wajid area. Therefore high-grade rutiles from the Saq Formation must have been derived from a source north of the Wajid catchment area and could not be sourced from the Abas Gneiss Terrane. Rutile varietal studies have proven to be a powerful tool with great potential, yet more data from other units is needed. This would open up the possibility to map out catchment areas and sediment transport routes.
Garnet varietal studies revealed striking similarities in the distribution patterns of garnet host rock lithologies of upper Palaeozoic units from the two study areas. Garnet populations are dominated by garnets derived from amphibolite-facies metasediments and intermediate to felsic igneous rocks. These are abundand in an around the ANS. They also contain high-grade garnets, which were probably derived from paragneisses in the Abas Gneiss Terrane, Yemen.

An integrated multi-proy provenance analysis revealed four distinct changes in provenance ('provenance events') in Palaeozoic sandstones from southern, central and northern Saudi Arabia:
The Cambrian–Ordovician formations (Saq, Qasim, Dibsiyah) are first-cycle sediments, largely derived from the nearby Neoproterozoic basement of the ANS, but with varying transport distances. A first provenance change (PE 1), probably confined to the Tabuk area, from the Saq Formation to the Qasim Formation has been observed through rutile varietal studies and trace element geochemistry. A second provenance change (PE 2) happened with the onset of the Late Ordovician glaciation. The Hirnantian formations are not derived from the basement of the ANS but rather from recycled sedimentary sources, as is indicated by heavy mineral data. Similarities point to the Cambrian–Ordovician sandstones as a major source, with minor contributions from Neoproterozoic basement. The third provenance change (PE 3) occurred either at the base of the Devonian; upper Palaeozoic units display an increasing input of fresh basement detritus. This is seen in trace element concentrations and heavy mineral assemblages. The event can be linked to an increased tectonic segmentation of north-eastern Gondwana during conversion from a passive to an active continental margin in Devonian-Carboniferous time (Sharland et al., 2001). The most prominent feature of this tectonic activity is the 'Hercynian' unconformity. A fourth and last provenance change (PE 4) has been related to the Carboniferous–Permian glaciation in the Wajid area. Trace element concentrations, heavy mineral assemblages and rutile varietal studies suggest a shift in provenance between the Khusayyayn and Juwayl formations, towards a source containing more metamorphic rocks. This provenance change is also tentatively assumed for the Unayzah Formation from the Tabuk area, but more conclusive evidence is needed.

The Palaeo- to Neoproterozoic Khida Terrane lies on the southeastern margin of the Arabian Shield. It is a potential proximal source area for Palaeozoic sandstones. The Khida Terrane contains siliciclastic metasediments that could have supplied recycled material for highly mature sandstones from the Wajid area. Primary igneous garnets from an alkali-feldspar monzogranite are a possible source for Type Bi garnets in the Juwayl Formation. SHMA, single-grain EMP analyses on thin sections and isotopic dating could provide new and valuable insights into this enigmatic block of continental crust within the ANS.

While some of the main questions have been successfully answered in this study, there are still holes left to be plugged and new issues have arisen. Further research efforts should be laid on the following points:

- Chemostratigraphy and geochemical correlations showed potential, but the data base was found to be insufficient to develop robust markers. A cheap and quick way to generate large amounts of usable geochemical data would be to analyse hand specimen with handheld XRF analysers.
- SHMA has proven to be an effective, yet time-consuming, tool in this provenance study. Future investigations should direct the attention on the already identified provenance events in order to increase resolution and to further contrain them.
- Best results have been obtained with single-grain analyses. Consequently, subsequent studies should focus on these techniques. Tourmaline is ultra-stable, available in abundance in the Palaeozoic sandstones and can be analysed reltively easily with the EMP. Chemical data from tourmaline is of limited use when employed independently (Morton et al., 2011), but could serve as a valuable supplementary to other analyses.
- While the idea of identifying magmatic and metamorphic events in zircons and using these events as provenance signals is promising, the method of manually assigning morphotypes using CL images did not yield meaningful results. A better suited approach would be to use CL imaging in conjunction with chemical single-grain data, obtained via EMP or LA-ICP-MS, to reduce the potential for operator bias.
- The most obvious next step is U–Pb isotopic dating of detrital zircons. This method has been applied successfully in other provenance studies targeting the Palaeozoic of northern Gondwana (Avigad et al., 2003, 2005; Kolodner et al., 2006; Linnemann et al., 2011; Meinhold et al., 2011, 2013b; Garzanti et al., 2013). So far only little data is available from Saudi Arabia (Garzanti et al., 2013). Detrital zircon U–Pb ages are important to tie in with the growing age data base of northern Gondwana and to remove the 'white spot' that is the Arabian Peninsula on the palaeogeographic map. They open up the possibility to further constrain geographical source areas, sedimentary dispersal systems and their development through time.

Acknowledgements

The work on this thesis – let alone its completion – would not have been possible without the invaluable support of many people. I am very grateful for their support throughout these years and want to express my personal thanks and profound gratitute.

First and foremost I want to mention Stefanie Redlberger, who was there for me throughout every phase of my PhD. Be it my absence during month-long field work in the Arabian desert, analytical campaigns in Göttingen, workshops and conferences or weekends spent at the Institute writing my thesis – she never complained. Thank you, Steffi, for always listening to my stories about old rocks!

Secondly, I am forever indebted to my parents Marlies and Giorgio Bassis. They enabled me to pursue my dream career as a geologist and supported me both morally and financially during this entire time.

Without Prof. Dr. Matthias Hinderer this whole project would have never come into existence. He accepted me as a PhD student, assisted me through the various stages of funding and helped me to greatly improve the quality not only of this thesis, but also of two publications as well as countless presentations and posters. Thank you, Matthias, for this opportunity!

In this place, Dr. Guido Meinhold deserves a special mention. First during field work in Saudi Arabia, then from my several stays at Göttingen and through countless phone calls I learned much and more about many field and aspects of geology. Thank you, Guido, for your guidance, patience, your professional and helpful input, and of course for letting me crash on your couch in Göttingen more than once!

I want to thank Prof. Dr. Christoph Schüth for his assistance during the starting phase and his multidisciplinary input.

During my studies at the TU Darmstadt I had the opportunity and privilege to meet many great colleagues. Among these I want to mention Nils Michelsen, with whom I had many inspiring discussions and Sandra Schneider, who helped me to figure out the finer details of heavy mineral studies and sample preparation. I want to especially mention Dennis Brüsch, with whom I not only shared my office, but also my passion for photography.

Furthermore, I want to express my sincere thanks to Nora Groschopf from the University of Mainz and to Dr. Gerald Hartmann, Dr. Klaus Simon and Dr. Andreas Kronz from the University of Göttingen for their help with various geochemical analyses. My warmest greetings go to the staff of the Geoscience Center at the University of Göttingen, especially to Irina Ottenbacher. I also want to mention my fellow PhD student Anne Krippner, with whom I had insightful scientific discussions and many a great night out in Göttingen.

I am especially indebted to the staff at the Riyadh office of GIZ/DornierConsulting. Without their logistical support and knowledge of the country, a successful field campaign would have been unimaginable. Among the many people there I want to especially mention Prof. Dr. Randolf Rausch and Prof. Dr. Martin Keller.

Last but by no means least I have to thank Dr. Olfa Lenz from our working group in Darmstadt. Olaf always had an open ear for any kind of problem, especially concerning statistics.

References

Abu-Ali, M.D., 2005. Organic Petrology, Maturation, Thermal and Burial History Analysis, and Hydrocarbon Generation and Migration Modeling of the Saudi Arabian Paleozoic Petroleum Systems. Dissertation, Faculty of Georesources and Materials Engineering, RWTH Aachen, pp. 202.

Agar, R.A., 1987. The Najd fault system revisited; a two-way strike-slip orogen in the Saudi Arabian Shield. Journal of Structural Geology 9(1), 41–48.

Agar, R.A., Stacey, J.S., Whitehouse, M.J., 1992. Archean to Late Proterozoic evolution of the southern Afif terrane: a geochronologic study. Saudi Arabian Deputy Ministry for Mineral Resources, open file report DGMR-OF-03-12. Cited in Whitehouse et al. (2001).

Akarish, A.I.M., El-Gohary, A.M., 2008. Petrography and geochemistry of lower Paleozoic sandstones, East Sinai, Egypt: Implications for provenance and tectonic setting. Journal of African Earth Sciences 52, 43–54.

Al-Ajmi, H.F., 2005. Geology of Sakaka Area Northern Saudi Arabia. Master thesis, Department of Geology, King Saud University, Saudi Arabia, pp. 249.

Al-Ajmi, H.F., 2013. Sedimentology, stratigraphy and reservoir quality of the Paleozoic Wajid Sandstone in SW Saudi Arabia. Dissertation, Technische Universität Darmstadt, Darmstadt, pp. 119.

Al-Ajmi, H.F., Hinderer, M., Keller, M., Rausch, R. 2008. New insights into the facies distribution of the Wajid Sandstone in its western outcrop area and implication on reservoir properties. The 3rd International Conference on Water Resources and Arid Environments. http://www.icwrae-psipw.org

Al-Ajmi, H.F., Hinderer, M., Rausch, R., Hornung, J., Bassis, A., Keller, M., Schüth, C., 2014. Matrix versus fracture permeability in a regional sandstone aquifer (Wajid sandstone, SW Saudi Arabia). Grundwasser – Zeitschrift der Fachsektion Hydrogeologie 19, 151–157.

Al-Ajmi H.F, Keller, M., Hinderer, M., Filomena, C.M., 2015. Lithofacies, depositional environments and stratigraphic architecture of the Wajid Group outcrops in southern Saudi Arabia. GeoArabia 20 (1), 49–94.

Al-Ghazi, A., 2007. New evidence for the Early Devonian age of the Jauf Formation in northern Saudi Arabia. Revue de micropaléontologie 50, 59–72.

Al-Hajri, S., 1995. Biostratigraphy of the Ordovician Chitinozoa of Northwestern Saudi Arabia. Review of Palaeobotany and Palynology 89, 27–48.

Al-Hajri, S.A., Filatoff, J., Wender, L.E., Norton, A.K., 1999. Stratigraphy and operational palynology of the Devonian System in Saudi Arabia. GeoArabia 4(1), 53–68.

Al-Hajri, S., Paris, F., 1998. Age and palaeoenvironment of the Sharawra Member (Silurian of northwestern Saudi Arabia). Geobios 31(1), 3–12.

Al-Harbi, O.A., Khan, M.M., 2005. Mineralogy and Geochemistry of Unayzah Formation, Central Saudi Arabia: Implications for Provenance Interpretation. Journal of King Saud University 18, 35–49.

Al-Harbi, O.A., Khan, M.M., 2008. Provenance, diagenesis, tectonic setting and geochemistry of Tawil Sandstone (Lower Devonian) in Central Saudi Arabia. Journal of Asian Earth Sciences 33, 278–287.

Al-Harbi, O.A., Khan, M.M. 2011. Source and origin of glacial paleovalley-fill sediments (Upper Ordovician) of Sarah Formation in central Saudi Arabia. Arabian Journal of Geosciences 4, 825–835.

Al-Husseini, M.I., 2004. Pre-Unayzah unconformity, Saudi Arabia. GeoArabia Special Publication 3, 15–59.

Al-Laboun, A.A., 1982. The subsurface stratigraphy of the pre-Khuff formations in central and northwestern Arabia. Dissertation, King Abdulaziz University, Jeddah, Saudi Arabia, pp. 102. Cited in Laboun (2013).

Al-Laboun, A.A., 1986. Stratigraphy and Hydrocarbon Potential of the Paleozoic Succession in both Tabuk and Widyan Basins, Arabia. In: Halbouty, M.T. (Ed.), Future petroleum provinces of the world. AAPG Memoir 40, 373–397. Cited in Laboun (2013).

Al-Laboun, A.A., 1993. Lexicon of the Palaeozoic and lower Mesozoic of Saudi Arabia, Part 1, lithostratigraphic units, nomenclature review. Al-Hudhud Publishers, Riyadh, pp. 509. Cited in Al-Laboun (2010).

Al-Laboun, A.A., 2000a. Lithostratigraphy and oil and gas fields of Saudi Arabia. 4th edition, Saudi Society for Earth Sciences, King Saud University, Riyadh.

Al-Laboun, A.A., 2000b. The Paleozoic geology of the Wajid area: a new approach. 4th Middle East Geosciences Conference, GEO 2000, Abstract. GeoArabia 5(1), 26–27.

Al-Laboun, A.A., 2009. Tectonostratigraphy of the exposed Silurian deposits in Arabia. Arabian Journal of Geosciences 2, 119–131.

Al-Laboun, A.A., 2010. Paleozoic tectono-stratigraphic framework of the Arabian Peninsula. Journal of King Saud University (Science) 22, 41–50.

Al-Laboun, A.A., 2011. Tectono-History of the Silurian Sharawra Formation in Northwestern and Central Arabia. Egyptian Journal of Pure and Applied Sciences 49(2), 1–7.

Al-Ramadan, K.A., Hussain, M., Imam, B., Saner, S., 2004. Lithologic characteristics of the Devonian Jauf sandstone at Ghawar Field, Eastern Saudi Arabia. Marine and Petroleum Geology 21, 1221–1234.

Al-Saleh, A., 2012. The Kirsh gneiss dome: an extensional metamorphic core complex from the SE Arabian Shield. Arabian Journal of Geosciences 5, 335–344.

Alsharhan, A.S., 1994. Geology and hydrocarbon occurrences of the clastic Permo-Carboniferous in the central and eastern Arabian Basin. Geologie en Mijnbouw 73a, 63–73.

Alsharhan, A.S., Nairn, A.E.M., 1997. Sedimentary Basins and Petroleum Geology of the Middle East. Elsevier, Amsterdam, pp. 843.

Anthony, J.W., Bideaux, R.A., Bladh, K.W., Nichols, M.C., 2015. Handbook of Mineralogy. Mineralogical Society of America, Chantilly, VA 20151-1110, USA. http://www.handbookofmineralogy.org/. Accessed 15.10.2015.

Armstrong-Altrin, J.S., Verma, S.P., 2005. Critical evaluation of six tectonic setting discrimination diagrams using geochemical data of Neogene sediments from known tectonic settings. Sedimentary Geology 177(1–2), 155–129.

Avigad, D., Kolodner, K., McWilliams, M., Persing, H., Weissbrod, T., 2003. Origin of northern Gondwana Cambrian sandstone revealed by detrital zircon SHRIMP dating. Geology 31 (3), 227–230.

Avigad, D., Sandler, A., Kolodner, K., Stern, R.J., McWilliams, M., Miller, N., Beyth, M., 2005. Mass-production of Cambro-Ordovician quartz-rich sandstone as a consequence of chemical weathering of Pan-African terranes: Environmental implications. Earth Planetary Science Letters 240, 818–826.

Babalola, L.O., 1999. Depositional Environments and Provenance of the Wajid Sandstone, Abha-Khamis Mushayt Area, Southwestern Saudi Arabia. MSc Thesis, King Fahd University of Petroleum and Minerals, Dhahran, Saudi Arabia, pp. 239.

Babalola L.O., Hussain, M., Hariri, M.M., 2003. Origin of iron-rich beds in the basal Wajid Sandstone, Abha-Khamis Mushayt area, Southwest Saudi Arabia. Arabian Journal of Science and Engineering 28(1A), 3–24.

Bahlburg, H., Dobrzinski, N., 2011. A review of the Chemical Index of Alteration (CIA) and its application to the study of Neoproterozoic glacial deposits and climate transitions. Geological Society of London Memoirs 36, 81–92.

Bateman, R.M., Catt, J.A., 1985. Modification of heavy mineral assemblags in English coversands by acid pedochemical weathering. Catena 12, 1–21.

Bates, R.L., Jackson, J.A., 1987. Glossary of geology (third edition). Alexandria, Virginia, American Geological Institute, pp. 788.

Bauluz, B., Mayayo, M.J., Fernandez-Nieto, C., Lopez, J.M.G., 2000. Geochemistry of Precambrian and Paleozoic siliciclastic rocks from the Iberian Range (NE Spain): implications for source-area weathering, sorting, provenance, and tectonic setting. Chemical Geology 168, 135–150.

Besems, R.E., Schuurman, W.M.L., 1987. Palynostratigraphy of late Paleozoic glacial deposits of the Arabian Peninsula with special reference to Oman. Palynology 11, 37–53.

Bhatia, M.R., 1983. Plate tectonics and geochemical composition of sandstones. The Journal of Geology 91(6), 611–627.

Bhatia, M.R., 1985. Rare earth element geochemistry of Australian Paleozoic graywackes and mudrocks: provenance and tectonic control. Sedimentary Geology 45, 97–113.

Bhatia, M.R., Crook, K.A.W., 1986. Trace element characteristics of graywackes and tectonic setting discrimination of sedimentary basins. Contributions to Mineralogy and Petrology 92, 181–193.

Bishop, D.T., 1982. Appraisal of gold potential in the Bi'r Juqjuq-North Tathlith region, Kingdom of Saudi Arabia. Saudi Arabian Deputy Ministry for Mineral Resources, open file report RF-OF-04-4, pp. 26. Cited in Thieme (1988).

Bishop, R.S., 1995. Maturation History of the Lower Palaeozoic of the Eastern Arabian Platform. In: Al-Husseini, M.I. (Ed), Middle East Petroleum Geosciences, GEO'94 1, 180–189. Cited in Sharland et al. (2001).

Bracciali, L., Marroni, M., Pandolfi, L., Rocchi, S., 2007. Geochemistry and petrography of Western Tethys Cretaceous sedimentary covers (Corsica and Northern Apenninces): from source areas to configuration of margins. In: Arribas, J., Critelli, S., Johnsson, M.J. (Eds.), Sedimentary Provenance and Petrogenesis: Perspectives from Petrography and Geochemistry, Geological Society of America Special Paper 420, 73–93.

Breuer, P., Al-Ghazi, A., Al-Ruwaili, M., Higgs, K.T., Steemans, P., Wellman, C.H., 2007. Early to Middle Devonian miospores from northern Saudi Arabia. Revue de micropaléontologie 50, 27–57.

Breuer, P., Miller, M.A., Leszczyński, S., Steemans, P., 2015. Climate-controlled palynofacies and miospore stratigraphy of the Jauf Formation, Lower Devonian, northern Saudi Arabia. Review of Palaeobotany and Palynology 212, 187–213.

BRGM, 1985. Water, Agriculture and soil studies of Saq and overlying aquifers. Unpublished report, Ministry of Agriculture and Water, Water Resources Development Department, Kingdom of Saudi Arabia. Cited in Al-Laboun (2010).

Brown, G.F., Coleman, R.G., 1972. Tectonic framework of the Arabian Peninsula. Proceedings of the 24th International Geological Congress, Montreal, 300–305.

Cardenas, A.A., Girty, G.H., Hanson, A.D., Lahren, M.M., Knaack, C., Johnson, D., 1996. Assessing Differences in Composition between Low Metamorphic Grade Mudstones and High-Grade Schists Using Logratio Techniques. The Journal of Geology 104, 279–293.

Chandler, F.W., 1988. Quartz arenites: review and interpretation. Sedimentary Geology 58, 105–126.

Chappel, B.W., White, A.J.R., 1974. Two contrasting granite types. Pacific Geology 8, 173–174.

Chen, R.X., Zheng, Y.F., Xie, L., 2010. Metamorphic growth and recrystallization of zircon: Distinction by simultaneous in-situ analyses of trace elements, U-Th-Pb and Lu-Hf isotopes in zircons from eclogite-facies rocks in the Sulu orogen. Lithos 114, 132–154.

Clark-Lowes, D.D., 1980. Sedimentology and mineralization potential of Saq and Tabuk formations. Imperial College Science and Technology, London, Open-File Report CRC/IC 7, pp. 88. Cited in Al-Laboun (2010).

Clark-Lowes, D.D., 2005. Arabian glacial deposits: recognition of palaeovalleys within the Upper Ordovician Sarah Formation, Al Qasim district, Saudi Arabia. Proceedings of the Geologists' Association 116(3–4), 331–347.

Clayton, G., Owens, B., Al-Hajri, S., Filatoff, J., 2000. Latest Devonian and Early Carboniferous miospore assemblages from Saudi Arabia. In: Al-Hajri S and Owens B (eds) Stratigraphic Palynology of the Palaeozoic of Saudi Arabia. GeoArabia Special Publication 1, 146–153.

Corfu, F., Hanchar, J.M., Hoski, P.W., Kinny, P., 2003. Atlas of zircon textures. Reviews in mineralogy and geochemistry 53(1), 469-500.

Cosca, M.A., Shimron, A., Caby, R., 1999. Late Precambrian metamorphism and cooling in the Arabian-Nubian Shield: Petrology and 40Ar/39Ar geochronology of metamorphic rocks of the Elat area (southern Israel). Precambrian Research 98, 107–127.

Cross, W., Iddings, J.P., Pirsson, L.V., Washington, H.S., 1902. A Quantitative Chemico-Mineralogical Classification and Nomenclature of Igneous Rocks. The Journal of Geology 10(6), 555–690.

Darbyshire, D.P.F., Jackson, N.J., Ramsay, C.R., Roobol, M.J., 1983. Rb-Sr isotope study of latest Proterozoic volcano-sedimentary belts in the central Arabian Shield. Journal of the Geological Society of London 140, 201–213.

Das, B.K., Al-Mikhlafi, A.S., Kaur, P., 2006. Geochemistry of Mansar Lake sediments, Jammu, India: Implication for source-area weathering, provenance, and tectonic setting. Journal of Asian Earth Sciences 26(6), 649–668.

Delfour, J., Dhellemmes, P., Elsass, D., Vaslet, J., Brosse, Y., Le Nindre, Y.M., Dottin, O., 1983. Geologic Map of the Ad-Dawadimi quadrangle, Sheet 24G. Saudi Deputy Ministry for Mineral Resources, Jeddah. Cited in Hussain and Abdullatif (2004).

Denèle, Y., Leroy, S., Pelleter, E., Pik, R., Talbot, J.-Y., Khanbari, K., 2012. The Cryogenian arc formation and successive high-K calc-alkaline plutons of Socotra Island (Yemen). Arabian Journal of Geosciences 5 (5), 903–924.

Dickinson, W.R., 1970. Interpreting detrital modes of greywacke and arkose. Journal of Sedimentary Petrology 40, 695–707.

Dickinson, W.R., Suczek, C.A., 1979. Plate Tectonics and Sandstone Composition. American Association of Petroleum Geologists Bulletin 63, 2164–2182.

Dickinson, W.R., Beard, L.S., Brackenbridge, G.R., Erjavec, J.L., Ferguson, R.C., Inman, K.F., Knepp, R.A., Lindberg, F.A., Ryberg, P.T., 1983. Provenance of North American Phanerozoic sandstones in relation to tectonic setting. Geological Society of America Bulletin 94, 222–235.

Drake, M.J., Weill, D.F., 1975. Partition of Sr, Ba, Ca, Y, Eu2+, Eu3+, and other REE between plagioclase feldspar and magmatic liquid: an experimental study. Geochimica et Cosmochimica Acta 39, 689–712.

Dryden, A.L., Dryden, C., 1946. Comparative rates of weathering of some common heavy minerals. Journal of Sedimentary Petrology 16, 91–96.

du Bray, E.A., 1983. Mineral potential of selected felsic plutons in the eastern and southeastern Arabian Shield, Kingdom of Saudi Arabia. Saudi Arabian Deputy Ministry for Mineral Resources, open file report USGS-OF-83-370, pp. 58.

du Bray, E.A., 1988. Garnet compositions and their use as indicators of peraluminous granitoid petrogenesis – southeastern Arabian Shield. Contributions to Mineralogy and Petrology 100, 205–212.

du Bray, E.A., Stoeser, D.B., 1983. Geochemical evaluation of felsic plutonic rocks in the eastern and southeastern Arabian Shield, Kingdom of Saudi Arabia. Saudi Arabian Deputy Ministry for Mineral Resources, open file report USGS-OF-83-369, pp. 57.

Duzgoren-Aydin, N.S., Aydin, A., Malpas, J., 2002. Re-assessment of chemical weathering indices: case study on pyroclastic rocks of Hong Kong. Engineering Geology 63, 99–119.

Edgell, H.S., 1997. Aquifers of Saudi Arabia and their Geological Framework. The Arabian Journal for Science and Engineering 22(1C), 3–31.

El-Khayal, A.A., 1987. Silurian graptolites from the Qusayba Shale (Llandovery) of central Saudi Arabia. Bulletin of the Geological Society of Denmark 35, 125–133.

Etemad-Saeed, N., Hosseini-Barzi, M., Armstrong-Altrin, J.S., 2011. Petrography and geochemistry of clastic sedimentary rocks as evidences for provenance of the Lower Cambrian Lalun Formation, Posht-e-badam block, Central Iran. Journal of African Earth Sciences 61, 142–159.

Evans, D.S., Lathon, R.B., Senalp, M., Connally, T.C., 1991. Stratigraphy of the Wajid Sandstone of southwestern Saudi Arabia. Proceedings of the 7th Society of Petroleum Engineers Middle East Oil Show, Bahrain, 16-19th November, 1991, SPE Paper 21449, 947–960.

Fedo, C.M., Nesbitt, H.W., Young, G.M., 1995. Unraveling the effects of potassium metasomatism in sedimentary rocks and paleosols, with implications for paleoweathering conditions and provenance. Geology 23, 921–924.

Ferguson, G.S., Chambers, T.M., 1991. Subsurface stratigraphy, depositional history, and reservoir development of the Early-to-Late Permian Unayzah Formation in central Saudi Arabia. Proceedings of the 7th Society of Petroleum Engineers Middle East Oil Show, Bahrain, 16-19th November, 1991, SPE Paper 21394, 487–496.

Fleet, W.F., 1926. Petrological notes on the Old Red Sandstone of the West Midlands. Geological Magazine 63(11), 505–516.

Foley, S.F., Barth, M.G., Jenner, G.A., 2000. Rutile/melt partition coefficients for trace elements and an assessment of the influence of rutile on the trace element characteristics of subduction zone magmas. Geochimica et Cosmochimica Acta 64, 933–938.

Forey, P.L., Young, V.T., McClure, H.A., 1992. Lower Devonian fishes from Saudi Arabia. Bulletin of the British Museum, Natural History (Geology) 48, 25–43.

Friis, H., Poulsen, M.L.K., Svendsen, J.B., Hamberg, L., 2007. Discrimination of density flow deposits using elemental geochemistry – Implications for subtle provenance differentiation in a narrow submarine canyon, Palaeogene, Danish North Sea. Marine and Petroleum Geology 24, 221–235.

Fritz, H., Dallmeyer, D.R., Wallbrecher, E., Loizenbauer, J., Hoinkes, G., Neumayr, P., Khudeir, A.A., 2002. Neoproterozoic tectonothermal evolution of the Central Eastern Desert, Egypt: a slow velocity tectonic process of core complex exhumation. Journal of African Earth Sciences 34, 137–155.

Fritz, H., Abdelsalam, M., Ali, K.A., Bingen, B., Collins, A.S., Fowler, A.R., Ghebreab, W., Hauzenberger, C.A., Johnson, P.R., Kusky, T.M., Macey, P., Muhongo, S., Stern, R.J., Viola, G., 2013. Orogen styles in the East African Orogen: A review of the Neoproterozoic to Cambrian tectonic evolution. Journal of African Earth Sciences 86, 65–106.

Frost, B.R., Barnes, C.G., Collins, W.J., Arculus, R.J., Ellis, D.J., Frost, C.D., 2001. A Geochemical Classification for Granitic Rocks. Journal of Petrology 42(11), 2033–2048.

Garzanti, E., Andò, S., Vezzoli, G., 2008. Settling-equivalence of detrital minerals and grain-size dependence of sediment composition. Earth and Planetary Science Letters 273, 138–151.

Garzanti, E., Andò, S., Vezzoli, G., 2009. Grain-size dependence of sediment composition and environmental bias in provenance studies. Earth and Planetary Science Letters 277, 422–432.

Garzanti, E., Vermeesch, P., Andò, S., Vezzoli, G., Valagussa, M., Allen, K., Kadi, K.A., Al-Juboury, A.I.A., 2013. Provenance and recycling of Arabian desert sand. Earth-Science Reviews 120, 1–19.

Gazzi, P., 1966. Le Arenarie del Flysch Sopracretaceo dell'Appennino Modenese: Correlazioni con il Flysch di Monghidoro. Mineralogica e Petrografica Acta 12, 69–97.

Ghebreab, W., 1999. Tectono-metamorphic history of Neoproterozoic rocks in eastern Eritrea. Precambrian Research 98, 83–105.

Ghienne, J.F., 2003. Late Ordovician sedimentary environments, glacial cycles, and post-glacial transgression in the Taoudeni Basin, West Africa. Palaeogeography, Palaeoclimatology, Palaeoecology 189, 117–145.

Ghienne, J.F., Deynoux, M., 1998. Large-scale channel-fi ll structures in Late Ordovician glacial deposits in Mauritania, western Sahara. Sedimentary Geology 119, 141–159.

Ghienne, J.F., Deynoux, M., Manatschal, G., Rubino, J.L., 2003. Palaeovalleys and fault-controlled depocentres in the Late Ordovician glacial record of the Murzuq Basin (central Libya). Comptes Rendus Geosciences 335, 1091–1100.

Glasmann, J.R., 1992. The fate of feldspar in Brent Group reservoirs, North Sea: A regional synthesis of diagenesis in shallow, intermediate, and deep burial environments. Geological Society London Special Publications 61, 329–350.

Goldich, S.S., 1938. A study in rock weathering. Journal of Geology 46, 17–58.

Götze, J., Kempe, U., Habermann, D., Nasdala, L., Neuser, R.D., Richter, D.K., 1999. High-resolution cathodoluminescence combined with SHRIMP ion probe measurements of detrital zircons. Mineralogical Magazine 63(2), 179–187.

Grant, M.L., Wilde, S.A., Wu, F., Yang, J., 2009. The application of zircon cathodoluminescence imaging, Th-U-Pb chemistry and U–Pb ages in interpreting discrete magmatic an high-grade metamorphic events in the North China Craton at the Archean/Proterozoic boundary. Chemical Geology 261, 155–171.

Grew, E.S., Locock, A.J., Mills, S.J., Galuskina, I.O., Galuskin, E.V., Hålenius, U., 2013. Nomenclature of the garnet supergroup. American Mineralogist 98, 785–811.

Grimm, W.D., 1973. Stepweise heavy mineral weathering in the residual quartz gravel, Bavarian Molasse (Germany). Contributions to Sedimentology 1, 103–125.

GTZ/DCo, 2009. Detailed water resources studies of Wajid and overlying aquifers, Volume 10, Drilling Investigations. Unpublished report, Ministry of Water and Electricity, Riyadh.

Hadley, D.G., Schmidt, D.L., 1974. Nonglacial origin for conglomerate beds in the Wajid sandstone of Saudi Arabia. United States Geological Survey, open file report PR-174, pp. 27.

Hammer, Ø., Harper, D.A.T., Ryan, P.D., 2001. PAST: Paleontological statistics software package for education and data analysis. Palaeontologia Electronica 4(1), 1–9.

Hanchar, J.M., Miller, C.F., 1993. Zircon zonation patterns as revealed by cathodoluminescence and backscattered electron images: Implications for interpretation of complex crustal histories. Chemical Geology 110, 1–13.

Hanchar, J.M., Rudnick, R.L., 1995. Revealing hidden structures: The application of cathodoluminescence and back-scattered electron imaging to dating zircons from lower crustal xenoliths. Lithos 36, 289–303.

Harris, N.B.W., Pearce, J.A., Tindle, A.G., 1986. Geochemical characteristics of collision-zone magmatism. Geological Society London Special Publications 19, 67–81.

Hartmann, L.A., Leite, J.A.D., Silva, I.C., Remus, M.V.D., McNaughton, N.J., Groves, D.J., Fletcher, I.R., Santos, J.O.S., Vasconce-Ilos, M.A.Z., 2000. Advances in SHRIMP geochronology and their impact on understanding the tectonic and metallogenic evolution of southern Brazil. Australian Journal of Earth Sciences 47, 829–844.

Helal, A.H., 1964. On the occurrence of lower Paleozoic rocks in the Tabuk area, Saudi Arabia. Neues Jahrbuch für Geologie und Paläontologie, Monatshefte 7, 391–415. Cited in Al-Laboun (2011).
Hildred, G.V., Ratcliffe, K.T., Wright, A.M., Zaitlin, B.A., Wray, D.S., 2010. Chemostratigraphic applications to low-accomodation fluvial incised-valley settings: an example from the lower Mannville Formation of Alberta, Canada. Journal of Sedimentary Research 80, 1032–1045.

Hinderer, M., Keller, M., Al-Ajmi, H., Rausch, R., 2009. Tales of two Glaciations in the Paleozoic of SW Saudi Arabia: Implications for Ice Shield Dynamics and Paleogeography of the SW Arabain Platform and Adjacent Areas. Report, Abu Dhabi.

Hints, O., Paris, F., Al-Hajri, S., 2015. Late Ordovician scolecodonts from the Qusaiba-1 core hole, central Saudi Arabia, and their paleogeographical affinities. Review of Palaeobotany and Palynology 212, 85–96.

Hoppe, G., 1963. Die Verwendbarkeit morphologischer Erscheinungen an akzessorischen Zirkonen für petrogenetische Auswertungen. Abhandlungen der Deutschen Akademie der Wissenschaften Berlin 1, 1–131.

Hoskin, P.W.O., Schaltegger, U., 2003. The Composition of Zircon and Igneous and Metamorphic Petrogenesis. Reviews in Mineralogy and Geochemistry 53(1), 27–62.

Howes, D.R., 1982. Prospecting for gold in the Jabal Ayyanah area, Bi'r Juqjuq-North Tathlith District, Southern Najd-Eastern Asir. Saudi Arabian Deputy Ministry for Mineral Resources, open file report RF-OF-02-16, pp. 38. Cited in Thieme (1988).

Hubert, J.F., 1962. A zircon-tourmaline-rutile maturity index and the interdependence of the composition of heavy mineral assemblages with the gross composition and texture of sandstones. Journal of Sedimentary Research 32, 440–450.

Huntsman-Mapila, P., Tiercelin, J.-J., Benoit, M., Ringrose, S., Diskin, S., Cotton, J., Hémond, C., 2009. Sediment geochemistry and tectonic setting: Application of discrimination diagrams to early stages of intracontinental rift evolution, with examples from the Okavango and Southern Tanganyika rift basins. Journal of African Earth Sciences 53, 33–44.

Hussain, M., 2001. Framework mineralogy, diagenesis and provenance of the Wajid sandstone in Asir region, Southwestern Saudi Arabia. Report, KACST Project no. LPG 283, pp. 75.

Hussain, M., 2007. Elemental chemistry as a tool of stratigraphic correlation: A case study involving lower Paleozoic Wajid, Saq, and Qasim formations in Saudi Arabia. Marine and Petroleum Geology 24, 91–108.

Hussain, M., Abdullatif, O.M., 2004. Trace Element Geochemistry and Heavy Mineral Assemblage of the Cambro-Ordovician Saq Sandstone of the Tabuk Basin and its Possible Correlation with the Wajid Sandstone of the Wajid Basin, Southwest Saudi Arabia. Report, KACST Project LGP 6-54, pp. 108.

Hussain, M., Babalola, L.O., Hariri, M., 2000. Provenance of the Wajid Sandstone, Southeastern Margin of the Arabian Shield: Geochemical and Petrographic Approach. American Association of Petroleum Geologists National Conference, New Orleans, USA, April 16, 1999, Extended Abstracts with Programs, pp. 7.

Hussain, M., Babalola, L.O., Hariri, M.M., 2004. Heavy minerals in the Wajid Sandstone from Abha-Khamis Mushayt area, southwestern Saudi Arabia: implications on provenance and regional tectonic setting. GeoArabia 9(4), 77–102.

Hutchison, C.S., 1974. Laboratory Handbook of Petrographic Techniques. John Wiley & Sons, New York, pp. 527.

Hutchison, C.S., 1975. The norm, its variations, their calculation and relationships. Schweizer Mineralogische und Petrographische Mitteilungen 55, 243–256.

Jackson, N.J., Al Yazidi, S., 1985. Reconnaissance prospecting of felsic plutons in the Demar area (21/44C). Saudi Arabian Deputy Ministry for Mineral Resources, open file report DGMR-OF-05-25, pp. 35. Cited in Thieme (1988).

Jackson, N.J., Douch, C.J., 1986. Jabal Hamra REE-mineralized silexite, Hijaz region, Kingdom of Saudi Arabia. Journal of African Earth Sciences 4, 269–274.

Jackson, N.J., Walsh, J.N., Pegram, E., 1984. Geology, geochemistry and petrogenesis of late Precambrian granitoids in the Central Hijaz Region of the Arabian Shield. Contributions to Mineralogy and Petrology 87, 205–219.

Janjou, D., Halawani, M.A., Al-Muallem, M.S., Robelin, C., Brosse, J.-M., Courbouleix, S., Dagain, J., Genna, A., Razin, P., Roobol, M.J., Shorbaji, H., Wyns, R., 1996. Geologic map of the Al Qalibah quadrangle, Sheet 28C, Kingdom of Saudi Arabia (with text). Saudi Arabian Deputy Ministry for Mineral Resources Geoscience Map GM-135, 1:250,000. Cited in Al-Laboun (2009).

Janoušek, V., Farrow, C.M., Erban, V., 2006. Interpretation of whole-rock geochemical data in igneous geochemistry: introducing Geochemical Data Toolkit (GCDkit). Journal of Petrology 47(6), 1255–1259.

Johnson, P.R., 2014. An expanding Arabian-Nubian Shield geochronologic and isotopic dataset: Defining limits and confirming the tectonic setting of a Neoproterozoic accretionary orogen. The Open Geology Journal 8, 3–33.

Johnson, P.R., Woldehaimanot, B., 2003, Development of the Arabian-Nubian Shield: perspectives on accretion and deformation in the northern East African Orogen and the assembly of Gondwana. In: Yoshida, M., Windley, B.F., Dasgupta, S. (Eds.), Proterozoic East Gondwana: Supercontinent Assembly and Breakup. Geological Society, London, Special Publication 206, 289–325.

Johnson, P.R., Kattan, F.H., 2008. Lithostratigraphic revision in the Arabian Shield: the impact of geochronology and tectonic analysis. The Arabian Journal for Science and Engineering 33(1C), 3–16.

Johnson, P.R., Kattan, F.H., 2012. The Geology of the Saudi Arabian Shield. Saudi Geological Survey, Jiddah, pp. 479.

Johnson, P.R., Kattan, F.H., Al-Saleh, A.M., 2004. Neoproterozoic ophiolites in the Arabian Shield: Field relations and structure. Developments in Precambrian Geology 13, 129–162.

Johnson, P.R., Andresen, A., Collins, A.S., Fowler, A.R., Fritz, H., Ghebreab, W., Kusky, T., Stern, R.J., 2011. Late Cryogenian-Ediacaran history of the Arabian-Nubian Shield: A review of depositional, plutonic, structural, and tectonic events in the closing stages of the northern East African Orogen. Journal of Petrology 61, 167–232.

Johnson, P.R., Halverson, G.P., Kusky, T.M., Stern, R.J., Pease, V., 2013. Volcanosedimentary Basins in the Arabian-Nubian Shield: Markers of Repeated Exhumation and Denudation in a Neoproterozoic Accretionary Orogen. Geosciences 3, 389–445.

Johnsson, M.J., 1993. The system controlling the composition of clastic sediments. In: Johnsson, M.J., Basu, A. (Eds.), Processes Controlling the Composition of Clastic Sediments, Geological Society of America Special Papers 284, 1–20.

Keller, M., Hinderer, M., Al-Ajmi, H.F., Rausch, R., 2011. Palaeozoic glacial depositional environments of SW Saudi Arabia: Process and product. In: Martini, I.P., French, H.M., Pérez Alberti, A. (Eds.), Icemarginal and periglacial processes and sediments. Geological Society London Special Publications 354, 129–152.

Kellmann, S., 2014. Schwermineraluntersuchungen zur Eingrenzung potentieller Grundwasserradioaktivitätsquellen in Sandsteinaquiferen. Master thesis, Technische Universität Darmstadt, Darmstadt, pp. 65.

Kellogg, K.S., Beckmann, G.E.J., 1982. Paleomagnetic investigations of upper Proterozoic rocks in the Eastern Arabian Shield, Kingdom of Saudi Arabia. Saudi Arabian Deputy Ministry for Mineral Resources, open file report USGS-OF-02-63, pp. 33. Cited in Thieme (1988).

Kellogg, K.S., Janjou, D., Minoux, L., Fourniguet, J., 1986. Explanatory notes to the geologic map of the Wadi Tathlith Quadrangle, Kingdom of Saudi Arabia. Geoscience Map GM-103C, scale 1:250,000, sheet 20G. Deputy Ministry for Mineral Resources, Ministry of Petroleum and Mineral Resources, Kingdom of Saudi Arabia, pp. 27. Cited in Al-Ajmi et al. (2015).

Khalifa, M.A., 2015. Glacial and post-glacial deposits of the Unayzah Formation (Carboniferous-Permian), Saudi Arabia: facies analysis and sequence stratigraphy. Carbonates and Evaporites 30, 207–227.

Klein, G.DeV., 1963. Analysis and review of sandstone classifications in the North American geological literature, 1940–1960. Geological Society of America Bulletin 74(5), 555–576.

Knox, R.W.O'B., Franks, S.G., Cocker, J.D., 2007. Stratigraphic evolution of heavy-mineral provenance signatures in the sandstones of the Wajid Group (Cambrian to Permian), southwestern Saudi Arabia. GeoArabia 12(4), 65–96.

Knox, R.W.O'B., Cocker, J.D., Filatoff, J., 2010. Heavy mineral stratigraphy of the Unayzah Formation and Basal Khuff Clastics (Carboniferous to Permian) of Central Saudi Arabia. GeoArabia 15(3), 17–80.

Kolodner, K., Avigad, D., McWilliams, M., Wooden, J.L., Weissbrod, T., Feinstein, S., 2006. Provenance of north Gondwana Cambrian–Ordovician sandstone: U–Pb SHRIMP dating of detrital zircons from Israel and Jordan. Geological Magazine 143, 367–391.

Konert, G., Al-Afifi, A.M., Al-Hajri, S.A., Droste, H.J., 2001. Paleozoic stratigraphy and hydrocarbon habitat of the Arabian Plate. GeoArabia 6(3), 407–442.

Krippner, A., Meinhold, G., Morton, A.C., von Eynatten, H., 2014. Evaluation of garnet discrimination diagrams using geochemical data of garnets derived from various host rocks. Sedimentary Geology 306, 36–52.

Krippner, A., Meinhold, G., Morton, A.C., Russell, E., von Eynatten, H., 2015. Grain-size dependence of garnet composition revealed by provenance signatures of modern stream sediments from the western Hohe Tauern (Austria). Sedimentary Geology, 321, 25–38.

Kröner, A., Roobol, M.J., Ramsay, C.R., Jackson, N.J., 1979. Pan African ages of some gneissic rocks in the Saudi Arabian Shield. Journal of the Geological Society of London 136, 455–461.

Kröner, A., Linnebacher, P., Stern, R.J., Reischmann, T., Manton, W., Hussein, I.M., 1991. Evolution of Pan-African island arc assemblages in the southern Red Sea Hills, Sudan, and in southwestern Arabia as exemplified by geochemistry and geochronology. Precambrian Research 52, 99–118.

Krynine, P.D., 1941. Paleogeographic and tectonic significance of arkoses. Geological Society of America Bulletin 52, 1918–1919.

Laboun, A.A., 2013. Regional tectonic and megadepositional cycles of the Paleozoic of northwestern and central Saudi Arabia. Arabian Journal of Geosciences 6, 971–984.

Le Hérissé, A., Al-Ruwaili, M., Miller, M., Vecoli, M., 2007. Environmental changes reflected by palynomorphs in the early Middle Ordovician Hanadir Member of the Qasim Formation, Saudi Arabia. In: Paris F, Owens B, Miller MA (eds) Palaeozoic Palynology of the Arabian Plate and Adjacent Areas. Revue de micropaléontologie 50(1), 3–16.

Le Hérissé, A., Molyneux, S.G., Miller, M.A., 2015. Late Ordovician to early Silurian acritarchs from the Qusaiba-1 shallow core hole, central Saudi Arabia. Review of Palaeobotany and Palynology 212, 22–59.

Le Heron, D.P., Sutcliffe, O., Bourgig, K., Craig, J., Visentin, C., Whittington, R., 2004. Sedimentary architecture of Upper Ordovician tunnel valleys, Gargaf Arch, Libya: Implications for the genesis of a hydrocarbon reservoir. GeoArabia 9(2), 137–160.

Le Heron, D.P., Sutcliffe, O.E., Whittington, R.J., Craig, J., 2005. The origins of glacially related softsediment deformation structures in Upper Ordovician glaciogenic rocks: Implication for ice sheet dynamics. Palaeogeography, Palaeoclimatology, Palaeoecology 218, 75–103.

Le Heron, D.P., Craig, J., Etienne, J.P., 2009. Ancient glaciations and hydrocarbon accumulations in North Africa and the Middle East. Earth-Science Reviews 93, 47–76.

Le Heron, D.P., Armstrong, H.A., Wilson, C., Howard, J.P., Gindre, L., 2010. Glaciation and deglaciation of the Libyan Desert: The Late Ordovician record. Sedimentary Geology 223, 100–125.

Le Heron, D.P., Meinhold, G., Bergig, K., 2013. Neoproterozoic–Devonian stratigraphic evolution of the eastern Murzuq Basin, Libya: a tale of tilting in the central Sahara. Basin Research 25, 52–73.

Le Heron, D.P., Meinhold, G., Elgadry, M., Abutarruma, Y., Boote, D., 2015. Early Palaeozoic evolution of Libya: perspectives from Jabal Eghei with implications for hydrocarbon exploration in Al Kufrah Basin. Basin Research 27, 60–83.

Lemcke, K., von Engelhardt, W., Füchtbauer, H., 1953. Geologische und sedimentpetrographische Untersuchungen im Westteil der ungefalteten Molasse des süddeutschen Alpenvorlandes. Beiheft des Geologischen Jahrbuchs 11, 1–128.

Leo, G.W., 1986. Geochemical Reconnaissance of Late Proterozoic Volcanic and Mafic Plutonic Rocks of the Al 'Awshaziyah Quadrangle and Related Rocks in the Qufar Quadrangle, Northern Arabian Shield. United States Geological Survey Bulletin 1680, pp. 16.

Linnemann, U., Ouzegane, K., Drareni, A., Hofmann, M., Becker, S., Gärtner, A., Sagawe, A., 2011. Sands of West Gondwana: An archive of secular magmatism and plate interactions—A case study from the Cambro-Ordovician section of the Tassili Ouan Ahaggar (Algerian Sahara) using U–Pb–LA-ICP-MS detrital zircon ages. Lithos 123, 188–203.

Ludwig, R., 1874. Geologische Bilder aus Italien. Bulletin de la Société Impériale des Naturalistes de Moscou 48, 42–131.

Luvizotto, G.L., Zack, T., Meyer, H.P., Ludwig, T., Triebold, S., Kronz, A., Münker, C., Stockli, D.F., Prowatke, S., Klemme, S., Jacob, D.E., von Eynatten, H., 2009. Rutile crystals as potential trace element and isotope mineral standards for microanalysis. Chemical Geology 261 (3-4), 346–369.
Lüning, S., Craig, J., Loydell, D.K., Štorch, P., Fitches, B., 2000. Lower Silurian 'hot shales' in North Africa and Arabia: regional distribution and depositional model. Earth-Science Reviews 49, 121–200.

Mahmoud, M.D., Vaslet, D., Husseini, M.I., 1992. The lower Silurian Qalibah Formation of Saudi Arabia: an important hydrocarbon source rock. American Association of Petroleum Geologists Bulletin 76(10), 1491–1506.

Mange, M.A., Maurer, H.F.W., 1992. Heavy minerals in Colour. Chapman and Hall, London, pp. 147.

Mange, M.A. Morton, A.C., 2007. Geochemistry of heavy minerals. In: Mange, M.A., Wright, D.T. (Eds.), Heavy Minerals in Use. Developments in Sedimentology 58. Elsevier, Amsterdam, 345–391.

Mange, M.A., Wright, D.T., 2007. Heavy Minerals in Use. Developments in Sedimentology 58, Elsevier, Amsterdam, pp. 1328.

Marshall, D., 1988. Cathodoluminescence of Geologic Materials. Unwin Hyman, Boston, pp. 146.

McBride, E.F., 1963. A classification of common sandstones. Journal of Sedimentary Petrology 33(3), 664–669.

McClure, H.A., 1978. Early Paleozoic glaciation in Arabia. Palaeogeography, Palaeoclimatology, Palaeoecology 25, 315–326.

McClure, H.A., 1980. Permian-Carboniferous Glaciation in the Arabian Peninsula. Geological Society of America Bulletin 91(1), 707–712.

McDonough, W.F., Sun, S.S., 1995. The composition of the Earth. Chemical Geology 120, 223–253.

McGillivray, J.G., Husseini, M.I., 1992. The Paleozoic petroleum geology of Central Arabia. Bulletin of the American Association of Petroleum Geologists 76(10), 1473–1490.

McLennan, S.M., 1989. Rare earth elements in sedimentary rocks: influence of provenance and sedimentary processes. In: Lipin, B.R., McKay, G.A. (Eds.), Geochemistry and Mineralogy of Rare Earth Elements. Reviews in Mineralogy 21, 169–200.

McLennan, S.M., 2001. Relationships between the trace element composition of sedimentary rocks and upper continental crust. Geochemistry, Geophysics, Geosystems 2(4). doi:10.1029/2000GC000109

McLennan, S.M., Hemming, S., McDaniel, D.K., Hanson, G.N., 1993. Geochemical approaches to sedimentation, provenance and tectonics. In: Johnsson, M.J., Basu, A. (Eds.), Processes Controlling the Composition of Clastic Sediments, Geological Society of America Special Papers 285, 21–40.

Meert, J.G., 2003. A synopsis of events related to the assembly of eastern Gondwana. Tectonophysics 362(1), 1–40.

Meert, J.G., van der Voo, R., 1997. The assembly of Gondwana 800-550 Ma. Journal of Geodynamics 23(3), 223–235.

Meinhold, G., 2010. Rutile and its applications in earth sciences. Earth-Science Reviews 102, 1–28.

Meinhold, G., Kostopoulos, D., Reischmann, T., 2007. Geochemical constraints on the provenance and depositional setting of sedimentary rocks from the islands of Chios, Inousses and Psara, Aegean Sea, Greece: implications for the evolution of Palaeotethys. Journal of the Geological Society 164, 1145–1163.

Meinhold, G., Anders, B., Kostopoulos, D., Reischmann, T., 2008. Rutile chemistry and thermometry as provenance indicator: An example from Chios Island, Greece. Sedimentary Geology 203, 98–111.

Meinhold, G., Morton, A.C., Fanning, C.M., Frei, D., Howard, J.P., Phillips, R.J., Strogen, D., Whitham, A.G., 2011. Evidence from detrital zircons for recycling of Mesoproterozoic and Neoproterozoic crust recorded in Paleozoic and Mesozoic sandstones of southern Libya. Earth and Planetary Science Letters 312, 164–175.

Meinhold, G., Howard, J.P., Strogen, D., Kaye, M.D., Abutarruma, Y., Elgadry, M., Thusu, B., Whitham, A.G., 2013a. Hydrocarbon source rock potential and elemental composition of lower Silurian subsurface shales of the eastern Murzuq Basin, southern Libya. Marine and Petroleum Geology 48, 224–246.

Meinhold, G., Morton, A.C., Avigad, D., 2013b. New insights into peri-Gondwana paleogeography and the Gondwana super-fan system from detrital zircon U–Pb ages. Gondwana Research 23(2), 661–665.

Meissner, C.R. Jr., Mytton, J.W., Riddler, G.P., van Eck, M., Aspinall, N.C., Farasini, A.M., Dini, S.M., 1989. Preliminary Geological Map of the Al Jawf Quadrangle, sheet 39D, Kingdom of Saudi Arabia. United States Geological Survey, Open-File Report 89-342, pp. 42.

Melvin, J., 2015. Lithostratigraphy and depositional history of Upper Ordovician and lowermost Silurian sediments recovered from the Qusaiba-1 shallow core hole, Qasim region, central Saudi Arabia. Review of Palaeobotany and Palynology 212, 3–21.

Melvin, J., Norton, A.K., 2013. Advances in Arabian stratigraphy: Comparative studies of glaciogenic Juwayl and lower Unayzah strata (Carboniferous–Permian) of Saudi Arabia. GeoArabia 18(1), 97–134.

Melvin, J., Sprague, R.A., Heine, C.J., 2010. From bergs to ergs: The late Paleozoic Gondwanan glaciation and its aftermath in Saudi Arabia. In: Lopez-Gamundi, O.R., Buatois, L.A. (Eds.), Late Paleozoic Glacial Events and Postglacial Transgressions in Gondwana. Geological Society of America Special Paper 468, 37–80.

Meunier, S., 1877. Composition et origine du sable diamantifere de Du Toit's Pan (Afrique australe). Comptes Rendus de l'Académie des Sciences 84, 250–252.

Michel Lévy, A., 1878. Note sur quelques minéraux contenus dans les sables du Mesvrin, pres Autun. Bulletin, Société Minéralogique de France 1, 39–41.

Middlemost, E.A.K., 1994. Naming materials in the magma/igneous rock system. Earth-Science Reviews 37, 215–224.

Mongelli, G., Critelli, S., Perri, F., Sonnino, M., Perrone, V., 2006. Sedimentary recycling, provenance and paleoweathering from chemistry and mineralogy of Mesozoic continental redbed mudrocks, Peloritani mountains, southern Italy. Geochemical Journal 40, 197–209.

Morag, N., Avigad, D., Gerdes, A., Belousova, E., Harlavan, Y., 2011. Detrital zircon Hf isotopic composition indicates long-distance transport of North Gondwana Cambrian–Ordovician sandstones. Geology 39 (10), 955–958.

Morton, A.C., 1985. Heavy minerals in provenance studies. In: Zuffa, G.G. (Ed.), Provenance of Arenites. Riedel, Dortrecht, pp. 249–277.

Morton, A.C., 1987. Influences of provenance and diagenesis on detrital garnet suites in the Forties sandstone, Paleocene, central North Sea. Journal of Sedimentary Petrology 57, 1027–1032.

Morton, A.C., Hallsworth, C.R., 1994. Identifying provenance-specific features of detrital heavy mineral assemblages in sandstones. Sedimentary Geology 90, 241–256.

Morton, A.C. Hallsworth, C.R., 1999. Processes controlling the composition of heavy mineral assemblages in sandstones. Sedimentary Geology 124, 3–29.

Morton, A.C., Hallsworth, C., 2007. Stability of Detrital Heavy Minerals During Burial Diagenesis. In: Mange, M.A., Wright, D.T. (Eds.), Heavy Minerals in Use. Developments in Sedimentology 58, Elsevier, Amsterdam, 215–245.

Morton, A.C., Chenery, S., 2009. Detrital Rutile Geochemistry and Thermometry as Guides to Provenance of Jurassic–Paleocene Sandstones of the Norwegian Sea. Journal of Sedimentary Research 79, 540–553.

Morton, A.C., Davies, J.R., Waters, R.A., 1992. Heavy minerals as a guide to turbidite provenance in the Lower Paleozoic southern Welsh basin: a pilot study. Geological Magazine 129 (5), 573–580.

Morton, A., Hallsworth, C., Chalton, B., 2004. Garnet compositions in Scottish and Norwegian basement terrains: a framework for interpretation of North Sea sandstone provenance. Marine and Petroleum Geology 21, 393–410.

Morton, A.C., Meinhold, G., Howard, J.P., Phillips, R.J., Strogen, D., Abutarruma, Y., Elgadry, M., Thusu, B., Whitham, A.G., 2011. A heavy mineral study of sandstones from the eastern Murzuq Basin, Libya: Constraints on provenance and stratigraphic correlation. Journal of African Earth Sciences 61, 308–330.

Murali, A.V., Parthasarathy, R., Mahadevan, T.M., Das, M.S., 1983 Trace element characteristics, REE patterns and partition coefficients of zircons from different geological environments – A case study on Indian zircons. Geochimica et Cosmochimica Acta 47, 2047–2052.

Nehlig, P., Genna, A., Asfirane, F., 2002. A review of the Pan-African evolution of the Arabian Shield. GeoArabia 7(1), 103–124.

Nesbitt, H.W., Young, G.M., 1982. Early Proterozoic climates and plate motions inferred from major element chemistry of lutites. Nature 299, 715–717.

Nesbitt, H.W., Young, G.M., 1984. Prediction of some weathering trends of plutonic and volcanic rocks based on thermodynamic and kinetic considerations. Geochimica et Cosmochimica Acta 48, 1523–1534.

Nesbitt, H.W., Young, G.M., 1996. Petrogenesis of sediments in the absence of chemical weathering: effects of abrasion and sorting on bulk composition and mineralogy. Sedimentology 43, 341–458.

Nesbitt, H.W., Young, G.M., McLennan, S.M., Keays, R.R., 1996. Effects of Chemical Weathering and Sorting on the Petrogenesis of Siliciclastic Sediments, with Implications for Provenance Studies. The Journal of Geology 104(5), 525–542.

Okada, H., 1971. Classification of sandstone: analysis and proposal. The Journal of Geology 79(5), 509-525.

Paris, F., Miller, A.M., Al-Hajri, S., Zalasiewicz, J., 2015a. Early Silurian chitinozoans from the Qusaiba type area, North Central Saudi Arabia. Review of Palaeobotany and Palynology 212, 127–186.
Paris, F., Verniers, J., Miller, A.M., Al-Hajri, S., Melvin, J., Wellman, C.H., 2015b. Late Ordovician-earliest Silurian chitinozoans from the Qusaiba-1 core hole (North Central Saudi Arabia) and their relations to the Hirnantian glaciation. Review of Palaeobotany and Palynology 212, 60–84.

Pearce, J.A., Harris, N.B.W., Tindle, A.G., 1984. Trace Element Discrimination Diagrams for the Tectonic Interpretation of Granitic Rocks. Journal of Petrology 25(4), 956–983.

Pearce, T.J., Besly, B.M., Wray, D.S., Wright, D.K., 1999. Chemostratigraphy: a method to improve interwell correlation in barren sequences – a case study using onshore Duckmantian/Stephanian sequences (West Midlands, U.K.). Sedimentary Geology 124, 197–220.

Pettijohn, F.J., 1941. Persistence of heavy minerals and geologic age. Journal of Geology 49, 610–625.

Pettijohn, F.J., 1954. Classification of sandstones. Jouernal of Geology 62, 360–365.

Piller, H., 1951. Über den Schwermineralgehalt von anstehendem und verwittertem Brockengranit nördlich St. Andreasberg. Heidelberger Beiträge zur Mineralogie und Petrographie 2, 523–537.

Poldervaart, A., 1955. Zircons in rocks 1: Sedimentary rocks. American Journal of Science 253, 433–461.

Poldervaart, A., 1956. Zircons in rocks 2: Igneous rocks. American Journal of Science 254, 521–554.

Pollastro, R.M., 2003. Total petroleum systems of the Paleozoic and Jurassic, greater Ghawar uplift and adjoining provinces of Central Saudi Arabia and Northern Arabian-Persian Gulf. U.S. Geological Survey Bulletin, 2202-H, pp. 100.

Pollastro, R.M., Karshbaum, A.S., Viger, R.J., 1998. Maps showing geology, oil and gas fields and geologic provinces of the Arabian Peninsula. United States Geological Survey, Open-File Report 97-470B, pp. 14.

Poller, U., Huth, J., Hoppe, P., Williams, I.S., 2001. REE, U, Th, and Hf distribution in zircon from western Carpathian Variscan granitoids: a combined cathodoluminescence and ion microprobe study. American Journal of Science 301, 858–876.

Powell, J.H., Mohammed, B.K., Masri, A., 1994. Late Ordovician-Early Silurian glaciofluvial deposits preserved in palaeovalleys in south Jordan. Sedimentary Geology 89, 303–314.

Powers, R.W., 1968. Lexique stratigraphique international. Volume III, Asie, Fas. 10 b1, Arabia Saoudite. Centre National de la Recherche Scientifique, Paris, pp. 117.

Powers, R.W., Ramirez, L.F., Redmond, C.D., Elberg, E.L. Jr., 1966. Geology of the Arabian Peninsula: Sedimentary geology of Saudi Arabia. United States Geological Survey Professional Paper 560-D, pp. 147.

Pupin, J.P., 1980. Zircon and Granite Petrology. Contributions to Mineralogy and Petrology 73, 207–220.

Quennell, A.M., 1951. The geology and mineral resources of (former) Trans-Jordan. Colonial Geology and Mineral Resources 2(2), 85–115.

Ramsay, C.R., 1982. Dahul granite belt: exploration targets related to post-tectonic plutons. Saudi Arabian Deputy Ministry for Mineral Resources, open file report DGMR-OF-02-28, pp. 45. Cited in Thieme (1988).
Ramsay, C.R., Drysdall, A.R., Clark, M.D., 1986. Felsic plutonic rocks of the Midyan region, Kingdom of Saudi Arabia – I. Distribution, classification and resource potential. Journal of African Earth Sciences 4, 63–77.

Richter, D.K., Götte, Th., Götze, J., Neuser, R.D., 2003. Progress in application of cathodoluminescence (CL) in sedimentary petrology. Mineralogy and Petrology 79, 127–166.

Roser, B.P., Korsch, R.J., 1986. Determination of tectonic setting of sandstone-mudstone suites using SiO_2 content and K_2O/Na_2O ratio. The Journal of Geology 94(5), 635–650.

Roser, B.P., Korsch, R.J., 1988. Provenance signatures of sandstone-mudstone suites determined using discriminant function analysis of major-element data. Chemical Geololgy 67, 119–139.

Rubey, W.W., 1933. The size-distribution of heavy minerals within a water-laid sandstone. Journal of Sedimentary Research 3(1), 3–29

Rudnick, R.L., Gao, S., 2003. Composition of the Continental Crust. In: Rudnick R, Holland HD, Turekian KK (eds) Treatise on Geochemistry 3, 1–64.

Retgers, J.W., 1895. Über die mineralogische und chemische Zusammensetzung der Dünensande Hollands und über die Wichtigkeit von Fluss-und Meeressanduntersuchungen im allgemeinen. Neues Jahrbuch für Mineralogie, Geologie und Paläontologie 1, 16–74.

Sabaou, N., Ait-Salem, H., Zazoun, R.S., 2009. Chemostratigraphy, tectonic setting and provenance of the Cambro-Ordovician clastic deposits of the subsurface Algerian Sahara. Journal of African Earth Sciences 55, 158–174.

Salman, A.S., Zaidi, F.K., Hussein, M.T., 2014. Evaluation of groundwater quality in northern Saudi Arabia using multivariate analysis and stochastic statistics. Environmental Earth Sciences. doi:10.1007/s12665-014-3803-7, pp. 69.

Schermaier, A., Haunschmid, B., Schubert, G., Frasl, G., 1992. Diskriminierung von S-Typ und I-Typ Graniten auf der Basis zirkontypologischer Untersuchungen. Frankfurter Geowissenschaftliche Arbeiten Serie A, 149–153.

Schubert, M., Schüth, C., Michelsen, N., Rausch, R., Al-Saud, M., 2011. Investigation and Treatment of Natural Radioactivity in Large-Scale Sandstone Aquifer Systems. International Journal of Water Resources and Arid Environments 1(1), 25–32.

Schwab, F.L., 1978. Modern and Ancient Sedimentary Utah. Sedimentology 25, 97–109.

Selley, R.C., 1972. Diagnosis of marine and non-marine environments from the Cambro-Ordovician sandstones of Jordan. Journal of the Geological Society, London 128, 135–150.

Senalp, M., Al-Duaiji, A., 1995. Stratigraphy and sedimentation of the Unayzah reservoir, central Saudi Arabia. In: Al-Husseini, M.I. (Ed.), Middle East Petroleum Geosciences Conference, GEO'94, Gulf PetroLink, Bahrain, 837–847.

Senalp. M., Al-Laboun, A.A., 2000. New evidence on the Late Ordovician glaciation in central Saudi Arabia. Saudi Aramco Journal of Technology, Spring 2000, 11–40.

SGS, 2013. Phanerozoic Stratigraphy of Saudi Arabia Part 1 – Paleozoic Successions of the Arabian Shelf (Cover Rocks). Saudi Stratigraphic Committee Special Publication SGS-SP-2012-1.

Sharland, P.R., Archer, R., Casey, D.M., Davies, R.B., Hall, S.H., Heward, A.P., Horbury, A.D., Simmons, M.D., 2001. Arabian Plate sequence stratigraphy. GeoArabia Special Publication 2, Gulf PetroLink, Bahrain, pp. 371.

Sharland, P.R., Casey, D.M., Davies, R.B., Simmons, M.D., Sutcliffe, O.E., 2004. Arabian Plate Sequence Stratigraphy. GeoArabia 9(1), 199–214.

Solomon, J.D., 1932. On the Heavy Mineral Assemblages of the Great Chalky Boulder-Clay and Cannon-shot Gravels of East Anglia, and their significance. Geological Magazine 69(07), 314–320.

Squire, R.J., Campbell, I.H., Allen, Ch.M., Wilson, J.L., 2006. Did the Transgondwanan supermountain trigger the explosive radiation of animals on Earth? Earth and Planetary Science Letters 250, 116–133.

Stacey, J.S., Hedge, C.E., 1984. Geochronologic and isotopic evidence for early Proterozoic crust in the eastern Arabian Shield. Geology, 12(5), 310–313.

Stacey, J.S., Agar, R.A., 1985. U–Pb isotopic evidence for the accretion of a continental microplate in the Zalm region of the Saudi Arabian Shield. Journal of the Geological Society 142(6), 1189–1203.

Stacey, J.S., Doe, B.R., Roberts, R.J., Delevaux, M.H., Gramlich, J.W., 1980. A Lead Isotope Study of Mineralization in the Saudi Arabian Shield. Contributions to Mineralogy and Petrology 74, 175–188.

Steemans, P., Wellman, C.H., Filatoff, J., 2007. Palaeophytogeographical and palaeoecological implications of a miospore assemblage of earliest Devonian (Lochkovian) age from Saudi Arabia. Palaeogeography, Palaeoclimatology, Palaeoecology 250, 237–254.

Steineke, M.R.A., Bramkamp, R.A., Sander, N.J., 1958. Stratigraphic relations of Arabian Jurassic oil. In: Weeks, L.G. (Ed.), Habitat of Oil. American Association of Petroleum Geologists Symposium, Tulsa, OK, pp. 1294–1329.

Stephenson, M.H., 2004. Early Permian Spores from Oman and Saudi Arabia. GeoArabia Special Publication 3, 185–215.

Stern, R.J., Dawoud, A.S., 1991. Late Precambrian (740 Ma) Charnockite, Enderbite, and Granite from Jebel Moya, Sudan: A Link between the Mozambique Belt and the Arabian-Nubian-Shield?. The Journal of Geology 99 (5), 649–659.

Stern, R.J., Johnson, P., 2010. Continental lithosphere of the Arabian Plate: a geologic, petrologic, and geophysical synthesis. Earth-Science Reviews 101(1), 29–67.

Stern, R.J., Ali, K.A., Liégeois, J.P., Johnson, P.R., Kozdroj, W., Kattan, F.H., 2010. Distribution and significance of pre-Neoproterozoic zircons in juvenile Neoproterozoic igneous rocks of the Arabian-Nubian Shield. American Journal of Science 310, 791–811.

Stoeser, D.B., Camp, V., 1985. Pan-African microplate accretion of the Arabian Shield. Geological Society of America Bulletin 96(7), 817–826.

Stoeser, D.B., Frost, C.D., 2006. Nd, Pb, Sr, and O isotopic characterization of Saudi Arabian Shield Terranes. Chemical Geology 226, 163–188.

Stoeser, D.B., Stacey, J.S., 1988. Evolution, U–Pb geochronology, and isotope geology of the Pan African Nabitah orogenic belt of the Saudi Arabian Shield. In: El Gaby, S., Greiling, R.O. (Eds), The Pan African belt of Northeast African and Adjacent Areas. Friedrich, Viewig and Sohn, Braunschweig/ Wiesbaden, 227–288.

Stoeser, D.B., Whitehouse, M.J., Stacey, J.S., 2001. The Khida Terrane – Geology of Paleoproterozoic Rocks in the Mhuayil Area, Eastern Arabian Shield, Saudi Arabia. Gondwana Research 4(2), 192–194.

Streckeisen, A.L., 1974. Classification and Nomenclature of Plutonic Rocks. Recommendations of the IUGS Subcommission on the Systematics of Igneous Rocks. Geologische Rundschau 63(2), 773–785.

Strother, P.K., Traverse, A., Vecoli, M., 2015. Cryptospores from the Hanadir Shale Member of the Qasim Formation, Ordovician (Darriwilian) of Saudi Arabia: taxonomy and systematics. Review of Palaeobotany and Palynology 212, 97–110.

Stuckless, J.S., Futa, K., 1987. Rb Sr isotopic studies of postorogenic granites from the eastern Arabian Shield, Kingdom of Saudi Arabia. Saudi Arabian Deputy Ministry for Mineral Resources, open file report USGS-OF-07-8, pp. 26.

Stuckless, J.S., Van Trump, G. Jr., Moore, W.J., Bartel, A.J., Vaughn, R.B., Bush, C.A., 1985. Geochemistry and preliminary assessment of resource potential for postorogenic granites of the east-central Arabian Shield, Kingdom of Saudi Arabia. United States Geological Survey, Open-File Report USGS-OF-05-26, pp. 59.

Stuckless, J.S., Vaughn, R.B., Van Trump, G. Jr., 1986. Trace-element contents of postorogenic granites of the eastern Arabian Shield, Kingdom of Saudi Arabia. United States Geological Survey, Open-File Report USGS-OF-06-2, pp. 49.

Stump, T.E., Al-Hajri, S., van der Eem, J.G., 1995. Geology and biostratigraphy of the Late Precambrian through Paleozoic sediments of Saudi Arabia. Review of Palaeobotany and Palynology 89, 5–17.

Stump, T.E., van der Eem, J.G., 1995. The stratigraphy, depositional environments and periods of deformation of the Wajid outcrop belt, southwestern Saudi Arabia. Journal of African Earth Sciences 21(3), 421–441.

Sutcliffe, O.E., Dowdeswell, J.A., Whittington, R.J., Theron, J.N., Craig, J., 2000. Calibrating the Late Ordovician glaciation and mass extinction by the eccentricity cycles of Earth's orbit. Geology 28(11), 967–970.

Suttner, L.J., Basu, A., Mack, G.H., 1981. Climate and the Origin of Quartz Arenites. Journal of Sedimentary Petrology 54(4), 1235–1246.

Taylor, S.R., McLennan, S.M., 1985. The continental crust: its composition and evolution. Blackwell, Oxford, pp. 312.

Taylor, S.R., McLennan, S.M., 2009. Planetary Crusts: Their Composition, Origin and Evolution. Cambridge University Press, Cambridge, pp. 378.

Thieme, J.G., 1988. Geologic map of the Jabal Khida quadrangle, sheet 21G, Kingdom of Saudi Arabia. Saudi Arabian Directorate General of Mineral Resources Geoscience Map GM-90C, pp. 35.

Thralls, H.W., Hasson, R.C., 1956. Geology and oil resources of eastern Saudi Arabia. 20th International Geology Congress, Mexico and Symposium sobre Yacimentos de Petroleum and Gas 2, 9–32. Cited in Al-Laboun (2011).

Thürach, H., 1884. Über das Vorkommen mikroskopischer Zirkone und Titan-Mineralien in den Gesteinen. Verhandlungen der Physikalischen-Medizinischen Gesellschaft zu Würzburg 18, 203–284.

Tomkins, H.S., Powell, R., Ellis, D.J., 2007. The pressure dependence of the zirconium-in-rutile thermometer. Journal of Metamorphic Geology 25, 703–713.

Triebold, S., von Eynatten, H., Luvizotto, G.L., Zack, T., 2007. Deducing source rock lithology from detrital rutile geochemistry: an example from the Erzgebirge, Germany. Chemical Geology 244, 421–436.

Triebold, S., von Eynatten, H., Zack, T., 2012. A recipe for the use of rutile in sedimentary provenance analysis. Sedimentary Geology 282, 268–275.

Turner, B.R., Makhlouf, I.M., Armstrong, H.A., 2005. Late Ordovician (Ashgillian) glacial deposits in southern Jordan. Sedimentary Geology 181, 73–91.

U.S. Geological Survey and Arabian-American Oil Company (1963) Geologic map of the Arabian Peninsula. United States Geological Survey, Miscellaneous Geologic Investigations Map I-270A, Scale 1:2,000,000.

Van Loon, A.J.T., Mange, M.A., 2007. 'In Situ' Dissolution of Heavy Minerals through Extreme Weathering, and the Application of the Surviving Assemblages and their Dissolution Characteristics to Correlation of Dutch and German Silver Sands. In: Mange, A.A., Wright, D.T. (Eds.), Heavy Minerals in Use, Developments in Sedimentology 58, Elsevier, Amsterdam, 189–213.

Vaslet, D., 1990. Upper Ordovician glacial deposits in Saudi Arabia. Episodes 13(3), 147–161. Cited in Sharland et al. (2001).

Vaslet, D., Kellogg, K.S., Berthiaux, A., Le Strat, P., Vincent, P.-L., 1987. Explanatory notes to the geologic map of the Baq'a Quadrangle, Kingdom of Saudi Arabia. Geoscience Map GM-116 C, scale 1:250,000, sheet 27F. Deputy Ministry for Mineral Resources, Ministry of Petroleum and Mineral Resources, Kingdom of Saudi Arabia, pp. 45.

Vavra, G., Schmid, R., Gebauer, D., 1999. Internal morphology, habit and U-Th-Pb microanalysis of amphibolite-to-granulite facies zircons: geochronology of the Ivrea Zone (Southern Alps). Contributions to Mineralogy and Petrology 134, 380–404.

Verma, S.P., Agrawal, S., 2011. New tectonic discrimination diagrams for basic and ultrabasic volcanic rocks through log-transformed ratios of high field strength elements and implications for petrogenetic processes. Revista Mexicana de Ciencias Geológicas 25(1), 24–44.

Verma, S.P., Armstrong-Altrin, J.S., 2013. New multi-dimensional diagrams for tectonic discrimination of siliciclastic sediments and their application to Precambrian basins. Chemical Geology 355, 117–133.

Verma, S.P., Torres-Alvarado, I.S., Sotelo-Rodríguez, Z.T., 2002. SINCLAS: standard igneous norm and volcanic rock classification system. Computers & Geosciences 28, 711–715.

Verma, S.K., Pandarinath, K., Verma, S.P., 2012. Statistical evaluation of tectonomagmatic discrimination diagrams for granitic rocks and proposal of new discriminant-function-based multi-dimensional diagrams for acid rocks. International Geology Review 54, 325–347.

Verma, S.P., Pandarinath, K., Verma, S.K., Agrawal, S., 2013. Fifteen new discriminant-function-based multi-dimensional robust diagrams for acid rocks and their application to Precambrian rocks. Lithos 168-169, 113–123.

von Eynatten, H., Dunkl, I., 2012. Assessing the sediment factory: The role of single grain analysis. Earth-Science Reviews 115, 97–120.
von Eynatten, H., Tolosana-Delgado, R., Karius, V., 2012. Sediment generation in modern glacial settings: Grain-size and source-rock control on sediment composition. Sedimentary Geology 280, 80–92.

Wahed, M.A., Zoheir, B., Hamimi, Z., Al-Selwi, Kh., 2006. Tectonic evolution of the Archaean-Neoproterozoic basement complex of Dhi Na'im-Al Bayda District, Republic of Yemen. Proceedings, 1st International Conference on Geology of the Arab World, Cairo University, Egypt.

Wanas, H.A., Abdel-Maguid, N.M., 2006. Petrography and geochemistry of the Cambro-Ordovician Wajid Sandstone, southwest Saudi Arabia: Implications for provenance and tectonic setting. Journal of Asian Earth Sciences 27(4), 416–429.

Watson, E.B., Wark, D.A., Thomas, J.B., 2006. Crystallisation thermometers for zircon and rutile. Contributions to Mineralogy and Petrology 151, 413–433.

Wedepohl, K.H., 1978. Handbook of Geochemistry, Volume II, Part 2. Springer, Berlin, Heidelberg, New York, pp. 1546.

Wegener, W., Wörner, G., Harmon, R.S., Jicha, B.R., 2011. Magmatic history and evolution of the Central American Land Bridge in Panama since Cretaceous times. Geological Society of America Bulletin 132(3–4), 703–724.

Weibel, R., Johannessen, P.N., Dybkjær, K., Rosenberg, P., Knudsen, C., 2010. Chemostratigraphy of upper Jurassic reservoir sandstones, Danish Central Graben, North Sea. Marine and Petroleum Geology 27, 1572–1594.

Weissbrod, T. and Bogoch, R., 2007. Distribution pattern and provenance implications of the heavy minerals in Neoproterozoic to Mesozoic siliciclastic successions in the Arabo-Nubian Shield and its northern periphery: a review. In: Mange, A.A., Wright, D.T. (Eds.), Heavy Minerals in Use, Developments in Sedimentology 58, Elsevier, Amsterdam, 647–676.

Wellman, C.H., Steemans, P., Miller, M.A., 2015. Spore assemblages from Upper Ordovician and lowermost Silurian sediments recovered from the Qusaiba-1 shallow core hole, Qasim region, central Saudi Arabia. Review of Palaeobotany and Palynology 212, 111–156.

Weltje, G.J., 2002. Quantitative analysis of detrital modes: statistically rigorous confidence regions in ternary diagrams and their use in sedimentary petrology. Earth-Science Reviews 57, 211–253.

Weltje, G.J, 2004. A quantitative approach to capturing the compositional variability of modern sands. Sedimentary Geology 171, 59–77.

Weltje, G.J., 2006. Ternary sandstone composition and provenance: an evaluation of the 'Dickinson model'. In: Buccianti, A., Mateu-Figueras, G., Pawlowsky-Glahn, V. (Eds.), Compositional Data Analysis: From Theory to Practice. Geological Society Special Publications 264, 611–627.

Weltje, G.J., von Eynatten, H., 2004. Quantitative provenance analysis of sediments: review and outlook. Sedimentary Geology 171, 1–11.

Weltje, G.J., Meijer, X.D., de Boer, P.L., 1998. Stratigraphic inversion of siliciclastic basin fills: a note on the distinction between supply signals resulting from tectonic and climatic forcing. Basin Research 10, 129–153.

Wender, L.E., Bryant, J.W., Dickens, M.F., Neville, A.S., Al-Moqbel, A.M., 1998. Paleozoic (pre-Khuff) hydrocarbon geology of the Ghawar area, eastern Saudi Arabia. GeoArabia 3(2), 273–302.

Weyl, R., Werner, H., 1951. Schwermineraluntersuchungen im Jungtertiär und Altquartär Schleswig-Holsteins. In: Proceedings, 3rd International Sedimentology Congress, Groningen-Wageningen, p. 293–303.

Whitlow, J.W., 1966. A mineral reconnaissance of the Jabal Khida quadrangle (21/44C, D). United States Geological Survey, Technical Letter TL-61, pp. 18.

Whitehouse, M.J., Stoeser, D.B., Stacey, J.S., 2001. The Khida Terrane – Geochsonology and Isotopic Evidence for Paleoproterozoic and Archean Crust in the Eastern Arabian Shield of Saudi Arabia. Gondwana Research 4(2), 200–202.

Wilkinson, M., Milliken, K.L., Haszeldine, R.S., 2001. Systematic destruction of K-feldspar in deeply buried rift and passive margin sandstones. Journal of the Geological Society London 158, 675–683.

Williams, P.L., Vaslet, D., Johnson, P.R., Berthiaux, A., Le Start, P., Fourniguet, J., 1987. Geologic map of the Jabal Habashi quadrangle, sheet 26F, Kingdome of Saudi Arabia (with text). Deputy Ministry for Mineral Resources, Ministry of Petroleum and Mineral Resources, Kingdom of Saudi Arabia. Cited in Al-Laboun (2010).

Woldehaimanot, B., 2001. Extensional Tectonics in the High-Grade Metamorphic Terrain of Upper Anseba Region, Central Eritrea. Gondwana Research 4, 207–208.

Wronkiewicz, D.J., Condie, K.C., 1987. Geochemistry of Archean shales from the Witwatersrand Supergroup, South Africa: Source-area weathering and provenance. Geochimica et Cosmochimica Acta 51, 2401–2416.

Zack, T., Kronz, A., Foley, S.F., Rivers, T., 2002. Trace element abundances in rutiles from eclogites and associated garnet mica schists. Chemical Geology 184, 97–122.

Zack, T., von Eynatten, H., Kronz, A., 2004a. Rutile geochemistry and its potential use in quantitative provenance studies. Sedimentary Geology 171, 37–58.

Zack, T., Moraes, R., Kronz, A., 2004b. Temperature dependence of Zr in rutile: empirical calibration of a rutile thermometer. Contributions to Mineralogy and Petrology 148, 471–488.

Zack, T., Luvizotto, G.L., 2006. Application of rutile thermometry to eclogites. Mineralogy and Petrology 88, 69–85.

Annex

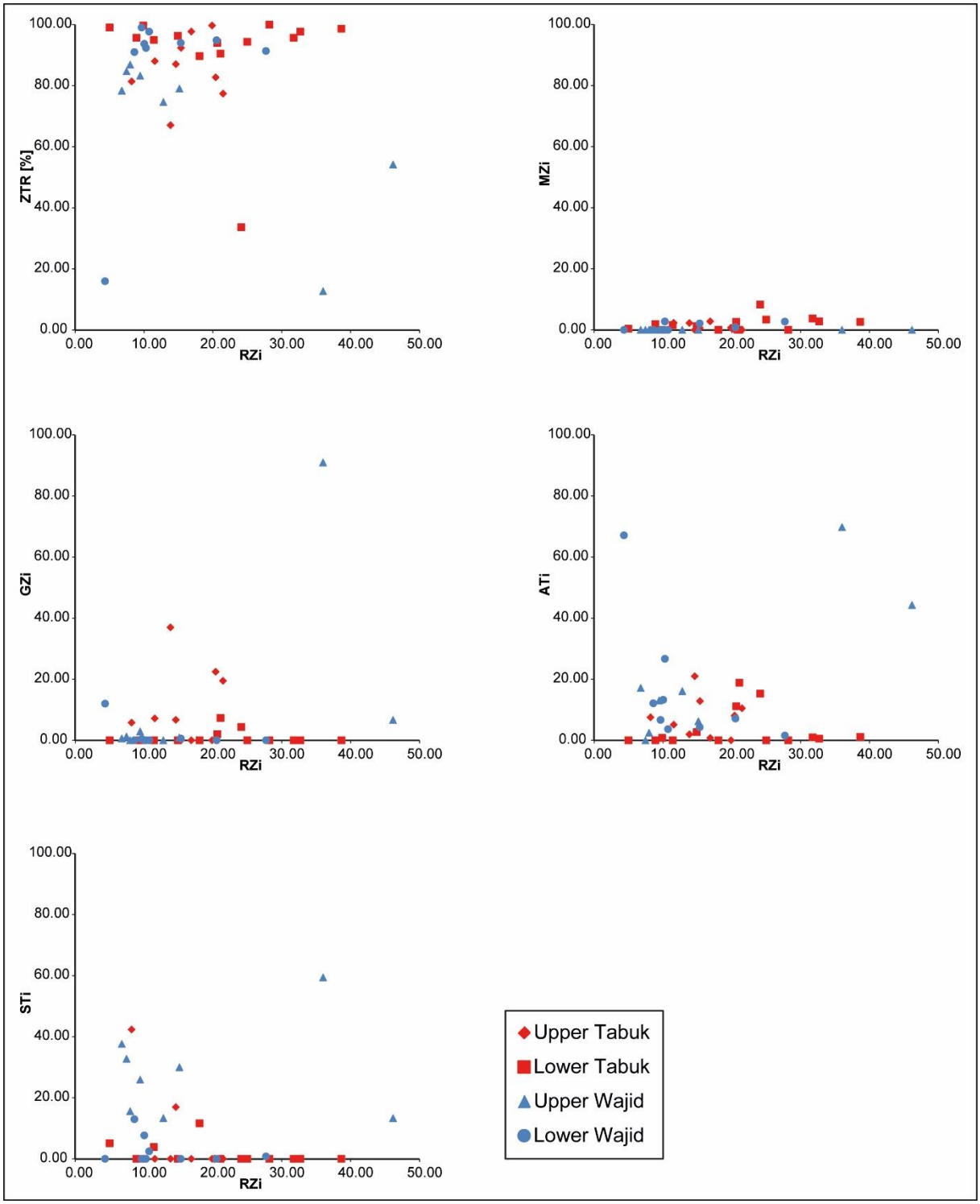

Figure A1: Crossplots of different heavy mineral indices versus the RZi.

Table A1: Results of zircon morphotype analysis in total counts.

Sample	Formation	zoned	core/rim zoned	regrowth features	convoluted	patchy	core/rim unzoned	un-zoned	n
Tabuk area									
AB-SA120	Unayzah	68	13	28	8	3	11	11	142
AB-SA129	Unayzah	50	16	19	8	2	8	6	109
AB-SA150	Jubah	21	12	18	5	2	4	7	69
AB-SA152	Jubah	53	17	30	8	0	13	13	134
AB-SA160/T	Jauf	41	12	19	4	2	13	6	97
AB-SA164	Jauf	2	5	3	0	0	0	1	11
AB-SA156	Tawil	54	21	18	16	8	21	16	154
AB-SA157	Tawil	43	12	31	5	6	17	13	127
AB-SA128	Sharawra	6	1	2	2	1	4	2	18
AB-SA132/1	Zarqa	51	6	12	15	1	7	6	98
AB-SA123/2	Sarah	69	18	29	17	6	16	8	163
AB-SA124	Qasim	56	30	50	10	9	30	8	193
AB-SA126	Qasim	15	11	10	9	5	5	5	60
AB-SA145	Qasim	37	14	15	14	3	13	10	106
AB-SA144/1	Qasim	49	13	18	16	2	11	13	122
AB-SA170	Saq	55	18	29	15	1	25	6	149
AB-SA169	Saq	76	14	14	24	6	11	10	155
Wajid area									
AB-SA98	Juwayl	13	6	2	4	1	2	0	28
AB-SA100	Juwayl	69	10	27	3	6	9	13	137
AB-SA87	Khusayyayn	65	20	17	1	3	8	10	124
AB-SA90	Khusayyayn	27	17	15	8	1	5	6	79
AB-SA118	Khusayyayn	65	24	25	13	1	7	13	148
AB-SA62	Sanamah	43	11	17	6	0	10	5	92
AB-SA73	Sanamah	65	12	35	11	5	9	9	146
AB-SA74	Dibsiyah	83	31	29	3	3	3	24	176
AB-SA79	Dibsiyah	71	8	30	45	5	8	4	171
per study area									
Upper Tabuk		332	108	166	54	23	87	73	843
Lower Tabuk		414	125	179	122	34	122	68	1064
Upper Wajid		239	77	86	29	12	31	42	516
Lower Wajid		262	62	111	65	13	30	42	585

Table A2: Results of zircon morphotype analysis as percentages.

Sample	Formation	zoned	core/rim zoned	regrowth features	convoluted	patchy	core/rim unzoned	un-zoned	n
Tabuk area									
AB-SA120	Unayzah	47.9	9.2	19.7	5.6	2.1	7.7	7.7	142
AB-SA129	Unayzah	45.9	14.7	17.4	7.3	1.8	7.3	5.5	109
AB-SA150	Jubah	30.4	17.4	26.1	7.2	2.9	5.8	10.1	69
AB-SA152	Jubah	39.6	12.7	22.4	6.0	0.0	9.7	9.7	134
AB-SA160/T	Jauf	42.3	12.4	19.6	4.1	2.1	13.4	6.2	97
AB-SA164	Jauf	18.2	45.5	27.3	0.0	0.0	0.0	9.1	11
AB-SA156	Tawil	35.1	13.6	11.7	10.4	5.2	13.6	10.4	154
AB-SA157	Tawil	33.9	9.4	24.4	3.9	4.7	13.4	10.2	127
AB-SA128	Sharawra	33.3	5.6	11.1	11.1	5.6	22.2	11.1	18
AB-SA132/1	Zarqa	52.0	6.1	12.2	15.3	1.0	7.1	6.1	98
AB-SA123/2	Sarah	42.3	11.0	17.8	10.4	3.7	9.8	4.9	163
AB-SA124	Qasim	29.0	15.5	25.9	5.2	4.7	15.5	4.1	193
AB-SA126	Qasim	25.0	18.3	16.7	15.0	8.3	8.3	8.3	60
AB-SA145	Qasim	34.9	13.2	14.2	13.2	2.8	12.3	9.4	106
AB-SA144/1	Qasim	40.2	10.7	14.8	13.1	1.6	9.0	10.7	122
AB-SA170	Saq	36.9	12.1	19.5	10.1	0.7	16.8	4.0	149
AB-SA169	Saq	49.0	9.0	9.0	15.5	3.9	7.1	6.5	155
Wajid area									
AB-SA98	Juwayl	46.4	21.4	7.1	14.3	3.6	7.1	0.0	28
AB-SA100	Juwayl	50.4	7.3	19.7	2.2	4.4	6.6	9.5	137
AB-SA87	Khusayyayn	52.4	16.1	13.7	0.8	2.4	6.5	8.1	124
AB-SA90	Khusayyayn	34.2	21.5	19.0	10.1	1.3	6.3	7.6	79
AB-SA118	Khusayyayn	43.9	16.2	16.9	8.8	0.7	4.7	8.8	148
AB-SA62	Sanamah	46.7	12.0	18.5	6.5	0.0	10.9	5.4	92
AB-SA73	Sanamah	44.5	8.2	24.0	7.5	3.4	6.2	6.2	146
AB-SA74	Dibsiyah	47.2	17.6	16.5	1.7	1.7	1.7	13.6	176
AB-SA79	Dibsiyah	41.5	4.7	17.5	26.3	2.9	4.7	2.3	171
per study area									
Upper Tabuk		39.4	12.8	19.7	6.4	2.7	10.3	8.7	843
Lower Tabuk		38.9	11.7	16.8	11.5	3.2	11.5	6.4	1064
Upper Wajid		46.3	14.9	16.7	5.6	2.3	6.0	8.1	516
Lower Wajid		44.8	10.6	19.0	11.1	2.2	5.1	7.2	585
Tabuk (total)		39.1	12.2	18.1	9.2	3.0	11.0	7.4	1907
Wajid (total)		45.5	12.6	17.9	8.5	2.3	5.5	7.6	1101

Table A3: Major element composition as well as CIA and PIA values of Saudi Arabian Palaeozoic sandstones. Element concentrations were measured with XRF and are given in weight-%. The laboratory responsible for analysis is also listed. n/d – not determined.

Sample	Lab	SiO_2	TiO_2	Al_2O_3	MnO	MgO	CaO	Na_2O	K_2O	P_2O_5	Fe_2O_3t	Sum%	CIA	PIA
Tabuk area														
AB-SA120	Göttingen	87.41	0.17	4.97	0.00	0.00	0.16	0.03	2.44	0.01	0.31	95.50	62.5	87.3
AB-SA129	Mainz	98.22	0.07	0.80	0.00	0.00	0.19	0.00	0.30	0.00	0.25	99.83	54.4	57.9
AB-SA130	Mainz	97.73	0.04	1.21	0.00	0.00	0.26	0.00	0.21	0.00	0.09	99.54	63.4	67.5
AB-SA150	Mainz	81.18	0.62	8.19	0.04	0.15	0.16	0.18	5.27	0.04	2.82	98.65	56.6	80.9
AB-SA152	Mainz	85.35	1.00	6.19	0.02	0.12	0.61	0.09	3.93	0.03	0.73	98.07	52.9	60.6
AB-SA153	Mainz	85.53	0.40	6.31	0.02	0.19	0.13	0.11	4.48	0.02	1.29	98.48	54.5	77.8
AB-SA160/T	Göttingen	83.40	0.71	11.24	0.02	0.00	1.56	0.25	6.48	0.05	1.37	105.08	52.3	56.5
AB-SA161	Mainz	71.79	0.65	12.62	0.02	0.67	0.58	0.09	6.39	0.10	3.46	96.37	60.9	82.6
AB-SA164	Mainz	82.37	0.13	2.35	0.13	1.68	9.39	0.00	0.88	0.05	0.76	97.74	n/a	n/a
AB-SA154	Mainz	99.80	0.06	0.09	0.00	0.00	0.05	0.00	0.03	0.01	0.11	100.15	42.2	38.8
AB-SA156	Göttingen	85.45	0.58	4.94	0.01	0.00	1.86	0.00	0.05	0.09	1.42	94.40	59.0	59.1
AB-SA157	Mainz	94.96	0.15	2.03	0.01	0.00	0.08	0.00	1.20	0.02	0.73	99.18	58.4	83.4
AB-SA128	Göttingen	71.43	0.65	11.86	0.02	0.54	0.81	0.07	5.88	0.07	2.90	94.23	59.9	77.6
AB-SA127	Göttingen	72.75	0.62	12.35	0.02	0.24	0.15	0.27	5.74	0.05	2.11	94.29	64.1	89.5
AB-SA132/1	Göttingen	65.28	0.10	2.92	0.26	0.10	13.19	0.00	1.96	0.19	2.37	86.38	n/a	n/a
AB-SA132/2	Mainz	89.24	0.57	5.21	0.07	0.12	0.09	0.47	2.33	0.02	0.83	98.95	60.1	74.2
AB-SA123/2	Mainz	95.09	0.69	1.93	0.01	0.00	0.55	0.00	0.05	0.02	0.52	98.86	64.7	65.2
AB-SA122/2	Göttingen	92.76	0.17	1.49	0.01	0.00	0.04	0.01	0.12	0.02	0.16	94.79	86.6	93.3
AB-SA124	Mainz	93.75	0.38	3.49	0.00	0.00	0.22	0.00	0.35	0.06	0.44	98.69	81.8	88.6
AB-SA126	Göttingen	69.68	2.33	8.20	0.08	0.00	0.66	0.37	4.53	0.13	3.20	89.17	55.0	64.6
AB-SA145	Göttingen	94.98	0.12	1.72	0.00	0.00	0.23	0.27	0.06	0.05	0.55	97.98	65.0	65.7
AB-SA144/1	Göttingen	90.68	0.30	4.54	0.01	0.00	0.06	0.00	0.08	0.08	0.53	96.28	95.9	97.6
AB-SA142/2	Mainz	87.70	0.49	5.07	0.06	0.09	2.23	0.00	0.07	0.07	0.49	96.27	55.1	55.2
AB-SA170	Mainz	94.61	0.20	2.86	0.00	0.00	0.47	0.00	0.04	0.02	0.10	98.30	76.1	76.7
AB-SA167	Mainz	91.79	0.80	4.36	0.00	0.00	0.22	0.00	0.02	0.06	0.63	97.88	91.2	91.6
AB-SA169	Mainz	88.44	0.23	3.97	0.01	0.17	2.35	0.00	0.07	0.04	0.90	96.18	n/a	n/a
Wajid area														
AB-SA98	Göttingen	46.82	0.05	4.97	0.12	9.05	12.92	0.29	1.84	0.03	1.21	77.30	n/a	n/a
AB-SA80	Mainz	95.27	0.14	1.26	0.02	0.13	1.34	0.00	0.09	0.03	0.36	98.64	33.2	32.3
AB-SA100	Göttingen	92.78	0.13	2.69	0.01	0.00	0.44	0.00	0.08	0.01	0.30	96.45	75.2	76.5
AB-SA87	Mainz	90.27	0.07	4.14	0.02	0.06	1.41	0.00	1.17	0.02	0.33	97.49	51.9	52.9
AB-SA89	Göttingen	90.23	0.08	3.85	0.01	0.00	0.69	0.03	0.82	0.02	0.27	96.00	63.7	69.4
AB-SA90	Göttingen	88.39	0.06	2.60	0.04	0.00	2.06	0.00	0.71	0.03	1.28	95.16	36.5	32.8
AB-SA118	Mainz	96.47	0.05	1.50	0.01	0.00	0.07	0.00	0.18	0.00	1.51	99.79	82.3	91.1
AB-SA32	Göttingen	91.35	0.03	0.99	0.17	0.00	6.84	0.02	0.11	0.03	3.78	103.31	n/a	n/a
AB-SA115	Göttingen	71.55	0.43	12.57	0.07	0.69	0.65	0.06	3.48	0.09	4.14	93.73	71.4	87.3
AB-SA62	Göttingen	85.88	0.15	4.09	0.01	0.00	1.63	0.00	0.03	0.05	2.54	94.38	57.7	57.8
AB-SA63	Göttingen	95.79	0.09	1.58	0.00	0.00	0.31	0.00	0.02	0.02	0.11	97.92	73.0	73.4
AB-SA64	Göttingen	91.74	0.18	3.27	0.01	0.00	0.81	0.00	0.04	0.03	0.51	96.58	68.3	68.7
AB-SA73	Göttingen	91.36	0.08	4.07	0.00	0.00	0.50	0.00	0.02	0.03	0.31	96.37	81.4	81.7
AB-SA74	Göttingen	92.59	0.18	1.65	0.01	0.00	0.23	0.01	0.03	0.02	0.27	94.98	77.8	78.6
AB-SA76	Göttingen	92.08	0.13	2.10	0.01	0.00	0.36	0.01	0.03	0.02	0.34	95.08	75.0	75.5
AB-SA72	Göttingen	80.95	0.39	11.84	0.00	0.00	0.39	0.00	0.07	0.08	0.54	94.27	93.8	94.3
AB-SA69	Göttingen	92.03	0.21	1.46	0.01	0.00	0.11	0.03	0.06	0.02	0.31	94.23	82.3	84.8
AB-SA79	Göttingen	90.22	0.23	3.39	0.01	0.00	0.28	0.00	0.03	0.02	2.48	96.67	86.2	86.8
JUW/315	Actlabs	93.44	0.10	3.51	0.00	0.01	0.60	0.08	0.03	0.02	0.69	98.48	73.7	74
JUW-BAS/314	Actlabs	91.32	0.09	1.36	0.07	0.05	2.50	0.00	0.04	0.02	0.56	96.00	22.9	22.5
Wuh-1-4/18	Actlabs	98.14	0.08	1.09	0.00	0.03	0.20	0.00	0.03	0.00	0.33	99.90	73.3	74.4
Wuh-4-2/66	Actlabs	96.89	0.18	1.26	0.00	0.02	0.41	0.01	0.04	0.03	0.28	99.12	61.0	61.5
Wuh-5-32-33/110	Actlabs	93.77	0.49	2.61	0.02	0.06	0.37	0.00	0.04	0.02	0.41	97.79	78.5	79.2
KSA 25/313	Actlabs	96.39	0.09	0.82	0.06	0.16	0.28	0.03	0.07	0.02	0.82	98.74	56.4	57.1
WKh-T-1/24	Actlabs	94.87	0.10	2.43	0.00	0.04	0.56	0.03	0.52	0.02	0.34	98.91	59.8	63.6
WKh-T-12/15	Actlabs	88.62	0.26	4.43	0.02	0.06	1.53	0.04	0.86	0.02	0.65	96.48	54.0	55.1
WKh-T-8/62	Actlabs	93.17	0.09	3.59	0.01	0.06	0.80	0.04	0.71	0.03	0.49	98.99	61.1	65
S2/312	Actlabs	96.36	0.13	1.06	0.15	0.10	0.66	0.02	0.07	0.07	1.35	99.98	44.8	44.4
WDSK-4/310	Actlabs	92.01	0.30	4.24	0.01	0.11	1.14	0.00	0.03	0.03	0.41	98.27	66.8	67
WDSK-5/32	Actlabs	96.58	0.07	1.33	0.00	0.06	0.31	0.02	0.05	0.06	0.69	99.17	67.2	68.1
WDSK-5-b/11	Actlabs	94.69	0.06	1.01	0.01	0.09	1.48	0.00	0.01	0.03	0.53	97.91	27.2	27.1
WDh-1-13/55	Actlabs	96.53	0.04	1.16	0.00	0.03	0.15	0.01	0.01	0.03	0.31	98.28	79.5	79.9
WDh-1-52/52	Actlabs	92.16	0.37	3.67	0.01	0.03	1.31	0.01	0.03	0.04	0.26	97.88	60.2	60.3
WDh-1-top/19	Actlabs	90.69	0.23	5.81	0.00	0.01	0.77	0.01	0.03	0.04	0.24	97.83	80.0	80.3
DIB/311	Actlabs	95.32	0.26	1.93	0.01	0.02	0.73	0.00	0.01	0.03	0.38	98.68	59.1	59.1

Table A4: Trace element composition and selected ratios of Saudi Arabian Palaeozoic sandstones. Element concentrations were measured with ICP-MS and are given in ppm. n/d – not determined; bdl – below detection limit.

Sample	Li	Sc	Cr	Ni	Cu	Zn	Ga	Y	Zr	Nb	Mo	Cd	Sn	Sb	Rb	Sr	Cs	Ba	La	Ce	Pr	Nd	Sm	Eu	Gd	Tb	Dy	Ho	Er	Tm	Yb	Lu
Tabuk area																																
AB-SA120	13.22	1.15	40.48	3.78	70.18	8.86	5.03	9.94	109.91	9.20	0.35	-0.06	16.63	0.09	35.83	58.36	0.61	1656.44	9.98	19.27	2.30	8.26	1.75	0.41	1.57	0.27	1.81	0.38	1.03	0.14	1.05	0.14
AB-SA129	9.01	3.70	23.23	9.08	1.81	14.62	0.92	3.86	43.40	1.00	0.80	0.03	0.17	0.07	5.54	13.09	0.03	86.26	6.72	10.95	1.23	4.46	0.91	0.16	0.82	0.11	0.75	0.15	0.46	0.06	0.44	0.07
AB-SA130	6.27	0.42	21.65	4.41	1.11	5.00	0.70	4.38	26.73	0.03	0.28	-0.01	0.15	0.08	3.09	11.17	0.03	31.39	12.10	25.31	2.79	10.82	1.98	0.40	2.03	0.25	1.18	0.18	0.49	0.05	0.39	0.05
AB-SA150	11.39	9.89	34.23	14.03	10.42	17.00	9.30	30.35	390.01	15.04	0.66	0.00	1.60	0.17	141.66	178.72	1.65	1264.72	40.13	80.13	9.12	32.48	6.74	1.25	5.89	0.91	5.79	1.16	3.42	0.49	3.35	0.50
AB-SA152	7.89	6.96	29.94	14.14	10.03	12.18	6.34	28.09	501.59	17.90	0.72	0.03	1.56	0.09	91.82	128.10	0.95	882.80	63.69	127.70	14.39	50.05	9.43	1.11	7.43	1.00	5.88	1.08	3.23	0.42	3.04	0.45
AB-SA153	6.02	5.68	30.98	8.96	4.22	9.44	7.56	12.90	157.63	9.42	0.56	0.02	0.99	0.12	117.71	149.89	1.12	1148.60	18.15	37.00	4.05	14.81	2.94	0.82	2.67	0.39	2.45	0.49	1.48	0.19	1.39	0.19
AB-SA160/T	13.68	8.22	37.09	6.75	5.34	11.83	9.05	33.28	498.14	15.02	0.59	0.10	1.70	0.20	121.79	163.69	1.36	1189.83	51.33	103.98	11.96	42.27	8.12	1.35	6.30	0.92	5.96	1.18	3.70	0.51	3.72	0.58
AB-SA161	22.09	11.41	46.70	26.00	7.49	31.11	19.17	32.13	482.65	16.86	1.21	0.02	2.65	0.44	164.35	756.05	2.52	1419.74	83.64	164.31	16.54	57.17	9.40	1.80	7.08	0.97	6.58	1.31	4.12	0.60	4.19	0.66
AB-SA164	n/a	n/a	n/a	n/a	n/a	n/a	n/a	n/a	n/a	n/a	n/a	n/a	n/a	n/a	n/a	n/a	n/a	n/a	n/a	n/a	n/a	n/a	n/a	n/a	n/a	n/a	n/a	n/a	n/a	n/a	n/a	n/a
AB-SA154	5.74	1.12	23.57	4.56	1.09	2.81	0.51	3.06	45.40	0.49	0.39	0.01	0.21	0.05	0.49	8.35	0.01	21.83	4.10	8.07	0.88	3.01	0.62	0.09	0.55	0.07	0.61	0.13	0.35	0.05	0.38	0.06
AB-SA156	11.05	2.97	48.60	8.33	6.47	23.52	4.64	13.13	226.11	10.57	0.53	0.12	1.01	0.09	1.18	59.99	0.04	102.27	24.56	52.14	5.67	19.29	3.66	0.53	2.87	0.40	2.43	0.47	1.46	0.19	1.45	0.22
AB-SA157	6.32	3.68	22.03	11.76	3.09	13.62	2.64	7.71	81.14	2.28	0.71	0.14	0.84	0.03	25.24	91.30	0.30	280.12	14.58	33.95	3.69	13.86	2.73	0.57	2.08	0.27	1.62	0.31	0.86	0.12	0.81	0.12
AB-SA128	28.06	10.45	46.88	43.93	23.62	42.77	11.84	41.27	454.24	15.45	2.06	0.00	2.01	0.28	159.52	175.99	3.76	1554.18	35.59	69.18	8.16	30.51	5.47	1.13	5.48	0.93	6.39	1.48	4.74	0.74	5.88	0.83
AB-SA127	24.08	5.34	43.76	17.04	16.84	22.76	9.74	28.29	282.39	12.73	0.38	-0.01	1.61	0.15	130.27	140.56	1.84	1300.07	29.17	57.90	6.64	24.24	4.03	0.94	3.99	0.62	4.30	1.00	3.14	0.49	3.72	0.56
AB-SA132/1	6.27	5.80	50.66	9.51	3.41	4.87	3.32	9.23	117.40	2.57	1.60	0.00	0.37	0.10	55.64	172.52	0.61	570.31	28.31	44.20	3.71	11.19	1.85	0.49	1.71	0.25	1.51	0.31	0.94	0.14	0.96	0.15
AB-SA132/2	8.94	5.61	30.12	6.19	5.41	11.14	4.97	13.82	524.40	8.16	0.56	0.02	0.98	0.09	58.97	154.18	0.71	754.78	35.96	73.44	7.66	25.91	4.37	0.81	3.05	0.44	2.63	0.55	1.72	0.28	2.03	0.32
AB-SA123/2	7.80	4.26	27.25	7.41	6.14	11.48	2.08	12.16	779.42	0.93	0.33	0.03	0.65	0.05	1.13	50.65	0.01	33.74	20.28	39.96	4.07	14.32	2.30	0.28	2.06	0.28	1.80	0.42	1.42	0.25	2.19	0.34
AB-SA122/2	8.16	3.43	23.76	5.57	3.40	5.14	1.24	6.52	239.10	1.37	0.40	0.01	0.29	0.07	3.89	37.24	0.04	64.63	13.00	25.68	2.63	8.99	1.50	0.26	1.20	0.17	1.08	0.24	0.73	0.11	0.92	0.13
AB-SA124	13.66	2.65	25.48	7.49	4.53	21.70	4.02	9.14	365.50	2.98	0.45	0.02	0.67	0.17	12.06	122.07	0.19	425.93	26.35	54.62	5.98	20.90	3.55	0.63	2.72	0.35	1.93	0.37	1.07	0.16	1.22	0.19
AB-SA126	32.08	18.44	86.66	23.43	28.47	90.69	10.95	129.75	3245.68	55.92	0.76	0.07	5.07	0.39	138.04	310.70	1.72	1428.57	287.72	583.07	67.71	247.23	42.58	5.60	34.84	4.87	25.91	4.94	13.85	1.89	14.54	2.07
AB-SA145	1.99	4.30	22.47	6.31	3.11	9.96	1.85	7.97	59.91	2.31	0.33	0.04	0.40	0.04	0.65	74.28	0.04	15.24	11.16	21.70	2.59	9.37	1.87	0.38	1.51	0.23	1.42	0.32	0.98	0.14	1.06	0.16
AB-SA144/1	13.20	4.72	24.20	4.30	6.64	8.19	5.86	13.10	138.00	8.13	0.43	0.02	2.15	0.11	3.30	164.26	0.11	212.70	36.65	70.91	8.37	30.62	5.78	0.86	4.44	0.54	2.80	0.50	1.49	0.20	1.45	0.22
AB-SA142/2	14.39	4.91	91.08	6.92	6.64	13.31	6.25	18.02	446.58	10.12	0.56	0.06	1.54	0.16	2.18	151.86	0.09	289.38	23.37	47.39	5.75	21.01	4.44	0.96	3.61	0.51	3.15	0.68	2.07	0.32	2.20	0.35
AB-SA170	n/a	n/a	n/a	n/a	n/a	n/a	n/a	n/a	n/a	n/a	n/a	n/a	n/a	n/a	n/a	n/a	n/a	n/a	n/a	n/a	n/a	n/a	n/a	n/a	n/a	n/a	n/a	n/a	n/a	n/a	n/a	n/a
AB-SA167	n/a	n/a	n/a	n/a	n/a	n/a	n/a	n/a	n/a	n/a	n/a	n/a	n/a	n/a	n/a	n/a	n/a	n/a	n/a	n/a	n/a	n/a	n/a	n/a	n/a	n/a	n/a	n/a	n/a	n/a	n/a	n/a
AB-SA169	7.65	6.78	44.75	7.50	5.62	8.30	4.58	42.17	100.02	5.48	0.52	0.02	0.72	0.13	2.15	65.77	0.09	46.65	13.76	25.64	3.18	11.51	2.24	0.56	2.54	0.50	4.46	1.18	3.92	0.56	3.76	0.56
Wajid area																																
AB-SA98	7.54	5.02	221.73	10.78	3.29	13.98	4.76	20.28	32.72	1.50	1.56	0.11	0.36	0.15	36.71	465.12	1.11	540.98	10.15	25.17	2.99	11.97	2.92	0.74	2.89	0.50	3.34	0.73	2.01	0.29	1.98	0.29
AB-SA80	12.57	3.20	21.78	9.28	26.95	11.13	1.94	5.53	99.28	2.65	0.62	0.03	5.28	0.10	3.25	27.28	0.13	125.87	9.24	18.84	2.18	8.32	1.88	0.23	1.47	0.19	1.07	0.21	0.64	0.08	0.63	0.09
AB-SA100	8.65	1.88	19.36	5.14	3.45	11.21	2.22	6.36	113.89	2.35	0.63	0.06	0.77	0.16	2.60	8.26	0.10	57.39	8.16	14.71	1.98	7.75	1.57	0.34	1.20	0.19	1.24	0.24	0.76	0.10	0.82	0.11
AB-SA87	11.52	4.57	20.01	8.32	62.62	6.95	4.31	6.04	60.01	1.53	0.47	0.04	14.27	0.05	33.88	54.83	0.51	261.50	11.51	23.51	2.55	9.51	2.01	0.55	1.49	0.22	1.30	0.24	0.65	0.09	0.60	0.09
AB-SA89	13.03	5.29	20.31	5.62	20.95	7.06	3.91	6.70	64.24	2.05	0.44	0.01	4.73	0.04	26.15	42.33	0.39	191.72	9.96	21.99	2.19	7.69	1.71	0.38	1.34	0.20	1.27	0.26	0.72	0.11	0.76	0.10
AB-SA90	10.48	3.70	30.27	13.55	40.54	15.25	2.85	7.52	60.37	1.46	0.71	0.10	9.18	0.07	22.60	46.32	0.39	193.39	9.62	20.36	2.18	7.46	1.52	0.40	1.22	0.20	1.30	0.28	0.85	0.13	0.85	0.13
AB-SA118	10.31	2.33	31.26	5.76	9.76	11.72	1.52	3.54	44.32	0.54	3.82	0.00	1.68	0.06	4.22	9.49	0.05	72.71	2.61	6.72	0.71	2.77	0.63	0.13	0.56	0.10	0.63	0.14	0.42	0.06	0.47	0.06
AB-SA32	4.22	4.52	21.57	13.54	12.89	14.57	0.96	9.32	32.71	0.17	10.66	0.05	2.17	0.16	2.46	41.36	0.04	137.93	11.66	33.42	4.61	23.17	5.63	0.76	3.19	0.38	2.06	0.36	1.05	0.16	1.30	0.19
AB-SA115	36.09	11.16	54.91	21.71	10.03	108.66	13.53	17.18	198.79	10.21	3.18	0.02	1.82	0.17	91.43	109.89	1.21	812.50	23.54	47.72	5.76	20.24	3.82	0.84	3.07	0.49	3.37	0.70	2.05	0.29	2.00	0.31
AB-SA62	5.34	2.17	31.65	3.70	34.74	6.59	5.24	4.97	100.21	2.74	7.52	0.01	7.27	0.23	0.65	64.29	0.02	38.77	11.69	22.80	2.49	8.90	2.01	0.42	1.45	0.19	1.08	0.21	0.65	0.09	0.74	0.11
AB-SA63	5.41	0.98	26.58	4.97	35.57	2.88	1.55	3.35	83.90	0.40	0.34	0.03	7.03	0.03	0.47	33.08	0.01	24.59	8.45	15.57	1.72	6.13	1.15	0.23	0.82	0.11	0.69	0.14	0.41	0.06	0.53	0.07
AB-SA64	4.76	2.17	21.54	4.36	37.48	3.89	3.05	3.96	119.63	1.92	0.31	-0.02	7.76	0.05	0.99	38.45	0.03	27.14	9.74	19.30	2.23	8.07	1.53	0.37	1.02	0.15	0.87	0.17	0.50	0.07	0.59	0.09
AB-SA73	3.50	2.69	25.44	5.34	28.93	5.32	4.48	5.47	58.71	1.76	0.28	-0.02	6.36	0.04	0.38	62.25	0.01	28.26	11.87	23.11	2.54	8.86	1.62	0.37	1.23	0.20	1.10	0.23	0.64	0.09	0.68	0.09
AB-SA74	4.43	1.79	31.55	6.40	30.85	6.32	1.83	4.82	156.57	0.64	0.40	-0.01	6.16	0.04	0.58	30.00	0.01	27.03	10.97	21.60	2.52	8.74	1.69	0.25	1.11	0.18	1.02	0.19	0.58	0.09	0.65	0.11
AB-SA76	5.03	5.00	34.95	6.74	55.46	5.55	2.89	5.26	124.68	2.04	0.55	-0.01	11.09	0.07	0.91	34.54	0.01	32.00	11.03	23.13	2.61	9.71	1.75	0.36	1.39	0.20	1.16	0.22	0.59	0.08	0.63	0.09
AB-SA72	5.85	8.81	35.05	7.24	5.58	11.27	17.19	23.95	174.52	9.97	0.23	0.01	2.03	0.10	2.49	253.60	0.06	95.24	80.34	162.51	18.63	67.80	12.61	2.50	8.99	1.21	6.71	1.09	2.64	0.31	2.15	0.30
AB-SA69	7.18	3.18	68.07	12.39	57.15	7.64	2.15	7.21	283.88	0.55	0.70	0.03	12.23	0.07	1.63	23.61	0.01	25.72	15.81	31.93	3.75	14.10	2.53	0.37	1.84	0.25	1.46	0.27	0.85	0.12	0.99	0.15
AB-SA79	4.48	6.39	25.52	7.76	41.77	5.77	4.82	7.90	165.36	4.94	0.43	0.00	8.75	0.08	0.57	52.29	0.02	26.77	14.64	28.89	3.31	12.10	2.43	0.47	1.82	0.28	1.74	0.32	0.93	0.14	0.97	0.14
JUW/315	n/a	n/a	n/a	n/a	n/a	n/a	4.00	4.00	80.00	2.00	n/a	n/a	n/a	n/a	n/a	40.00	n/a	42.00	9.43	19.90	2.05	6.69	1.06	0.23	0.74	0.12	0.68	0.14	0.39	0.06	0.40	0.07
JUW-BAS/314	n/a	n/a	n/a	n/a	n/a	n/a	1.00	4.80	75.00	1.40	n/a	n/a	n/a	n/a	n/a	37.00	n/a	168.00	7.44	17.70	2.13	8.50	1.69	0.26	1.13	0.16	0.83	0.16	0.46	0.07	0.47	0.08
Wuh-1-4/18	n/a	n/a	n/a	n/a	n/a	n/a	1.00	4.40	89.00	1.20	n/a	n/a	n/a	n/a	n/a	10.00	n/a	63.00	4.09	8.26	0.89	3.30	0.68	0.13	0.63	0.10	0.65	0.13	0.41	0.06	0.42	0.07
Wuh-4-2/66	n/a	n/a	n/a	n/a	n/a	n/a	1.00	5.30	145.00	3.50	n/a	n/a	n/a	n/a	n/a	8.00	n/a	30.00	8.51	16.80	1.89	7.08	1.27	0.14	0.96	0.14	0.85	0.16	0.49	0.08	0.52	0.09
Wuh-5-32-33/110	n/a	n/a	n/a	n/a	n/a	n/a	3.00	15.40	761.00	7.60	n/a	n/a	n/a	n/a	n/a	11.00	n/a	73.00	22.40	46.20	5.03	18.10	3.49	0.41	2.86	0.43	2.43	0.49	1.48	0.23	1.68	0.31
KSA 25/313	n/a	n/a	n/a	n/a	n/a	n/a	1.00	3.90	119.00	1.80	n/a	n/a	n/a	n/a	n/a	12.00	n/a	115.00	6.02	11.80	1.24	4.51	0.93	0.12	0.71	0.11	0.66	0.13	0.39	0.06	0.42	0.08
WKh-T-1/24	n/a	n/a	n/a	n/a	n/a	n/a	3.00	5.60	82.00	2.70	n/a	n/a	n/a	n/a	n/a	25.00	n/a	120.00	9.84	20.70	2.20	7.89	1.51	0.32	1.33	0.19	1.00	0.19	0.53	0.08	0.52	0.09
WKh-T-12/15	n/a	n/a	n/a	n/a	n/a	n/a	5.00	9.60	176.00	4.70	n/a	n/a	n/a	n/a	n/a	42.00	n/a	195.00	13.50	28.60	2.87	10.70	1.97	0.42	1.66	0.27	1.61	0.33	0.99	0.15	1.09	0.18
WKh-T-8/62	n/a	n/a	n/a	n/a	n/a	n/a	4.00	6.60	88.00	1.90	n/a	n/a	n/a	n/a	n/a	30.00	n/a	163.00	8.70	18.60	1.88	6.97	1.24	0.35	1.10	0.19	1.13	0.22	0.64	0.10	0.68	0.11
S2/312	n/a	n/a	n/a	n/a	n/a	n/a	2.00	5.80	143.00	4.20	n/a	n/a	n/a	n/a	n/a	15.00	n/a	219.00	6.90	13.80	1.50	5.22	1.00	0.14	0.84	0.15	0.89	0.18	0.55	0.08	0.55	0.09
WDSK-4/310	n/a	n/a	n/a	n/a	n/a	n/a	4.00	6.10	253.00	3.40	n/a	n/a	n/a	n/a	n/a	49.00	n/a	33.00	11.60	23.50	2.51	9.41	1.73	0.43	1.28	0.19	1.08	0.20	0.61	0.10	0.71	0.13
WDSK-5/32	n/a	n/a	n/a	n/a	n/a	n/a	2.00	2.90	62.00	2.20	n/a	n/a	n/a	n/a	n/a	14.00	n/a	20.00	4.24	8.67	1.03	3.80	0.71	0.14	0.53	0.10	0.56	0.11	0.32	0.05	0.33	0.06
WDSK-5-b/11	n/a	n/a	n/a	n/a	n/a	n/a	1.00	2.40	59.00	0.80	n/a	n/a	n/a	n/a	n/a	22.00	n/a	17.00	4.84	10.10	1.15	4.21	0.73	0.15	0.56	0.08	0.46	0.09	0.25	0.04	0.28	0.05
WDh-1-13/55	n/a	n/a	n/a	n/a	n/a	n/a	2.00	6.50	56.00	0.70	n/a	n/a	n/a	n/a	n/a	88.00	n/a	30.00	11.40	26.80	2.93	11.00	2.18	0.46	1.81	0.26	1.50	0.26	0.59	0.08	0.49	0.08
WDh-1-52/52	n/a	n/a	n/a	n/a	n/a	n/a	4.00	6.20	434.00	6.20	n/a	n/a	n/a	n/a	n/a	32.00	n/a	29.00	6.74	12.70	1.31	4.54	0.82	0.18	0.75	0.14	0.96	0.22	0.69	0.11	0.82	0.15
WDh-1-top/19	n/a	n/a	n/a	n/a	n/a	n/a	7.00	5.60	153.00	3.90	n/a	n/a	n/a	n/a	n/a	39.00	n/a	29.00	7.56	14.60	1.50	5.25	0.96	0.23	0.82	0.15	0.96	0.20	0.59	0.09	0.61	0.10
DIB/311	n/a	n/a	n/a	n/a	n/a	n/a	2.00	3.80	202.00	3.30	n/a	n/a	n/a	n/a	n/a	25.00	n/a	45.00	8.95	16.60	1.95	7.05	1.18	0.25	0.91	0.13	0.71	0.14	0.41	0.07	0.45	0.08

Table A4 (continued)

Sample	Hf	Ta	Tl	Pb	Bi	Th	U	V	ΣLREE	ΣHREE	ΣREE	ΣLREE/ΣHREE	Eu/Eu*	$(La/Yb)_c$	$(La/Sm)_c$	$(Gd/Yb)_c$
Tabuk area																
AB-SA120	2.84	2.06	0.10	3.41	0.02	2.66	0.79	15.00	43.54	4.54	48.08	9.58	0.75	6.44	3.56	1.21
AB-SA129	1.25	1.97	0.00	2.34	0.01	1.29	0.54	11.00	25.27	1.91	27.17	13.23	0.57	10.38	4.59	1.51
AB-SA130	0.81	0.02	0.00	0.62	0.01	0.87	0.35	8.00	55.42	2.49	57.91	22.26	0.60	21.30	3.81	4.26
AB-SA150	10.60	5.35	0.68	18.33	0.06	21.02	5.14	n/a	175.74	14.63	190.36	12.01	0.60	8.13	3.72	1.42
AB-SA152	13.61	4.16	0.40	15.25	0.03	40.25	6.89	27.00	273.80	14.23	288.02	19.25	0.41	14.25	4.22	1.98
AB-SA153	4.29	5.91	0.58	14.59	0.03	7.60	2.22	n/a	80.43	6.20	86.63	12.96	0.89	8.89	3.85	1.56
AB-SA160/T	12.85	4.19	0.64	13.80	0.04	22.32	2.95	24.00	225.32	15.49	240.81	14.55	0.58	9.37	3.95	1.37
AB-SA161	12.90	2.76	0.86	27.14	0.11	21.24	3.18	n/a	339.95	17.16	357.11	19.81	0.67	13.57	5.56	1.37
AB-SA164	n/a	n/a	n/a	n/a	n/a	n/a	n/a	29.00	n/a	n/a	n/a	n/a	n/a	n/a	n/a	n/a
AB-SA154	1.27	1.53	0.00	0.41	0.03	0.86	0.43	n/a	17.31	1.54	18.85	11.26	0.48	7.34	4.16	1.17
AB-SA156	6.33	2.32	0.01	7.63	0.03	13.77	1.98	30.00	108.71	6.21	114.92	17.50	0.50	11.49	4.19	1.60
AB-SA157	2.27	4.09	0.05	4.11	0.02	4.61	1.21	14.00	71.47	3.87	75.34	18.46	0.73	12.18	3.34	2.07
AB-SA128	12.33	1.92	0.76	16.42	0.10	16.63	3.22	60.00	155.52	19.43	174.95	8.01	0.63	4.11	4.06	0.75
AB-SA127	7.85	2.01	0.54	13.85	0.08	12.34	2.07	39.00	126.92	12.78	139.70	9.93	0.72	5.33	4.52	0.87
AB-SA132/1	2.93	1.95	0.27	7.91	0.01	6.03	1.22	17.00	91.47	3.97	95.44	23.06	0.84	20.11	9.57	1.45
AB-SA132/2	13.57	2.58	0.21	8.90	0.05	12.88	2.37	n/a	151.19	7.37	158.56	20.52	0.67	12.02	5.14	1.21
AB-SA123/2	21.69	0.35	0.00	1.36	0.04	18.23	2.42	21.00	83.27	6.11	89.38	13.62	0.39	6.28	5.51	0.76
AB-SA122/2	6.45	1.03	0.00	1.42	0.02	5.41	1.30	10.00	53.27	3.15	56.41	16.93	0.60	9.55	5.40	1.05
AB-SA124	10.32	0.74	0.02	9.55	0.03	9.65	2.29	19.00	114.75	4.94	119.69	23.22	0.62	14.64	4.64	1.80
AB-SA126	92.70	5.98	0.80	24.96	0.18	165.57	24.47	78.00	1268.74	64.11	1332.86	19.79	0.44	13.44	4.22	1.94
AB-SA145	1.86	4.33	0.00	2.26	0.03	3.60	1.40	14.00	48.57	4.00	52.57	12.13	0.68	7.15	3.73	1.15
AB-SA144/1	3.97	3.80	0.12	5.93	0.05	10.80	1.93	22.00	157.63	6.78	164.41	23.25	0.52	17.13	3.96	2.47
AB-SA142/2	12.13	1.51	0.08	14.26	0.07	12.07	3.07	21.00	106.53	8.60	115.13	12.39	0.73	7.23	3.29	1.33
AB-SA170	n/a	n/a	n/a	n/a	n/a	n/a	n/a	14.00	n/a	n/a	n/a	n/a	n/a	n/a	n/a	n/a
AB-SA167	n/a	n/a	n/a	n/a	n/a	n/a	n/a	25.00	n/a	n/a	n/a	n/a	n/a	n/a	n/a	n/a
AB-SA169	2.87	3.72	0.03	5.66	0.03	4.69	1.56	16.00	59.42	13.82	73.25	4.30	0.71	2.49	3.84	0.55
Wajid area																
AB-SA98	0.69	1.18	0.20	3.44	0.01	2.78	0.86	17.00	56.83	8.56	65.39	6.64	0.77	3.49	2.17	1.18
AB-SA80	2.68	4.45	0.01	4.71	0.01	4.10	1.06	11.00	42.2	2.73	44.88	15.44	0.43	9.96	3.07	1.88
AB-SA100	3.04	3.21	0.03	6.11	0.02	1.44	1.38	14.00	35.7	3.24	38.95	11.02	0.75	6.74	3.25	1.18
AB-SA87	1.67	4.26	0.19	7.01	0.01	3.40	1.36	n/a	51.1	3.00	54.14	17.05	0.97	12.98	3.57	2.01
AB-SA89	1.85	2.83	0.15	6.33	0.01	3.83	1.88	19.00	45.3	3.21	48.47	14.09	0.76	8.92	3.64	1.43
AB-SA90	1.77	3.94	0.11	6.10	0.01	3.34	1.61	16.00	42.8	3.48	46.24	12.28	0.90	7.67	3.96	1.15
AB-SA118	1.28	1.02	0.01	2.39	0.01	1.06	0.67	11.00	14.1	1.76	15.88	8.04	0.65	3.75	2.60	0.95
AB-SA32	1.06	0.04	0.22	2.29	0.10	5.95	8.47	9.00	82.43	5.15	87.58	16.02	0.55	6.08	1.29	1.98
AB-SA115	5.14	1.52	0.46	15.84	0.04	5.61	2.69	45.00	104.98	8.60	113.58	12.20	0.74	7.99	3.85	1.24
AB-SA62	2.80	1.85	0.02	10.73	0.03	4.02	2.80	33.00	49.77	2.88	52.65	17.28	0.75	10.72	3.63	1.58
AB-SA63	2.34	0.21	0.00	2.59	0.01	3.09	1.24	10.00	34.07	1.89	35.95	18.05	0.72	10.84	4.59	1.25
AB-SA64	3.33	1.03	0.00	3.65	0.02	3.90	1.78	18.00	42.27	2.27	44.53	18.65	0.91	11.26	3.98	1.41
AB-SA73	1.75	2.88	0.00	4.58	0.01	3.87	0.86	15.00	49.6	2.86	52.46	17.35	0.80	11.83	4.57	1.46
AB-SA74	4.33	0.17	0.00	1.32	0.01	6.20	1.09	12.00	46.87	2.61	49.48	17.93	0.55	11.46	4.05	1.39
AB-SA76	3.67	2.02	0.00	1.57	0.02	5.81	1.24	10.00	49.98	2.81	52.79	17.79	0.71	11.92	3.93	1.79
AB-SA72	4.82	2.28	0.01	14.34	0.04	12.11	2.99	20.00	353.39	13.80	367.19	25.61	0.72	25.33	3.98	3.38
AB-SA69	7.55	0.15	0.00	1.13	0.01	10.99	1.63	13.00	70.32	3.82	74.14	18.42	0.52	10.80	3.90	1.49
AB-SA79	4.81	5.46	0.01	4.25	0.02	7.50	1.67	49.00	63.65	4.23	67.88	15.05	0.68	10.30	3.76	1.52
JUW/315	2.00	0.18	n/a	n/a	n/a	4.98	0.59	14.00	40.10	1.73	41.83	23.18	0.77	16.02	5.56	1.50
JUW-BAS/314	1.90	0.15	n/a	n/a	n/a	2.98	0.97	17.00	38.85	2.08	40.93	18.68	0.58	10.75	2.75	1.95
Wuh-1-4/18	2.20	0.13	n/a	n/a	n/a	2.07	1.39	11.00	17.98	1.71	19.69	10.51	0.59	6.62	3.76	1.21
Wuh-4-2/66	3.60	0.29	n/a	n/a	n/a	5.06	1.07	11.00	36.65	2.16	38.81	16.97	0.38	11.12	4.18	1.49
Wuh-5-32-33/110	18.30	0.76	n/a	n/a	n/a	15.10	3.01	26.00	98.49	6.51	105.00	15.13	0.40	9.06	4.01	1.38
KSA 25/313	3.00	0.21	n/a	n/a	n/a	3.64	0.89	15.00	25.33	1.71	27.04	14.81	0.46	9.74	4.04	1.37
WKh-T-1/24	2.10	0.24	n/a	n/a	n/a	4.41	1.05	11.00	43.79	2.43	46.22	18.02	0.69	12.85	4.07	2.07
WKh-T-12/15	4.40	0.41	n/a	n/a	n/a	7.48	2.24	21.00	59.72	4.29	64.01	13.92	0.70	8.41	4.28	1.23
WKh-T-8/62	2.30	0.20	n/a	n/a	n/a	3.27	1.17	12.00	38.84	2.86	41.70	13.58	0.91	8.69	4.38	1.31
S2/312	3.70	0.35	n/a	n/a	n/a	4.37	1.70	35.00	29.40	2.32	31.72	12.67	0.46	8.52	4.31	1.24
WDSK-4/310	6.50	0.32	n/a	n/a	n/a	6.77	4.24	23.00	50.46	2.79	53.25	18.09	0.88	11.10	4.19	1.46
WDSK-5/32	1.70	0.21	n/a	n/a	n/a	2.65	0.80	14.00	19.12	1.42	20.54	13.46	0.67	8.73	3.73	1.30
WDSK-5-b/11	1.70	0.08	n/a	n/a	n/a	3.26	0.77	16.00	21.74	1.16	22.90	18.74	0.72	11.74	4.14	1.62
WDh-1-13/55	1.40	0.08	n/a	n/a	n/a	4.92	0.90	10.00	56.58	3.10	59.68	18.25	0.70	15.80	3.27	2.99
WDh-1-52/52	10.10	0.52	n/a	n/a	n/a	6.46	1.58	23.00	27.04	2.83	29.87	9.55	0.69	5.58	5.13	0.74
WDh-1-top/19	3.70	0.30	n/a	n/a	n/a	5.15	1.11	25.00	30.92	2.51	33.43	12.32	0.79	8.42	4.92	1.09
DIB/311	5.00	0.29	n/a	n/a	n/a	4.89	0.93	13.00	36.89	1.84	38.73	20.05	0.74	13.51	4.74	1.64

Table A5: Single-grain heavy mineral chemical data for rutiles.

JEOL JXA-8900RL Geowissenschaftliches Zentrum Universitaet G(

25.0kV — mass-% correction: Phi-rho-Z — Detection Limits [mass-%] 1-sigma count.Stat — Standard Deviations [% relative] 1-sigma count.Stat

No.	Sample	Nb_2O_5	Al_2O_3	Cr_2O_3	TiO_2	ZrO_2	SnO_2	SiO_2	FeO	V_2O_3	WO_3	wt-total	Nb_DL	Al_DL	Cr_DL	Ti_DL	Zr_DL	Sn_DL	Si_DL	Fe_DL	V_DL	W_DL	Nb_SD	Al_SD	Cr_SD	Ti_SD	Zr_SD	Sn_SD	Si_SD	Fe_SD	V_SD	W_SD
188	AB-SA100	0.0088	0.0177	0.01	97.44	0.0283	0	0.0752	0.3658	0.2219	0	98.17	0.0036	0.001	0.0016	0.0193	0.0027	0.0036	0.003	0.002	0.002	0.0051	42.79	8.8	28.8	0.22	9.18	62.33	5	1.02	0.72	100
189	AB-SA100	0.0665	0	0.0447	99.59	0.0084	0.01	0.0271	0.3847	0.1206	0	100.25	0.0039	0.0009	0.0017	0.0204	0.0027	0.0038	0.0028	0.002	0.002	0.0051	6.46	29.7	5.06	0.22	29.57	63.44	12.83	0.98	0.81	100
190	AB-SA100	0.0244	0.01	0.01	98.9	0.0351	0.01	0.0307	0.5493	0.1234	0	99.68	0.0039	0.0009	0.0017	0.0201	0.0027	0.0038	0.0028	0.002	0.002	0.0051	16.68	21.06	35.1	0.22	7.52	56.72	11.4	0.78	0.81	100
191	AB-SA100	0.0982	0	0.1284	98.5	0.0547	0	0.0306	0.3286	0.3154	0.0292	99.49	0.0039	0.001	0.0017	0.0197	0.0027	0.0038	0.0029	0.002	0.002	0.0051	4.43	126.5	2.08	0.22	4.97	156.01	11.52	1.1	0.66	23.03
192	AB-SA100	0.0345	0.0318	0.0894	98.31	0.0995	0.0066	0.0225	0.2973	0.2737	0	99.17	0.0039	0.001	0.0017	0.0206	0.0027	0.0037	0.0028	0.002	0.002	0.0051	11.99	4.8	2.76	0.22	2.9	48.01	15.51	1.17	0.68	100
193	AB-SA100	0.0319	0.01	0	98.34	0.0186	0.0151	0.0254	0.5249	0.1552	0	99.12	0.0039	0.001	0.0017	0.0208	0.0027	0.0038	0.0028	0.002	0.002	0.0051	12.88	29.24	75.03	0.22	13.6	21.31	13.74	0.8	0.78	100
158	AB-SA144/1	0.1625	0	0.0293	98.34	0.0203	0	0.0261	1.2389	0.2032	0	100.03	0.0038	0.001	0.0017	0.0206	0.0027	0.0037	0.0029	0.002	0.002	0.0052	2.82	100	7.47	0.22	12.56	112.82	13.65	0.48	0.73	100
167	AB-SA144/1	0.0847	0.01	0.0653	99.81	0.0115	0.01	0.0319	0.3504	0.1064	0	100.47	0.0038	0.0009	0.0017	0.0202	0.0027	0.0038	0.0028	0.002	0.002	0.0052	5.06	24.98	3.59	0.22	22.09	57.3	10.94	1.05	0.82	1077.91
168	AB-SA144/1	0.0361	0	0	100.08	0.0298	0	0.029	0.615	0.0892	0	100.89	0.0039	0.0009	0.0017	0.0207	0.0027	0.0038	0.0028	0.002	0.002	0.0051	11.39	31.71	211.44	0.22	8.7	79.96	12.1	0.73	0.84	100
169	AB-SA144/1	0.0295	0.01	0.0151	99.66	0.0165	0	0.0346	0.4693	0.119	0.01	100.36	0.0039	0.0009	0.0017	0.019	0.0027	0.0038	0.0028	0.002	0.002	0.0051	13.85	23.12	14.01	0.22	15.3	103.98	10.11	0.86	0.81	110.47
170	AB-SA144/1	0.2852	0.0151	0.0892	99.9	0.0858	0	0.0194	0.1327	0.1356	0.0251	100.69	0.0039	0.001	0.0017	0.0203	0.0027	0.0038	0.0028	0.002	0.002	0.0051	1.77	9.97	2.77	0.22	3.32	83.79	18.07	2.17	0.79	26.67
171	AB-SA144/1	0.2387	0	0.1266	99.96	0.0934	0.0108	0.0219	0.0805	0.3307	0.0157	100.89	0.0039	0.001	0.0017	0.0195	0.0027	0.0038	0.0029	0.002	0.002	0.0051	2.05	30.76	2.09	0.22	3.09	29.8	16.04	3.28	0.64	42.76
172	AB-SA144/1	0.0533	0	0.0372	99.59	0.0326	0	0.0284	0.5732	0.0909	0	100.42	0.0039	0.0009	0.0017	0.02	0.0027	0.0038	0.0028	0.002	0.002	0.0052	7.9	35.74	5.92	0.22	8.01	104.25	12.33	0.76	0.84	203.95
173	AB-SA144/1	0.0878	0	0.0599	99.7	0.0428	0.0086	0.0306	0.4984	0.1493	0	100.57	0.0038	0.0009	0.0017	0.0196	0.0027	0.0038	0.0028	0.002	0.002	0.0051	4.88	100	3.9	0.22	6.19	37.22	11.43	0.83	0.78	2251.94
372	AB-SA144/1	0.0872	0	0.0677	97.97	0.0558	0	0.0221	0.454	0.157	0	98.82	0.0038	0.0009	0.0017	0.0198	0.0027	0.0038	0.0028	0.002	0.002	0.0051	4.92	66.24	3.49	0.22	4.82	610.67	15.9	0.88	0.77	217.39
175	AB-SA144/1	0.6333	0.0191	0.0647	98.33	0.0374	0.0175	0.0238	0.5528	0.091	0.0659	99.83	0.0039	0.0009	0.0017	0.0202	0.0027	0.0038	0.0028	0.002	0.002	0.0052	0.95	7.87	3.65	0.22	7.05	18.64	14.66	0.78	0.85	10.42
176	AB-SA144/1	0.5793	0	0.0085	98.19	0.0669	0.0202	0.0294	0.7805	0.1954	0.0855	99.96	0.0039	0.001	0.0017	0.0195	0.0027	0.0038	0.0029	0.002	0.002	0.0052	1.02	38.02	24.03	0.22	4.15	16.21	11.94	0.63	0.74	8.09
159	AB-SA144/1	0.4726	0	0.0992	96.94	0.0387	0.1661	0.0266	1.0621	0.1926	0.5557	99.55	0.0039	0.001	0.0017	0.0207	0.0027	0.0038	0.0029	0.002	0.002	0.0052	1.2	40.17	2.51	0.22	6.91	2.23	12.88	0.52	0.75	1.36
177	AB-SA144/1	0.4343	0	0.5965	98.42	0.011	0.0425	0.0213	0.4845	0.1448	0.0087	100.16	0.0039	0.001	0.0017	0.0202	0.0027	0.0038	0.0028	0.002	0.002	0.0052	1.26	122.8	0.7	0.22	22.82	7.86	16.24	0.84	0.79	78.97
178	AB-SA144/1	0.5395	0	0	98.4	0.0234	0.0275	0.0242	0.6037	0.0656	0.01	99.7	0.0038	0.0009	0.0016	0.0216	0.0027	0.0038	0.0028	0.002	0.002	0.0052	1.07	30.33	46.84	0.22	10.94	12.04	14.38	0.73	0.88	128.69
179	AB-SA144/1	0.0565	0.01	0.1351	99.11	0.0591	0.01	0.0291	0.5058	0.0779	0.0261	100.01	0.0039	0.001	0.0017	0.0205	0.0027	0.0038	0.0028	0.002	0.002	0.0051	7.47	22.19	1.96	0.22	4.59	62.81	12.05	0.82	0.86	25.75
180	AB-SA144/1	0.1921	0.0161	0.1907	97.95	0.1432	0.0105	0.0243	0.0751	0.3938	0.0205	99.02	0.0039	0.0009	0.0017	0.0198	0.0027	0.0038	0.0028	0.002	0.002	0.0051	2.46	9.22	1.52	0.22	2.13	30.7	14.37	3.48	0.61	32.73
181	AB-SA144/1	0.2203	0.01	0.0367	98.44	0.1205	0.01	0.026	0.5433	0.0776	0	99.48	0.0039	0.0009	0.0017	0.0207	0.0027	0.0038	0.0028	0.002	0.002	0.0051	2.18	25.36	6.02	0.22	2.47	52.53	13.45	0.79	0.86	376.9
182	AB-SA144/1	0.1503	0.01	0.01	98.25	0	0.0112	0.0282	0.7764	0.116	0.011	99.36	0.0039	0.001	0.0017	0.0205	0.0027	0.0038	0.0028	0.002	0.002	0.0051	3.05	25.05	28.96	0.22	100	28.79	12.41	0.63	0.82	61.13
183	AB-SA144/1	0.3394	0.01	0.0714	98.07	0.0798	0.01	0.0287	0.4627	0.1973	0.0962	99.36	0.0039	0.0009	0.0017	0.0203	0.0027	0.0038	0.0028	0.002	0.002	0.0051	1.53	14.85	3.35	0.22	3.5	60.51	12.2	0.87	0.74	7.13
373	AB-SA144/1	0.1641	0	0.2085	98.02	0.0524	0	0.0205	0.1221	0.143	0	98.74	0.0039	0.0009	0.0017	0.02	0.0027	0.0038	0.0028	0.0019	0.002	0.0051	2.81	63.37	1.43	0.22	5.08	79.61	16.97	2.29	0.79	100
185	AB-SA144/1	0.0348	0.01	0.1637	98.23	0.0551	0.0242	0.0283	0.0717	0.516	0.0092	99.14	0.0039	0.001	0.0017	0.0204	0.0027	0.0038	0.0028	0.002	0.002	0.0051	11.95	17.37	1.71	0.22	4.84	13.5	12.31	3.61	0.56	72.55
186	AB-SA144/1	0.0962	0.01	0.0297	97.9	0.0315	0.0123	0.0322	0.3496	0.1767	0.0662	98.7	0.0039	0.0009	0.0017	0.0205	0.0027	0.0038	0.0028	0.002	0.002	0.0051	4.53	23.64	7.3	0.22	8.25	26.28	10.81	1.05	0.76	10.3
160	AB-SA144/1	0.1548	0	0.1859	99.32	0.0241	0	0.0239	0.2922	0.0769	0.01	100.09	0.0039	0.0009	0.0017	0.0203	0.0027	0.0038	0.0028	0.002	0.002	0.0051	2.94	74.45	1.55	0.22	10.67	132.13	14.7	1.19	0.86	128.25
187	AB-SA144/1	0.1382	0	0.0907	98.17	0.01	0	0.0274	0.7012	0.121	0	99.25	0.0039	0.0009	0.0017	0.0196	0.0027	0.0038	0.0028	0.002	0.002	0.0052	3.27	1408.65	2.71	0.22	38.82	100	12.75	0.67	0.81	100
161	AB-SA144/1	0.1448	0.01	0.0423	99.39	0.0921	0.01	0.0286	0.1942	0.2009	0.0118	100.13	0.0038	0.0009	0.0017	0.0203	0.0027	0.0038	0.0028	0.002	0.002	0.0051	3.12	19.04	5.25	0.22	3.12	32.39	12.27	1.6	0.73	57.2
162	AB-SA144/1	0.3849	0	0.0147	98.82	0.0513	0.0291	0.0307	0.6877	0.119	0.0379	100.18	0.0038	0.001	0.0017	0.0197	0.0027	0.0038	0.0028	0.002	0.002	0.0051	1.38	178.84	14.2	0.22	5.24	11.24	11.38	0.68	0.81	17.88
163	AB-SA144/1	0.2942	0	1.1675	98.18	0.01	0.1325	0.014	0.2768	0.0087	0.3252	100.4	0.0039	0.001	0.0017	0.0203	0.0027	0.0038	0.0029	0.002	0.002	0.0051	1.72	24486.09	0.48	0.22	37.83	2.7	24.18	1.23	0.98	2.22
371	AB-SA144/1	0.0663	0	0.076	98.3	0.0353	0.0129	0.0278	0.1974	0.2338	0.0367	98.98	0.0039	0.0009	0.0017	0.0201	0.0027	0.0038	0.0028	0.002	0.002	0.0051	6.45	148.81	3.17	0.22	7.4	24.86	12.61	1.58	0.71	18.36
165	AB-SA144/1	0.1567	0	0.0725	99.57	0.0582	0	0.0239	0.4875	0.056	0	100.43	0.0039	0.0009	0.0017	0.0207	0.0027	0.0038	0.0029	0.002	0.002	0.0051	2.92	100	3.28	0.22	4.63	118.08	14.73	0.84	0.89	405.18
166	AB-SA144/1	0.0175	0.0112	0.0699	99.8	0.0144	0	0.0303	0.3627	0.0944	0	100.4	0.0039	0.0009	0.0017	0.0202	0.0027	0.0038	0.0028	0.002	0.002	0.0051	23.63	13.08	3.4	0.22	17.77	100	11.51	1.02	0.84	4330.31
2	AB-SA152	0.2647	0.01	0.0712	98.39	0	0.011	0.0382	0.643	0.1606	0.0293	99.62	0.0038	0.001	0.0017	0.0201	0.0027	0.0037	0.0029	0.002	0.002	0.0052	1.84	19.95	3.35	0.22	51.29	28.74	9.41	0.71	0.78	23.31
11	AB-SA152	0.2543	0.0151	0.108	98.51	0.3003	0	0.0234	0.2235	0.2333	0	99.67	0.0039	0.0009	0.0017	0.0206	0.0028	0.0038	0.0028	0.002	0.002	0.0052	1.95	9.81	2.38	0.22	1.21	77.46	14.96	1.45	0.71	100
356	AB-SA152	0.0935	0.0126	0.021	99.02	0.0957	0	0.0277	0.3648	0.1138	0.0085	99.75	0.0039	0.0009	0.0017	0.0204	0.0027	0.0038	0.0028	0.002	0.002	0.0051	4.67	11.43	10.22	0.22	3	100	12.6	1.01	0.81	78.1
13	AB-SA152	0.3404	0	0.0184	98.35	0.0119	0.2304	0.0287	0.4942	0.162	0.0256	99.67	0.0039	0.0009	0.0017	0.0198	0.0027	0.0038	0.0029	0.002	0.002	0.0053	1.54	46.27	11.5	0.22	21.36	1.67	11.62	0.84	0.78	26.94
14	AB-SA152	1.0669	0.1297	0.0183	97.93	0.1234	0.0271	0.0244	0.4642	0.0812	0	99.87	0.0039	0.0009	0.0017	0.0197	0.0027	0.0038	0.0029	0.002	0.002	0.0053	0.67	1.32	11.62	0.22	2.41	12.22	14.36	0.88	0.87	100
15	AB-SA152	0.286	0	0.6323	98.54	0.0585	0.0142	0.024	0.0612	0.1596	0	99.77	0.0039	0.0009	0.0017	0.0202	0.0027	0.0038	0.0029	0.002	0.002	0.0052	1.76	205.05	0.68	0.22	4.67	22.97	14.66	4.2	0.78	100
16	AB-SA152	0.0352	0	0	99.24	0.0434	0.0095	0.0306	0.3369	0.1048	0	99.81	0.0039	0.0009	0.0017	0.0197	0.0027	0.0038	0.0028	0.002	0.002	0.0052	11.75	100	62.37	0.22	6.16	34.03	11.39	1.09	0.84	145.9
17	AB-SA152	0.0968	0.0123	0.1045	99.68	0.1028	0	0.0281	0.1919	0.0509	0	100.27	0.0039	0.0009	0.0017	0.0197	0.0028	0.0038	0.0029	0.002	0.002	0.0052	4.55	11.95	2.45	0.22	2.87	66.49	12.55	1.62	0.9	100
18	AB-SA152	0.2789	0.014	0.0114	98.03	0.0386	0.086	0.0295	0.4456	0.1773	0.069	99.18	0.0039	0.001	0.0017	0.0201	0.0027	0.0038	0.0029	0.002	0.002	0.0052	1.81	10.7	18.22	0.22	6.83	4.02	11.83	0.9	0.76	10.06
19	AB-SA152	0.6538	0.0133	0.0253	95.77	0.0578	0.1326	0.024	1.1954	0.1696	0.9964	99.04	0.0039	0.001	0.0017	0.0209	0.0028	0.0039	0.0029	0.002	0.002	0.0053	0.95	11.33	8.55	0.23	4.86	2.78	14.42	0.49	0.78	0.84
20	AB-SA152	0.0782	0.01	0.0098	98.99	0.0164	0	0.0353	0.3151	0.2323	0.012	99.7	0.0039	0.001	0.0017	0.0206	0.0027	0.0038	0.0029	0.002	0.002	0.0052	5.53	17.55	21.29	0.22	15.4	106.99	10.05	1.14	0.71	57.09
3	AB-SA152	0.6207	0	0.3904	97.79	0.016	0.0226	0.0214	0.5228	0.0626	0.0708	99.51	0.0039	0.001	0.0017	0.0202	0.0027	0.0037	0.0028	0.002	0.002	0.0052	0.97	100.93	0.93	0.22	15.95	14.39	16.29	0.81	0.89	9.79
21	AB-SA152	0.0394	0	0.0204	99.74	0.0964	0	0.0245	0.02	0.5936	0	100.54	0.0039	0.0009	0.0017	0.0202	0.0027	0.0038	0.0028	0.002	0.002	0.0052	10.59	103.76	10.47	0.22	2.98	220.74	14.26	11.89	0.53	1683.98
22	AB-SA152	0.0439	0	0.0919	98.84	0.0129	0	0.0305	0.4495	0.2071	0	99.68	0.0039	0.0009	0.0017	0.0193	0.0027	0.0038	0.0028	0.002	0.002	0.0052	9.48	55.3	2.71	0.22	19.65	121.95	11.47	0.89	0.73	100
23	AB-SA152	0.2854	0.0473	0.2691	98.17	0.2564	0	0.0254	0.1608	0.3857	0.0146	99.62	0.0039	0.0009	0.0017	0.0204	0.0027	0.0038	0.0028	0.002	0.002	0.0052	1.77	3.25	1.19	0.22	1.35	86.87	13.81	1.87	0.62	46.63
357	AB-SA152	0.3284	0.01	0.297	98.25	0.1214	0.0239	0.0183	0.0215	1.0979	0.0821	100.24	0.0039	0.0009	0.0017	0.0199	0.0027	0.0038	0.0029	0.002	0.002	0.0051	1.57	24.54	1.11	0.22	2.45	13.84	19.2	10.93	0.42	8.28
25	AB-SA152	0.1359	0	0.302	98.49	0.0701	0.0216	0.0224	0.0344	0.8416	0.089	100.01	0.0039	0.0009	0.0017	0.02	0.0028	0.0038	0.0028	0.002	0.002	0.0052	3.32	100	1.11	0.22	4.02	15.16	15.54	7.04	0.47	7.84
26	AB-SA152	0.2814	0	0.4508	98.72	0.0848	0	0.0248	0.1655	0.1194	0.0138	99.87	0.0039	0.0009	0.0017	0.0199	0.0027	0.0038	0.0028	0.002	0.002	0.0052	1.78	100	0.84	0.22	3.37	109.17	14.15	1.82	0.82	49.8
27	AB-SA152	0.0871	0.0268	0.0163	97.07	0.0132	0	0.0608	0.5647	0.1371	0	97.98	0.0046	0.0008	0.0017	0.0195	0.0028	0.0041	0.0024	0.002	0.002	0.0053	5.72	5.08	13.27	0.22	19.7	180.79	5.02	0.78	0.8	623.43
28	AB-SA152	0.2291	0.0166	0.257	98.65	0.0275	0.01	0.044	0.2244	0.0893	0.0502	99.6	0.004	0.0009	0.0017	0.0206	0.0027	0.0038	0.0028	0.002	0.002	0.0052	2.14	8.81	1.23	0.22	9.45	53.65	7.97	1.44	0.85	13.72
29	AB-SA152	0.0326	0.0301	0.0137	99.41	0.0394	0	0.0794	0.3777	0.0996	0.0246	100.11	0.0035	0.001	0.0017	0.0201	0.0028	0.0036	0.003	0.002	0.002	0.0052	11.61	5.2	15.27	0.22	6.86	370.74	4.68	1	0.84	27.57
30	AB-SA152	0.2017	0	0.165	99.22	0.032	0.0168	0.0265	0.1471	0.2763	0.0362	100.12	0.0039	0.001	0.0017	0.0192	0.0027	0.0038	0.0029	0.002	0.002	0.0052	2.36	30.68	1.69	0.22	8.25	19.33	13.38	2.01	0.68	18.95
4	AB-SA152	2.94	0.0238	0.058	93.24	0.0423	0.0075	0.0283	2.08	0.04	0.0337	98.5	0.004	0.001	0.0017	0.0204	0.0028	0.0038	0.0029	0.002	0.002	0.0053	0.36	6.44	4.06	0.23	6.48	44.6	12.74	0.36	0.96	20.61
31	AB-SA152	0.4089	0.0475	0.01	97.56	0.037	0.0688	0.0745	0.4572	0.0868	0.066	98.82	0.0038	0.001	0.0017	0.0207	0.0028	0.0037	0.0029	0.002	0.002	0.0052	1.3	3.29	33.64	0.22	7.32	4.81	4.79	0.88	0.86	10.45
32	AB-SA152	0.2282	0.1159	0.0493	98.29	0.095	0.0219	0.2212	0.829	0.035	0.0718	99.96	0.0029	0.001	0.0016	0.0211	0.0029	0.0031	0.0032	0.002	0.002	0.0052	1.78	1.55	4.52	0.22	3.21	12.55	1.87	0.61	0.94	9.67
33	AB-SA152	0.14	0	0.1159	99.03	0.0384	0.0128	0.0249	0.5274	0.11	0	100.01	0.0039	0.001	0.0017	0.0206	0.0027	0.0038	0.0029	0.002	0.002	0.0052	3.22	43.71	2.24	0.22	6.85	25.17	14.14	0.8	0.82	136.11
358	AB-SA152	0.065	0.01	0.2564	99.94	0.1027	0	0.0286	0.1134	0.0733	0	100.59	0.0038	0.0009	0.0017	0.0199	0.0027	0.0038	0.0028	0.0019	0.002	0.0051	6.46	17.86	1.22	0.22	2.82	100	12.2	2.42	0.86	519.31
35	AB-SA152	2.37	0.0641	0.0376	95.05	0.0727	0.0635	0.0259	1.67	0.0817	0.0805	99.51	0.004	0.001	0.0017	0.0192	0.0028	0.0038	0.0029	0.002	0.002	0.0053	0.41	2.51	5.93	0.23	3.92	5.46	13.68	0.41	0.88	8.74
36	AB-SA152	0.1718	0	0.0248	99.23	0.0145	0.0091	0.0266	0.5292	0.1108	0.0169	100.14	0.0039	0.0009	0.0017	0.0198	0.0027	0.0038	0.0028	0.002	0.002	0.0052	2.71	160.76	8.72	0.22	17.63	35.27	13.17	0.8	0.82	40.49
37	AB-SA152	0.0457	0	0.0536	98.47	0.0455	0.01	0.0284	0.5006	0.0793	0.0131	99.24	0.0039	0.0009	0.0017	0.0202	0.0027	0.0038	0.0028	0.002	0.002	0.0052	9.14	208.69	4.31	0.22	5.89	59.29	12.36	0.83	0.87	52.21
38	AB-SA152	0.289	0.0321	0	98.94	0.0556	0.0279	0.0276	0.3728	0.0262	0.0687	99.84	0.0039	0.001	0.0017	0.0205	0.0027	0.0038	0.0028	0.002	0.002	0.0052	1.74	4.76	100	0.22	4.88	11.72	12.63	1.01	0.94	10.09
39	AB-SA152	0.0546	0	0.1722	98.97	0.0118	0.0358	0.0286	0.1655	0.202	0.0215	99.66	0.0039	0.0009	0.0017	0.0202	0.0027	0.0038	0.0028	0.002	0.002	0.0052	7.75	37.86	1.64	0.22	21.27	9.29	12.16	1.84	0.74	31.86
40	AB-SA152	0.3178	0	0.2274	98.1	0.0849	0.0243	0.0272	0.3859	0.2422	0.0105	99.42	0.0039	0.0009	0.0017	0.0211	0.0027	0.0038	0.0029	0.002	0.002	0.0052	1.62	141.57	1.34	0.22	3.31	13.48	12.91	0.99	0.71	65.56
5	AB-SA152	0.0822	0	0.012	98.53	0.0572	0	0.0288	0.6108	0.2061	0	99.53	0.0039	0.001	0.0017	0.0199	0.0027	0.0038	0.0028	0.002	0.002	0.0052	5.27	100	17.45	0.22	4.76	122.63	12.16	0.73	0.73	100
41	AB-SA152	0.157	0	0.0404	98.95	0.0815	0.0105	0.0228	0.4387	0.0467	0.0933	99.85	0.0039	0.0009	0.0017	0.0205	0.0027	0.0038	0.0028	0.002	0.002	0.0052	2.93	42.58	5.52	0.22	3.49	30.88	15.39	0.9	0.91	7.46
42	AB-SA152	0.1696	0.0214	0.01	98.66	0.0658	0	0.0339	0.552	0.1538	0.0213	99.69	0.0039	0.001	0.0017	0.0204	0.0027	0.0038	0.0029	0.002	0.002	0.0052	2.73	7.05	34.8	0.22	4.17	116.82	10.43	0.78	0.78	32.02
43	AB-SA152	0.0638	0.01	0.418	97.98	0.1713	0.0321	0.0185	0.0437	0.5239	0	99.27	0.0039	0.0009	0.0017	0.0197	0.0027	0.0038	0.0028	0.002	0.002	0.0052	6.7	14.58	0.89	0.22	1.85	10.28	18.7	5.67	0.56	155.74
359	AB-SA152	0.2397	0.01	0.0123	99.79	0.0443	0.0244	0.0421	0.3265	0.0383	0	100.53	0.0038	0.0009	0.0017	0.0204	0.0027	0.0038	0.0028	0.002	0.002	0.0051	2.02	19.26	16.93	0.22	6.05	13.35	8.25	1.1	0.91	316.92
45	AB-SA152	2.17	0.0758	0	93.68	0.0392	0.0865	0.0349	1.54	0.0926	0.11	97.84	0.004	0.001	0.0017	0.0195	0.0028	0.0038	0.0029	0.002	0.002	0.0053	0.43	2.15	89.51	0.23	6.92	4.1	10.11	0.42	0.87	6.46
46	AB-SA152	0.1885	0	0.1059	97.65	0.0404	0.0211	0.0245	0.018	0.4316	0	98.48	0.0039	0.0009	0.0017	0.0197	0.0027	0.0038	0.0029	0.002	0.002	0.0052	2.5	100	2.41	0.22	6.55	15.46	14.27	12.91	0.6	319.92
47	AB-SA152	0.6964	0	0.0542	96.58	0.036	0.0107	0.0289	1.0326	0.0162	0.0675	98.52	0.0039	0.0009	0.0017	0.0199	0.0027	0.0038	0.0029	0.002	0.002	0.0052	0.9	90.92	4.27	0.22	7.34	30.66	12.23	0.53	0.97	10.25
48	AB-SA152	0.62	0.0114	0.0556	96.33	0.0663	0.0118	0.0307	0.6754	0.1151	0.022	97.94	0.0039	0.0009	0.0017	0.019	0.0027	0.0038	0.0028	0.002	0.002	0.0052	0.98	13.01	4.18	0.22	4.19	27.76	11.42	0.69	0.84	31.12
49	AB-SA152	0.3007	0	0.0931	97.32	0.0784	0.0064	0.0311	0.6817	0.1166	0.0326	98.66	0.0039	0.001	0.0017	0.0206	0.0027	0.0038	0.0029	0.002	0.002	0.0052	1.71	280.86	2.67	0.22	3.59	50.91	11.37	0.68	0.83	21.02
50	AB-SA152	0.6069	0.0292	0.1019	97.32	0.1034	0.0075	0.0444	0.7143	0.0388	0.0193	98.98	0.0039	0.001	0.0017	0.0206	0.0027	0.0038	0.0029	0.002	0.002	0.0052	0.99	5.22	2.5	0.22	2.83	43.46	8.01	0.67	0.93	35.67
6	AB-SA152	0.1802	0	0.1056	98.33	0.1068	0	0.0265	0.378	0.1258	0	99.25	0.0039	0.0009	0.0017	0.0201	0.0027	0.0038	0.0028	0.002	0.002	0.0052	2.59	100	2.42	0.22	2.75	100	13.19	1	0.81	100
51	AB-SA152	0.3768	0	0.0477	97.2	0.0111	0.0592	0.0351	0.6048	0.0817	0	98.42	0.0039	0.0009	0.0017	0.019	0.0027	0.0038	0.0028	0.002	0.002	0.0052	1.42	86.84	4.76	0.22	22.62	5.7	9.89	0.74	0.87	359.9
52	AB-SA152	0.2031	0	0.0686	97.92	0.0175	0.0286	0.0247	0.6531	0.1664	0.0631	99.15	0.0039	0.001	0.0017	0.0202	0.0027	0.0038	0.0029	0.002	0.002	0.0052	2.35	30.22	3.45	0.22	14.73	11.42	14.2	0.71	0.77	10.97
53	AB-SA152	0.1726	0	0.0427	98.94	0.0246	0.0445	0.0333	0.4448	0.1592	0.0144	99.88	0.0038	0.0009	0.0017	0.0206	0.0027	0.0038	0.0029	0.002	0.002	0.0052	2.67	37.74	5.27	0.22	10.54	7.49	10.53	0.9	0.77	47.37
360	AB-SA152	0.0899	0.0344	0.0895	100.38	0.163	0	0.0267	0.084	0.3156	0.0069	101.19	0.0039	0.0009	0.0017	0.0201	0.0027	0.0038	0.0028	0.002	0.002	0.0051	4.82	4.27	2.73	0.22	1.91	94.98	13.07	3.15	0.65	95.96
7	AB-SA152	0.7915	0.038	0.1829	97.14	0.1006	0.0677	0.0322	0.2178	0.4103	0.1507	99.13	0.0039	0.001	0.0017	0.0196	0.0028	0.0038	0.0028	0.002	0.002	0.0052	0.82	4.06	1.58	0.22	2.92	5.06	10.77	1.48	0.61	4.67
8	AB-SA152	0.1496	0	0.0143	98.96	0.0482	0.1378	0.0233	0.3665	0.2547	0.041	100	0.0039	0.0009	0.0017	0.021	0.0027	0.0038	0.0028	0.002	0.002	0.0052	3.03	55.6	14.79	0.22	5.65	2.59	14.43	1.02	0.7	16.74
9	AB-SA152	0.3471	0.035	0.0974	98.67	0.2007	0.0086	0.0244	0.1371	0.2871	0.0111	99.81	0.0039	0.0009	0.0017	0.02	0.0027	0.0038	0.0028	0.002	0.002	0.0052	1.52	4.36	2.57	0.22	1.64	37.56	14.37	2.11	0.68	60.93
10	AB-SA152	0.2598	0.0218	0.0995	98.3	0.1113	0.0069	0.0266	0.0634	0.4158	0	99.31	0.0039	0.001	0.0017	0.0198	0.0027	0.0038	0.0028	0.002	0.002	0.0052	1.9	6.9	2.56	0.22	2.65	46.79	13.09	4.04	0.61	100
115	AB-SA170	0.0785	0.01	0.0275	99.46	0.0777	0.0065	0.0322	0.4633	0.127	0	100.29	0.0042	0.001	0.0017	0.0205	0.0027	0.0038	0.0029	0.002	0.002	0.0052	5.84	16.26	7.92	0.22	3.63	50.13	11.1	0.87	0.81	100
367	AB-SA170	0.0386	0.0231	0	99.34	0.0625	0.01	0.0319	0.3226	0.0572	0.0159	99.91	0.0039	0.0009	0.0017	0.0201	0.0027	0.0038	0.0028	0.002	0.002	0.0051	10.67	6.35	73.47	0.22	4.36	52.68	10.95	1.1	0.89	41.68
125	AB-SA170	0.0092	0	0.1543	101.07	0.0133	0.01	0.0174	0.4373	0.1068	0.019	101.83	0.0039	0.001	0.0017	0.0199	0.0027	0.0038	0.0029	0.002	0.002	0.0051	43.32	1341.47	1.79	0.22	19.2	55.97	20.31	0.91	0.82	35.35
126	AB-SA170	0.5946	0.0553	0	98.3	0.0313	0.0311	0.0241	0.7873	0.1057	0.1391	100.07	0.0039	0.001	0.0017	0.0201	0.0027	0.0038	0.0029	0.002	0.002	0.0052	1.01	2.88	45.54	0.22	8.38	10.8	14.61	0.63	0.84	5.03
127	AB-SA170	0.2581	0	0.2598	99.43	0.0203	0.0149	0.0263	0.1059	0.1847	0.0425	100.35	0.0039	0.001	0.0017	0.0206	0.0027	0.0038	0.0029	0.002	0.002	0.0052	1.92	80.78	1.23	0.22	12.7	21.93	13.43	2.62	0.75	16.02
128	AB-SA170	0.0729	0.01	0.0123	99.29	0.0601	0.0174	0.0223	0.3118	0.1997	0.0525	100.04	0.0039	0.001	0.0017	0.0208	0.0027	0.0038	0.0029	0.002	0.002	0.0051	5.9	23.98	16.98	0.22	4.51	18.51	15.74	1.14	0.74	12.96
129	AB-SA170	0.2491	0.0353	0.161	98.9	0.0985	0.0169	0.0228	0.1305	0.4968	0.127	100.24	0.0039	0.001	0.0017	0.0207	0.0027	0.0038	0.0029	0.002	0.002	0.0052	1.99	4.37	1.73	0.22	2.96	19.4	15.41	2.22	0.57	5.48
130	AB-SA170	0.2347	0.0406	0.0569	99.25	0.0192	0.023	0.0301	0.1881	0.2389	0.013	100.09	0.0039	0.001	0.0017	0.0207	0.0027	0.0038	0.0028	0.002	0.002	0.0052	2.08	3.82	4.11	0.22	13.5	14.23	11.58	1.65	0.71	52.48
131	AB-SA170	2.33	0.0259	0.0417	95.07	0.0353	0.0656	0.0657	1.51	0.1967	0.0738	99.42	0.004	0.001	0.0017	0.0195	0.0028	0.0038	0.0029	0.002	0.002	0.0053	0.42	5.99	5.44	0.23	7.61	5.38	5.55	0.43	0.76	9.46
132	AB-SA170	0.0802	0.01	0.0492	98.98	0.0333	0	0.0251	0.6131	0.1261	0	99.91	0.0039	0.001	0.0017	0.0205	0.0027	0.0038	0.0029	0.002	0.002	0.0052	5.37	23.22	4.73	0.22	7.9	100	14.16	0.73	0.81	244.26
133	AB-SA170	0.1301	0.0105	0.045	99.76	0.0201	0.01	0.0304	0.2927	0.1053	0.0116	100.41	0.0038	0.001	0.0017	0.0211	0.0027	0.0038	0.0029	0.002	0.002	0.0052	3.43	14.21	5.06	0.22	12.81	63.14	11.59	1.2	0.83	58.22

Table A5 (continued)

JEOL JXA-8900RL Geowissenschaftliches Zentrum Universitaet G

25.0kV mass-% correction: Phi-rho-Z | Detection Limits [mass-%] 1-sigma count.Stat | Standard Deviations [% relative] 1-sigma count.Stat

No.	Sample	Nb_2O_5	Al_2O_3	Cr_2O_3	TiO_2	ZrO_2	SnO_2	SiO_2	FeO	V_2O_3	WO_3	wt-total	Nb_DL	Al_DL	Cr_DL	Ti_DL	Zr_DL	Sn_DL	Si_DL	Fe_DL	V_DL	W_DL	Nb_SD	Al_SD	Cr_SD	Ti_SD	Zr_SD	Sn_SD	Si_SD	Fe_SD	V_SD	W_SD
116	AB-SA170	0.2208	0.01	0.1474	99.89	0.5442	0	0.0292	0.0885	0.3702	0	101.3	0.004	0.001	0.0017	0.0201	0.0028	0.0038	0.0029	0.002	0.002	0.0052	2.21	20.42	1.86	0.22	0.8	100	12.33	3.05	0.63	100
368	AB-SA170	0.1425	0	0.1359	98.56	0.1193	0.0074	0.0233	0.3954	0.1458	0.018	99.55	0.0039	0.0009	0.0017	0.0201	0.0027	0.0038	0.0028	0.002	0.002	0.0051	3.17	201.31	1.97	0.22	2.48	43.84	15.02	0.96	0.78	37.01
135	AB-SA170	0.1076	0	0.021	98.86	0.0201	0	0.0249	0.4042	0.1171	0.0169	99.58	0.0039	0.001	0.0017	0.0205	0.0027	0.0038	0.0028	0.002	0.002	0.0052	4.09	42.88	10.23	0.22	12.71	159.89	14.14	0.96	0.82	40.18
136	AB-SA170	0.0915	0	0.0292	99.24	0.0139	0	0.0276	0.2155	0.1542	0	99.78	0.0039	0.001	0.0017	0.0204	0.0028	0.0038	0.0028	0.002	0.002	0.0052	4.8	34.17	7.46	0.22	18.57	79.39	12.74	1.49	0.78	100
137	AB-SA170	0.1169	0.0183	0.0232	99.88	0.0411	0.0066	0.029	0.1715	0.2111	0.0175	100.52	0.0039	0.0009	0.0017	0.0206	0.0027	0.0038	0.0029	0.002	0.002	0.0052	3.81	8.21	9.31	0.22	6.51	48.44	12.15	1.77	0.73	38.66
138	AB-SA170	0.0184	0.0131	0.018	98.86	0.0348	0	0.0246	0.5595	0.1187	0.0225	99.67	0.0039	0.0009	0.0017	0.0204	0.0027	0.0038	0.0029	0.002	0.002	0.0052	22.33	11.32	11.84	0.22	7.59	143.25	14.36	0.77	0.82	30.17
139	AB-SA170	0.0486	0	0.299	98.15	0.01	0	0.0255	0.6846	0.0418	0	99.26	0.0039	0.001	0.0017	0.021	0.0027	0.0038	0.0028	0.002	0.002	0.0052	8.72	100	1.11	0.22	45.12	71.57	13.78	0.68	0.92	175.96
140	AB-SA170	0.1002	0	0.0752	99.05	0.0348	0.0089	0.0273	0.9141	0.2073	0	100.41	0.0039	0.001	0.0017	0.0207	0.0027	0.0038	0.0029	0.002	0.002	0.0052	4.42	100	3.18	0.22	7.56	36.32	12.94	0.57	0.73	100
141	AB-SA170	0.2701	0.01	0.1768	98.34	0.2185	0.01	0.0238	0.1195	0.2491	0	99.42	0.0039	0.0009	0.0017	0.0203	0.0027	0.0038	0.0029	0.002	0.002	0.0051	1.85	18.35	1.6	0.22	1.52	58.02	14.78	2.34	0.7	180.24
142	AB-SA170	0.1205	0.01	0.068	98.83	0.0386	0.01	0.0312	0.4134	0.2208	0	99.73	0.0039	0.0009	0.0017	0.0198	0.0027	0.0038	0.0028	0.002	0.002	0.0051	3.69	24.04	3.49	0.22	6.78	63.37	11.25	0.94	0.72	188.59
143	AB-SA170	0.0654	0.0167	0.01	96.97	0.0081	0	0.0778	1.83	0.0452	0.0187	99.05	0.0039	0.0009	0.0017	0.0208	0.0027	0.0038	0.0028	0.002	0.002	0.0051	6.5	8.98	32.17	0.22	30.66	103.04	4.62	0.38	0.92	35.96
117	AB-SA170	0.2665	0.0266	0.0712	97.62	0.3448	0	0.0374	0.4092	0.3606	0	99.14	0.004	0.0009	0.0017	0.0198	0.0028	0.0038	0.0029	0.002	0.002	0.0052	1.91	5.66	3.4	0.22	1.09	100	9.46	0.95	0.64	100
369	AB-SA170	0.1345	0.0103	0.0188	98.58	0.0237	0.01	0.0253	0.5725	0.0969	0.0126	99.48	0.0039	0.0009	0.0017	0.0198	0.0027	0.0038	0.0028	0.0019	0.002	0.0051	3.33	13.87	11.1	0.22	10.77	62.27	13.79	0.75	0.83	52.57
145	AB-SA170	0.6836	0	0.0232	97.51	0.0415	0.0178	0.0284	0.9393	0.1287	0.0359	99.42	0.0039	0.001	0.0017	0.0212	0.0027	0.0038	0.0028	0.002	0.002	0.0051	0.91	31.77	9.31	0.22	6.4	18.4	12.28	0.56	0.81	18.83
146	AB-SA170	0.01	0.0189	0.014	98.66	0.0533	0	0.0325	0.4378	0.0845	0	99.31	0.0039	0.001	0.0017	0.0206	0.0027	0.0038	0.0028	0.002	0.002	0.0052	62.78	7.91	14.82	0.22	5.06	100	10.84	0.91	0.86	344.58
147	AB-SA170	0.0674	0.01	0.0637	99.12	0.0748	0.01	0.0206	0.1038	0.2797	0	99.75	0.0038	0.001	0.0017	0.0198	0.0027	0.0038	0.0028	0.002	0.002	0.0052	6.27	23.68	3.71	0.22	3.75	57.25	16.95	2.64	0.68	231.34
148	AB-SA170	0.1887	0	0.0092	98.91	0.0389	0.0091	0.0274	0.4792	0.1877	0	99.85	0.0039	0.001	0.0017	0.0207	0.0027	0.0038	0.0028	0.0019	0.002	0.0052	2.5	100	22.88	0.22	6.84	35.56	12.77	0.85	0.75	100
149	AB-SA170	0.1334	0.0286	0.0744	98.77	0.2262	0	0.023	0.0983	0.3322	0.0166	99.7	0.0039	0.001	0.0017	0.0204	0.0028	0.0038	0.0029	0.002	0.002	0.0052	3.4	5.34	3.25	0.22	1.49	97.72	15.3	2.78	0.65	40.98
150	AB-SA170	0.285	0	0.0762	98.54	0.0131	0	0.0254	0.4595	0.0976	0	99.5	0.0039	0.001	0.0017	0.0205	0.0027	0.0038	0.0028	0.002	0.002	0.0052	1.77	174.97	3.2	0.22	19.45	100	13.88	0.88	0.84	100
151	AB-SA170	0.282	0.01	0.0548	99.07	0.0357	0.0123	0.0272	0.4488	0.1088	0	100.05	0.0039	0.0009	0.0017	0.0206	0.0027	0.0037	0.0028	0.002	0.002	0.0052	1.77	21.93	4.23	0.22	7.4	26.14	12.85	0.89	0.83	100
152	AB-SA170	0.2153	0.092	0.0809	98.13	0.0237	0.0129	0.1648	0.3164	0.2208	0	99.26	0.0039	0.001	0.0017	0.0197	0.0027	0.0038	0.0028	0.002	0.002	0.0051	2.22	1.78	3.01	0.22	10.81	25.12	2.23	1.12	0.72	529.95
153	AB-SA170	0.0321	0.5314	0.0772	96.33	0.01	0	0.736	1.78	0.162	0.009	99.67	0.0038	0.0009	0.0017	0.019	0.0027	0.0038	0.0028	0.002	0.002	0.0051	12.78	0.44	3.14	0.22	41.46	183.91	0.58	0.39	0.78	73.86
118	AB-SA170	0.4056	0.01	0.0182	99.36	0.0576	0.0087	0.0277	0.4118	0.1642	0	100.46	0.0039	0.001	0.0017	0.0204	0.0027	0.0038	0.0029	0.002	0.002	0.0052	1.34	16.36	11.65	0.22	4.76	37.08	12.84	0.95	0.77	100
370	AB-SA170	0.0373	0.0796	0.0555	99.31	0.0383	0	0.0276	0.1842	0.1186	0.0164	99.86	0.0038	0.0009	0.0017	0.0188	0.0027	0.0038	0.0028	0.0019	0.002	0.0051	10.92	1.95	4.13	0.22	6.87	100	12.65	1.66	0.81	40.8
155	AB-SA170	0.2749	0.0155	0.1222	98.65	0.1817	0.01	0.0203	0.0941	0.5841	0	99.95	0.0039	0.0009	0.0017	0.021	0.0027	0.0038	0.0028	0.002	0.002	0.0051	1.82	9.56	2.15	0.22	1.75	61.07	17.26	2.87	0.54	398.93
156	AB-SA170	0.1179	0.0121	0.0922	99.73	0.1074	0	0.0269	0.0922	0.3244	0	100.51	0.0039	0.001	0.0017	0.0203	0.0027	0.0038	0.0028	0.002	0.002	0.0052	3.76	12.32	2.7	0.22	2.73	135.92	13.07	2.9	0.65	353.88
157	AB-SA170	0.5254	0.0203	0.1066	98.6	0.0272	0.0229	0.0281	0.319	0.3491	0.0188	100.02	0.0039	0.0009	0.0017	0.0208	0.0027	0.0038	0.0028	0.0019	0.002	0.0052	1.09	7.41	2.39	0.22	9.65	14.29	12.43	1.11	0.64	35.94
119	AB-SA170	0.1226	0	0.0531	99.59	0.1039	0	0.0242	0.5564	0.1682	0	100.62	0.0038	0.001	0.0017	0.0202	0.0027	0.0038	0.003	0.0019	0.002	0.0051	3.61	100	4.34	0.22	2.82	167.69	15.14	0.77	0.77	4511.11
120	AB-SA170	0.3027	0.01	0.3635	99.45	0	0.0064	0.0251	0.1546	0.1525	0	100.47	0.0039	0.001	0.0017	0.0207	0.0027	0.0038	0.0029	0.002	0.002	0.0052	1.69	18.93	0.97	0.22	80.5	50.34	14.14	1.91	0.78	100
121	AB-SA170	0.0197	0	0.0944	98.95	0.0081	0	0.0356	0.4802	0.1131	0	99.7	0.004	0.0009	0.0017	0.0207	0.0027	0.0039	0.0028	0.002	0.002	0.0052	21.47	40.33	2.65	0.22	31.08	100	9.85	0.85	0.82	100
122	AB-SA170	0.887	0.032	0.0408	98.03	0.0501	0.0132	0.0247	0.5611	0.1662	0.0108	99.82	0.0039	0.001	0.0017	0.0216	0.0027	0.0038	0.0029	0.002	0.002	0.0052	0.76	4.84	5.52	0.22	5.35	24.77	14.51	0.78	0.77	63.2
123	AB-SA170	0.4961	0.0223	0.0637	100.94	0.0115	0	0.0273	0.3888	0.1259	0.0225	102.1	0.0039	0.001	0.0017	0.0193	0.0027	0.0038	0.0029	0.002	0.002	0.0052	1.15	6.8	3.73	0.22	22	73.4	12.95	0.98	0.8	30.11
55	AB-SA73	0.1168	0.01	0.3897	97.24	0.0099	0.0086	0.0291	0.1439	0.1758	0	98.12	0.0042	0.0009	0.0017	0.0201	0.0027	0.0039	0.0028	0.002	0.002	0.0052	4.03	25.62	0.93	0.22	25.42	38.42	11.99	2.04	0.77	100
361	AB-SA73	0.0945	0	0	99	0.0644	0	0.0297	0.6045	0.1302	0	99.93	0.0039	0.0009	0.0017	0.0194	0.0027	0.0038	0.0028	0.0019	0.002	0.0051	4.65	96.03	67.21	0.22	4.28	155.2	11.81	0.73	0.8	689.05
65	AB-SA73	0.114	0.0829	0	99.81	0.0441	0.0117	0.0305	0.1474	0.0724	0.0134	100.33	0.0039	0.001	0.0017	0.0191	0.0027	0.0038	0.0028	0.002	0.002	0.0052	3.91	1.97	87.49	0.22	6.06	27.83	11.51	1.99	0.86	50.51
66	AB-SA73	0.1362	0	0.0236	99.12	0.0551	0.0184	0.0261	0.397	0.2076	0.0375	100.03	0.0039	0.001	0.0017	0.0198	0.0027	0.0038	0.0029	0.002	0.002	0.0052	3.31	100	9.08	0.22	4.93	17.85	13.42	0.97	0.73	18.27
67	AB-SA73	0.2997	0.0246	0	98.84	0.086	0.0109	0.028	0.345	0.1347	0	99.78	0.0039	0.001	0.0017	0.0197	0.0028	0.0038	0.0029	0.002	0.002	0.0052	1.69	6.19	61.77	0.22	3.35	29.6	12.56	1.07	0.8	251.21
68	AB-SA73	0.2324	0.01	0	98.79	0.0359	0.0271	0.0258	0.862	0.0216	0	100	0.0039	0.0009	0.0017	0.0204	0.0027	0.0038	0.0028	0.002	0.002	0.0052	2.09	18.89	329.21	0.22	7.38	12.17	13.56	0.59	0.95	225.1
69	AB-SA73	0.0991	0.0261	0.0943	99.24	0.0339	0.0113	0.0275	0.089	0.1856	0	99.8	0.0039	0.0009	0.0017	0.0201	0.0027	0.0038	0.0028	0.002	0.002	0.0052	4.42	5.77	2.66	0.22	7.65	28.57	12.77	3.04	0.75	100
70	AB-SA73	0.0414	0	0	98.98	0.08	0	0.027	0.4393	0.1327	0.0556	99.76	0.0039	0.001	0.0017	0.0204	0.0027	0.0038	0.0029	0.002	0.002	0.0052	10.04	60.92	139.81	0.22	3.54	81.17	13.09	0.91	0.8	12.36
71	AB-SA73	0.2299	0.0563	0	97.69	0.049	0.034	0.029	0.5683	0.1037	0.0492	98.81	0.0039	0.0009	0.0017	0.02	0.0027	0.0038	0.0028	0.002	0.002	0.0052	2.11	2.79	316.15	0.22	5.5	9.78	11.97	0.77	0.84	13.85
72	AB-SA73	0.0509	0.01	0	98.56	0.0624	0.0151	0.0265	0.4018	0.1092	0.0092	99.25	0.0039	0.0009	0.0017	0.0207	0.0027	0.0038	0.0028	0.002	0.002	0.0052	8.22	14.72	50.67	0.22	4.39	21.43	13.12	0.96	0.83	74.5
73	AB-SA73	0.8721	0.01	0.0142	97.23	0.0879	0	0.0294	0.8524	0.0857	0.011	99.19	0.004	0.001	0.0017	0.0212	0.0027	0.0038	0.0029	0.002	0.002	0.0052	0.77	29.07	14.95	0.22	3.25	81.18	12	0.6	0.86	62.14
56	AB-SA73	0.0415	0.01	0.0563	98.91	0.031	0	0.0345	0.3846	0.145	0	99.61	0.0039	0.0009	0.0017	0.019	0.0027	0.0038	0.0028	0.002	0.002	0.0052	9.95	20.24	4.09	0.22	8.43	187.54	10.21	1	0.79	100
362	AB-SA73	0.3493	0	0.0616	99.36	0.0162	0	0.0283	0.4858	0.1069	0	100.41	0.0039	0.0009	0.0017	0.0197	0.0027	0.0038	0.0028	0.002	0.002	0.0051	1.49	100	3.76	0.22	15.45	100	12.37	0.84	0.82	170.93
75	AB-SA73	1.71	0.0099	0.0324	94.05	0.1209	0.0407	0.0291	1.48	0.2908	0.1756	97.93	0.004	0.001	0.0017	0.0198	0.0028	0.0038	0.0029	0.002	0.002	0.0053	0.5	15.34	6.93	0.23	2.51	8.43	12.3	0.44	0.69	4.1
76	AB-SA73	0.3814	0.0297	0.2028	97.62	0.0963	0.0135	0.0126	0.3068	0.1439	0.3104	99.12	0.0039	0.001	0.0017	0.02	0.0028	0.0038	0.0029	0.002	0.002	0.0052	1.41	5.15	1.45	0.22	3.04	24.23	27.82	1.16	0.8	2.33
77	AB-SA73	0.2175	0.0249	0.2007	98.33	0.1187	0.0091	0.0263	0.0387	0.3871	0.0187	99.37	0.0039	0.0009	0.0017	0.0208	0.0027	0.0038	0.0028	0.002	0.002	0.0052	2.21	6.08	1.47	0.22	2.52	35.23	13.33	6.36	0.62	36.34
78	AB-SA73	0.0329	0	0.0209	98.02	0.1239	0.0136	0.0222	0.2829	0.3129	0.0705	98.9	0.0039	0.001	0.0017	0.0209	0.0027	0.0038	0.0028	0.002	0.002	0.0052	12.58	100	10.1	0.22	2.42	23.89	15.74	1.22	0.66	9.71
79	AB-SA73	0.1074	0.0135	0.0236	98.11	0.1131	0	0.0314	0.2778	0.256	0	98.94	0.0039	0.001	0.0017	0.0201	0.0027	0.0038	0.0028	0.002	0.002	0.0052	4.11	11.04	9.17	0.22	2.63	170.78	11.19	1.24	0.7	209.2
80	AB-SA73	0.3679	0.0123	0.1041	98.88	0.1907	0.01	0.0235	0.0353	0.5541	0.0079	100.19	0.0039	0.001	0.0017	0.0205	0.0028	0.0038	0.0028	0.002	0.002	0.0052	1.44	12.13	2.46	0.22	1.72	52.18	14.87	6.97	0.55	86.64
81	AB-SA73	0.1992	0	0.1065	98.84	0.0265	0.0142	0.0692	0.563	0.0533	0.0947	99.97	0.0039	0.001	0.0017	0.0207	0.0027	0.0038	0.0028	0.0019	0.002	0.0052	2.38	121.75	2.42	0.22	9.8	22.9	5.16	0.77	0.9	7.28
82	AB-SA73	0.0107	0	0.0178	100.04	0.056	0	0.0259	0.3832	0.1612	0.0134	100.71	0.0039	0.001	0.0017	0.02	0.0027	0.0038	0.0028	0.002	0.002	0.0052	37.27	72.67	11.91	0.22	4.87	580.9	13.53	0.99	0.77	50.38
57	AB-SA73	0.0089	0	0.0741	99.39	0.0254	0	0.0317	0.3651	0.1064	0	100	0.0038	0.0009	0.0017	0.0207	0.0027	0.0038	0.0029	0.002	0.002	0.0052	44.61	854.71	3.25	0.22	10.27	100	11.18	1.03	0.83	5098.82
58	AB-SA73	0.0443	0.0131	0.0267	99	0.093	0	0.0229	0.153	0.0873	0.0159	99.46	0.0039	0.0009	0.0017	0.0203	0.0027	0.0038	0.0028	0.002	0.002	0.0052	9.41	11.38	8.07	0.22	3.08	66.79	15.17	1.94	0.85	42.83
59	AB-SA73	0	0.01	0.01	99.15	0.0225	0	0.0223	0.2908	0.3007	0.0351	99.84	0.0039	0.0009	0.0017	0.0196	0.0027	0.0038	0.0029	0.0019	0.002	0.0052	204.61	20.74	35.22	0.22	11.36	109.54	15.81	1.19	0.67	19.53
60	AB-SA73	0.042	0	0.0161	98.76	0.056	0	0.0263	0.519	0.1521	0	99.57	0.0039	0.0009	0.0017	0.0195	0.0027	0.0038	0.0028	0.002	0.002	0.0052	9.84	86.82	13	0.22	4.86	618.02	13.31	0.81	0.78	100
61	AB-SA73	0.1739	0.0104	0.1663	99.29	0.1416	0.0072	0.0234	0.0742	0.3017	0.0092	100.19	0.0039	0.0009	0.0017	0.0206	0.0027	0.0038	0.0028	0.002	0.002	0.0052	2.68	14.22	1.69	0.22	2.15	44.77	14.92	3.53	0.66	74.81
62	AB-SA73	0.0727	0.0158	0.1199	98.96	0.0589	0.0163	0.0269	0.0959	0.3035	0.0154	99.69	0.0039	0.001	0.0017	0.0202	0.0027	0.0038	0.0028	0.002	0.002	0.0052	5.93	9.41	2.17	0.22	4.64	19.77	12.95	2.82	0.67	44.49
63	AB-SA73	0	0	0.0116	99.3	0.0911	0.0082	0.0262	0.3833	0.0777	0	99.91	0.0039	0.001	0.0017	0.0208	0.0027	0.0038	0.0028	0.002	0.002	0.0052	100	82.72	17.99	0.22	3.15	38.94	13.36	0.99	0.87	189.65
83	AB-SA79	0.2835	0	0.0352	99.17	0.0177	0.0079	0.0334	0.2217	0.1583	0	99.93	0.0039	0.001	0.0017	0.0209	0.0027	0.0038	0.0028	0.002	0.002	0.0052	1.78	31.46	6.21	0.22	14.52	41.17	10.49	1.46	0.78	100
92	AB-SA79	0.0756	0.0103	0.01	99.11	0.0822	0.0271	0.0335	0.2771	0.2666	0.0134	99.9	0.0039	0.001	0.0017	0.0208	0.0027	0.0038	0.0028	0.002	0.002	0.0052	5.68	14.35	40.94	0.22	3.46	12.14	10.47	1.25	0.69	50.42
93	AB-SA79	0.1136	0.01	0.1803	98.64	0.0227	0	0.0269	0.5437	0.0714	0	99.6	0.004	0.001	0.0017	0.0197	0.0027	0.0038	0.0028	0.002	0.002	0.0051	3.97	24.3	1.58	0.22	11.32	669.93	13.08	0.79	0.87	174.37
391	AB-SA79	1.0822	0	0.5207	97.35	0.01	0.0176	0.0207	0.6193	0.1078	0	99.73	0.0039	0.0009	0.0017	0.0195	0.0027	0.0038	0.0029	0.002	0.002	0.0052	0.66	30.78	0.76	0.22	43.36	18.63	17.13	0.72	0.83	100
95	AB-SA79	1.0929	0.1255	0	96.34	0.0534	0.0252	0.5248	1.0212	0.0164	0.0093	99.21	0.0039	0.001	0.0017	0.0213	0.0028	0.0038	0.0029	0.002	0.002	0.0052	0.66	1.36	59.84	0.22	5.17	13.4	0.78	0.54	0.97	72.11
96	AB-SA79	0.2233	0.0227	0.01	99.11	0.0634	0.01	0.0299	0.3187	0.199	0.0143	99.99	0.0039	0.001	0.0017	0.0209	0.0027	0.0038	0.0029	0.002	0.002	0.0052	2.18	6.69	40.41	0.22	4.35	52.44	11.79	1.13	0.74	47.77
97	AB-SA79	0.1212	0	0.271	98.33	0.1264	0.01	0.0229	0.0173	0.5859	0.0441	99.53	0.0039	0.001	0.0017	0.0191	0.0027	0.0038	0.0028	0.002	0.002	0.0052	3.7	100	1.19	0.22	2.39	53.44	15.22	13.68	0.54	15.43
98	AB-SA79	0.1225	0	0.0244	98.74	0.024	0	0.0291	0.351	0.1211	0	99.42	0.0039	0.001	0.0017	0.0201	0.0027	0.0038	0.0028	0.002	0.002	0.0052	3.66	100	8.78	0.22	10.75	133.3	12.04	1.05	0.82	100
99	AB-SA79	0.0159	0	0.0163	98.58	0.0311	0	0.0269	0.4781	0.1497	0.01	99.31	0.0039	0.001	0.0017	0.0205	0.0027	0.0038	0.0028	0.002	0.002	0.0051	25.47	215.2	13.12	0.22	8.4	100	13.07	0.86	0.79	110.97
100	AB-SA79	0.0195	0	0.0399	98.63	0	0.0071	0.0216	0.3763	0.1173	0	99.21	0.0039	0.001	0.0017	0.0203	0.0027	0.0038	0.0028	0.002	0.002	0.0051	20.91	43.86	5.62	0.22	122.08	44.82	16.19	1	0.82	100
101	AB-SA79	0.5628	0	0.0506	98.54	0.0647	0.0329	0.0239	0.7141	0.0705	0.0064	100.07	0.0039	0.001	0.0017	0.0202	0.0027	0.0038	0.0029	0.002	0.002	0.0052	1.05	35.23	4.56	0.22	4.25	10.09	14.62	0.67	0.88	105.72
363	AB-SA79	0.0742	0	0.2798	99.75	0.0424	0	0.0263	0.1687	0.0858	0	100.43	0.0039	0.0009	0.0017	0.0201	0.0027	0.0038	0.0029	0.0019	0.002	0.0051	5.73	38.57	1.15	0.22	6.22	174.14	13.43	1.76	0.84	100
102	AB-SA79	0	0	0.0093	99.33	0.0184	0	0.0275	0.433	0.0873	0	99.91	0.0038	0.0009	0.0017	0.0209	0.0027	0.0038	0.0028	0.002	0.002	0.0051	100	32.69	22.27	0.22	13.95	2476.62	12.7	0.91	0.86	100
103	AB-SA79	0.0295	0.01	0.0665	99.51	0.017	0	0.0243	0.3946	0.1907	0.0174	100.25	0.0039	0.001	0.0017	0.0201	0.0027	0.0038	0.0029	0.002	0.002	0.0051	14.01	21.2	3.54	0.22	15.12	100	14.54	0.98	0.74	38.83
365	AB-SA79	0.5492	0.01	0.01	98.1	0.0264	0.0103	0.035	0.9151	0.0528	0.02	99.72	0.0039	0.0009	0.0017	0.0201	0.0027	0.0038	0.0028	0.002	0.002	0.0051	1.06	22.11	33.57	0.22	9.84	31.57	10.04	0.57	0.89	33.72
105	AB-SA79	0.165	0	0.0242	98.6	0.0425	0.01	0.0259	0.5411	0.073	0	99.47	0.0039	0.001	0.0017	0.0201	0.0027	0.0038	0.0029	0.002	0.002	0.0051	2.81	91.68	8.89	0.22	6.28	55.96	13.63	0.79	0.88	100
106	AB-SA79	0.048	0	0.0154	99.46	0.0363	0	0.0356	0.5198	0.1349	0	100.26	0.0039	0.001	0.0017	0.0208	0.0027	0.0038	0.0029	0.002	0.002	0.0051	8.75	36.36	13.63	0.22	7.24	91.21	9.95	0.81	0.8	100
107	AB-SA79	0.0889	0.0098	0.1878	99.51	0.0193	0	0.0301	0.3348	0.1253	0	100.31	0.0039	0.001	0.0017	0.0207	0.0027	0.0038	0.0028	0.002	0.002	0.0052	4.92	15.17	1.54	0.22	13.15	67.28	11.59	1.09	0.81	100
108	AB-SA79	0	0	0.0301	99.92	0.0335	0	0.0335	0.2939	0.1226	0	100.44	0.0039	0.001	0.0017	0.0202	0.0027	0.0038	0.0028	0.002	0.002	0.0052	100	34.47	7.24	0.22	7.76	65.54	10.47	1.19	0.81	100
109	AB-SA79	0.0807	0.0121	0.1	100.13	0.0603	0.0117	0.021	0.1019	0.2252	0.0474	100.79	0.0039	0.001	0.0017	0.0209	0.0027	0.0038	0.0029	0.002	0.002	0.0052	5.35	12.25	2.54	0.22	4.57	27.73	16.76	2.71	0.72	14.42
110	AB-SA79	0.1785	0.0226	0.0154	100.23	0.0766	0.0081	0.0292	0.25	0.2321	0.013	101.05	0.0039	0.0009	0.0017	0.0201	0.0027	0.0038	0.0029	0.002	0.002	0.0051	2.63	6.65	13.82	0.22	3.69	39.92	12.07	1.34	0.71	51.83
111	AB-SA79	0.0745	0	0.0196	98.09	0.0268	0	0.0346	1.59	0.2048	0.1456	100.19	0.0039	0.001	0.0017	0.0199	0.0028	0.0038	0.0028	0.002	0.002	0.0052	5.84	62.16	10.98	0.22	9.9	123	10.22	0.42	0.74	4.8
85	AB-SA79	0.0398	0	0.0457	99.31	0.0378	0	0.0269	0.3756	0.1233	0	99.97	0.0039	0.001	0.0017	0.0205	0.0027	0.0038	0.0029	0.002	0.002	0.0052	10.44	29.67	4.96	0.22	7.03	122.1	13.14	1	0.81	545.57
112	AB-SA79	0.1205	0.01	0	99.58	0.0395	0.0079	0.0322	0.5001	0.1275	0.0102	100.43	0.0039	0.001	0.0017	0.0202	0.0027	0.0038	0.0028	0.002	0.002	0.0051	3.72	19.74	63.37	0.22	6.76	41.14	10.95	0.83	0.81	66.23
113	AB-SA79	0.219	0.01	0.1568	99.19	0.057	0	0.0429	0.4107	0.0996	0.0661	100.26	0.0039	0.001	0.0017	0.0204	0.0027	0.0038	0.0029	0.002	0.002	0.0052	2.2	21.39	1.77	0.22	4.81	88.04	8.28	0.95	0.84	10.34
366	AB-SA79	4.89	0.0202	0.0618	88.61	0.0766	0.0458	0.0349	3.62	0.1038	0.0382	97.5	0.0041	0.0009	0.0017	0.02	0.0027	0.0039	0.003	0.0021	0.002	0.0055	0.27	7.4	3.83	0.23	3.72	7.87	10.56	0.26	0.88	18.68
86	AB-SA79	0.066	0.0097	0.1461	99.56	0.0499	0.01	0.0255	0.3421	0.0746	0	100.28	0.0039	0.001	0.0017	0.0191	0.0027	0.0038	0.0028	0.002	0.002	0.0052	6.4	15.32	1.87	0.22	5.39	54.64	13.78	1.08	0.87	536.25
87	AB-SA79	0.021	0.01	0.0178	99.42	0.0257	0	0.029	0.3772	0.1176	0	100.02	0.0039	0.001	0.0017	0.0196	0.0027	0.0038	0.0029	0.002	0.002	0.0052	19.6	20.67	11.82	0.22	10.03	100	12.2	1	0.81	100
88	AB-SA79	0.033	0.0118	0.0293	99.51	0.0389	0	0.0269	0.196	0.1392	0	99.99	0.0039	0.0009	0.0017	0.0197	0.0027	0.0038	0.0028	0.002	0.002	0.0052	12.52	12.56	7.36	0.22	6.83	786.16	13.02	1.6	0.8	100
89	AB-SA79	0.1042	0.01	0.1035	99.33	0.1816	0.0109	0.0224	0.0747	0.3678	0	100.2	0.0039	0.0009	0.0017	0.021	0.0028	0.0038	0.0029	0.002	0.002	0.0052	4.25	24.94	2.47	0.22	1.78	29.88	15.65	3.52	0.63	173.7
90	AB-SA79	0.2301	0.0134	0.6449	98.82	0.1309	0.0088	0.019	0.0316	0.2773	0.0438	100.22	0.0039	0.001	0.0017	0.0207	0.0027	0.0038	0.0029	0.002	0.002	0.0051	2.1	11.2	0.68	0.22	2.32	36.56	18.45	7.62	0.68	15.51
91	AB-SA79	0.0408	0	0.0666	99.46	0.0557	0	0.0291	0.5846	0.116	0	100.36	0.0039	0.0009	0.0017	0.0202	0.0027	0.0038	0.0028	0.002	0.002	0.0052	10.17	104.71	3.54	0.22	4.88	194.81	12.05	0.75	0.82	153.14
392	AB-SA98	0.3014	0.01	0.1628	98.58	0.0604	0	0.0247	0.4329	0.1061	0	99.68	0.0039	0.0009	0.0017	0.0203	0.0027	0.0038	0.0029	0.002	0.002	0.0051	1.68	22.71	1.71	0.22	4.54	115.45	14.36	0.9	0.83	496.65
195	AB-SA98	0.1603	0.0117	0.1012	98.64	0.0474	0.01	0.0282	0.2163	0.161	0.0139	99.39	0.0039	0.0009	0.0017	0.0206	0.0027	0.0038	0.0028	0.002	0.002	0.0051	2.87	12.68	2.51	0.22	5.67	53.02	12.37	1.48	0.77	48.4
196	AB-SA98	0.9533	0.2018	0.2377	94.73	0.0193	0	0.206	1.1844	0.2332	0.1045	97.88	0.0031	0.001	0.0017	0.02	0.0029	0.0033	0.0032	0.0019	0.002	0.0051	0.68	0.97	1.29	0.23	14.05	67.55	2.01	0.49	0.73	6.54
197	AB-SA98	0.184	0	0.5839	99.25	0.0654	0.0152	0.025	0.0271	0.1301	0.0608	100.35	0.0038	0.001	0.0017	0.0202	0.0027	0.0038	0.0029	0.002	0.002	0.0051	2.52	78.59	0.71	0.22	4.2	21.29	14.19	8.8	0.8	11.15
198	AB-SA98	0.0208	0.0151	0.0864	98.93	0.1073	0	0.0304	0.2397	0.2257	0	99.65	0.0038	0.001	0.0017	0.02	0.0027	0.0038	0.0028	0.002	0.002	0.0051	19.18	9.9	2.84	0.22	2.73	109.94	11.53	1.37	0.71	100
199	AB-SA98	0.0332	0	0.0139	99.69	0.0175	0	0.0301	0.6737	0.126	0	100.59	0.0039	0.0009	0.0017	0.0202	0.0027	0.0038	0.0028	0.002	0.002	0.0051	12.58	31.18	15.08	0.22	14.49	138.45	11.52	0.69	0.8	100
200	AB-SA98	0.0753	0.0137	0.048	94.48	0	0	0.0528	0.4196	0.1021	0.0092	95.2	0.0038	0.001	0.0016	0.0195	0.0027	0.0037	0.0029	0.002	0.002	0.005	5.61	11.16	4.66	0.23	58.19	104.09	6.89	0.93	0.85	71.87

Table A6: Single-grain heavy mineral chemical data for garnets.

JEOL JXA-8900RL Geowissenschaftliches Zentrum Universitaet Goettingen (GZG) Abt. Geochemie; Dr. A. Kronz

15.0kV		mass-%	correction: Phi-rho-Z								Detection Limits [mass-%] 1-sigma count.Stat								Standard Deviations [% relative] 1-sigma count.Stat							
No.	**Sample**	**SiO_2**	**MgO**	**CaO**	**TiO_2**	**FeO**	**Al_2O_3**	**Cr_2O_3**	**MnO**	**wt-total**	**Si_DL**	**Mg_DL**	**Ca_DL**	**Ti_DL**	**Fe_DL**	**Al_DL**	**Cr_DL**	**Mn_DL**	**Si_SD**	**Mg_SD**	**Ca_SD**	**Ti_SD**	**Fe_SD**	**Al_SD**	**Cr_SD**	**Mn_SD**
8	AB-SA164	39.35	9.29	5.03	0.0482	23.17	22.22	0.1896	0.4789	99.77	0.0159	0.0109	0.0141	0.011	0.0212	0.0138	0.0131	0.0119	0.31	0.71	1.02	25.33	0.56	0.42	8.03	3.85
10	AB-SA164	38.07	4.31	6.54	0.0093	25.36	21.61	0.023	3.79	99.71	0.0162	0.0095	0.0135	0.0116	0.0217	0.0134	0.0134	0.0126	0.32	1.08	0.88	132.07	0.53	0.42	60.65	1.06
12	AB-SA164	37.7	2.42	7.17	0.0434	29.86	21.19	0.0238	1.2714	99.68	0.0164	0.0095	0.0139	0.0118	0.0235	0.0146	0.0136	0.0127	0.32	1.49	0.84	29.44	0.49	0.43	58.81	2.01
13	AB-SA164	39.56	13.1	0.8467	0.01	22.4	22.62	0	0.1524	98.68	0.0152	0.0114	0.0137	0.0113	0.0211	0.0137	0.013	0.0116	0.31	0.59	2.83	166.36	0.57	0.42	100	9.44
15	AB-SA152	38.04	1.5737	12.29	0.084	11.61	21.19	0.0235	15.63	100.45	0.0162	0.0096	0.0142	0.0118	0.0207	0.0136	0.0134	0.0131	0.31	1.87	0.64	15.86	0.79	0.42	61.44	0.5
16	AB-SA152	37.68	2.71	6.31	0.0152	14.27	21.5	0.0154	17.07	99.57	0.0153	0.0092	0.0141	0.0117	0.0222	0.0138	0.0136	0.0137	0.32	1.38	0.9	79.77	0.71	0.42	94.15	0.48
18	AB-SA152	37.43	3.92	2.72	0.062	14.06	20.54	0	20.94	99.68	0.0156	0.0096	0.0115	0.0111	0.0218	0.0139	0.0138	0.0139	0.32	1.14	1.38	19.37	0.72	0.43	100	0.43
19	AB-SA152	37.56	3.28	5.93	0	23.09	20.9	0	8.97	99.72	0.0161	0.0095	0.0138	0.0119	0.022	0.0137	0.0138	0.0127	0.32	1.26	0.93	4200.19	0.56	0.43	100	0.66
21	AB-SA152	37.4	2.41	2.11	0.0185	21.93	21.21	0	14.76	99.84	0.0156	0.0094	0.0129	0.0119	0.0228	0.0141	0.0138	0.0137	0.32	1.5	1.61	66.16	0.57	0.43	100	0.51
22	AB-SA152	37.24	0.1178	14.87	0.0654	17.79	21.07	0	8.07	99.24	0.0159	0.0091	0.0146	0.0116	0.0213	0.0147	0.0136	0.0127	0.32	11.19	0.58	19.85	0.64	0.42	100	0.7
23	AB-SA152	37.91	3.69	3.98	0.0484	15.91	21.23	0	17.29	100.06	0.0158	0.0091	0.0133	0.0115	0.0217	0.0141	0.0134	0.0136	0.32	1.18	1.14	25.44	0.67	0.43	100	0.47
24	AB-SA152	37.35	0.2911	11.17	0.1266	7.8	20.65	0.0087	22.61	100	0.0162	0.0099	0.0138	0.0114	0.02	0.0144	0.0133	0.0137	0.32	5.73	0.67	10.51	0.98	0.43	164.86	0.41
25	AB-SA152	36.57	1.73	1.43	0.0146	18.75	20	0	21.01	99.51	0.0166	0.009	0.0138	0.0117	0.0219	0.014	0.0138	0.014	0.32	1.81	2.02	81.27	0.62	0.44	100	0.43
26	AB-SA152	37.69	1.2169	9.89	0.0283	21.54	21.12	0	8.53	100.02	0.016	0.0101	0.0146	0.0115	0.0215	0.0138	0.0137	0.0123	0.32	2.23	0.71	43.46	0.58	0.43	299.65	0.68
27	AB-SA152	37.73	1.442	8.99	0.0322	21.82	20.98	0	9.2	100.21	0.0166	0.0095	0.0141	0.0113	0.022	0.0141	0.0138	0.0125	0.32	1.99	0.75	37.79	0.57	0.43	100	0.66
28	AB-SA152	38.24	6.67	1.7	0	16.29	21.87	0.0579	14.84	99.67	0.0156	0.0097	0.0133	0.0119	0.0218	0.0135	0.0135	0.0134	0.32	0.86	1.83	100	0.67	0.42	25.13	0.51
29	AB-SA152	37.47	1.2156	9.23	0.2586	14.49	19.47	0.0085	17.86	100.01	0.0164	0.0095	0.0145	0.0118	0.0219	0.0132	0.0135	0.0136	0.32	2.21	0.74	5.79	0.71	0.44	167.94	0.47
30	AB-SA152	37.5	0.7229	10.19	0.0185	22.33	20.95	0.0253	8.14	99.87	0.0157	0.0091	0.0151	0.0117	0.0212	0.0142	0.0133	0.0122	0.32	3.01	0.7	66.73	0.57	0.43	55.59	0.7
31	AB-SA152	37.85	2.53	6.98	0.017	22.49	21.29	0.0432	9.16	100.37	0.0165	0.0099	0.0138	0.0119	0.0221	0.0138	0.0138	0.0131	0.32	1.46	0.85	74.06	0.56	0.43	33.78	0.66
32	AB-SA152	37.2	1.3997	6.52	0.031	13.45	19.62	0.0333	21.17	99.42	0.0161	0.0098	0.0133	0.0119	0.0214	0.0138	0.0134	0.014	0.32	2.05	0.88	40.22	0.73	0.44	43	0.43
33	AB-SA152	39.29	6.63	10.22	0.0485	21.57	21.79	0	0.4491	100.01	0.0162	0.0102	0.0141	0.011	0.0206	0.0134	0.0135	0.0117	0.31	0.85	0.71	25.27	0.58	0.42	100	4.02
34	AB-SA152	37.65	2.36	9.06	0.0353	11.5	20.1	0.0241	18.95	99.67	0.0162	0.0102	0.0139	0.0117	0.0221	0.0144	0.0137	0.0133	0.32	1.51	0.75	35.49	0.8	0.44	60.94	0.45
37	AB-SA152	40.42	12.48	7.16	0.051	16.6	23.05	0.0156	0.2271	100	0.0161	0.0113	0.0138	0.011	0.0208	0.0141	0.0125	0.0115	0.31	0.6	0.85	24.29	0.67	0.41	86.01	6.81
39	AB-SA164	39.02	9.28	5.17	0	23.34	22.21	0.1698	0.484	99.67	0.0156	0.0103	0.0134	0.0115	0.0214	0.0138	0.013	0.0116	0.32	0.72	1.01	269.18	0.56	0.42	8.81	3.78
41	AB-SA164	38.24	4.45	6.95	0.0435	25.26	21.48	0.01	3.46	99.88	0.0161	0.0099	0.0133	0.0117	0.0219	0.0141	0.0133	0.012	0.32	1.07	0.86	29.23	0.53	0.42	202.45	1.11
43	AB-SA152	37.93	3.77	2.53	0.0469	13.95	21.24	0.024	20.79	100.28	0.0157	0.009	0.0146	0.0116	0.0205	0.014	0.0134	0.0141	0.32	1.17	1.48	26.2	0.72	0.43	59.19	0.43
44	AB-SA152	36.62	3.33	5.85	0.0302	22.97	20.37	0	9.07	98.24	0.0157	0.0098	0.0143	0.0115	0.0218	0.0132	0.0138	0.0127	0.32	1.26	0.94	40.35	0.56	0.44	100	0.66
46	AB-SA152	37.98	3.84	4.26	0.0945	15.89	21.5	0.0174	16.6	100.18	0.0163	0.0101	0.013	0.0121	0.0225	0.0137	0.0136	0.0139	0.32	1.16	1.1	14.22	0.68	0.42	81.77	0.48
47	AB-SA152	37.08	1.66	1.3371	0.0201	18.21	20.73	0	21.32	100.37	0.0171	0.0087	0.0132	0.0117	0.0238	0.0143	0.0139	0.0138	0.32	1.84	2.09	59.47	0.63	0.43	100	0.42
48	AB-SA152	37.24	2.25	7.05	0.0264	22.13	21.23	0.044	9.88	99.84	0.0154	0.0095	0.0135	0.012	0.0221	0.0144	0.0134	0.0126	0.32	1.55	0.85	47.95	0.57	0.43	32.46	0.63
49	AB-SA152	38.83	6.67	10.25	0.0729	21.36	21.87	0.0307	0.4188	99.51	0.0161	0.0104	0.0139	0.0112	0.0219	0.0135	0.0129	0.0123	0.31	0.85	0.71	17.63	0.58	0.42	45.11	4.34
50	AB-SA98	37.95	6.6	1.3962	0.0522	30.92	21.7	0.0094	1.1443	99.77	0.0158	0.01	0.0129	0.0112	0.022	0.0136	0.0138	0.0121	0.32	0.87	2.05	23.47	0.48	0.43	148.06	2.13
51	AB-SA98	38.29	6.64	1.53	0.0089	30.75	21.88	0.0102	1.1129	100.22	0.0157	0.0104	0.0137	0.0118	0.0221	0.0135	0.0137	0.0122	0.32	0.87	1.97	137.92	0.48	0.42	137.62	2.17
52	AB-SA98	38.99	7.88	6.32	0.0624	24.09	21.77	0.0407	0.7458	99.91	0.016	0.0103	0.0138	0.0113	0.0209	0.0135	0.0133	0.012	0.31	0.78	0.91	20.39	0.55	0.42	34.84	2.84
53	AB-SA98	38.11	7.12	6.28	0.02	24.72	21.46	0.0312	0.8016	98.55	0.0158	0.0099	0.0137	0.0118	0.0207	0.0137	0.0134	0.0124	0.32	0.83	0.91	63.31	0.54	0.43	45.62	2.72
54	AB-SA98	37.07	0.4997	9.28	0.0407	29.82	20.67	0	2.43	99.81	0.0161	0.0092	0.0142	0.0119	0.0219	0.0144	0.0137	0.0122	0.32	3.88	0.74	31.64	0.49	0.43	100	1.35
55	AB-SA98	36.97	0.4275	9.91	0.0504	29.37	20.69	0	2	99.43	0.0158	0.0091	0.0145	0.0115	0.0226	0.0135	0.0137	0.0125	0.32	4.29	0.71	25.06	0.49	0.43	501.04	1.52
56	AB-SA98	37.87	3.53	6.77	0	27.19	21.28	0	3.13	99.77	0.016	0.0093	0.0137	0.0117	0.0219	0.0129	0.0136	0.0125	0.32	1.21	0.87	272.25	0.51	0.43	100	1.18
57	AB-SA98	37.64	3.18	6.98	0.037	27.1	21.41	0	3.63	99.98	0.0162	0.0094	0.0142	0.0117	0.0227	0.0134	0.0137	0.0128	0.32	1.28	0.86	34.1	0.51	0.43	100	1.09
58	AB-SA98	37.31	0.7312	9.53	0.13	21.36	20.58	0.01	10.44	100.08	0.0157	0.0089	0.0135	0.0117	0.0223	0.013	0.0135	0.0131	0.32	2.97	0.73	10.51	0.58	0.43	196.98	0.62
59	AB-SA98	36.99	1.001	8.74	0.0701	19.59	20.64	0	12	99.04	0.0162	0.0092	0.0137	0.0116	0.0226	0.0139	0.0138	0.0136	0.32	2.47	0.76	18.28	0.61	0.43	100	0.57
60	AB-SA98	38.36	5.21	2.84	0.0086	30.58	21.49	0	1.91	100.4	0.0165	0.0102	0.0138	0.0117	0.0215	0.0138	0.0137	0.0121	0.32	0.99	1.38	141.08	0.48	0.43	100	1.55
61	AB-SA98	37.91	5.18	2.78	0.0196	30.81	21.32	0.0189	1.88	99.93	0.0161	0.0096	0.0132	0.0116	0.0222	0.0132	0.0133	0.0125	0.32	0.99	1.39	62.25	0.48	0.43	71.48	1.58
62	AB-SA98	39.81	11.88	5.7	0.0397	19.38	22.52	0.1354	0.4896	99.95	0.0159	0.0108	0.0141	0.0111	0.0205	0.0141	0.013	0.012	0.31	0.62	0.96	31.12	0.61	0.41	10.98	3.82
63	AB-SA98	37.95	3.11	8.27	0	28.27	20.91	0	1.83	100.35	0.0155	0.0094	0.0139	0.0122	0.0223	0.0143	0.0137	0.0123	0.32	1.3	0.78	100	0.5	0.43	100	1.6
64	AB-SA98	37.69	3.07	8.42	0.0379	27.51	20.89	0	1.75	99.36	0.0153	0.0093	0.0148	0.0113	0.0214	0.0141	0.0135	0.0118	0.32	1.3	0.78	32.59	0.51	0.43	100	1.63
65	AB-SA98	36.9	0.3447	6.08	0.089	11.49	19.62	0	25.52	100.04	0.0158	0.0094	0.0134	0.012	0.0225	0.0142	0.0139	0.0144	0.32	5.05	0.91	14.74	0.8	0.44	100	0.39
66	AB-SA98	37.24	0.3658	6.16	0.0876	11.32	19.86	0	25.02	100.05	0.016	0.01	0.0143	0.0118	0.0227	0.0138	0.0138	0.0142	0.32	4.97	0.91	14.78	0.81	0.44	100	0.39
67	AB-SA98	37.93	4.65	6.74	0.0891	28.13	21.17	0	1.1677	99.88	0.0152	0.0098	0.0142	0.0116	0.0218	0.014	0.0136	0.0119	0.32	1.04	0.87	14.75	0.5	0.43	100	2.09
68	AB-SA98	37.74	4.22	6.7	0.0603	28	20.71	0	1.2564	98.69	0.0167	0.0104	0.0132	0.0114	0.0217	0.0139	0.0134	0.0126	0.32	1.11	0.87	20.93	0.5	0.43	321.8	2.03
69	AB-SA98	38.36	4.35	7.08	0.058	26.95	21.58	0	2.02	100.4	0.016	0.0101	0.0132	0.0111	0.0221	0.0137	0.0138	0.0125	0.32	1.08	0.85	21.3	0.52	0.42	100	1.52
70	AB-SA98	37.72	4.26	7.38	0.0326	26.54	21.41	0	2.01	99.35	0.0159	0.0091	0.0137	0.0114	0.0212	0.0143	0.0136	0.0122	0.32	1.09	0.83	37.93	0.52	0.42	100	1.51
71	AB-SA98	37.61	3.31	4.05	0.0221	26.13	20.97	0	8.06	100.14	0.0157	0.0097	0.0132	0.0116	0.0221	0.0145	0.0137	0.0131	0.32	1.26	1.13	55.42	0.52	0.43	100	0.7
72	AB-SA98	37.33	2.61	4.03	0.0225	23.4	20.85	0	11.34	99.58	0.0165	0.0098	0.0136	0.0116	0.022	0.0133	0.0137	0.0129	0.32	1.44	1.14	53.76	0.55	0.43	100	0.59
73	AB-SA98	37.6	3.16	5.27	0.0552	27.5	21.49	0.01	5.32	100.4	0.0162	0.0093	0.0134	0.0116	0.0218	0.0139	0.0133	0.0122	0.32	1.29	0.99	22.83	0.51	0.42	239.72	0.87
74	AB-SA98	37.82	3	5.23	0.0345	27.4	21.44	0	5.24	100.18	0.0159	0.0092	0.0132	0.0116	0.0232	0.014	0.0135	0.0129	0.32	1.32	0.99	36.01	0.51	0.42	376.89	0.88
75	AB-SA98	37.47	2.7	3.69	0.0237	27.92	21.2	0	6.72	99.73	0.0164	0.0102	0.0138	0.0117	0.0234	0.0137	0.0139	0.0128	0.32	1.42	1.19	51.8	0.5	0.43	100	0.77
76	AB-SA98	36.43	0.765	1.0205	0.0982	23.23	20.85	0	17.02	99.42	0.0165	0.0095	0.0129	0.0118	0.0223	0.0142	0.014	0.0137	0.32	2.99	2.44	13.21	0.55	0.43	100	0.47
77	AB-SA98	38.72	7.31	6.49	0.1433	24.93	21.39	0.0202	1.1325	100.13	0.0158	0.0104	0.0138	0.0111	0.0208	0.0142	0.0133	0.0117	0.31	0.82	0.89	9.33	0.54	0.43	69.01	2.13
78	AB-SA98	38.47	4.61	8.31	0.0394	26.18	21.8	0.0198	0.6145	100.04	0.0158	0.0096	0.014	0.0117	0.0214	0.0134	0.013	0.0122	0.32	1.04	0.78	32.36	0.52	0.42	69.17	3.25
79	AB-SA98	38.18	4.51	8.48	0.0433	26.16	21.71	0.0255	0.6028	99.72	0.0157	0.0096	0.0142	0.0113	0.0208	0.0137	0.0133	0.0122	0.32	1.05	0.77	28.72	0.52	0.42	54.88	3.29
80	AB-SA98	38.14	4.12	6.01	0.0285	26.5	21.48	0.0662	3.65	99.99	0.0153	0.0098	0.0129	0.0114	0.0213	0.0139	0.0133	0.0125	0.32	1.11	0.92	42.77	0.52	0.42	21.44	1.08
81	AB-SA98	37.7	4.12	5.67	0.0344	26.83	21.63	0.0501	3.9	99.93	0.0156	0.01	0.0138	0.0118	0.0225	0.0131	0.0133	0.0122	0.32	1.12	0.95	36.77	0.52	0.42	28.04	1.04
82	AB-SA98	37.62	4.17	1.98	0	32.08	21.4	0.0226	2.55	99.83	0.0158	0.0104	0.0136	0.0119	0.0222	0.0139	0.0135	0.0121	0.32	1.12	1.68	100	0.47	0.43	60.67	1.31
83	AB-SA98	37.54	2.9	1.87	0	32.35	21.36	0.01	4.42	100.45	0.0161	0.0091	0.0136	0.012	0.0211	0.0142	0.0138	0.0122	0.32	1.36	1.73	100	0.47	0.43	268.91	0.96
84	AB-SA98	38.06	4.37	8.49	0.1835	25.38	21.26	0.0098	1.93	99.68	0.0158	0.0103	0.014	0.0116	0.0219	0.0138	0.0132	0.0124	0.32	1.08	0.77	7.78	0.53	0.42	139.93	1.56
85	AB-SA98	37.82	4.32	8.04	0.0132	25.28	21.45	0.0123	2.43	99.36	0.0157	0.0099	0.014	0.0118	0.0227	0.0131	0.0132	0.0123	0.32	1.08	0.8	94.73	0.53	0.42	112.14	1.36
86	AB-SA98	38.65	5.42	10.1	0.0308	22.47	21.69	0.0076	1.84	100.2	0.0159	0.0094	0.0137	0.0114	0.0218	0.0137	0.0129	0.0121	0.31	0.95	0.71	40.37	0.57	0.42	181.17	1.6
87	AB-SA98	38.68	5.24	9.89	0.0394	22.48	21.49	0	1.82	99.64	0.0148	0.0095	0.0136	0.0113	0.0209	0.0137	0.0132	0.0123	0.31	0.97	0.72	31.71	0.57	0.42	463.66	1.61
88	AB-SA98	38.2	4.93	4.63	0.0345	29.19	21.44	0.0188	1.63	100.08	0.0156	0.0098	0.0135	0.0113	0.0222	0.0138	0.0134	0.0124	0.32	1.01	1.06	35.44	0.49	0.43	73.47	1.72
89	AB-SA98	37.73	1.85	7.13	0.0465	27.2	21.09	0	5.51	100.55	0.016	0.009	0.0142	0.0113	0.0224	0.0145	0.0137	0.013	0.32	1.72	0.84	26.39	0.51	0.43	100	0.86
90	AB-SA98	37.45	3.73	1.145	0	29.42	21.41	0.0154	6.59	99.77	0.016	0.0097	0.013	0.012	0.0224	0.0139	0.0136	0.0125	0.32	1.19	2.29	100	0.49	0.43	89.8	0.78
91	AB-SA98	37.85	1.5796	9.29	0.0389	22.31	21.23	0	8.17	100.48	0.0153	0.0099	0.0138	0.0118	0.0223	0.0139	0.0135	0.0132	0.32	1.9	0.73	32.84	0.57	0.42	100	0.7
92	AB-SA98	37.71	3.01	4.22	0.0462	31.67	21.56	0.0131	2.74	100.95	0.0153	0.0093	0.0138	0.0117	0.0229	0.0135	0.0134	0.0128	0.32	1.33	1.11	27.33	0.47	0.42	104.06	1.27
93	AB-SA98	38.08	3.36	10.15	0.018	25.06	21.38	0.0122	1.51	99.56	0.0162	0.0098	0.0152	0.0114	0.0225	0.0138	0.0133	0.0121	0.32	1.24	0.71	67.76	0.54	0.42	113.42	1.8
94	AB-SA98	37.63	2.84	5.09	0.0216	14.94	21.06	0	18.55	100.12	0.0152	0.009	0.0144	0.0115	0.0222	0.0139	0.0139	0.014	0.32	1.35	1.01	55.79	0.7	0.43	100	0.46
95	AB-SA98	37.87	4.04	4.34	0.033	24.83	21.41	0.0111	7.74	100.27	0.0158	0.009	0.0134	0.0115	0.023	0.0147	0.0133	0.0129	0.32	1.12	1.09	37.03	0.54	0.43	122.45	0.72
96	AB-SA98	37.64	0.8819	8.75	0.0696	30.1	21.29	0	1.91	100.65	0.0159	0.0095	0.0145	0.0115	0.0219	0.0141	0.0134	0.0123	0.32	2.7	0.76	18.4	0.49	0.42	294.87	1.56
97	AB-SA98	38.52	4.22	11.12	0.0993	24.42	21.09	0	0.5173	99.98	0.016	0.0095	0.014	0.0116	0.0206	0.0139	0.0135	0.0118	0.31	1.09	0.67	13.52	0.54	0.43	100	3.64
98	AB-SA98	38.57	4.15	10.98	0.1031	24.44	20.96	0	0.547	99.76	0.0161	0.0097	0.0151	0.0115	0.0216	0.0132	0.0134	0.0121	0.31	1.1	0.68	13.02	0.54	0.43	100	3.52
99	AB-SA98	37.8	4.8	1.1344	0.0173	30.77	21.6	0.0469	4.01	100.17	0.0165	0.0097	0.0136	0.012	0.0228	0.0138	0.0135	0.0127	0.32	1.04	2.33	72.24	0.48	0.43	29.61	1.02
100	AB-SA98	38.01	4.63	1.1987	0	30.52	21.86	0	4.02	100.25	0.0164	0.0097	0.0124	0.012	0.0214	0.0132	0.014	0.0126	0.32	1.05	2.22	100	0.48	0.42	100	1.02
101	AB-SA98	37.3	2.88	1.1568	0	28	21.54	0.0163	9.55	100.45	0.0163	0.0098	0.0135	0.012	0.0219	0.0136	0.0134	0.013	0.32	1.37	2.29	100	0.5	0.43	83.4	0.64
102	AB-SA98	37.62	1.0726	11.34	0.0868	21.38	21.22	0	7.36	100.09	0.0161	0.009	0.0152	0.0111	0.0207	0.0139	0.0137	0.0128	0.32	2.34	0.67	14.65	0.58	0.42	100	0.74
103	AB-SA98	38.39	5.99	1.1577	0	31.85	21.68	0.019	1.63	100.72	0.0162	0.0091	0.0133	0.0118	0.0225	0.0141	0.0134	0.0123	0.32	0.92	2.29	259.28	0.47	0.43	71.41	1.71
105	AB-SA153	38.42	3.14	11.58	0.1618	23.28	21.52	0	2.25	100.36	0.0159	0.0098	0.0146	0.0118	0.0221	0.014	0.0135	0.0121	0.31	1.28	0.66	8.82	0.56	0.42	100	1.42
106	AB-SA153	38.07	4.98	1.7	0.0119	17.49	21.81	0.0255	16.76	100.84	0.0162	0.01	0.0125	0.012	0.0216	0.0135	0.0135	0.0134	0.32	1.01	1.81	103.25	0.64	0.42	55.43	0.48
107	AB-SA153	37.95	2.79	9.13	0.01	14.28	21.53	0.0829	14.4	100.16	0.0162	0.0096	0.0144	0.0117	0.0228	0.0137	0.0133	0.013	0.32	1.36	0.74	187.04	0.72	0.42	17.85	0.52
108	AB-SA153	37.47	2.67	8.68	0.0148	14.23	21.21	0.1292	14.96	99.38	0.0156	0.0096	0.0139	0.0118	0.0219	0.0137	0.0135	0.0133	0.32	1.4	0.76	83.6	0.71	0.42	11.84	0.51
109	AB-SA153	38.09	5.22	2.6	0.0298	7.17	21.54	0.0107	25.51	100.19	0.0159	0.0105	0.0133	0.0113	0.0218	0.0133	0.0137	0.0138	0.32	0.98	1.44	39.73	1.03	0.42	136.27	0.39
114	AB-SA153	37.12	1.86	0.8682	0.01	15.9	20.97	0	23.86	100.59	0.0159	0.0093	0.0137	0.012	0.0221	0.0141	0.0142	0.014	0.32	1.73	2.73	163.03	0.67	0.43	100	0.4
115	AB-SA153	37.54	2.2	6.76	0.0188	19.44	20.68	0	13.47	100.1	0.016	0.0101	0.013	0.0117	0.0225	0.0143	0.0139	0.0129	0.32	1.58	0.86	65.21	0.61	0.43	100	0.54
116	AB-SA153	36.98	1.94	5.88	0.0236	18.47	20.53	0	15.28	99.11	0.0159	0.0094	0.014	0.0117	0.0224	0.0134	0.0137	0.0133	0.32	1.68	0.93	51.8	0.62	0.43	100	0.5
117	AB-SA153	39.49	7.82	9.68	0.1108	20.58	22.31	0.0538	0.4554	100.49	0.0159	0.0104	0.0137	0.0108	0.0205	0.0136	0.0134	0.0119	0.31	0.78	0.73	11.67	0.59	0.41	27.18	4
118	AB-SA153	37.5	1.2827	6.73	0.0556	24.08	21.18	0	9.62	100.44	0.0156	0.0092	0.0129	0.0117	0.0215	0.0143	0.0137	0.0127	0.32	2.14	0.86	22.77	0.54	0.43	551.92	0.64
121	AB-SA153	37.28	2.73	0.6164	0.0276	10.8	20.85	0.012	28.24	100.56	0.015	0.0092	0.0136	0.0115	0.0224	0.0133	0.0134	0.0142	0.32	1.39	3.4	42.83	0.82	0.43	117.82	0.37
123	AB-SA153	37.06	0.0839	2.9	0	21.54	20.83	0	18.12	100.54	0.0167	0.009	0.0146	0.0119	0.0219	0.0142	0.0138	0.0136	0.32	15.59	1.36	100	0.57	0.43	582.14	0.46
125	AB-SA153	37.05	0.8369	5.69	0.0155	22.78	20.25	0	13.07	99.69	0.0163	0.009	0.0134	0.0117	0.0228	0.0138	0.0138	0.0132	0.32	2.77	0.94	78.24	0.56	0.44	990.97	0.55
127	AB-SA153	38.43	3.56	8.56	0.079	12.55	21.79	0.0383	15.62	100.63	0.0155	0.0101	0.0135	0.0117	0.0222	0.0138	0.0134	0.0132	0.31	1.19	0.77	16.62	0.77	0.42	37.84	0.5
129	AB-SA153	39.51	8	9.11	0.033	20.73	22.3	0	0.5981	100.29	0.0158	0.011	0.0135	0.0114	0.0215	0.0144	0.013	0.0119	0.31	0.77	0.75	37.88	0.59	0.41	457.39	3.29
130	AB-SA153	38.47	5.96	6.55	0.0493	25.22	21.4	0.0138	2.25	99.92	0.0162	0.0097	0.0151	0.0112	0.0222	0.0142	0.0133	0.0121	0.32	0.91	0.89	25.08	0.53	0.43	100.84	1.42
133	AB-SA153	37.21	1.1513	9.93	0.5116	6.68	18.5	0.01	25.68	99.67	0.0165	0.0097	0.0143	0.0118	0.0223	0.0141	0.0138	0.0143	0.32	2.28	0.71	3.37	1.07	0.45	210.64	0.39
139	AB-SA153	40.15	12.1	2.07	0.0278	23.1	22.62	0.1038	0.2909	100.46	0.0159	0.0106	0.0138	0.0111	0.0213	0.013	0.0132	0.012	0.31	0.62	1.66	43.15	0.56	0.42	14.01	5.65
142	AB-SA150	36.67	0.5874	5	1.2448	14.64	20.32	0.0079	21.72	100.19	0.0168	0.0089	0.0147	0.0118	0.0223	0.0134	0.0137	0.014	0.32	3.44	1.02	1.81	0.7	0.44	178.89	0.42
143	AB-SA150	36.25	1.5468	2.27	0.0259	22.76	20.76	0.0148	14.51	98.15	0.0168	0.0086	0.0134	0.0118	0.0237	0.0152	0.014	0.0129	0.33	1.92	1.55	47.41	0.56	0.43	97.13	0.52
149	AB-SA150	37.54	2.43	5.14	0.1407	1.76	21.01	0.1042	31.45	99.58	0.0165	0.0095	0.0127	0.0114	0.0216	0.0146	0.0137	0.0149	0.32	1.47	0.99	9.37	2.32	0.43	14.89	0.35
150	AB-SA150	36.95	0.6037	4.05	0.1633	15.56	20.56	0.0104	22.47	100.36	0.016	0.0094	0.014	0.0116	0.0225	0.0141	0.0136	0.0145	0.32	3.45	1.13	8.33	0.68	0.43	137.38	0.41
152	AB-SA150	38.17	1.86	10.47	0.0162	21.78	21.62	0.03	6.95	100.91	0.0158	0.0097	0.0135	0.0117	0.0226	0.0138	0.0135	0.0127	0.32	1.72	0.69	76.78	0.58	0.42	47.63	0.76
153	AB-SA150	37.15	1.144	4.73	0.1445	15.72	21.14	0.0186	20.54	100.58	0.0156	0.0085	0.013	0.0118	0.0226	0.014	0.0139	0.0131	0.32	2.26	1.04	9.44	0.68	0.43	78.17	0.43
154	AB-SA150	37.29	1.4753	3.43	0.0641	9.08	20.9	0.0208	28.11	100.37	0.0163	0.0092	0.014	0.0118	0.0224	0.0142	0.014	0.0146	0.32	1.97	1.24	19.68	0.91	0.43	71.36	0.37
156	AB-SA150	37.89	3.12	4.31	0.021	6.23	21.41	0.1525	27.81	100.95	0.0164	0.0098	0.013	0.012	0.0214	0.0149	0.0136	0.014	0.32	1.29	1.09	59.21	1.11	0.42	10.33	0.37
163	AB-SA150	37.09	1.99	2.1	0.0175	21.52	20.45	0	16.72	99.88	0.0156	0.0098	0.0139	0.012	0.0224	0.0141	0.0138	0.0133	0.32	1.69	1.63	69.89	0.57	0.44	100	0.48

Table A7: Major and trace element composition of samples from the Khida Terrane. Major element concentrations were measured with XRF and are given in weight-%; trace element concentrations were measured with ICP-MS and are given in ppm.

Sample	SiO_2	TiO_2	Al_2O_3	MnO	MgO	CaO	Na_2O	K_2O	P_2O_5	Fe_2O_3	Sum%	Li	Sc	V
AB-SA39	71.96	0.01	13.43	0.13	0.07	0.82	4.29	3.67	0.04	1.06	95.48	114.86	3.03	8.00
AB-SA40	72.42	0.23	14.04	0.04	0.38	2.78	3.80	2.93	0.21	2.22	100.33	46.27	6.45	18.0(
AB-SA45	64.13	0.40	9.41	0.08	3.80	13.66	0.84	0.17	0.05	5.71	*97.88*	34.21	11.72	31.0(
AB-SA48	50.62	0.10	27.97	0.02	0.73	11.45	4.24	0.69	0.02	1.34	97.17	3.28	1.56	23.0(
AB-SA49	73.09	0.11	12.68	0.03	0.15	1.40	4.10	4.15	0.03	1.12	96.86	16.52	2.58	10.0(
AB-SA51	72.58	0.19	14.25	0.03	0.44	1.52	5.40	1.39	0.08	2.22	99.73	16.79	5.35	n/d
AB-SA57	74.39	0.07	13.54	0.02	0.10	1.44	3.27	4.75	0.01	1.14	100.05	21.33	1.57	n/d

Sample	Cr	Ni	Cu	Zn	Ga	Rb	Sr	Y	Zr	Nb	Mo	Cd	Sn	Sb
AB-SA39	45.74	6.24	1.77	51.37	24.59	344.47	6.26	33.29	40.01	21.06	0.79	0.10	9.63	0.08
AB-SA40	52.90	6.96	5.38	51.63	17.76	97.66	481.37	15.91	214.99	15.24	0.67	0.05	2.20	0.07
AB-SA45	664.39	44.40	10.91	16.25	21.78	12.48	482.60	29.48	173.34	20.99	3.14	0.04	7.62	0.47
AB-SA48	141.52	16.90	4.66	13.58	21.35	6.22	714.37	0.95	2.49	1.12	1.36	0.04	0.49	0.30
AB-SA49	65.70	7.42	4.84	36.95	18.13	130.22	117.36	13.06	104.20	9.26	1.96	0.14	1.57	0.15
AB-SA51	128.59	9.69	7.17	38.68	21.36	59.00	216.22	7.19	158.17	4.71	1.12	0.04	2.17	0.16
AB-SA57	218.99	14.78	6.66	13.24	14.08	154.65	248.10	6.96	95.71	9.15	1.81	0.01	1.29	0.11

Sample	Cs	Ba	La	Ce	Pr	Nd	Sm	Eu	Gd	Tb	Dy	Ho	Er	Tm
AB-SA39	10.02	12.83	7.31	20.75	2.79	9.94	4.28	0.01	4.40	0.90	5.93	1.10	3.08	0.45
AB-SA40	2.72	1694.92	73.89	140.24	15.13	52.75	8.84	1.45	6.15	0.67	3.53	0.62	1.69	0.22
AB-SA45	4.29	65.89	52.97	108.00	11.85	42.31	8.35	1.40	6.43	0.94	5.30	1.04	3.04	0.44
AB-SA48	0.33	214.97	3.13	5.08	0.55	2.11	0.34	1.74	0.28	0.04	0.20	0.04	0.09	0.01
AB-SA49	2.19	541.43	23.72	45.41	5.09	17.81	3.40	0.53	2.51	0.37	2.40	0.46	1.45	0.22
AB-SA51	0.44	272.63	17.02	34.33	4.12	15.53	3.14	0.66	2.38	0.30	1.60	0.26	0.67	0.08
AB-SA57	2.26	908.53	25.04	42.76	4.46	15.30	2.49	0.62	1.85	0.22	1.29	0.23	0.66	0.09

Sample	Yb	Lu	Hf	Ta	Tl	Pb	Bi	Th	U	ΣLREE	ΣHREE	ΣREE	ΣLREE/ ΣHREE	Eu/Eu
AB-SA39	3.05	0.40	3.14	5.22	1.39	9.00	5.39	11.64	3.22	49.48	14.05	63.54	3.52	0.01
AB-SA40	1.54	0.21	6.20	2.02	0.39	15.11	0.09	20.15	1.70	298.45	8.04	306.49	37.12	0.60
AB-SA45	2.87	0.43	4.68	3.18	0.05	2.42	0.32	21.77	4.07	231.32	13.19	244.51	17.54	0.58
AB-SA48	0.09	0.01	0.06	0.39	0.02	2.49	0.04	0.14	0.04	13.22	0.45	13.68	29.10	17.28
AB-SA49	1.65	0.23	4.14	1.38	0.59	18.55	0.06	18.11	3.55	98.48	6.33	104.81	15.56	0.55
AB-SA51	0.56	0.07	3.99	2.49	0.25	10.18	0.02	1.40	0.79	77.19	3.40	80.59	22.72	0.74
AB-SA57	0.77	0.10	3.32	2.72	0.47	29.12	0.01	8.31	2.55	92.53	3.18	95.71	29.09	0.88

Curriculum Vitae

Educational background

10/2012 – 10/2015	PhD, Institue for Applied Geoscienes, Darmstadt Technical University
23.03.2011	Diploma (MSc) in Geology, Ruprecht-Karls-University Heidelberg, Germany, Title of Diploma thesis: "*Fazielle Analyse des Calcimikroben-Archaeocyathen Bioherms von Funtana Colomba (Iglesiente, Südwest-Sardinien, Italien)*"
10/2005 – 03/2011	Geology and Palaeontology (Diploma) Ruprecht-Karls-University Heidelberg, Germany

Professional background

04/2012 – 10/2012:	Consultant, GIZ International Services GmbH, Darmstadt
01/2012 – 04/2012:	Wellsite geologist, GIZ International Services GmbH, Riyadh

Professional experience

- Shallow and deep water well supervision
- Sedimentological, petrographical and geochemical studies in the Palaeozoic sandstones in Saudi Arabia
- Provenance studies in highly mature siliciclastic successions

Training courses

- EAGE Geological Boot Camp, Esslingen, Germany, 04/2015
- Short course 'Sedimentary Provenance Analysis', Göttingen, Germany, 09/2012
- Short course 'Introduction to Sequence Stratigraphy', Hamburg, Germany, 09/2012

Fellowships, scientific visits and conferences

- Member in ‘Deutsche Geologische Gesellschaft - Geologische Vereinigung e. V. (DGGV)’
- Member in ‘Paläontologische Gesellschaft e. V.’ (PalGes)
- Visit to 'GeoBerlin', Berlin, Germany, 2015
- Visit to ‘GeoFrankfurt’, Frankfurt, Germany, 2014
- Attended ‘Working Group on Sediment Generation (WGSG), 2nd Workshop’, Göttingen, Germany, 2014
- Visit to ‘Joint Meeting DMG, GV & Sediment’, Tübingen, Germany, 2013
- Visit to ‘GV & Sediment Meeting "Of Land and Sea - Processes and Products"’, Hamburg, Germany, 2012

Publications and abstracts

- Bassis, A., Hinderer, M., Meinhold, G., 2016a. New insights into the provenance of Saudi Arabian Palaeozoic sandstones from heavy mineral analysis and single-grain geochemistry. Sedimentary Geology 333, 100–114.
- Bassis, A., Hinderer, M., Meinhold, G., 2016b. Petrography and geochemistry of Palaeozoic quartz-rich sandstones from Saudi Arabia: implications for provenance and chemostratigraphy. Arabian Journal of Geosciences 9(5), 1–26.
- Bassis, A., Hinderer, M., Meinhold, G., 2015. Provenance of Saudi Arabian Palaeozoic sandstones using whole rock and single grain geochemistry. In: Wagner, J., Elger, K. (Eds.), GeoBerlin2015 – Dynamic Earth from Alfred Wegener to today and beyond – Abstracts. Annual Meeting of DGGV and DMG, 4–7 October 2015, 76.
- Bassis, A., Hinderer, M., Meinhold, G., Schüth, C., Rausch, R., 2014a. Petrographical and geochemical data from Palaeozoic sandstones and Precambrian basement of the Arabian Peninsula. GeoFrankfurt 2014 / Abstract volume.
- Bassis, A., Hinderer, M., Meinhold, G., Schüth, C., Rausch, R., 2014b. Petrographical and geochemical data from Palaeozoic sandstones of the Arabian Peninsula. WGSG 2nd Workshop / Abstract volume.
- Al-Ajmi, H., Hinderer, M., Hornung, J., Bassis, A., Keller, M., Rausch, R., Schüth, C., 2014. Matrix versus fracture permeability in a regional sandstone aquifer (Wajid sandstone, SW Saudi Arabia). Grundwasser 19(2), 151–157.
- Bassis, A., Hinderer, M., Meinhold, G., Spiegel, C., 2013. Paleozoic source to sink relation along the Transgondwanan Mountain Belt (Saudi Arabia). DMG-Gv Meeting Tübingen / Abstract volume.
- Bassis, A., Hinderer, M., Rausch, R., Keller, M., Schüth, C., Al-Ajmi, H., Michelsen, N., 2012. Analysis of Radioactive Anomalies in Paleozoic-Mesozoic Aquifers of the Arabian Platform. In: Rausch, R., Schüth, C., Himmelsbach, T. (Eds.) Hydrogeology of Arid Environments, Proceedings, 200.